R&T 1998
Research & Technology

NASA

Lewis Research Center • Cleveland, Ohio

NASA/TM—1999-208815

About the cover:

Top: NASA Lewis has been responsible for developing the propulsion technologies required for a next-generation supersonic commercial transport, or High-Speed Civil Transport (HSCT). NASA personnel have made significant contributions to propulsion component and high-temperature engine materials technologies that will not only contribute to future HSCT aircraft and engine designs but will be utilized in a wide variety of other government and industry programs, both aerospace and nonaerospace.

Bottom: The agreement between Lewis and America True calls for detailed analysis of different sail and mast designs.

Research & Technology 1998

National Aeronautics and Space Administration

Lewis Research Center
Cleveland, Ohio 44135

NASA/TM—1999-208815

This report is available in electronic form at http://www.grc.nasa.gov/WWW/RT/.

Note that at the time of printing, the NASA Lewis Research Center was undergoing a name change to the NASA John H. Glenn Research Center at Lewis Field. URL's for the Center are gradually being changed from lerc.nasa.gov to grc.nasa.gov. This process was just starting at the time of this printing. If a URL given in this document does not work, try substituting "grc" for "lerc" or "lerc" for "grc", wherever they appear.

Available from

NASA Center for Aerospace Information
7121 Standard Drive
Hanover, MD 21076
Price Code: A10

National Technical Information Service
5285 Port Royal Road
Springfield, VA 22100
Price Code: A10

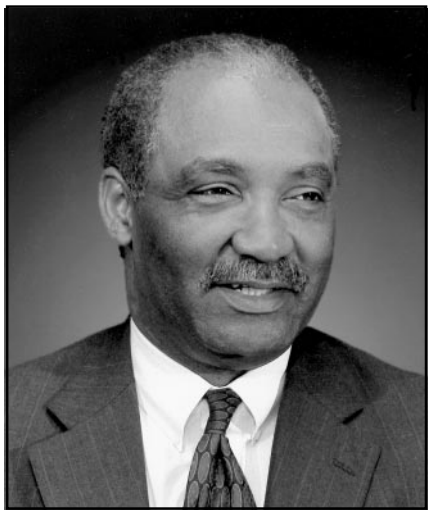

Introduction

NASA Lewis Research Center is responsible for developing and transferring critical technologies that address national priorities in aerospace propulsion and space applications in partnership with U.S. industries, universities, and other Government institutions.

As NASA's premier Center for aerospace propulsion, our role is to develop, demonstrate, and transfer relevant technologies to U.S. industry. As NASA's designated Center of Excellence in Turbomachinery, we develop new and innovative technologies that improve the reliability, performance, efficiency, affordability, capacity, and environmental compatibility of turbomachinery-based propulsion systems. We also maintain a science and technology development role in communications, space power, onboard propulsion, and microgravity fluid physics and combustion. We are committed to enabling U.S.-based aerospace and nonaerospace industries to benefit directly from the technologies developed through our programs. Our goal is to maximize the benefit of our efforts to the Nation and to optimize the return on each taxpayer's investment.

Over 3600 civil service employees and support service contractor personnel staff Lewis. Scientists and engineers comprise more than half of our workforce, with technical specialists, skilled workers, and an administrative staff supporting them. We aggressively strive for technical excellence through continuing education, diversity in our workforce, and continuous improvement in our management and business practices so we can extend the edge of technology in space and aeronautics.

The Lewis Research Center is a unique facility located in the southwest corner of Cleveland, Ohio. Situated on 350 acres of land adjacent to the Cleveland Hopkins International Airport, Lewis comprises more than 140 buildings, including 24 major facilities and over 500 specialized research and test facilities. Additional facilities are located at the Plum Brook Station, which is about 50 miles west of Cleveland.

Our end product is knowledge. This report is designed to help make this knowledge fully available to potential users—the aircraft engine industry, the space industry, the energy industry, the automotive industry, the aerospace industry, and others. It is organized so that a broad cross section of the community can readily use it. Each article begins with a short introductory paragraph that should prove to be a valuable tool for the layperson. These articles summarize the progress made during the year in various technical areas and portray the technical and administrative support associated with Lewis' technology programs. We hope that the information is useful to all.

At the time of publication, NASA Lewis was undergoing a name change to the NASA John H. Glenn Research Center at Lewis Field. If additional information is desired, readers are encouraged to contact the researchers identified in the articles and to visit NASA Glenn on the World Wide Web at http://www.grc.nasa.gov. This document is available on the World Wide Web (http://www.grc.nasa.gov/WWW/RT/).

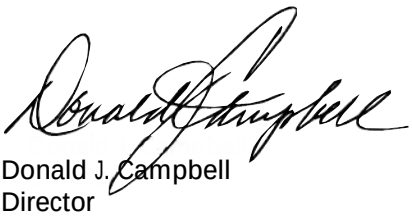

Donald J. Campbell
Director

NASA Lewis Research Center Senior Management

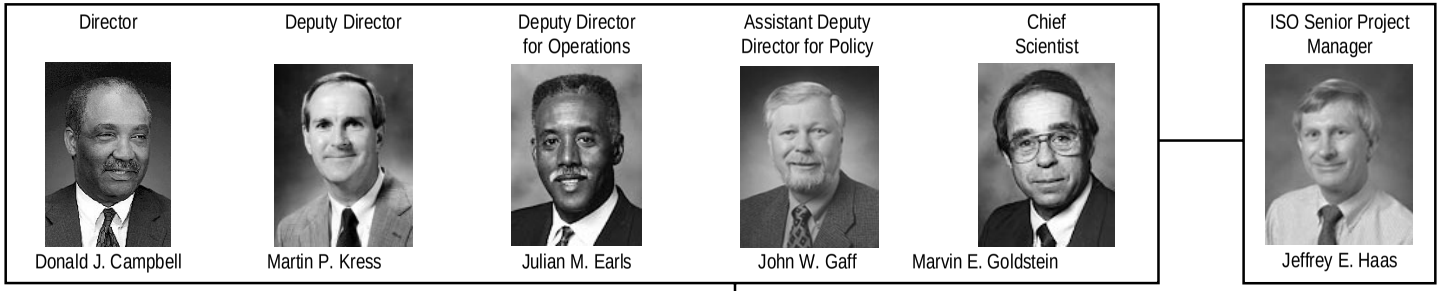

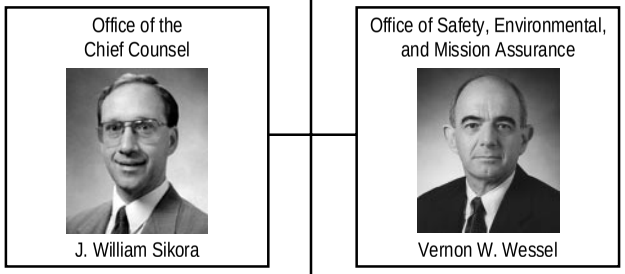

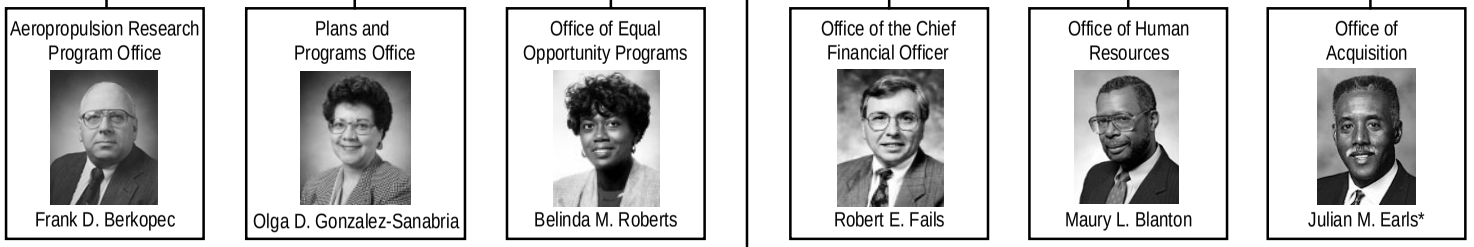

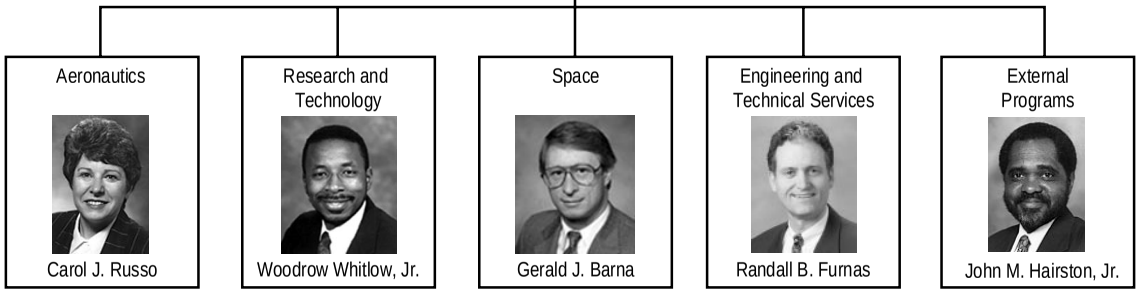

*Acting

CD-48534
February 1999

NASA Lewis Research Center

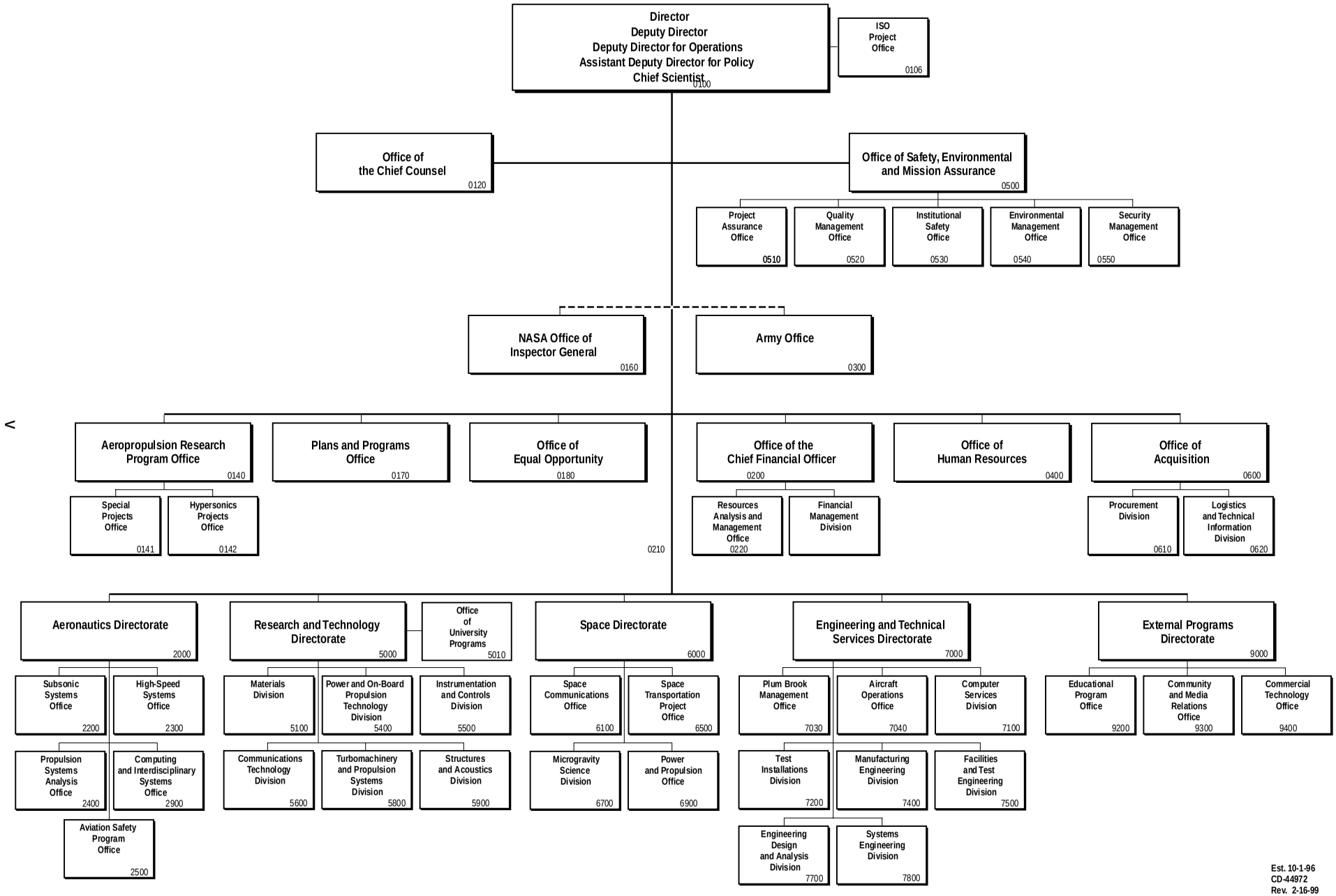

Est. 10-1-96
CD-44972
Rev. 2-16-99

Quality Council

Gerald J. Barna
Director of Space

Donald J. Campbell
Director

Woodrow Whitlow, Jr.
Director of Research
and Technology

Virginia A. Cantwell
President LESA

Donald R. Streibing
President AFGE

Julian M. Earls
Deputy Director for
Operations

Dennis M. Sender
Special Assistant to
the Quality Council

Robert E. Fails
Chief Financial Officer

Carol J. Russo
Director of Aeronautics

Randall B. Furnas
Director of Engineering
and Technical Services

Christopher J. Pestak
Support Service
Contractor Liaison

Marvin E. Goldstein
Chief Scientist

Martin P. Kress
Deputy Director

John M. Hairston, Jr.
Director of External Programs

The Quality Council was established in October 1992 to adopt and implement a Total Quality (TQ) plan for Lewis. It is composed of Executive Council members as well as the president of the American Federation of Government Employees (AFGE), Local 2812, and the president of the Lewis Engineers and Scientists Association (LESA), IFPTE Local 28. A representative of major onsite support service contractors serves as a liaison.

February 1999

Contents

Aeronautics

Research and Technology

Space

Engineering and Technical Services

Commercial Technology

Appendixes

Aeronautics

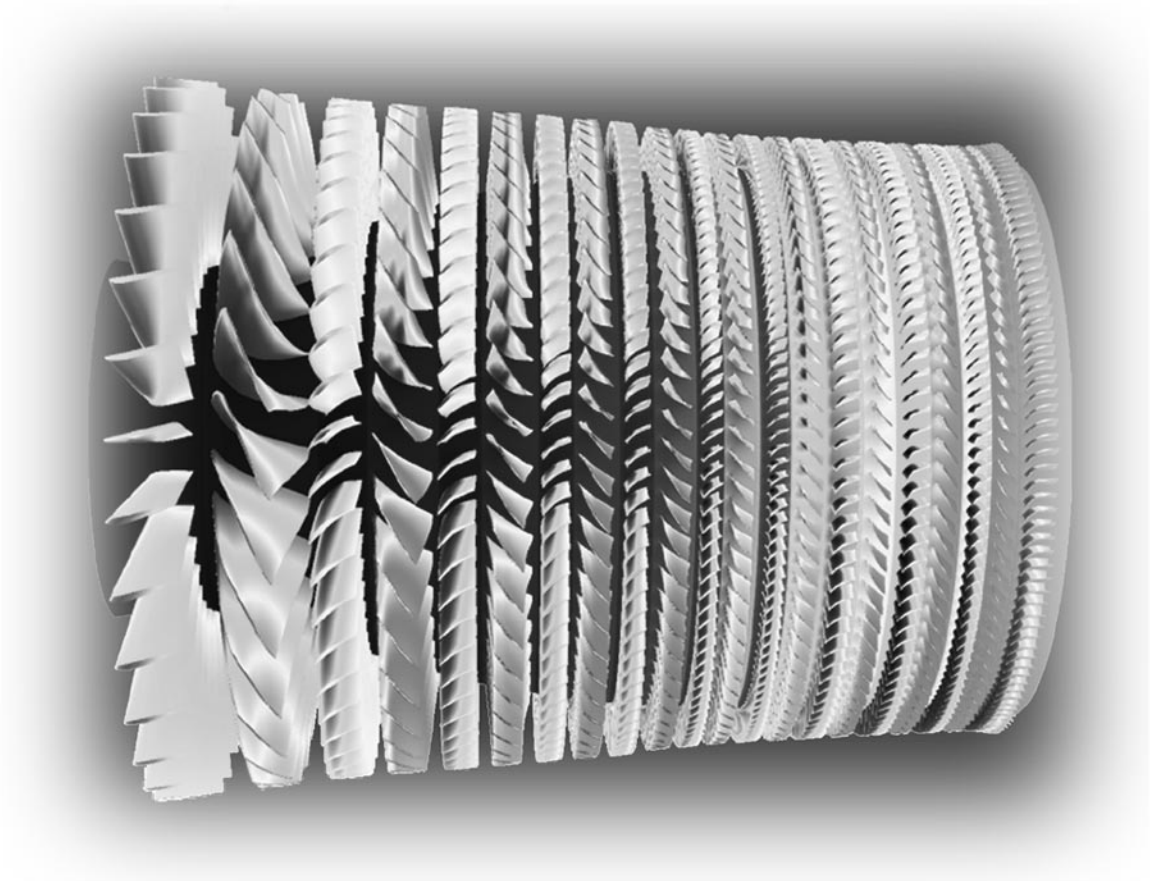

High-Speed Systems

High-Speed Research—Propulsion Project Accomplishments

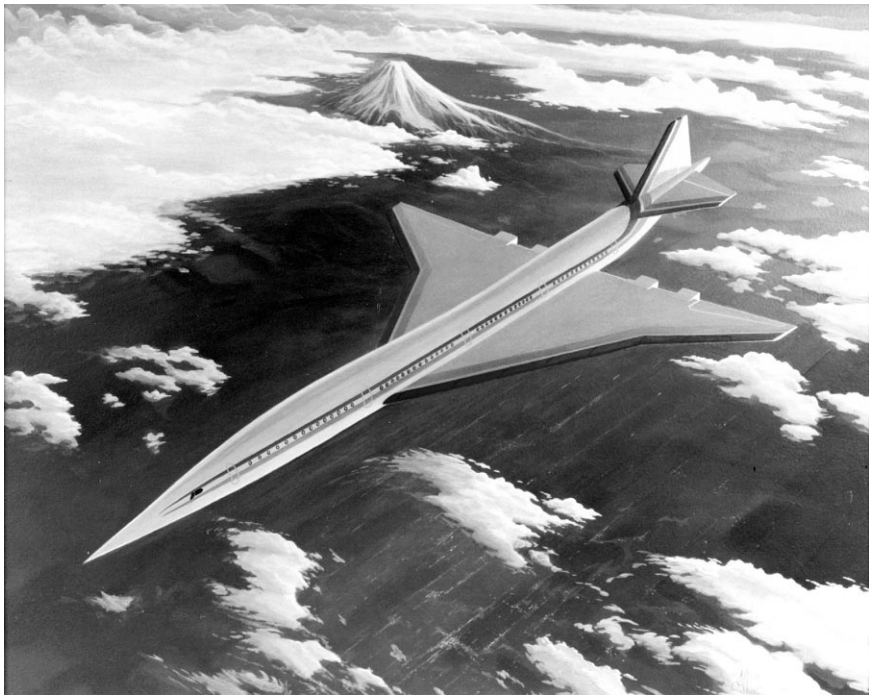

High-Speed Civil Transport (HSCT).

This past year has been one of great technical accomplishment for the propulsion element of NASA's High-Speed Research (HSR) Program. The HSR Program is a NASA/industry partnership to develop the high-risk/high-payoff airframe and propulsion technologies applicable to a second-generation supersonic commercial transport, or High-Speed Civil Transport (HSCT). The NASA Lewis Research Center manages the propulsion element, which also includes industry participation. These technologies will contribute greatly to U.S. industry's ability to make an informed product launch decision for an HSCT vehicle. Specific NASA Lewis accomplishments in 1998 include

• The lean premixed prevaporized combustor concept was selected for follow-on full-scale development. The combustor concept has demonstrated the ability to produce ultra-low emissions of less than 5 g of nitrogen oxides (NO_x) per kg of fuel burned while maintaining a combustion efficiency of greater than 99.9 percent with minimal technical or developmental risks.

• Combustor sector tests were initiated in CE–9 of the Engine Research Building to evaluate ceramic matrix composite parts in a realistic combustor environment.

• An alternative metal combustor liner was assessed. These tests showed that metal liners made from nickel-based superalloys and coated with a thick thermal barrier coating can meet HSR emission and life goals.

• The Large Scale Model 1 (LSM–1) test, which was conducted to test a nozzle design in a large-scale, more realistic engine environment, was completed. The goal was to improve confidence in the ability of the nozzle technologies being developed to meet the noise goals of the HSR Program. The test not only showed that the technologies are on track but successfully demonstrated the use of ceramic matrix composite tiles in HSCT engine applications.

• Over 18 000 hours of durability testing were completed for all four advanced materials systems in Lewis' materials laboratories. Superalloy, gamma-titanium aluminide, ceramic matrix composite, and thermal protection system performance were evaluated for HSCT nozzle applications.

• A turbomachinery disk alloy was selected for a large-scale processing effort. This alloy has mechanical properties far superior to current production materials and is projected to meet HSCT requirements.

• A concept for a second generation, two-dimensional, mixed-compression supersonic inlet was coupled to a turbojet engine and tested in Lewis' 10- by 10-Foot Supersonic Wind Tunnel. The extensive data base of results for inlet/engine operability and unstart conditions contributed to the maturation of inlet technologies for future commercial supersonic transport vehicles.

• Proactive transfer of HSR propulsion technologies to other NASA programs has been initiated. Specifically, an economic fabrication technique for sheet titanium

aluminide developed for the HSCT exhaust nozzle is being considered for use in the thermal protection system for both the reusable launch vehicle and X–33 programs.

For more information, visit Lewis' HSR and aeropropulsion facility sites on the World Wide Web:
HSR: http://www.grc.nasa.gov/WWW/HSR

Engine Research Building:
http://www.grc.nasa.gov/WWW/AFED/facilities/erb.html

Propulsion Systems Laboratory:
http://www.grc.nasa.gov/WWW/AFED/facilities/psl.html

Aero-Acoustic Propulsion Laboratory:
http://www.grc.nasa.gov/WWW/AFED/facilities/aapl.html

10- by 10-Foot Supersonic Wind Tunnel:
http://www.grc.nasa.gov/WWW/AFED/facilities/10x10.html

Lewis contacts:
Dr. Robert J. Shaw, (216) 977–7135, Robert.J.Shaw@grc.nasa.gov;
and Lori A. Manthey, (216) 433–2484, Lori.A.Manthey@grc.nasa.gov

Author: Lori A. Manthey

Headquarters program office: OAT

Programs/Projects: HSR, RLV, X–33

Propulsion Systems Analysis

Neural Network and Regression Approximations Used in Aircraft Design

NASA Lewis Research Center's CometBoards Test Bed was used to create regression and neural network models for a High-Speed Civil Transport (HSCT) aircraft. Both approximation models that replaced the actual analysis tool predicted the aircraft response in a trivial computational effort. The models allow engineers to quickly study the effects of design variables on constraint and objective values for a given aircraft configuration. For example, an engineer can change the engine size by 1000 lb of thrust and quickly see how this change affects all the output values without rerunning the entire simulation. In addition, an engineer can change a constraint and use the approximation models to quickly reoptimize the configuration. Generating the neural network and the regression models is a time-consuming process, but this exercise has to be carried out only once. Furthermore, an automated process can reduce calculations substantially.

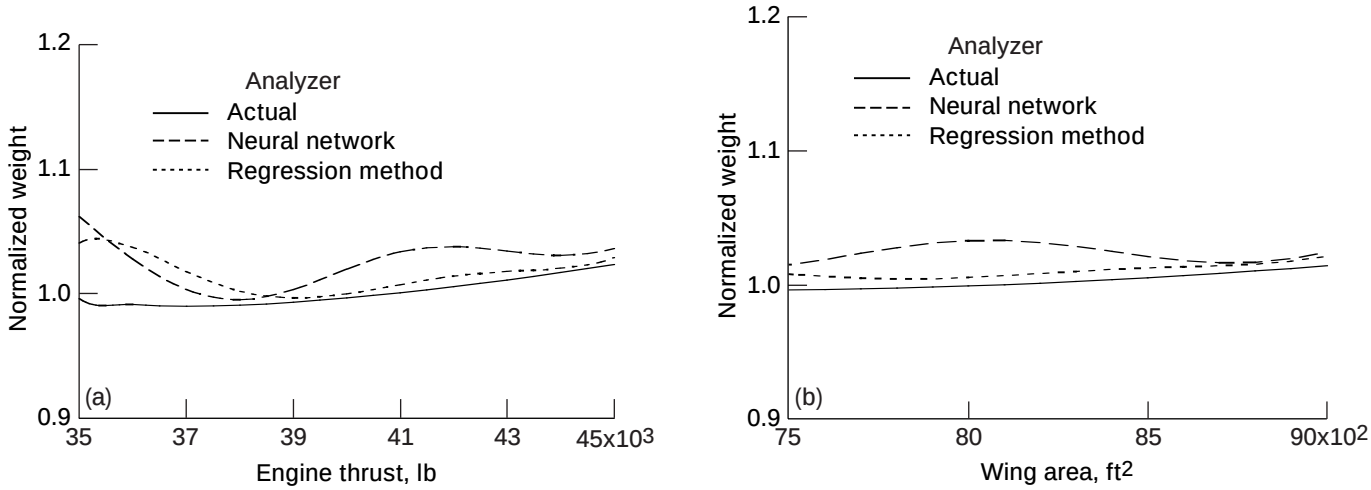

Comparison of aircraft weight obtained by using approximate methods and actual analysis. (a) As a function of engine thrust. (b) As a function of wing area.

One issue that needs to be addressed is the generation of output for a given set of design variables. The analysis tools must be smart enough to respond completely to changes in design values. For example, a change in the overall pressure ratio of an engine will affect several behavior parameters besides an increase in the pressure. For example, the overall efficiency of the compressor will change, the cooling flow temperature will rise, more cooling flow will be required, and the compressor will increase in weight. These problems, however, can be overcome with more capable tools and a little planning.

The figure shows how closely the neural network and regression techniques track the output value of aircraft gross weight from the actual analysis. Both approximation techniques have been shown to produce good agreement for all desired response parameters.

Lewis contacts:
Dr. Surya N. Patnaik, (216) 433–5916, Surya.N.Patnaik@grc.nasa.gov;
Dale A. Hopkins, (216) 433–3260, Dale.A.Hopkins@grc.nasa.gov; and
Thomas M. Lavelle, (216) 977–7042, Thomas.M.Lavelle@grc.nasa.gov

Authors: Dr. Surya N. Patnaik, Dale A. Hopkins, and Thomas M. Lavelle

Headquarters program office: OAT

Programs/Projects: HSCT, AST, HSR

Computing and Interdisciplinary Systems

Numerical System Solver Developed for the National Cycle Program

As part of the National Cycle Program (NCP), a powerful new numerical solver has been developed to support the simulation of aeropropulsion systems. This software uses a hierarchical object-oriented design. It can provide steady-state and time-dependent solutions to nonlinear and even discontinuous problems typically encountered when aircraft and spacecraft propulsion systems are simulated. It also can handle constrained solutions, in which one or more factors may limit the behavior of the engine system. Time-dependent simulation capabilities include adaptive time-stepping and synchronization with digital control elements. The NCP solver is playing an important role in making the NCP a flexible, powerful, and reliable simulation package.

The NCP solver uses a modified Newton-Raphson method. For any given system model of interest, a set of independent and dependent parameters are defined, either by the user or automatically by the model elements. The solver characterizes the effects of each independent parameter on all dependent variables through direct perturbation of the model. It uses this information as a guide as it attempts to find the set of independent values that will render all dependent errors equal to zero (the solution). This is typically achieved through a number of successive iterations. The NCP solver employs a sophisticated set of algorithms to enhance the model's convergence toward the solution, and it has a number of attributes that allow expert users to fine tune the solution process.

The NCP solver has a flexible, object-oriented design that allows appropriate solver information to be embedded in the model, even though the solver itself is part of the NCP infrastructure and is not model specific. The functions of the solver are also hierarchical, as illustrated in the figure. The Transient Executive controls the overall performance of time-dependent simulations, which consist of one or more individual solutions to the model at different points in time. The Transient Executive sends messages to the Solver Executive, requesting a solution at each individual point in time. The Solver Executive, in turn, sends messages to the independents and dependents to perform low-level functions as required (including integration with respect to time). This hierarchical approach provides a great deal of design flexibility and minimizes the need to keep multiple copies of data during execution.

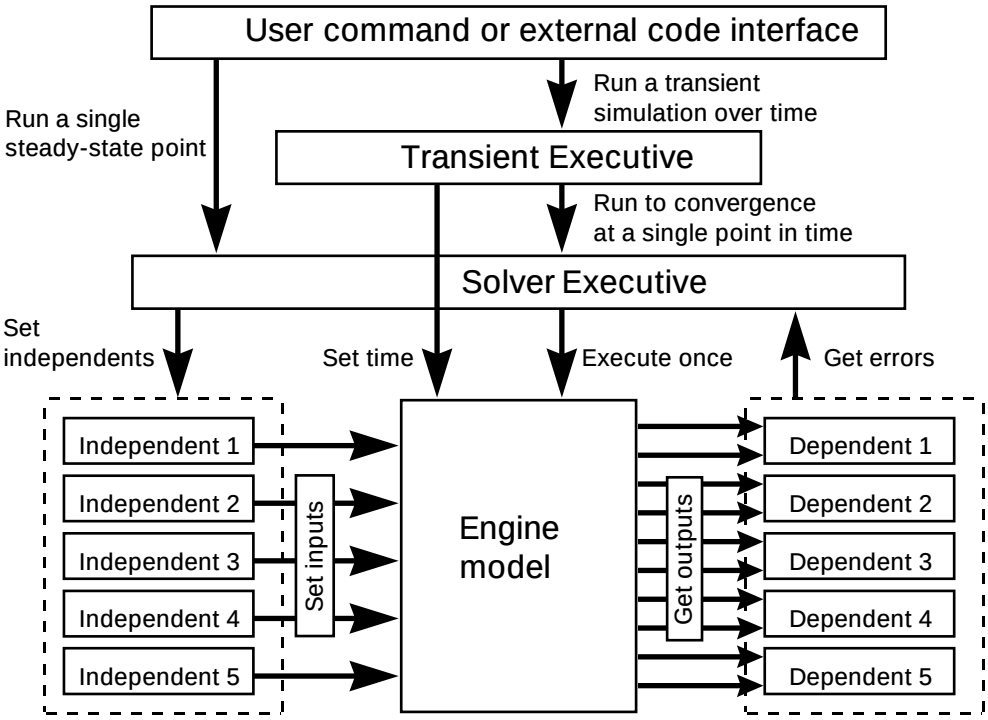

NCP solver subsystem hierarchy.

The NCP solver was developed at the NASA Lewis Research Center in cooperation with experts at each of the industry partner companies. It includes the best practices of each partner company in a single package.

The original version of the solver included steady-state analysis capabilities only. In fiscal year 1998, time-dependent simulation capabilities were added, including support for simulation of the digital control elements. In fiscal year 1999, the NCP solver will be enhanced to include special handling for high-frequency, spatially distributed models (dynamics). A framework for optimization will also be incorporated in the solver in 1999.

Bibliography

Evans, A.L.; Follen, G.; and Naiman, C.: Numerical Propulsion System Simulation's National Cycle Program. AIAA Paper 98–3113, 1998.

Ashleman, R.H.; Lavelle, T.; and Parsons, F.: The National Cycle Program: A Flexible System Modeling Architecture for Aircraft Engine Simulation. AIAA Paper 98–3114, 1998.

Dynacs Engineering Co., Inc. contact:
Michael P. Binder, (216) 977–1454, Michael.P.Binder@grc.nasa.gov

Lewis contacts:
James L. Felder, (216) 433–3956, James.L.Felder@grc.nasa.gov; and Cynthia G. Naiman, (216) 433–5238, Cynthia.G.Naiman@grc.nasa.gov

Author: Michael P. Binder

Headquarters program office: OAT

Programs/Projects: NCP, HPCCP, HSR

Inlet-Compressor Analysis Performed Using Coupled Computational Fluid Dynamics Codes

A thorough understanding of dynamic interactions between inlets and compressors is extremely important to the design and development of propulsion control systems, particularly for supersonic aircraft such as the High-Speed Civil Transport (HSCT). Computational fluid dynamics (CFD) codes are routinely used to analyze individual propulsion components. By coupling the appropriate CFD component codes, it is possible to investigate inlet-compressor interactions. The objectives of this work were to gain a better understanding of inlet-compressor interaction physics, formulate a more realistic compressor-face boundary condition for time-accurate CFD simulations of inlets, and to take a first step toward the CFD simulation of an entire engine by coupling multidimensional component codes. This work was conducted at the NASA Lewis Research Center by a team of civil servants and support service contractors as part of the High Performance Computing and Communications Program (HPCCP).

An inlet-compressor experiment (ref.1) conducted at the University of Cincinnati was chosen as the application for this CFD analysis because of the availability of experimental data for validation. A schematic of the experiment is shown in the figure. It consists of a constant-area annular inlet coupled to a GE T–58 engine (General Electric) that was modified for cold operation. The collapse of a flexible bump on the hub of the inlet produced a well-defined acoustic pulse that traveled downstream and interacted with the engine. Static-pressure time histories were measured at the four axial locations shown in the figure. NPARC, a general purpose CFD code, was used to simulate the inlet portion of the experiment. The engine was approximated by the first-stage rotor and was simulated with ADPAC, a turbomachinery code. Details concerning the code coupling approach and the issues involved are given in reference 2.

The NPARC domain was solved using a single grid block, whereas the ADPAC domain was divided into multiple blocks, with all the blocks computed in parallel to achieve faster execution. Simulation of the experiment for a 10.4-msec transient took about 32.5 hours for a seven-block ADPAC case and 12 hours for a 21-block case. A snapshot in time of flowfield pressure contour plots and the four pressure-sensor time histories are shown in the figure. (Only part of the NPARC domain is shown.) Although not shown in the figure, the computed pressure time histories were found to give reasonable agreement with the experimental data.

The investigation indicates that coupling inlet and turbomachinery CFD codes is a feasible approach to studying inlet-engine interaction problems. Additional investigation of code coupling issues and the means for reducing execution time is planned. This approach offers the possibility of including other specialized codes (e.g., combustor) to provide a full engine simulation. The coupled NPARC–ADPAC codes could also serve as a test bed for exploring other flow perturbations of interest and for validating simplified boundary conditions.

References

1. Freund, D.; and Sajben, M.: Reflection of Large Amplitude Acoustic Pulses From an Axial Flow Compressor. AIAA Paper 97–2879, 1997.
2. Suresh, A., et al.: Analysis of Compressor-Inlet Acoustic Interactions Using Coupled Component Codes. AIAA Paper 99–0749, 1999.

Lewis contact:
Gary L. Cole, (216) 433–3655, Gary.L.Cole@grc.nasa.gov

Dynacs Engineering Co., Inc. contacts:
Ambady Suresh, (216) 977–1384, Ambady.Suresh@grc.nasa.gov; and Scott Townsend, (216) 977–1080, Scott.Townsend@grc.nasa.gov

Authors: Gary L. Cole, Ambady Suresh, and Scott Townsend

Headquarters program office: OAT

Programs/Projects: HPCCP, NPSS

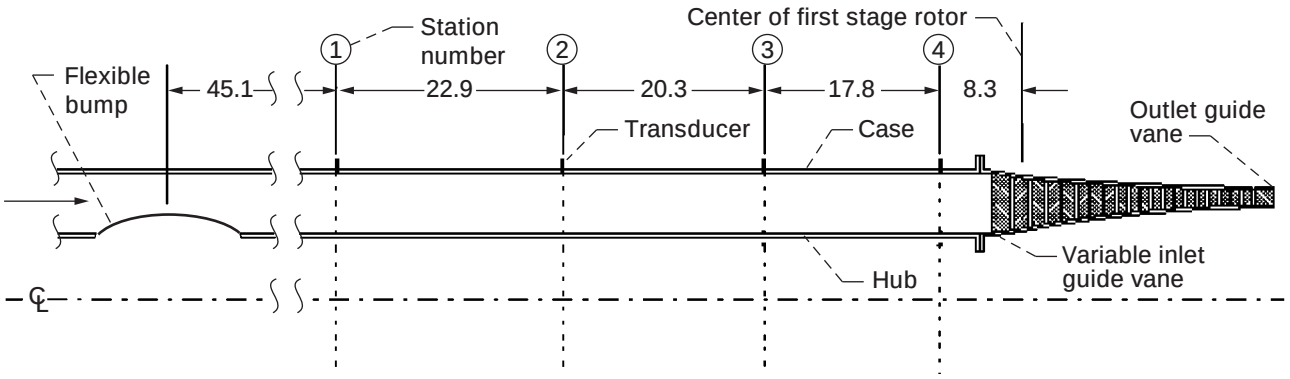

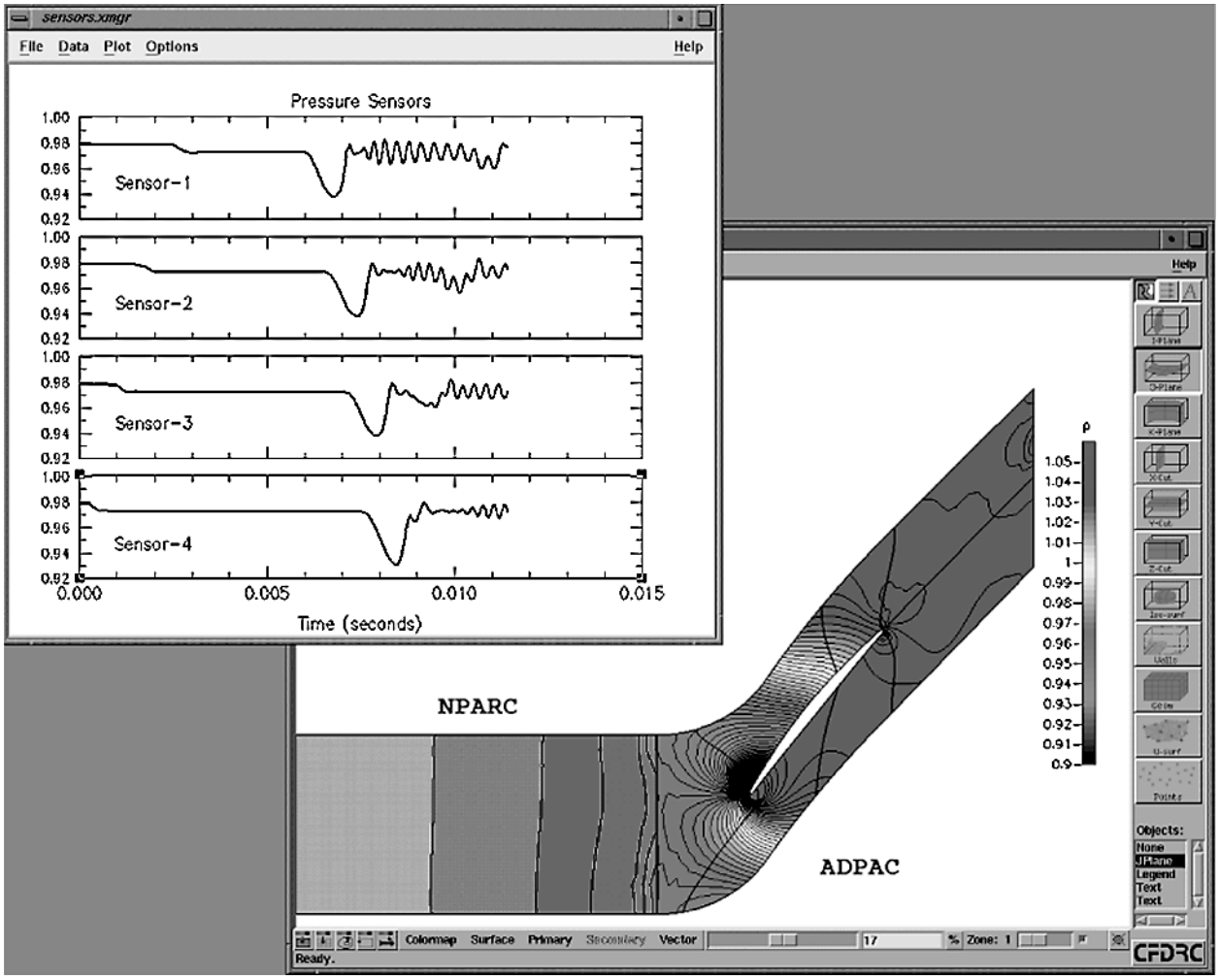

Snapshot of (partial) NPARC–ADPAC pressure contour plots and pressure time histories at sensor locations during simulation of the University of Cincinnati experiment. All dimensions in diagram at top are in centimeters.

FoilSim—Basic Aerodynamics Software Created

FoilSim is interactive software that simulates the airflow around various shapes of airfoils. The graphical user interface, which looks more like a video game than a learning tool, captures and holds the students' interest. The software is a product of NASA Lewis Research Center's Learning Technologies Project, an educational outreach initiative within the High Performance Computing and Communications Program (HPCCP).

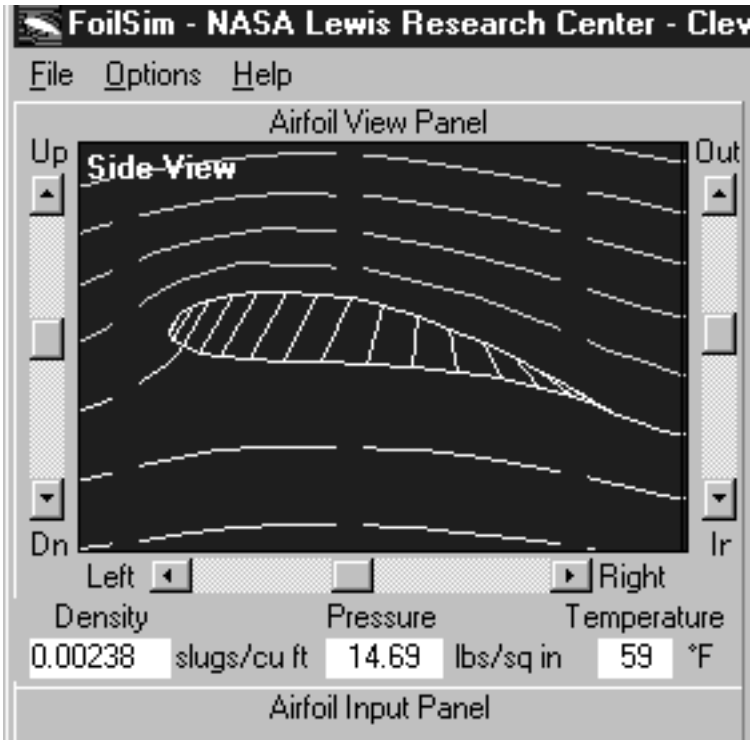

Airfoil view panel within FoilSim.

This airfoil view panel is a simulated view of a wing being tested in a wind tunnel. As students create new wing shapes by moving slider controls that change parameters, the software calculates their lift. FoilSim also displays plots of pressure or airspeed above and below the airfoil surface. A satisfied user comments, "To be able to change the parameters of the experiment with a click of a button is fantastic, as is the ability to observe the results instantaneously." An additional feature of the program is "Play Ball," where students learn more about aerodynamics through controlling the conditions of a baseball pitch, including altitude, speed of pitch, and spin of pitch.

Interactive lessons that accompany the package prompt students to engage in problem solving and discovery. Teachers are impressed at how well the software and lessons inspire students to explore their intellectual potential. One teacher says, "FoilSim allows students to hypothesize and provides them with immediate, nonthreatening feedback. They really seem to begin to appreciate the process of experimenting rather than just getting the correct answer."

Originally, the code was written for college level engineering students. Adjustment of the code to the high school level resulted in FoilSim, which was created and tested by a diverse team composed of NASA employees, contractors, educators, and students. Lewis' Learning Technologies Project is a part of NASA's agencywide Learning Technologies Project, which is managed by the NASA Ames Research Center.

Find out more about the Learning Technologies Project:
http://learn.ivv.nasa.gov/

Download FoilSim from the Web:
http://www.grc.nasa.gov/WWW/K-12/aerosim

Find supporting resources:
http://www.grc.nasa.gov/WWW/K-12

Lewis contact:
Beth Lewandowski, (216) 433–8873,
Beth.E.Lewandowski@grc.nasa.gov

Author: Ruth A. Petersen

Headquarters program office: OAT

Programs/Projects: HPCCP

Common Analysis Tool Being Developed for Aeropropulsion: the National Cycle Program Within the Numerical Propulsion System Simulation Environment

The NASA Lewis Research Center is developing an environment for analyzing and designing aircraft engines—the Numerical Propulsion System Simulation (NPSS). NPSS will integrate multiple disciplines, such as aerodynamics, structure, and heat transfer, and will make use of numerical "zooming" on component codes. Zooming is the coupling of analyses at various levels of detail. NPSS uses the latest computing and communication technologies to capture complex physical processes in a timely, cost-effective manner. The vision of NPSS is to create a "numerical test cell" enabling full engine simulations overnight on cost-effective computing platforms.

Through the NASA/Industry Cooperative Effort agreement, NASA Lewis and industry partners are developing a new engine simulation called the National Cycle Program (NCP). NCP, which is the first step toward NPSS and is its initial framework, supports the aerothermodynamic system simulation process for the full life cycle of an engine. U.S. aircraft and airframe companies recognize NCP as the future industry standard common analysis tool for aeropropulsion system modeling. The estimated potential payoff for NCP is a $50 million/yr savings to industry through improved engineering productivity.

NCP is being developed to provide all the features that currently exist in cycle simulations as well as the framework needed to enable NPSS concepts of coupling multidisciplinary tools at various levels of detail in a collaborative distributed environment while preserving an overall engine system view. What NCP now allows is illustrated by the following illustration.

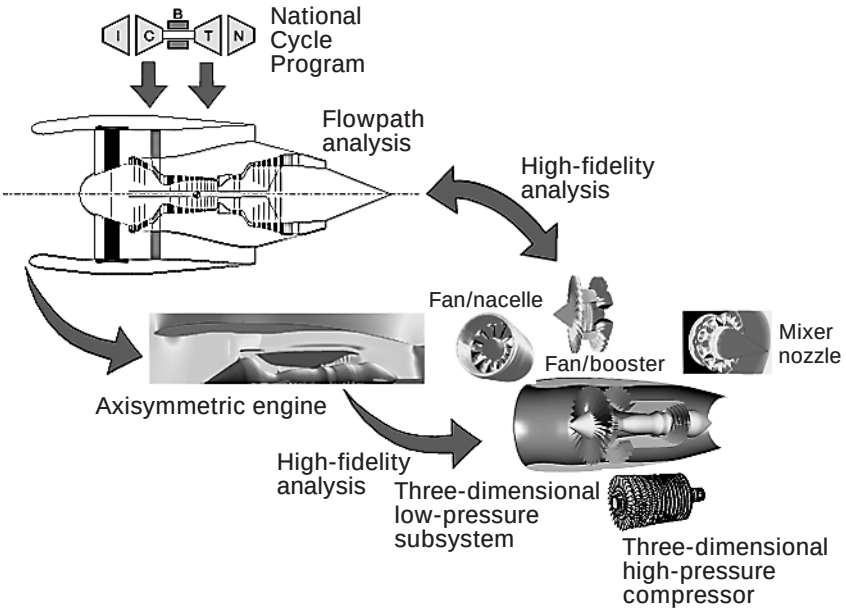

National Cycle Program makes it possible to zoom to a more detailed analysis.

The NPSS/NCP team consists of propulsion experts and software engineers from GE Aircraft Engines, Pratt & Whitney, the Boeing Company, AlliedSignal Engines, Allison, Williams International, Teledyne Ryan Aeronautical, Arnold Engineering Development Center, Wright Patterson Air Force Base, and NASA Lewis. Formal software development processes are followed to facilitate technology transfer.

In fiscal year 1998, the major accomplishment of the NCP team was the completion and distribution of NCP Version 1. New capabilities include transient analysis, test data reduction, a controls toolbox, and initial zooming. NCP applications to the NPSS architecture successfully demonstrated distributed simulations. Workshops were conducted throughout the year, training over 60 NCP users and component developers. NCP is being used as the modeling tool for in-house, High-Speed Research (HSR) at Lewis and GE Aircraft Engines.

In fiscal year 1999, the NCP team will complete the major pieces of the cycle system, including customer deck generation and dynamic solver capability, and will finish off the complete set of engine components. At the same time, NCP's development will shift to a major emphasis on zooming. As part of NPSS, the NCP is supported under the NASA High Performance Computing and Communications Program.

Bibliography

Evans, A.L.; Follen, G.; and Naiman, C.: Numerical Propulsion System Simulation's National Cycle Program. AIAA Paper 98–3113, 1998.

Ashleman, R.H.; Lavelle, T.; and Parsons, F.: The National Cycle Program: A Flexible System Modeling Architecture for Aircraft Engine Simulations. AIAA Paper 98–3114, 1998.

Lewis contacts:

Gregory J. Follen, (216) 433–5193, Gregory.J.Follen@grc.nasa.gov; and Cynthia G. Naiman, (216) 433–5238, Cynthia.G.Naiman@grc.nasa.gov

Authors: Gregory J. Follen and Cynthia G. Naiman

Headquarters program office: OAT

Programs/Projects: HPCCP, NCP

Flow of GE90 Turbofan Engine Simulated

The objective of this task was to create and validate a three-dimensional model of the GE90 turbofan engine (General Electric) using the APNASA (average passage) flow code. This was a joint effort between GE Aircraft Engines and the NASA Lewis Research Center. The goal was to perform an aerodynamic analysis of the engine primary flow path, in under 24 hours of CPU time, on a parallel distributed workstation system. Enhancements were made to the APNASA Navier-Stokes code to make it faster and more robust and to allow for the analysis of more arbitrary geometry. The resulting simulation exploited the use of parallel computations by using two levels of parallelism, with extremely high efficiency.

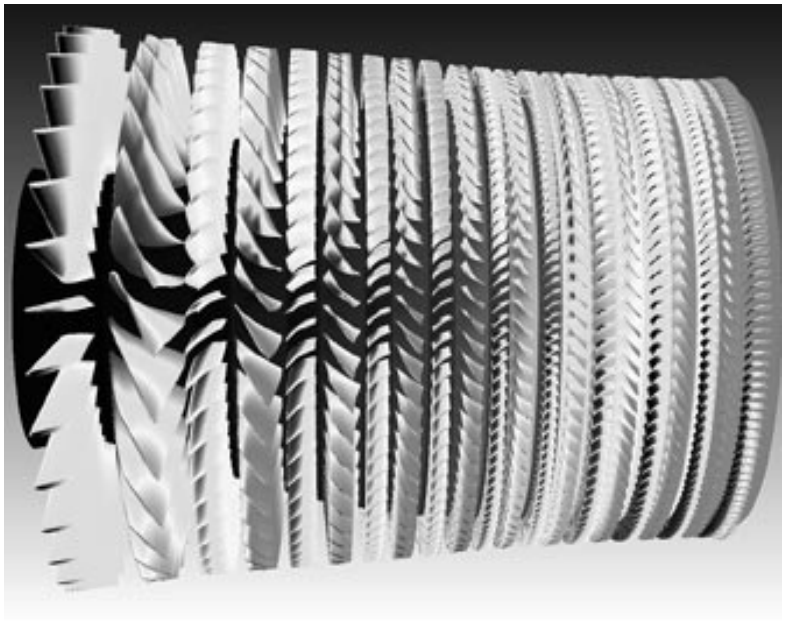

GE90 high-pressure compressor surface pressures. The figures are shown in color in the online version of this article (http://www.grc.nasa.gov/WWW/RT1998/2000/2900veres.htm).

The primary flow path of the GE90 turbofan consists of a nacelle and inlet, 49 blade rows of turbomachinery, and an exhaust nozzle. Secondary flows entering and exiting the primary flow path—such as bleed, purge, and cooling flows—were modeled macroscopically as source terms to accurately simulate the engine. The information on these source terms came from detailed descriptions of the cooling flow and from thermodynamic cycle system simulations. These provided boundary condition data to the three-dimensional analysis. A simplified combustor was used to feed boundary conditions to the turbomachinery. Flow simulations of the fan, high-pressure compressor, and high- and low-pressure turbines were completed with the APNASA code.

Two high-pressure compressors were modeled, the original and a new, improved design. The APNASA flow simulation of the new geometry predicted a significant performance improvement over the baseline design. APNASA has been further validated by these rig tests. The 128-processor SGI Origin at the NASA Ames Research Center was used to simulate the compression system, which comprises 31 blade rows, in 38 hours of elapsed time. The computer simulation time to convergence on the 18-blade-row, cooled, high- and low-pressure turbine simulation was 15 hours.

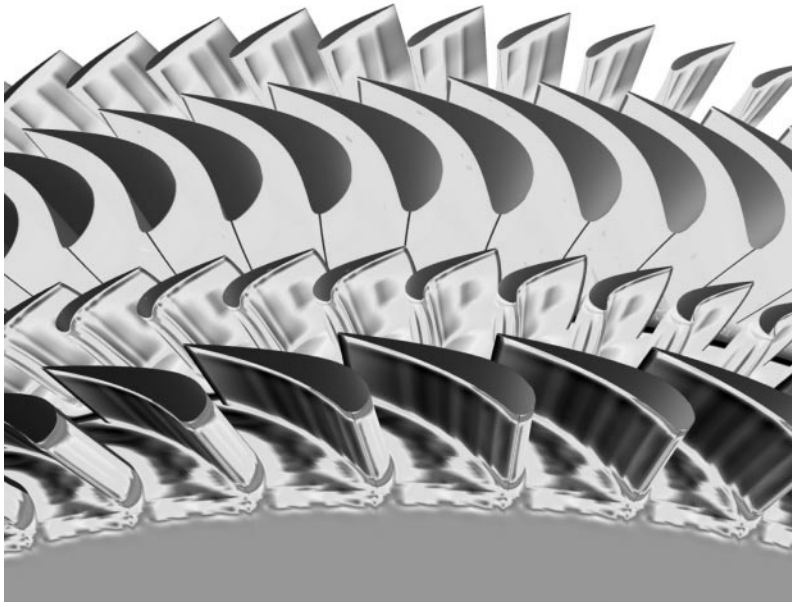

GE90 high-pressure cooled turbine flow simulation.

Because of its higher efficiency and reduced specific fuel consumption, the improved high-pressure compressor will significantly reduce the operating cost of the GE90 engine. The accurate predictive simulation capability of APNASA will increase design confidence in future versions of the baseline GE90 engine featuring higher levels of thrust. Increased design confidence will result in fewer test rigs and lower costs during development and certification.

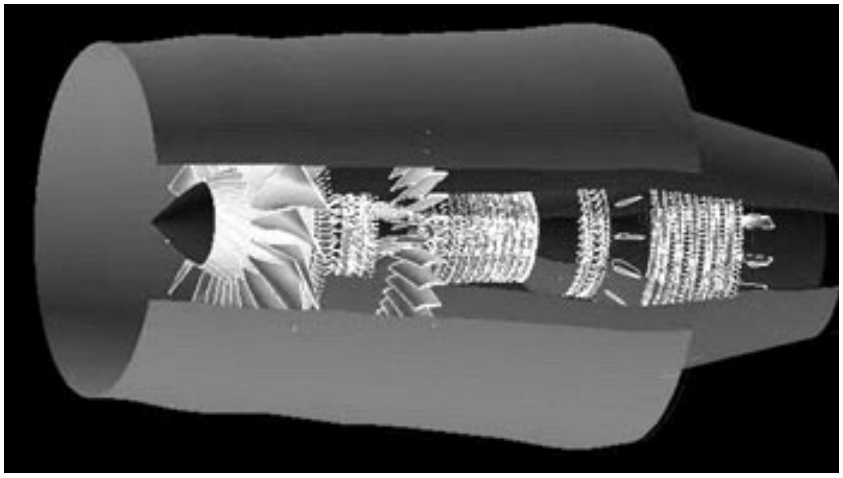

Full GE90 turbofan engine flow simulation (with simple combustor).

All the major engine components have been simulated with APNASA for 49 blade rows (see the final figure). This high-fidelity simulation will be used by GE to evaluate modifications for future versions of the GE90 to reduce derivative engine development time and cost. This work, which is a major element of the Numerical Propulsion System Simulation (NPSS), supports the High Performance Computing and Communication Program's (HPCCP) Grand Challenge milestone to "Demonstrate end-to-end reductions in cost and time to solution for aerospace propulsion design applications on heterogenous computing systems."

More information about this research is available on the World Wide Web:
http://hpcc/ge90/

Lewis contact:
Joseph P. Veres, (216) 433–2436,
Joseph.P.Veres@grc.nasa.gov

Author: Joseph P. Veres

Headquarters program office: OAT

Programs/Projects: HPCCP, NPSS

Research and Technology

Materials

$MoSi_2$-Base Structural Composite Passed Engine Test

The intermetallic compound molybdenum disilicide ($MoSi_2$) is an attractive high-temperature structural material for advanced engine applications. It has excellent oxidation resistance, a high melting point, relatively low density, and high thermal conductivity; and it is easily machined. Past research at the NASA Lewis Research Center has resulted in the development of a hybrid composite consisting of a $MoSi_2$ matrix reinforced with silicon nitride (Si_3N_4) particulate and silicon carbide (SiC) fibers. This composite has demonstrated attractive strength, toughness, thermal fatigue, and oxidation resistance, including resistance to "pest" oxidation. These properties attracted the interest of the Office of Naval Research and Pratt & Whitney, and a joint NASA/Navy/Pratt & Whitney effort was developed to continue to mature the $MoSi_2$ composite technology. A turbine blade outer air seal, which was part of the Integrated High Performance Turbine Engine Technology (IHPTET) program, was chosen as a first component on which to focus.

The first tasks of the materials development effort were to develop improved processing methods to reduce costs and to use fine-diameter fibers that enable the manufacturing of complex shapes. Tape-casting methods were developed to fully infiltrate the fine SiC fibers with matrix powders. The resulting composites were hot pressed to 100-percent density. Composites with cross-plied fiber architectures with 30 vol % Hi-Nicalon SiC fibers (Nippon Carbon Company, Japan) and 30 vol % nitride particles are now made routinely and demonstrate a good balance of properties.

The next task entailed the measurement of a wide variety of mechanical properties to confirm the suitability of this composite in engines. In particular, participants in this effort demonstrated that composites made with Hi-Nicalon fibers had strength and toughness properties equal to or better than those of the composites made with the large-diameter fibers that had been used previously. Another critically important property measured was impact resistance. Aircraft engine components require sufficient toughness to resist manufacturing defects, assembly damage, stress concentrations at notches, and foreign object damage. Engine company designers indicated that impact resistance would have to be measured before they would seriously consider these types of composites. The

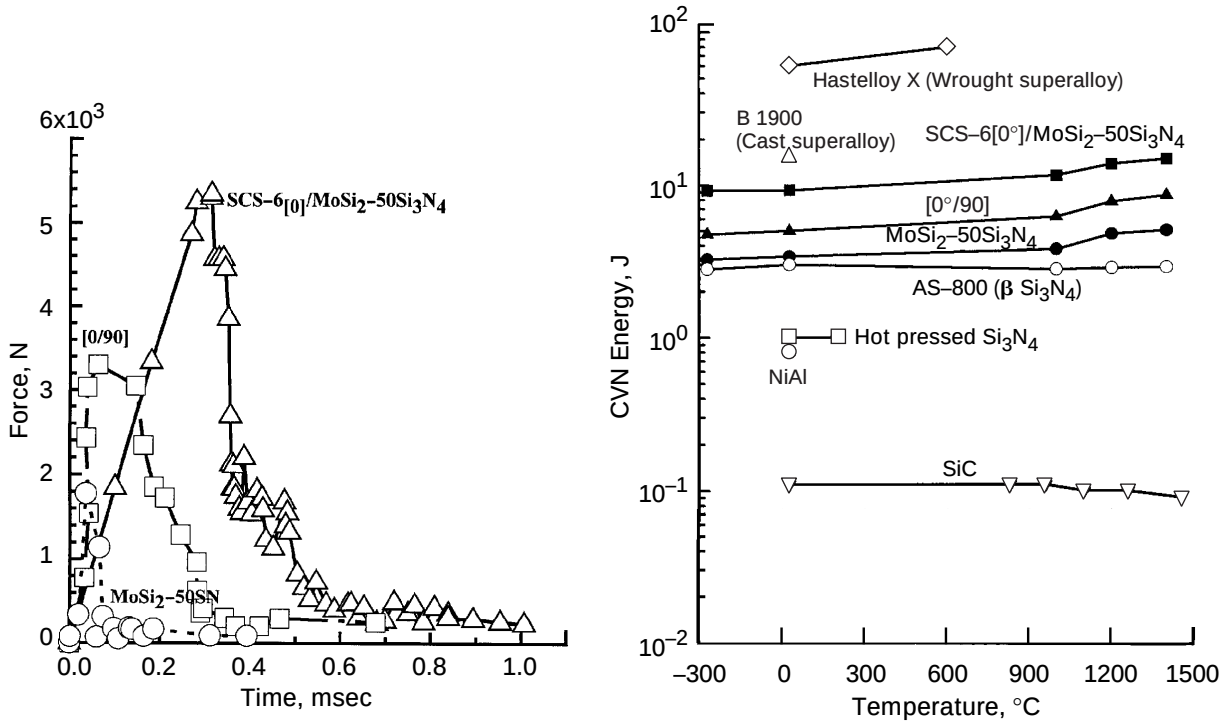

Charpy impact properties of $MoSi_2$ base composites compared with several competitive materials. Left: Force-time curves. Right: Charpy-V-Notch (CVN) energy plot.

Charpy V-Notch test was chosen to assess impact resistance, and both monolithic and composite versions of $MoSi_2$ were tested from –300 to 1400 °C. The results (see the preceding graphs) show that nitride-particulate-reinforced $MoSi_2$ exhibited impact resistance higher than that of many monolithic ceramics and intermetallics and that the fiber-reinforced composites had even higher values, approaching that of cast superalloys.

These and other results led to the decision to test the hybrid composite in the aggressive environment of a gas turbine engine. Test coupons were fabricated and tested in Pratt & Whitney's IHPTET XTC/66 demonstrator engine to simulate the thermal cycling conditions of a blade outer air seal. The composite was exposed to thermal cycles to 1200 °C, with a 600 °C gradient through the thickness of the coupon. It survived all 15 engine cycles without any appearance of distress (see the photomicrograph).

These results indicate that $MoSi_2$-base composites are still competitive with state-of-the-art ceramic composites as replacements for superalloys in jet engines. Further work on processing, fiber coatings, and mechanical and environmental durability is in progress.

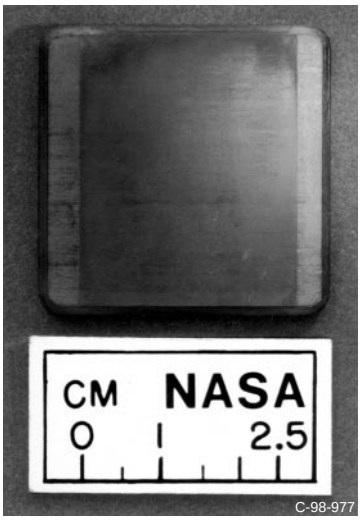

Hybrid composite coupon of $MoSi_2$/Si_3N_4 particulate/Hi-Nicalon SiC fiber after engine testing at Pratt & Whitney.

Bibliography

Hebsur, M.G; and Nathal, M.V.: Strong, Tough, and Pest Resistant $MoSi_2$-Base Hybrid Composite for Structural Applications. Structural Intermetallics 1997, M.V. Nathal, et al., eds., 1997, The Minerals, Metals and Materials Society, Warrandale, PA, pp. 949–958.

Lewis contacts:
Dr. Mohan G. Hebsur, (216) 433–3266, Mohan.G.Hebsur@grc.nasa.gov; and Dr. Michael V. Nathal, (216) 433–9516, Michael.V.Nathal@grc.nasa.gov

Office of Naval Research (ONR) contact:
Dr. A.K. Vasudevan, (703) 696–8181

Authors: Dr. Michael V. Nathal and Dr. Mohan G. Hebsur

Headquarters program office: OAT

Programs/Projects: P&PM

Deleterious Phase Formation in Next-Generation Nickel-Base Superalloys Predicted

Nickel- (Ni-) base superalloy single crystals represent the state-of-the-art for turbine engine airfoil applications because they offer the best balance of properties under the high operating temperatures required for efficient engine operation. Current trends in alloy design take advantage of improved creep rupture strength with the addition of higher levels of refractory elements. In particular, the addition of significantly higher levels of rhenium in third-generation superalloys is key for both microstructural stability and creep rupture strength. Although refractories provide strength benefits, alloys tend to be unstable when their refractory content is high because of topologically close-packed (TCP) phases. The formation of these phases in sufficient amount is detrimental to the performance of these alloys because of their brittle nature and because they deplete the Ni-rich matrix of potent solid-solution strengthening elements.

TCP phase formation in modern single-crystal superalloys is being investigated in-house at the NASA Lewis Research Center, where particular attention is being paid to the potential synergistic effects of alloying elements. The approach chosen in this investigation was to develop a model based on a design-of-experiments methodology. A design of experiments consisting of 44 alloys was set up to quantify both the linear and pairwise interactive effects of aluminum (Al), cobalt (Co), chromium (Cr), molybdenum (Mo), rhenium (Re), tantalum (Ta), and tungsten (W) in a third-generation Ni-base superalloy according to the resultant amount of TCP phase in the microstructure.

All alloys were produced by vacuum induction melting and were cast using high-purity melting stock. This was followed by a homogenization heat treatment and a simulated long–duration engine exposure.

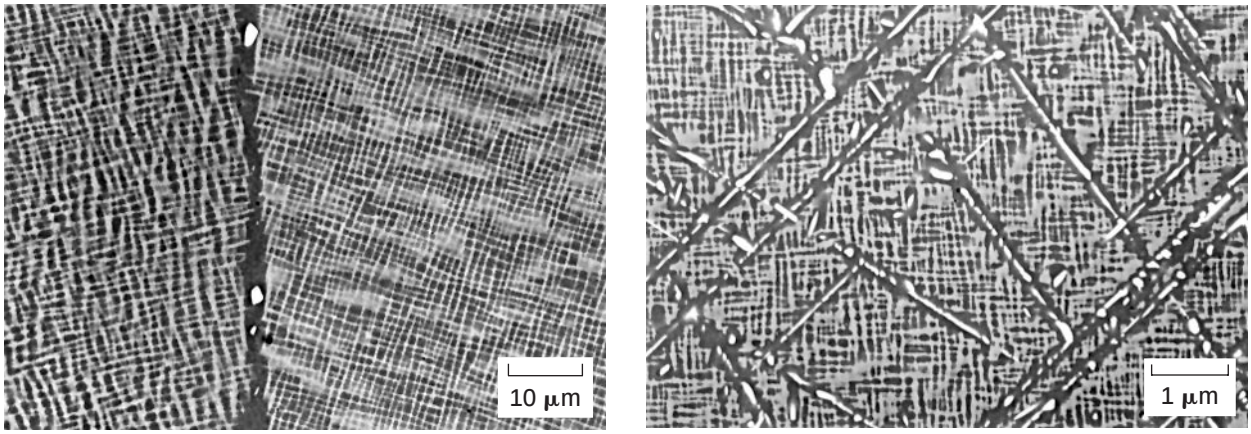

Third-generation, Ni-base, superalloy aged microstructures. Left: Group 2. Right: Group 3.

After alloys were aged at 1093 °C for 400 hours, an examination of all microstructures showed that the alloys fell into three groups on the basis of the TCP distribution. Group 1 alloys contained no TCP phase. Group 2 contained less than 3 vol % TCP, which formed exclusively at the grain boundaries. Group 3 contained between 3 and 17 vol % TCP, which formed within grains as well as at grain boundaries.

A regression model was developed to describe the presence of TCP phase in the microstructures of a polycrystalline third-generation superalloy on the basis of chemical content. The result of this analysis, in terms of atomic percent, follows:

$$
\begin{aligned}
(\text{vol \% TCP})^{1/2} = {} & 16.344782 - 1.019587(\text{Al}) - 2.624322(\text{Cr}) \\
& - 3.821997(\text{Mo}) + 1.109575(\text{Re}) - 3.207295(\text{Ta}) \\
& + 6.462984(\text{W}) - 2.271803(\text{Co}) + 0.052884(\text{Al})(\text{Co}) \\
& + 0.214059(\text{Al})(\text{Cr}) + 0.300698(\text{Al})(\text{Mo}) \\
& + 0.80011(\text{Co})(\text{Re}) + 0.257108(\text{Cr})(\text{Mo}) \\
& - 5.081598(\text{Re})(\text{W}) + 1.824441(\text{Ta})(\text{W})
\end{aligned}
$$

This relationship has been shown to explain 95 percent of the TCP variations seen in the experiments. It is also useful for identifying principal elemental effects as well as interactive effects toward TCP phase instability and for providing insight for stable alloy development. Additional efforts are underway to further refine these results.

Bibliography

Ritzert, F., et al.: The Effect of Alloying on Topologically Close Packed Phase Instability in Advanced Nickel-Based Superalloy Rene N6. NASA TM—1998-206622, 1998.

Lewis contact:
Frank J. Ritzert, (216) 433–8199, Frank.J.Ritzert@grc.nasa.gov

Author: Frank J. Ritzert

Headquarters program office: OAT

Programs/Projects: HITEMP

Affordable Manufacturing Technologies Being Developed for Actively Cooled Ceramic Components

Efforts to improve the performance of modern gas turbine engines have imposed increasing service temperature demands on structural materials. Through active cooling, the useful temperature range of nickel-base superalloys in current gas turbine engines has been extended, but the margin for further improvement appears modest. Because of their low density, high-temperature strength, and high thermal conductivity, in situ toughened silicon nitride ceramics have received a great deal of attention for cooled structures. However, high processing costs have proven to be a major obstacle to their widespread application. Advanced rapid prototyping technology, which is developing rapidly, offers the possibility of an affordable manufacturing approach.

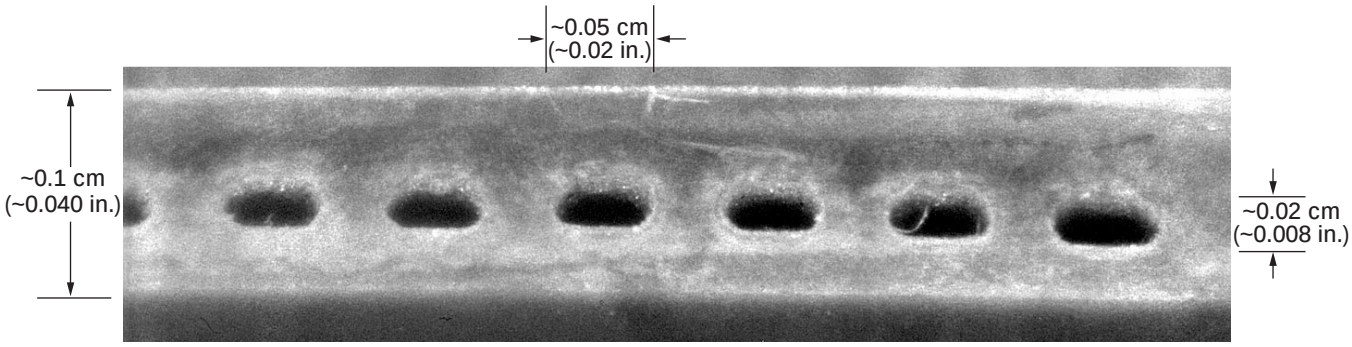

Silicon nitride (Si_3N_4) plate with cooling holes.

Researchers at the NASA Lewis Research Center, in cooperation with a local university and industry, are developing actively cooled and functionally graded ceramic structures. The objective of this program is to develop a cost-effective manufacturing technology and the analytical modeling capability to predict thermomechanical stresses in burner rig tests of thermal-barrier-coated, actively cooled, in situ toughened silicon nitride turbine nozzle vanes under simulated engine conditions. In the initial studies, green and sintered bodies of silicon nitride plates with cooling holes were successfully fabricated through the use of a Sanders prototype molding machine for mold detail fabrication, ceramic gel casting, and conventional sintering techniques. A two-dimensional analytical model was developed to optimize the cooling hole geometry and spacing, and to reduce thermal stresses.

Lewis contact: Dr. Ramakrishna T. Bhatt, (216) 433–5513, Ramakrishna.T.Bhatt@grc.nasa.gov

Author: Dr. Ramakrishna T. Bhatt

Headquarters program office: OAT

Programs/Projects: HITEMP

Sensor Lead Wires Positioned on SiC-Based Monolithic Ceramic and Fiber-Reinforced Ceramic Matrix Composite Subcomponents With Flat and Curved Surfaces

There is strong interest in the development of silicon carbide-based monolithic ceramic and composite materials and components for demanding, high-temperature applications. Thorough characterization of material properties, including high-temperature testing under simulated or actual operating conditions, is a high priority for programs involved in developing these silicon carbide- (SiC) based materials and components.

Members of the Sensors and Electronics Technology Branch at the NASA Lewis Research Center are developing minimally intrusive methods of measuring the properties (such as the surface temperature, strain, and heat flux characteristics) of components and subelements that are being tested or operated in hostile, high-temperature environments. Their primary goal is to instrument the test article or operating component with durable sensors that have a minimal effect on test conditions such as the gas flow across the surface of the item and the material response (including the through-thickness conduction of heat). Therefore, the main thrust of their work has been the development of thin-film sensors (e.g., thermocouples or strain gauges) for use on various advanced material test articles, including SiC/SiC composite components.

There was a need for a better method of securing sensor lead wires on SiC-based components and subelements that would be tested at temperatures to 1000 °C (or higher), to enhance the durability of the overall minimally intrusive sensor system. To address this need, Lewis researchers devised an alternative approach for positioning the sensor lead wires (which are connected to the thin-film sensors) on SiC or SiC/SiC components. A reaction-forming method of joining was used to strongly bond hoop-shaped monolithic SiC and SiC/SiC composite attachments of various sizes to both flat and curved surfaces of SiC/SiC composite

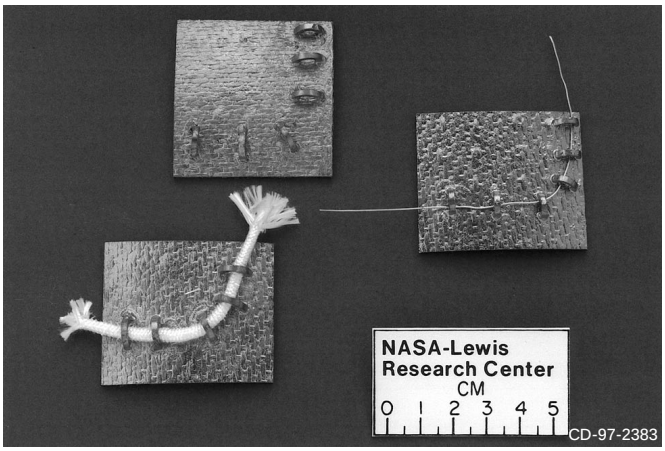

SiC hoops joined to SiC/SiC composite panels. These attachments are used to position and secure sensor lead wires.

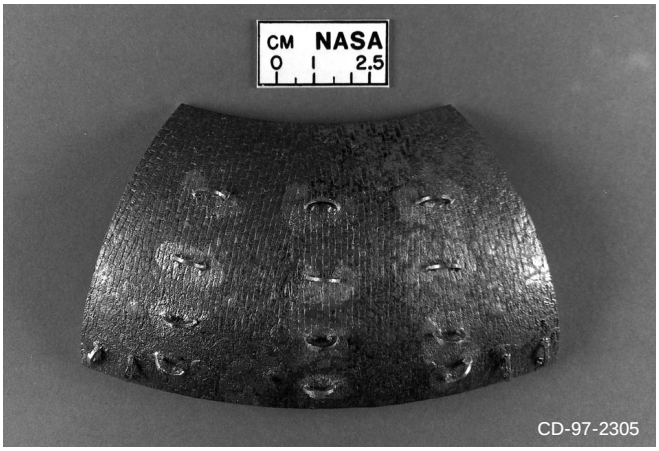

SiC hoops successfully attached (via reaction joining) to a SiC/SiC composite subelement having a curved surface.

subelements (see the photos). This approach is based on an affordable, robust ceramic joining technology, named ARCJoinT, which was developed at Lewis for the joining of SiC-based ceramics and fiber-reinforced composites.

The ability to join these attachments to a curved surface is important because many SiC/SiC components that need to be tested have some curved surfaces. The use of thin attachment hoops having a radius slightly larger than the diameter of the sensor lead wire cable should (1) prevent the wires from moving, which reduces the risk of sensor failure, (2) minimize the disruption of high-velocity combustion or cooling gas flow, and (3) minimize the influence of the attachments on component performance during testing under simulated engine conditions because the hoops have minimal contact with the test article. On the basis of results obtained in previous joining studies, the joined attachments should maintain their integrity at temperatures up to 1350 °C in air. Preliminary testing under static high-temperature conditions has yielded positive results.

The projected excellent high-temperature strength of the joined attachments should make it possible to obtain better sensor durability than has previously been achieved by using refractory, adhesive cement to secure lead wire assemblies. This novel approach is being evaluated further through burner rig testing of instrumented panels to determine the potential for obtaining enhanced durability, minimally intrusive, high-temperature sensor systems. The technology apparently could also be used to reinstall attachments on ceramic components that have been damaged in service.

For more information, visit Lewis on the World Wide Web:

Ceramics Branch: http://www.grc.nasa.gov/WWW/Ceramics/

Sensors and Electronics Technology Branch: http://www.grc.nasa.gov/WWW/sensors/

Lewis contacts:
James D. Kiser, (216) 433–3247, James.D.Kiser@grc.nasa.gov;
Dr. Jih-Fen Lei, (216) 433–3922, Jih-Fen.Lei@grc.nasa.gov; and
Lisa C. Martin, (216) 433–6468, Lisa.C.Martin@grc.nasa.gov

Dynacs Engineering Co., Inc. contact:
Dr. Mrityunjay Singh, (216) 433–8883, Mrityunjay.Singh@grc.nasa.gov

Authors:
James D. Kiser, Dr. Mrityunjay Singh, Dr. Jih-Fen Lei, and Lisa C. Martin

Headquarters program office: OAT

Programs/Projects: HITEMP, EPM

Modal Acoustic Emission Used at Elevated Temperatures to Detect Damage and Failure Location in Ceramic Matrix Composites

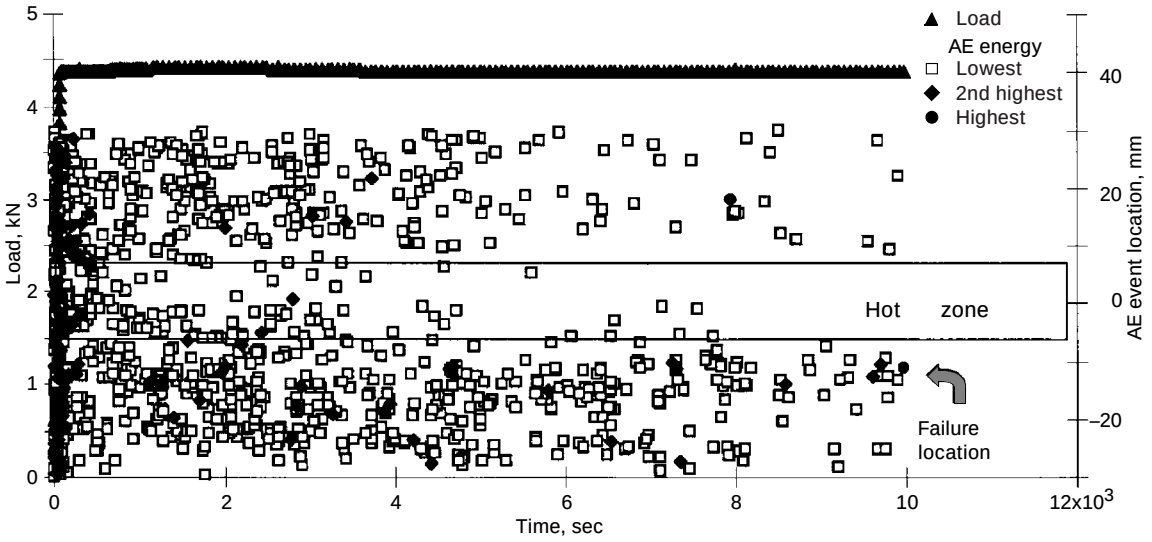

Acoustic emission (AE) event location and load versus time for stress-rupture experiment performed in air at 960 °C.

Ceramic matrix composites are being developed for elevated-temperature engine applications. A leading material system in this class of materials is silicon carbide (SiC) fiber-reinforced SiC matrix composites. Unfortunately, the nonoxide fibers, matrix, and interphase (boron nitride in this system) can react with oxygen or water vapor in the atmosphere, leading to strength degradation of the composite at elevated temperatures. For this study, constant-load stress-rupture tests were performed in air at temperatures ranging from 815 to 960 °C until failure. From these data, predictions can be made for the useful life of such composites under similar stressed-oxidation conditions.

During these experiments, the sounds of failure events (matrix cracking and fiber breaking) were monitored with a modal acoustic emission (AE) analyzer through transducers that were attached at the ends of the tensile bars. Such failure events, which are caused by applied stress and oxidation reactions, cause these composites to fail prematurely. Because of the nature of acoustic waveform propagation in thin tensile bars, the location of individual source events and the eventual failure event could be detected accurately.

The graph shows the load versus time and the AE event location versus time for an experiment performed at 960 °C. The AE events are plotted according to their respective energies; that is, the highest energy events are the loudest events and correspond to large matrix cracks. Also noted on this figure is the location of the hot zone, which is a 15-mm region of the furnace that is at 960 °C. Outside of this region the temperature decreases. It is evident that after a few thousand seconds very little activity occurs in the hot zone. However, just outside the hot zone, a significant amount of AE activity occurs, with eventual composite failure occurring at about 880 °C. For experiments performed at 815 °C, the failure location is always in the hot zone. Because at ~800 to 900 °C chemical reactions between the interphase and environment reduce the load-carrying ability of the reinforcing fibers, this constitutes the “pest” temperature regime for this material.

Modal AE accurately located the failure location of the composite. In addition, it detected a number of loud AE events in the same relative failure location prior to failure. Since eventual failure of these composites occurs at a specific location after a progression of smaller matrix cracks and fiber failures which weaken that area of the composite, this type of monitoring can be used to actually predict the location of composite failure.

Lewis contact:
Gregory N. Morscher, (216) 433–5512
Gregory.N.Morscher@grc.nasa.gov

Author: Gregory N. Morscher

Headquarters program office: OAT

Programs/Projects: HITEMP

High-Temperature Solid Lubricants Developed by NASA Lewis Offer Virtually “Unlimited Life” for Oil-Free Turbomachinery

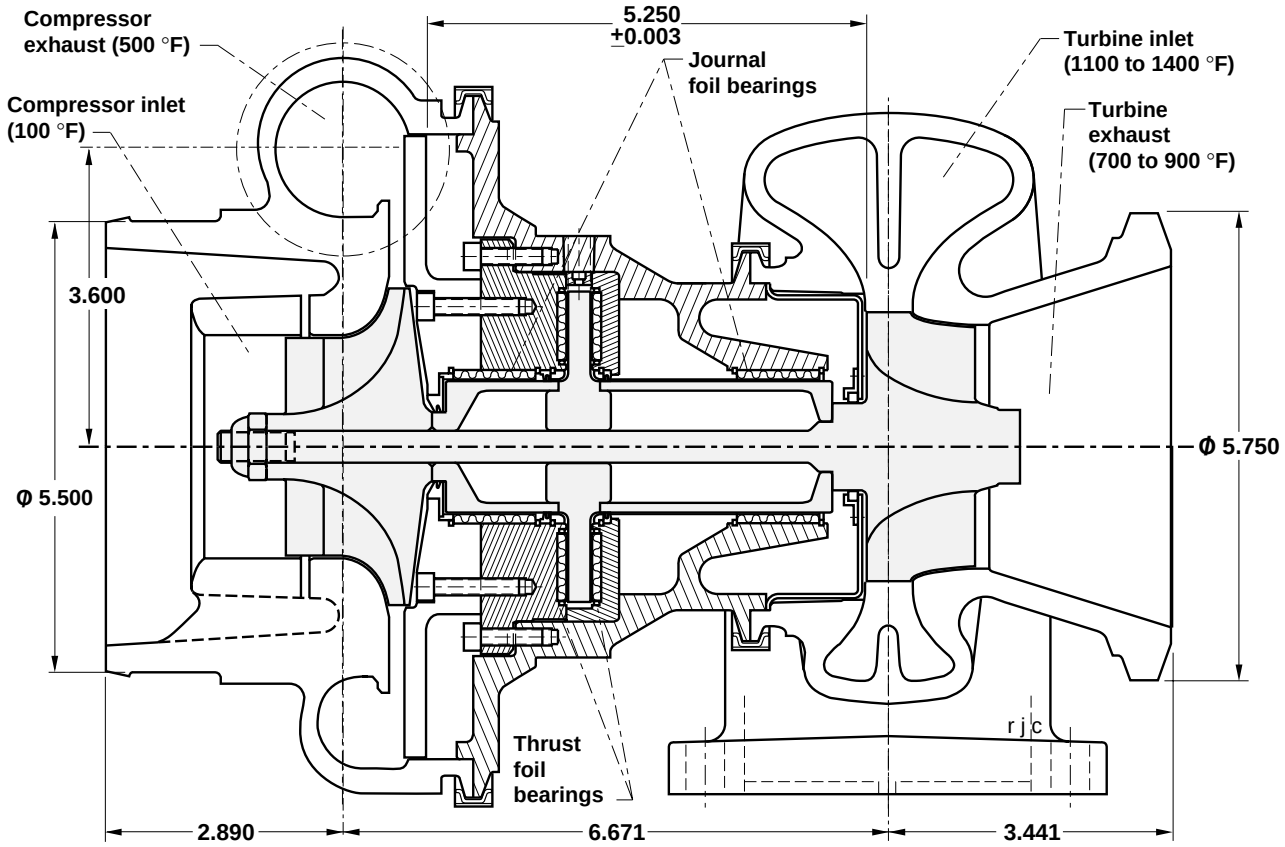

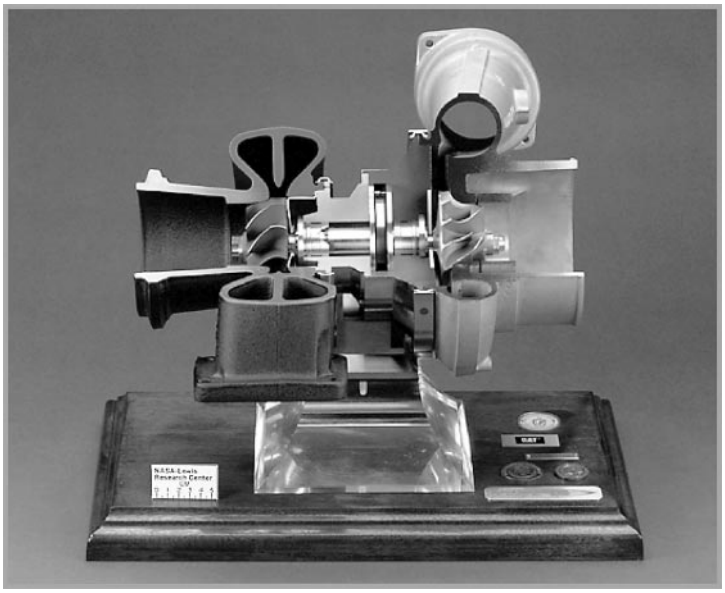

PS304-coated bearing after 100 000 cycles at 1000 °F. This oil-free turbocharger features two journal foil bearings, two thrust foil bearings, a NASA PS304 coating, and a rigid rotor. All dimensions are in inches.

The NASA Lewis Research Center is capitalizing on breakthroughs in foil air bearing performance, tribological coatings, and computer analyses to formulate the Oil-free Turbomachinery Program. The program's long-term goal is to develop an innovative, yet practical, oil-free aeropropulsion gas turbine engine that floats on advanced air bearings. This type of engine would operate at higher speeds and temperatures with lower weight and friction than conventional oil-lubricated engines. During startup and shutdown, solid lubricant coatings are required to prevent wear in such engines before the self-generating air-lubrication film develops.

NASA's Tribology Branch has created PS304, a chrome-oxide-based plasma spray coating specifically tailored for shafts run against foil bearings. PS304 contains silver and barium fluoride/calcium fluoride eutectic (BaF_2/CaF_2) lubricant additives that, together, provide lubrication from cold start temperatures to over 650 °C, the maximum use temperature for foil bearings. Recent lab tests show that bearings lubricated with PS304 survive over 100 000 start-stop cycles without experiencing any degradation in performance due to wear. The accompanying photograph shows a test bearing after it was run at 650 °C. The rubbing process created a "polished" surface that enhances bearing load capacity.

This type of bearing performance suggests virtually unlimited life for foil-bearing-supported, oil-free turbomachinery. By adapting these technologies, future aeropropulsion engines can run more efficiently and be maintenance free as well as oil free.

Lewis contacts: Dr. Christopher DellaCorte, (216) 433–6056, Christopher.DellaCorte@grc.nasa.gov; and Dr. Mark J. Valco, (216) 433–3717, Mark.J.Valco@grc.nasa.gov

Authors: Dr. Christopher DellaCorte and Dr. Mark J. Valco

Headquarters program office: OAT

Programs/Projects: P&PM, SGE

Special recognition:
A patent will be issued on this coating technology in January 1999.

New Vapor/Mist Phase Lubricant Formulated

To meet the increased thermal stresses of future advanced aircraft engines, new lubricants will have to be developed to replace the currently used ester-based liquid lubricants. If a suitable conventional replacement cannot be found, a different lubrication method will have to be used. The conventional method circulates bulk lubricant (stored in a sump) through a lubricating system containing cooling and filtering elements. Solid lubricants have been studied as a replacement for bulk liquid lubricants, and have been found to provide reasonable lubrication for lightly loaded systems. Solid lubricants, however, have proved inadequate for highly loaded, high-speed applications. Vapor/mist phase lubrication (VMPL), on the other hand, may be a viable alternative.

VMPL has been used successfully to lubricate high-temperature bearings or gears. It can be used as an emergency backup system or as the primary source of lubrication. With VMPL, minimal weight is added to the system and minimal debris is formed. It works over a wide temperature range. The concept is illustrated in the following figure.

The basis for the VMPL method stems from the idea that a "suitable" organic vapor or fine mist can react inside high-temperature sliding surfaces to form a lubricious film. The primary compounds used for VMPL studies have been organophosphates, which work well with only certain ferrous material. Their success is due to an initial, rapid formation of a predominant iron phosphate film, which is followed by the formation and growth (by cationic diffusion) of a lubricious pyrophosphate-type coating over the iron phosphate. As long as iron is present at a wearing surface,

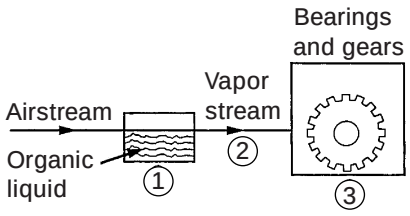

① A small quantity of an organic liquid is vaporized into the airstream (liquid in air, <1 wt%).

② The vapor steam is delivered to the bearings and gears.

③ A lubricating polymeric film is deposited at the wearing surfaces.

Vapor/mist phase lubrication method.

the VMPL method using organophosphates works well. Evidence, however, has been reported that continued organophosphate interaction with ferrous bearing material can lead to depletion of surface iron and to eventual lubrication failure. If VMPL is to work for prolonged periods of time, the depletion of surface iron must be circumvented.

Work at the NASA Lewis Research Center has resulted in a new organophosphate formulation that prevents surface iron depletion. This new formulation incorporates a soluble iron additive that reacts with the organophosphate to generate an iron phosphate film. This formulation was used to successfully vapor/mist phase lubricate a spur gearbox in a preliminary study. In a related study, this formulation was used to lubricate a silicon nitride pin-on-plate couple that used a reciprocating friction and wear apparatus at 500 °C.

Lewis contact:
Dr. Wilfredo Morales, (216) 433–6052, Wilfredo.Morales@grc.nasa.gov

Authors:
Dr. Wilfredo Morales and
Dr. Robert F. Handschuh

Headquarters program office: OAT

Programs/Projects: P&PM

Special recognition: A special achievement award was given for this work, and a patent was issued.

Monte Carlo Simulation of Alloy Design Techniques: Fracture and Welding Studied Using the BFS Method for Alloys

Large-scale simulations of dynamic processes at the atomic level have developed into one of the main areas of work in computational materials science. Until recently, severe computational restrictions, as well as the lack of accurate methods for calculating the energetics, resulted in slower growth in the area than that required by current alloy design programs.

The Computational Materials Group at the NASA Lewis Research Center is devoted to the development of powerful, accurate, economical tools to aid in alloy design. These include the BFS (Bozzolo, Ferrante, and Smith) method for alloys (ref. 1) and the development of dedicated software for large-scale simulations based on Monte Carlo-Metropolis numerical techniques, as well as state-of-the-art visualization methods. Our previous effort linking theoretical and computational modeling resulted in the successful prediction of the microstructure of a five-element intermetallic alloy, in excellent agreement with experimental results (refs. 2 and 3). This effort also produced a complete description of the role of alloying additions in intermetallic binary, ternary, and higher order alloys (ref. 4).

A natural continuation of this work includes dynamic processes. Preliminary results from Monte Carlo-Metropolis minimization techniques used in conjunction with the BFS method for calculating the energetics, show a promising and viable way to gain insight into the microscopic evolution of intermetallic fracture, as shown in the illustration on the facing page. In this example, a nickel-aluminide- (NiAl) ordered alloy in the B2 phase is uniformly stretched until the computational cell develops cracks, which ultimately lead to the sample's fracture. Beyond this point, the surfaces created during this process reconstruct, showing a strong preference for mixed-composition termination, as is to be expected. This Monte Carlo approach allows for individual atomic relaxations (which were exaggerated in the illustration for visualization purposes).

The final illustration shows a temperature-dependent process where the computational cell is divided in two halves with an intermediate copper (Cu) layer, in what amounts to the first simulation of the brazing process. In this example, the temperature is raised steadily in small increments that allow the sample to stabilize at each step. The Monte Carlo-Metropolis approach used in this example allows only for atomic exchanges between nearest neighbors, thus showing the increasing interdiffusion of Cu in the NiAl matrix as the temperature increases beyond the melting temperature of Cu.

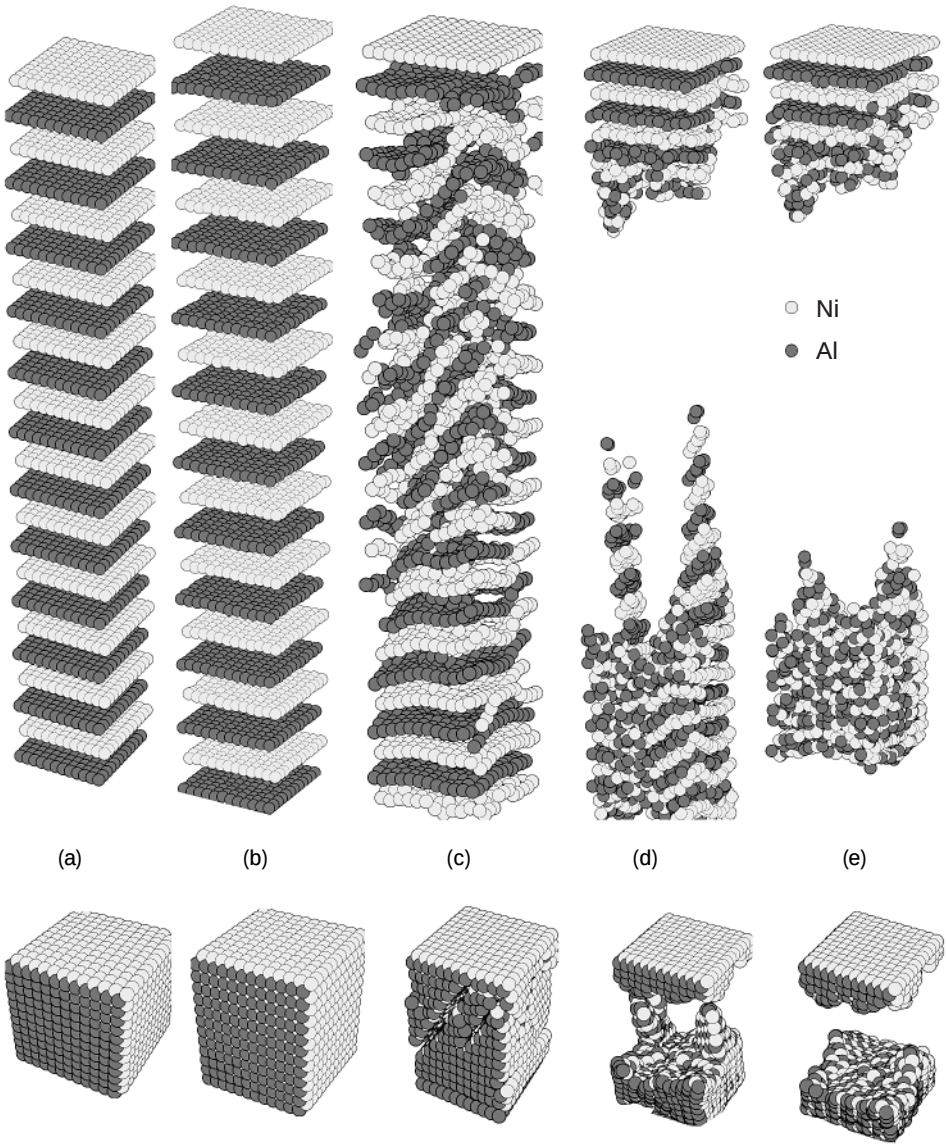

Onset of fracture for NiAl for various states of the computational cell. Ni and Al atoms are denoted with lighter and darker spheres, respectively. (This figure is shown in color in the online version of this article: http://www.grc.nasa.gov/WWW/RT1998/5000/5140noebe.htm.) (a) Beginning of the simulation. (b) After uniaxial strain, just before the onset of fracture. (c) Just after the onset of fracture. (d) During relaxation of the newly formed fracture surfaces. (e) After fracture relaxation is essentially complete.

Although Monte Carlo numerical techniques allow for a detailed visualization of the simulated process, the main advantage of this type of analysis is that it helps researchers to understand the underlying features that drive these processes. Because of the simplicity of the BFS method for the energetics used in these calculations, a detailed atom-by-atom analysis can be performed at any point in the simulation, providing necessary insight into the details of the process.

A main objective of this research program is to make the calculations as simple as possible. By reducing computational effort without losing physical accuracy, we expect that powerful simulation tools will be developed in the immediate future which will allow material scientists to easily visualize and analyze processes at a level not achievable experimentally.

References

1. Bozzolo, G.; Ferrante, J.; and Kobistek, R.: Modelling of Surfaces. J. Comput.-Aided Mater. Des., vol. 1, no. 3, 1994, pp. 305–324.

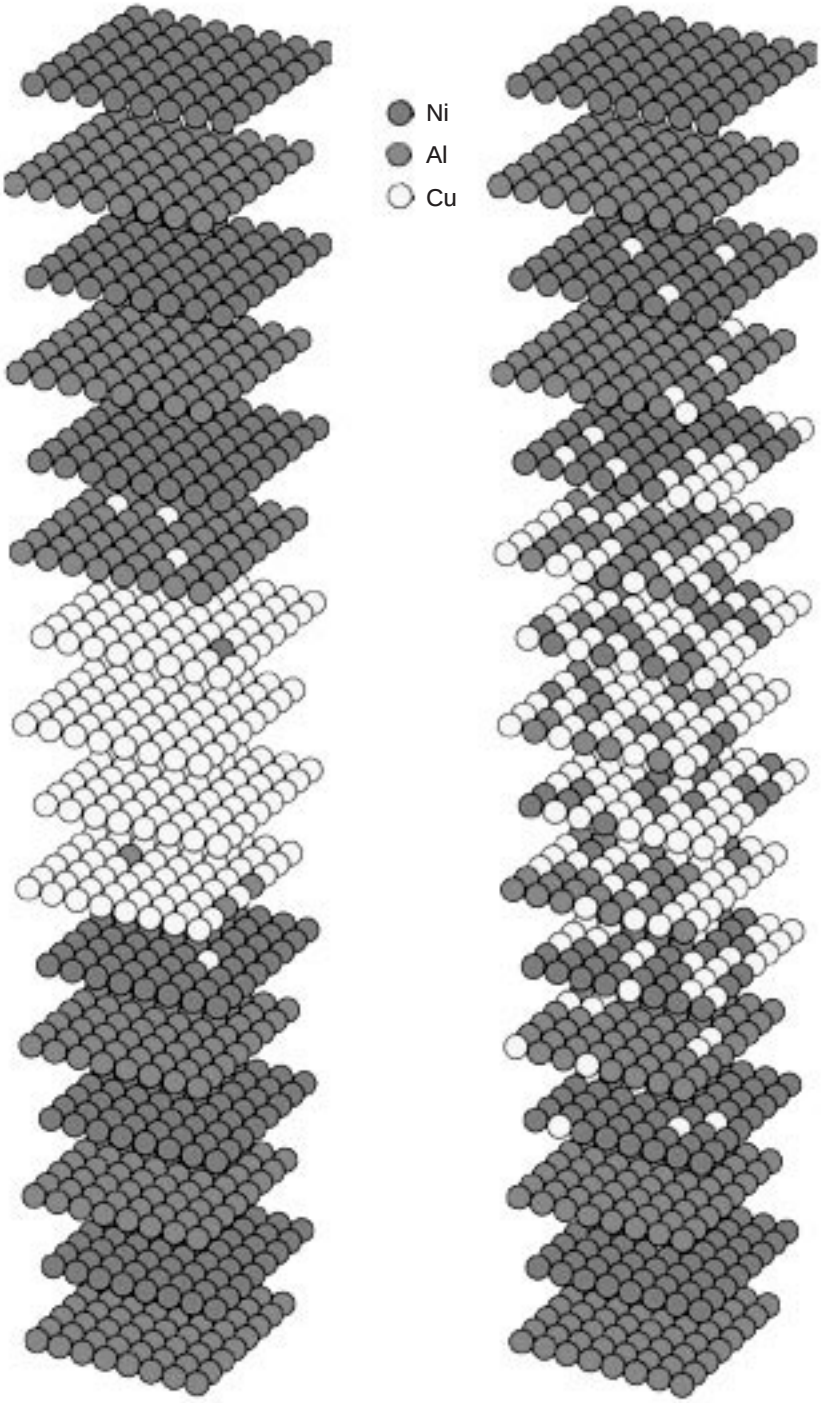

(a) (b)

NiAl + Cu computational cell. Ni, Al, and Cu atoms are denoted with medium, dark, and light spheres, respectively. (This figure is shown in color in the online version of this article: http://www.grc.nasa.gov/WWW/RT1998/5000/5140noebe.htm.) (a) Original cell, with four atomic layers of Cu between two identical NiAl cells. (b) After stabilization at 1400 °F.

2. Bozzolo, G., et al.: Progress in the Modelling of NiAl-Based Alloys Using the BFS Method. Structural Intermetallics 1997, M.V. Nathal, et al., eds., The Minerals, Metals and Materials Society, Warrendale, PA, 1997, pp. 655–664.

3. Noebe, R.D.: Research & Technology 1996. BFS Method for Alloys Optimized and Verified for the Study of Ordered Intermetallic Material. NASA TM–107350, 1997, pp. 49–50. (Available online: http:/www.grc.nasa.gov/WWW/RT1996/5000/5120b.htm)

4. Bozzolo, G.; Noebe, R.D.; and Honecy, F.: Modeling of Substitutional Site Preference in Ordered Intermetallic Alloys. The Minerals, Metals and Materials Society, Warrendale, PA, 1998, pp. 341–368.

Lewis contact:
Ronald D. Noebe, (216) 433–2093, Ronald.D.Noebe@grc.nasa.gov

Ohio Aerospace Institute contact:
Guillermo Bozzolo, Ohio Aerospace Institute, (440) 962–3103, Guillermo.H.Bozzolo@grc.nasa.gov

Authors:
Guillermo Bozzolo, Brian Good, Ronald D. Noebe, Frank Honecy, and Phillip Abel

Headquarters program office: OAT

Programs/Projects: HITEMP, P&PM

Low-Cost, High Glass-Transition Temperature, Thermosetting Polyimide Developed

PMR–15 polyimide, developed in the mid-1970's at the NASA Lewis Research Center, is recognized as a state-of-the-art high-temperature resin for composite applications in the temperature range of 500 to 550 °F (260 to 288 °C). PMR–15 offers easy processing and good property retention at a reasonable cost. For these reasons, it is widely used in both military and commercial aircraft engine components. Traditionally, polyimide composites have been designed for long-term use at 500 to 600 °F over thousands of hours. However, new applications in reusable launch vehicles (RLV's) require lightweight materials that can perform for short times (tens of hours) at temperatures between 800 and 1000 °F (425 and 538 °C). Current efforts at Lewis are focused on raising the use temperature of polyimide composites by increasing the glass-transition temperature of the matrix resins. Achieving this dramatic increase in the upper use temperature without sacrificing polymer and composite processability is a major technical challenge.

A recent development from these efforts is a low-cost, high glass-transition temperature, thermosetting polyimide (DMBZ–15), prepared from 3,3',4,4'-benzophenonetetracarboxylic acid dimethyl ester (BTDE) and 2,2'-dimethylbenzidine (DMBZ) with nadic ester as the endcap. The glass-transition temperature of a DMBZ–15 polyimide/T650–35 carbon fiber composite (414 °C) is much higher than that of the corresponding PMR–15 composite (348 °C). DMBZ–15 polyimide-based composites exhibit good compressive strengths at room and elevated temperatures (233 and 288 °C), as well as good hot/wet compressive strength. (See the left figure, where one hot/wet cycle consists of a 93 °C (200 °F) water soak to a gain of >1 wt %, followed by a dry out at 288 °C (500 °F) to <0.1 wt % moisture.) In addition, flexural strengths of PMR–15 and DMBZ–15 composites measured at room temperature, 288 °C, and 538 °C are comparable (see the right figure). These materials, along with other high-performance fiber-reinforced polymer matrix composites are currently being evaluated in Lewis/industry/university/Government cooperative efforts for potential use in reusable launch vehicles (RLV's) and other space vehicles.

Lewis contact:
Dr. Kathy C. Chuang, (216) 433–3227, Kathy.Chuang@grc.nasa.gov

Author: Dr. Kathy C. Chuang

Headquarters program office: OAT

Programs/Projects: HITEMP, RLV, AST

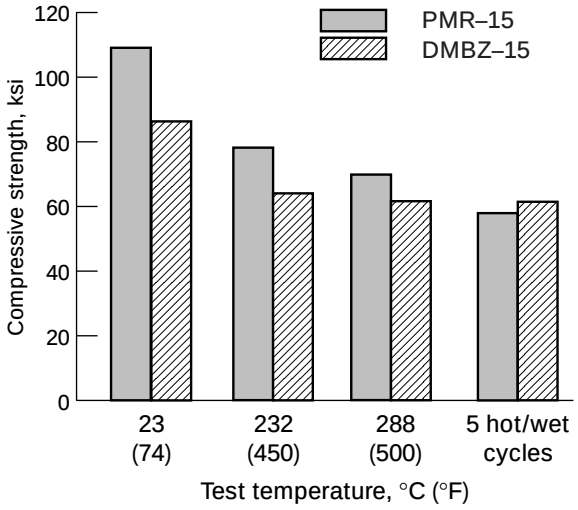

Compressive strength of polyimide/T650–35 composities.

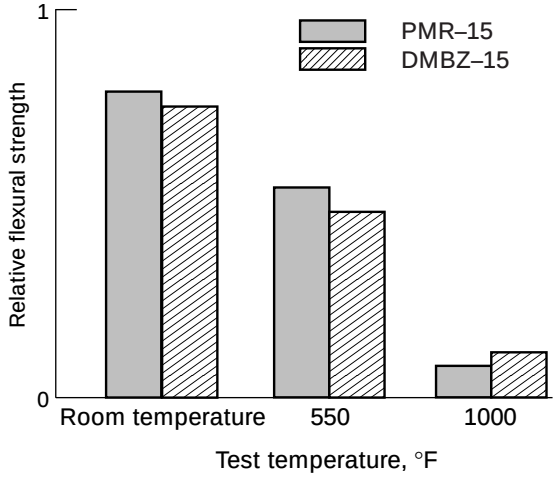

Flexure strength of DMBZ–15 and PMR–15 composites.

Novel Ultraviolet-Light-Curable Polyimides

Polyimides have found broad application in fiber-reinforced composites for aerospace components and as thin films for electronics packaging. Typical routes to processing these materials require temperatures above 200 °C. As a result, tooling costs for fabricating components from these composites can be quite high. Recent efforts within the Polymers Branch at the NASA Lewis Research Center have been aimed at developing radiation-curable (with light or electron beams) polyimides. Such materials may enable the processing of polymers and composites at or near room temperature, leading to reduced tooling requirements and costs.

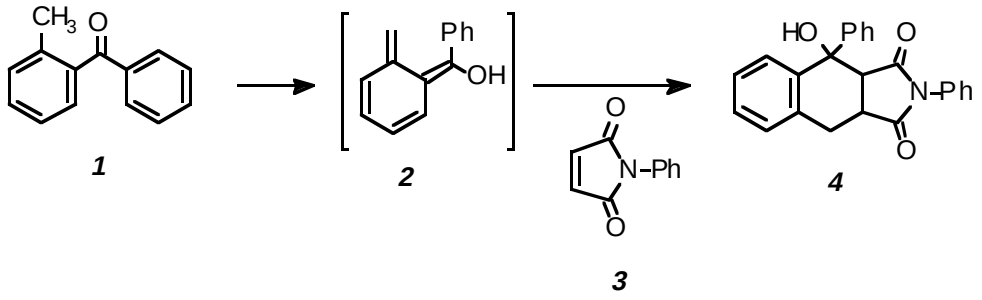

*Generation and trapping of photoenol, **2,** from o-methylbenzophenone, **1**.*

A new Diels-Alder route to polyimides has been developed that employs ultraviolet light (UV), rather than heat, to effect polymerization. This approach, which can be carried out at room temperature, is based on a well-known photochemical reaction—the photoenolization of *o*-methylphenyl ketones. Irradiation of *o*-methylphenyl ketones, such as ***1*** in the preceding figure, with UV wavelengths above 300 nm produces a photoenol, ***2***. This photoenol is unstable, but it persists long enough to undergo Diels-Alder reactions with good dienophiles, such as maleimide, ***3***. By utilizing a diketone, such as 2,5-dibenzoyl-*p*-xylene, ***5***, and a bismalemide, ***6***, this chemistry has been used to make a number of polyimides, ***7*** (see the figure on the following page).

These polyimides have glass-transition temperatures as high as 300 °C and have modest stabilities in both air and nitrogen. Onsets of decomposition, measured by thermal gravimetric analysis, were as high as 400 °C in air and 450 °C in nitrogen. Higher glass-transition temperatures and onsets of decomposition can be obtained by conversion of polyimide ***7*** into polyimide ***8*** through acid-catalyzed dehydration followed by dehydrogenation (as shown in the second figure). These polyimides have glass-transition temperatures as high as 330 °C and onsets of decomposition as high as 550 °C in air and 525 °C in nitrogen.

This chemistry has been demonstrated in solution (benzene or cyclohexanone). However, it should be easily adapted to achieve solid-state (solvent-free) curing, making it well-suited for thin-film applications (coatings, electronics packaging, and photonic and optical materials).

This new UV curing process could offer several advantages over other methods of preparing polyimides. UV-cured films should undergo less shrinkage during cure than thermally cured films. UV curing would also be useful for processing polyimides containing thermally sensitive groups or additives, such as photonic materials. Current efforts are aimed at modifying this chemistry to enable electron-beam curing of polyimides and polyimide-based composites for aeropropulsion and reusable launch vehicle applications.

Lewis contact: Dr. Michael A. Meador, (216) 433–9518, Michael.A.Meador@grc.nasa.gov

Author: Dr. Michael A. Meador

Headquarters program office: OAT

Programs/Projects: P&PM, RLV

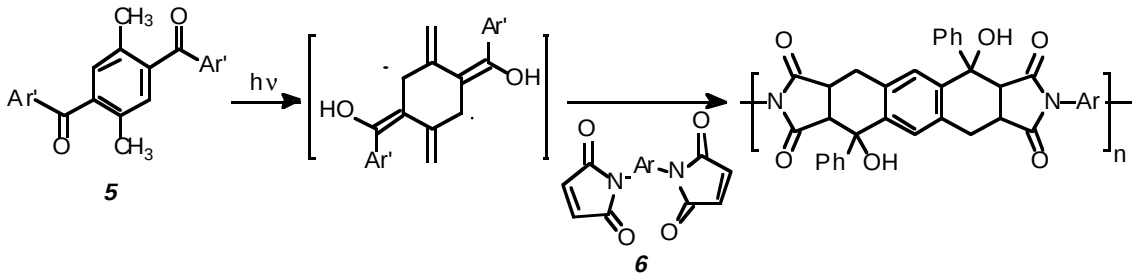

5 *6*

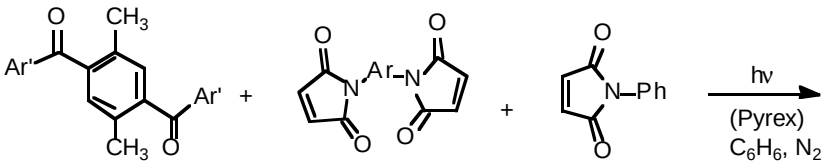

5 *6* *3*

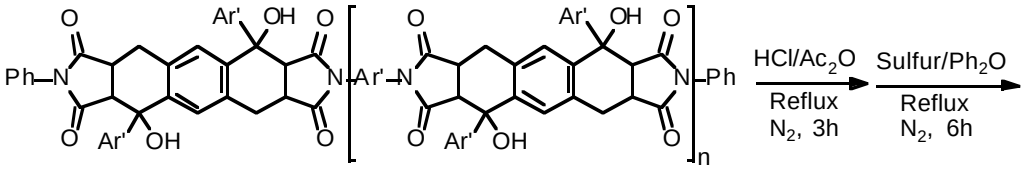

7

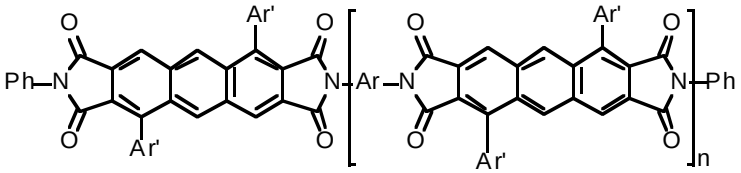

8

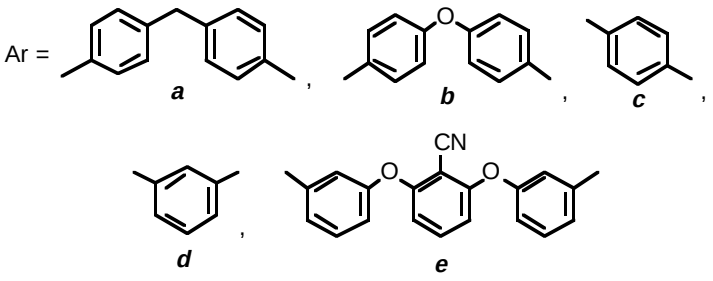

Ar' = Ph, *p*-($C_{12}H_{25}O$)Ph

Polyimides from Diels-Alder trapping of photochemically generated bisdienes.

10 000-hr Cyclic Oxidation Behavior of 68 High-Temperature Co-, Fe-, and Ni-Base Alloys Evaluated at 982 °C (1800 °F)

Power systems with operating temperatures in the range of 815 to 982 °C (1500 to 1800 °F) frequently require alloys that can operate for long times at these temperatures. A critical requirement is that these alloys have adequate oxidation resistance. The alloys used in these power systems require thousands of hours of operating life with intermittent shutdown to room temperature. Intermittent power plant shutdowns, however, offer the possibility that the protective scale will tend to spall (i.e., crack and flake off) upon cooling, increasing the rate of oxidative attack in subsequent heating cycles. Thus, it is critical that candidate alloys be evaluated for cyclic oxidation behavior. It was determined that exposing test alloys to ten 1000-hr cycles in static air at 982 °C (1800 °F) could give a reasonable simulation of long-time power plant operation.

Iron- (Fe-), nickel- (Ni-), and cobalt- (Co-) based high-temperature alloys with sufficient chromium (Cr) and/or aluminum (Al) content can exhibit excellent oxidation resistance. The protective oxides formed by these classes of alloys are typically Cr_2O_3 and/or Al_2O_3, and are usually influenced by their Cr, or Cr and Al, content. Sixty-eight Co-, Fe-, and Ni-base high-temperature alloys, typical of those used at this temperature or higher, were used in this study. (Detailed chemical compositions of these alloys are listed in ref. 1.)

At the NASA Lewis Research Center, the alloys were tested and compared on the basis of their weight change as a function of time, x-ray diffraction of the protective scale composition, and the physical appearance of the exposed samples. Although final appearance and x-ray diffraction of the final scale products were two factors used to evaluate the oxidation resistance of each alloy, the main criterion was the oxidation kinetics inferred from the specific weight change versus time data. These data indicated a range of oxidation behavior including parabolic (typical of isothermal oxidation), paralinear, linear, and mixed-linear kinetics. Paralinear kinetics was the most typical behavior, with scale growth at the operating temperature and scale spalling as the sample cooled between exposure cycles. Of the 132 cyclic oxidation tests (including replicates), 94 indicated paralinear behavior, only 4 showed parabolic behavior (scale growth only), and 34 were linear or mixed linear, where spalling tended to be massive.

The gravimetric data were fit to the basic paralinear equation:

$$\Delta W/A = k_1^{1/2} t^{1/2} + k_2 t \pm SEE$$

where ΔW is the change of sample weight (in milligrams) with time, A is the surface area in square centimeters, t is time in hours, SEE is the standard error of estimate by the multiple linear regression method, and depending upon the degree of fit, the significance and sign of the constants $k_1^{1/2}$ and k_2 define the kinetic model. (The use of this equation is discussed in detail in ref. 1.) The regression coefficients were combined into a single parameter, which along with the alloys' physical appearance, provided a relative ranking of the alloys' oxidation resistance.

Of the 68 alloys tested, 16 alloys were ranked as excellent, 18 good, 5 fair, 10 poor, and 19 catastrophic. The top bar graph shows 23 Cr-containing Ni-base alloys that formed a protective chromia/chromite scale. The bottom bar graph shows the best of the excellent-ranked alloys. They include four Ni-base and five Fe-base alloys. All of the most highly cyclic-oxidation-resistant alloys were protected by the formation of alumina and aluminate scales.

Reference

1. Barrett, C.A.: 10,000-Hour Cyclic Oxidation Behavior at 982 °C (1800 °F) of 68 High-Temperature Co-, Fe-, and Ni-Base Alloys. NASA TM–107394, 1997. (Available online: http://gltrs.grc.nasa.gov/cgi-bin/GLTRS/browse.pl?1997/TM-107394.html)

Lewis contact:
Charles A. Barrett, (216) 433–3163, Charles.A.Barrett@grc.nasa.gov

Author: Charles A. Barrett

Headquarters program office: OAT

Programs/Projects: HITEMP

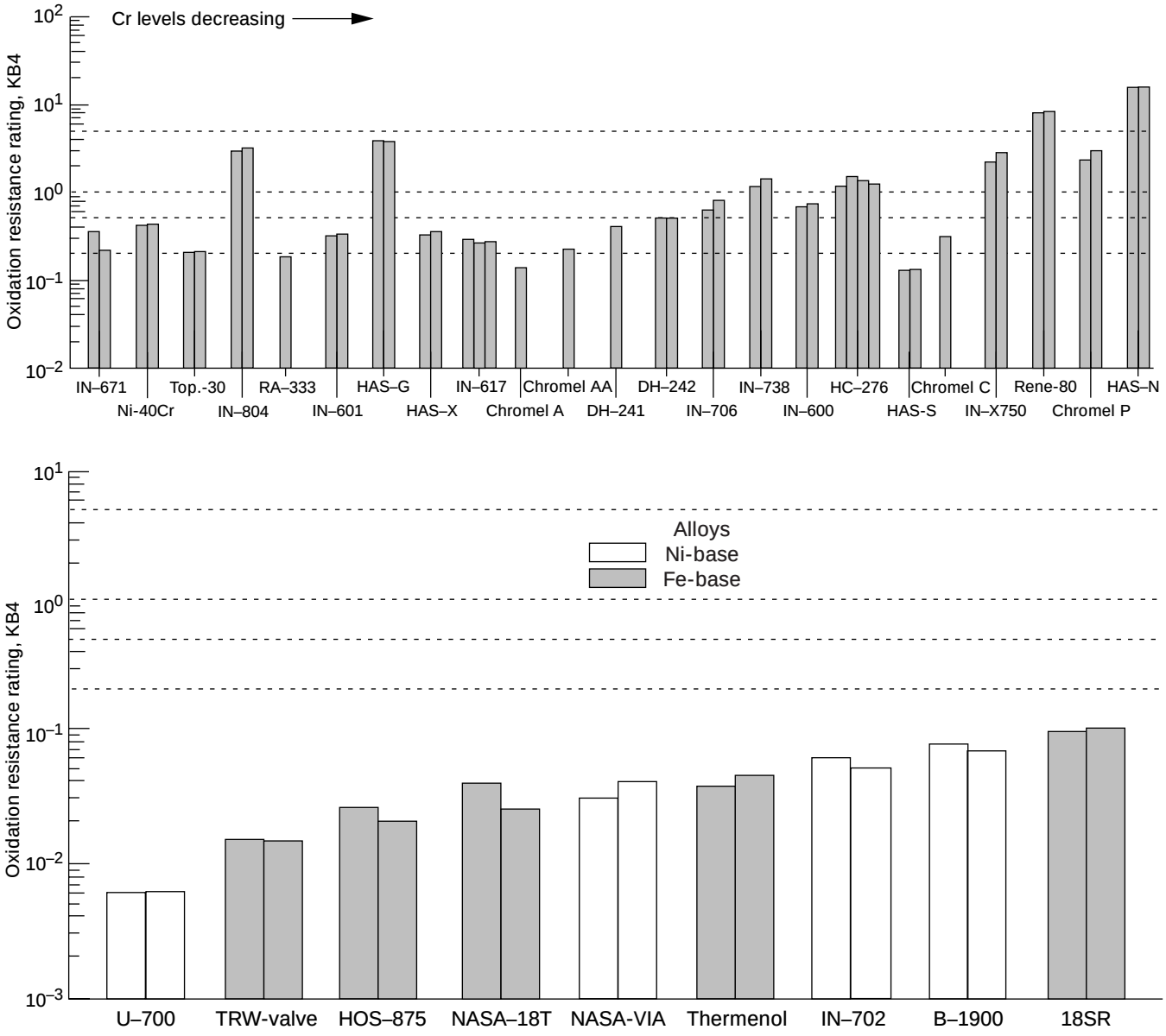

Relative oxidation attack resistance ratings. Dashed lines indicate cyclic oxidation resistance ratings, KB4: <0.2, excellent; 0.2 to 0.5, good; 0.5 to 1.0, fair; 1.0 to 5.0, poor; >5.0, catastrophic. Top: Chromia/chromite-forming Ni-base alloys (ten 1000-hr cycles at 982 °C). Bottom: The best of the excellent-ranked oxidation-resistant alloys (ten 1000-hr cycles at 982 °C).

Single-Crystal NiAl-X Alloys Tested for Hot Corrosion

Single-crystal nickel aluminide (NiAl) has been investigated extensively throughout the last several years as a potential structural material in aero-gas turbine engines. The attractive features of NiAl in comparison to Ni-base superalloys include a higher melting point, lower density, higher thermal conductivity, and excellent oxidation resistance. However, NiAl suffers from a lack of ductility and fracture toughness at low temperatures and a low creep strength at high temperatures. Alloying additions of hafnium (Hf), gallium (Ga), titanium (Ti), and chromium (Cr) have each shown some benefit to the mechanical properties over that of the binary alloy. However, the collective effect of these alloying additions on the environmental resistance of NiAl-X was unclear. Hence, the present study was undertaken to examine the hot corrosion behavior of these alloys. A companion study examined the cyclic oxidation resistance of these alloys.

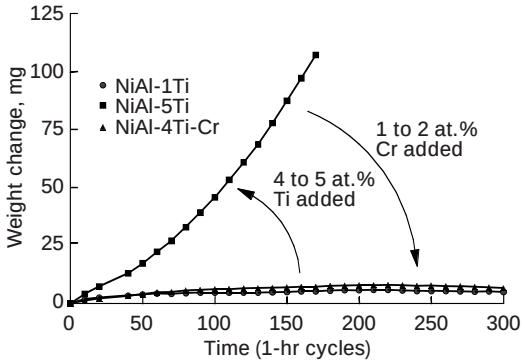

Weight change as a function of time for three single-crystal NiAl-X alloys.

Several single-crystal NiAl-X alloys (where X is Hf, Ti, Cr, or Ga) underwent hot corrosion testing in a Mach 0.3 burner rig at the NASA Lewis Research Center. Samples were tested for up to 300 1-hr cycles at a temperature of 900 °C. It was found that increasing the Ti content from 1 to 5 at.% degraded the hot corrosion behavior. This decline in the behavior was reflected in high weight gains and large corrosion mound formation during testing (see the figures). However, the addition of 1 to 2 at.% Cr to alloys containing 4 to 5 at.% Ti appeared to greatly reduce the susceptibility of these alloys to hot corrosion attack and negated the deleterious effect of the increased Ti addition.

After testing, the surface morphology consisted of either mounds or an inward, uniform attack that preserved surface features. The mounds initiated early and grew and coalesced through the 300 hours of testing. However, few new corrosion mounds were observed after 50 to 100 hours. Microstructurally, below the surface, the hot corrosion attack initiated as pits but evolved to a rampant attack consisting of the rapid inward growth of Al_2O_3 and TiO_2. This attack stage progressed rapidly inward, totally depleting the Al and Ti in the degraded regions.

It was also observed that the corrosion morphology was strongly affected by the surface preparation treatments. The sample surfaces were prepared by either electropolishing, chemically milling, or mechanical polishing. It was found that mechanical polishing changed the corrosion morphology and improved the hot corrosion response over that of chemically milled surfaces. Further details of this work are given in reference 1.

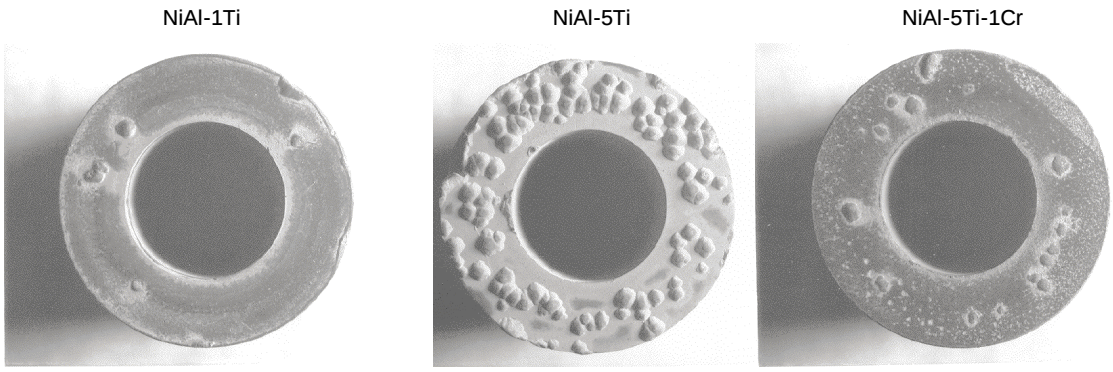

Hot corrosion of three single-crystal alloys.

Reference

1. Nesbitt, J.A.: Hot Corrosion of Single-Crystal NiAl-X Alloys. NASA TM–113128, 1998.

Lewis contact:
Dr. James A. Nesbitt, (216) 433–3275, James.A.Nesbitt@grc.nasa.gov

Author: Dr. James A. Nesbitt

Headquarters program office: OAT

Programs/Projects: HITEMP

Thermal Mechanical Stability of Single-Crystal-Oxide Refractive Concentrators Evaluated for High-Temperature Solar-Thermal Propulsion

Recently, refractive secondary solar concentrator systems were developed for solar thermal power and propulsion (ref. 1). Single-crystal oxides—such as yttria-stabilized zirconia (Y_2O_3-ZrO_2), yttrium aluminum garnet ($Y_3Al_5O_{12}$, or YAG), magnesium oxide (MgO), and sapphire (Al_2O_3)—are candidate refractive secondary concentrator materials. However, the refractive concentrator system will experience high-temperature thermal cycling in the solar thermal engine during the sun/shade transition of a space mission. The thermal mechanical reliability of these components in severe thermal environments is of great concern. Simulated mission tests are important for evaluating these candidate oxide materials under a variety of transient and steady-state heat flux conditions. In this research at the NASA Lewis Research Center, a controlled heat flux test approach was developed for investigating the thermal mechanical stability of the candidate oxide. This approach used a 3.0-kW continuous-wave (wavelength, 10.6 μm) carbon dioxide (CO_2) laser (ref. 2). The CO_2 laser is especially well-suited for single-crystal thermal shock tests because it can directly deliver well-characterized heat energy to the oxide surfaces. Since the oxides are opaque at the 10.6-μm wavelength of the laser beam, the light energy is absorbed at the surfaces rather than transmitting into the crystals, and thus generates the required temperature gradients within the specimens. The following figure is a schematic diagram of the test rig.

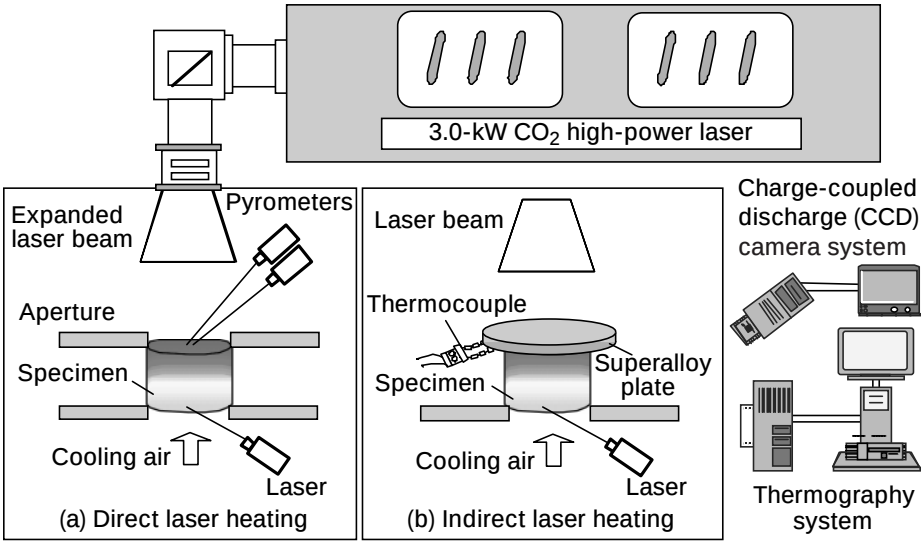

High-temperature thermal gradient testing of single-crystal-oxide refractive solar concentrator using a high-power laser.

The thermal stress fracture behavior and failure mechanisms of these oxide materials were investigated, and the critical temperature gradients and corresponding absorbed power densities imposed on the crystals to cause failure were determined under various temperature and heating conditions. Steady-state thermal gradient tests were conducted on thin-disk specimens of Y_2O_3-ZrO_2, YAG, MgO, and Al_2O_3 (diameter, 25.4 mm; thickness, 1 mm) to determine the critical temperature differences across the specimen thickness that will initiate cracking. The laser power was continuously increased at a slow rate to heat the specimen under near steady-state conditions and to increase the temperature gradient across the specimen thickness with the heating time. Because the disk specimen broke off as soon as the material began to crack, the onset of cracking and the fracture of the specimen were recorded as a sudden temperature drop in the pyrometer temperature reading. The average critical temperature differences at failure were 81±20 °C, 88±21 °C, and 200±35 °C for Y_2O_3-ZrO_2, YAG, and Al_2O_3, respectively. Because the thermal gradients established in the secondary solar concentrator systems are due to the heat receiver cavity heating/cooling cycles and to a small portion of solar light energy being absorbed in the crystal components, the information obtained from this experiment can be of great importance in component design. The crack origins were typically observed near the back edges of the specimen because of a tensile stress state near the backside, as shown in the photomicrograph on the left (Y_2O_3-ZrO_2).

Laser transient thermal shock tests were conducted on single-crystal cylindrical specimens (diameter, 12.7 mm; length, 12.7 mm) with a total heating time of 60 sec and a subsequently increased laser power. During the test, heating/cooling profiles and temperature distributions were experimentally measured with thermography and pyrometry. Results were compared with analytical solutions and one-dimensional finite difference models. The critical power densities for crystal failure were approximately 15.3 W/cm^2, 56.9 W/cm^2, 39.1 W/cm^2, and 109.4 W/cm^2 for Y_2O_3-ZrO_2, YAG, MgO, and Al_2O_3 (sapphire), respectively. In the materials with low thermal conductivity and high thermal expansion, Y_2O_3-ZrO_2 and MgO, high compressive stresses and/or compressive stress-induced (resolved) shear stresses initiated the surface cracks. On the other hand, in the materials with high thermal conductivity and low thermal expansion, Al_2O_3 and YAG, the cracks were more likely initiated deep in the crystals.

The photomicrograph on the right illustrates the surface shear-stress-initiated cleavage along the (110) plane in MgO. The modeled transient thermal stress distributions indicate that the surface compressive stresses and subsurface tensile stresses are responsible for the crystal failures observed under the laser transient heating conditions.

Single-crystal cylindrical specimens were also tested under a thermal gradient to simulate the heating/cooling cycles of a space mission. A typical thermography temperature distribution in a YAG specimen during the testing is illustrated in the final figure. Surface cracking was observed for the Y_2O_3-ZrO_2 and MgO specimens at a surface heating rate of approximately 15 °C/min at 1200 °C. The YAG and Al_2O_3 specimens did not crack

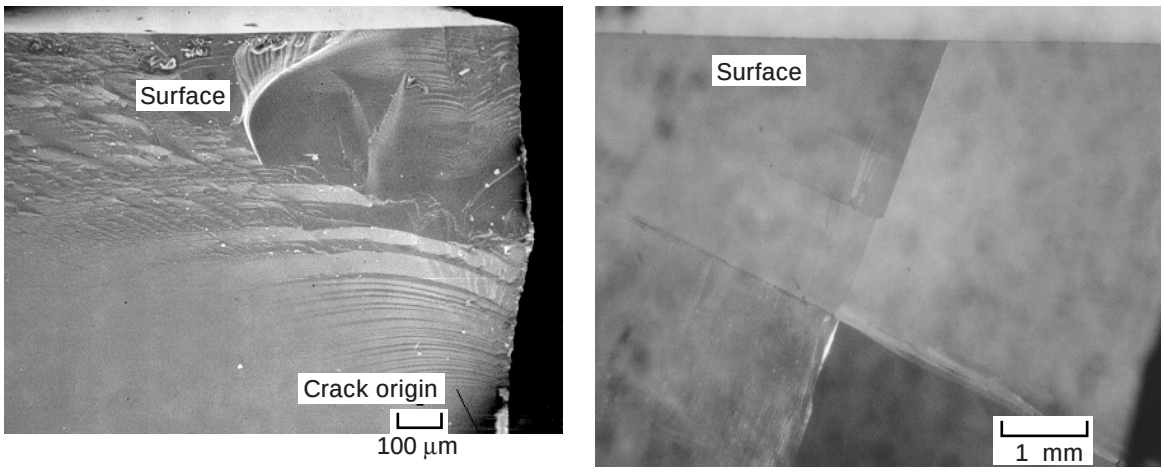

Crack and fracture morphologies of single-crystal oxides after laser testing. Left: SEM fractograph of the Y_2O_3-doped ZrO_2 disk specimen after laser steady-state thermal gradient testing. Right: Surface shear-stress-initiated cleavage along the (110) plane in MgO after laser thermal transient testing (optical microscopy).

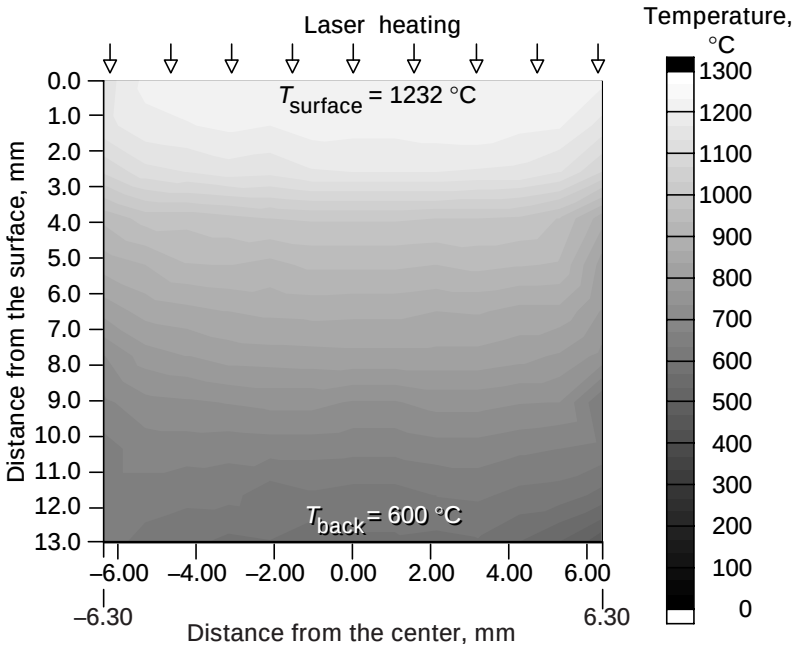

Thermography temperature distribution in a YAG specimen (diameter, 12.7 mm; length, 12.7 mm) during near-steady-state laser heating.

under the test conditions. Al_2O_3 (sapphire) exhibited the best thermal shock resistance of all oxide materials tested. The good thermal shock resistance of sapphire is attributed to its high strength, high thermal conductivity, and low thermal expansion coefficient.

References

1. Soules, J.A., et al.: Design and Fabrication of a Dielectric Total Internal Reflecting Solar Concentrator and Associated Flux Extractor for Extreme High Temperature (2500 K) Applications. NASA CR–204145, 1997.

2. Zhu, D.; Jacobson, N.S.; and Miller, R.A.: Thermal-Mechanical Stability of Single Crystal Oxide Refractive Concentrators for High-Temperature Solar Thermal Propulsion. NASA TM—1999-208899, 1999.

Ohio Aerospace Institute contact:
Dr. Dongming Zhu, (216) 433–5422, Dongming.Zhu@grc.nasa.gov

Lewis contact:
Dr. Nathan S. Jacobson, (216) 433–5498, Nathan.S.Jacobson@grc.nasa.gov

Authors:
Dr. Dongming Zhu, Dr. Nathan S. Jacobson, and Dr. Robert A. Miller

Headquarters program office: OAT

Programs/Projects:
Secondary Concentrator Project, Space Transfer Technology Program

Power and On-Board Propulsion Technology

Solar Array Verification Analysis Tool (SAVANT) Developed

Modeling solar cell performance for a specific radiation environment to obtain the end-of-life photovoltaic array performance has become both increasingly important and, with the rapid advent of new types of cell technology, more difficult. For large constellations of satellites, a few percent difference in the lifetime prediction can have an enormous economic impact. The tool described here automates the assessment of solar array on-orbit end-of-life performance and assists in the development and design of ground test protocols for different solar cell designs. Once established, these protocols can be used to calculate on-orbit end-of-life performance from ground test results.

The Solar Array Verification Analysis Tool (SAVANT) utilizes the radiation environment from the Environment Work Bench (EWB) model developed by the NASA Lewis Research Center's Photovoltaic and Space Environmental Effects Branch in conjunction with Maxwell Technologies. It then modifies and combines this information with the displacement damage model proposed by Summers et al. (ref. 1) of the Naval Research Laboratory to determine solar cell performance during the course of a given mission. The resulting predictions can then be compared with flight data.

The Environment WorkBench (ref. 2) uses the NASA AE8 (electron) and AP8 (proton) models of the radiation belts to calculate the trapped radiation flux. These fluxes are integrated over the defined spacecraft orbit for the duration of the mission to obtain the total omnidirectional fluence spectra.

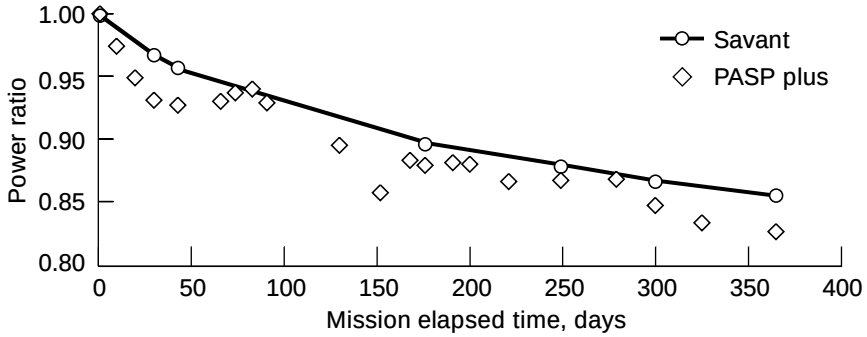

Normalized power ratio for the silicon module.

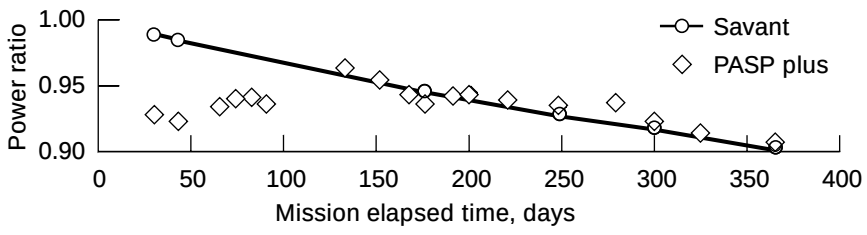

Normalized power ratio for the gallium arsenide module.

Components such as the solar cell coverglass, adhesive, and antireflective coatings can slow and attenuate the particle fluence reaching the solar cell. In SAVANT, a continuous slowing down approximation is used to model this effect.

The displacement damage model is based on a damage correlation using the "displacement damage dose" derived from the product of the calculated nonionizing energy loss and the fluence. It can very accurately predict the expected degradation of solar cell performance in a complex space radiation environment based on Earth-made measurements with only one proton energy and two electron energies, or proton and electron energy, and Co^{60} gammas.

The displacement damage dose is the nonionizing equivalent of the ionizing dose, and the nonionizing energy loss coefficients are the nonionizing counterpart to the collision stopping power. The displacement damage dose is calculated by integrating the product of the differential fluence and the nonionizing energy loss values over energy. This displacement damage dose is calculated for both electrons and protons, and the total dose is found by summing the two after the electron dose has been converted to an effective dose by dividing it by a dose ratio experimentally determined for the particular solar cell type. The displacement damage dose can then be related to solar cell power loss.

$$\frac{P_{\max}}{P_0} = 1 - C \ln\left[1 + \frac{D_T}{D_x}\right]$$

where P_{max} is the maximum power output of the cell, P_0 is the original

power output, C and D_x depend on the specific solar cell, and D_T is the total displacement damage dose.

A comparison of the SAVANT prediction with the albedo-free data from the Photovoltaic Array Space Power Plus Diagnostics (PASP Plus) flight experiment for the silicon and gallium arsenide modules is shown in the preceding page.

The SAVANT tool fully integrates the required models end to end, including the trapped particle environment, cell shielding, geometry and type, slowing of the incident fluence by shielding, resultant displacement damage dose, and effect on cell power output. Parameter trade studies are extremely easy to perform with SAVANT. The effect of shielding material or thickness, orbit parameters, mission length, or cell type can be examined. The SAVANT tool provides a time-effective way to compare a variety of array parameters.

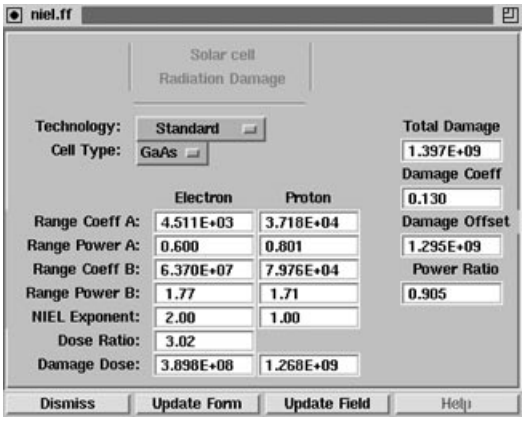

SAVANT screen capture showing solar cell radiation damage.

References

1. Summers, G.P.; Burke, E.A.; and Zapsos, M.A.: Displacement Damage Analogs to Ionizing Radiation Effects. Radiation Measurements, vol. 24, no. 1, 1995, pp. 1–8.

2. EWB: The Environment WorkBench. Online information: http://satori2.grc.nasa.gov/DOC/EWB/ewbhome.html

Lewis contact: Dr. Sheila G. Bailey, (216) 433–2228, fax (216) 433–6106, Sheila.G.Bailey@grc.nasa.gov

Authors:
Dr. Sheila G. Bailey, Kenwyn J. Long, Henry B. Curtis, Barbara Gardner, Victoria Davis, Scott Messenger, and Robert Walters

Headquarters program office:
OSS (ATMS)

Programs/Projects: Spacecraft for all solar-powered flight missions

Space Plasma Shown to Make Satellite Solar Arrays Fail

In 1997, scientists and engineers of the Photovoltaic and Space Environments Branch of the NASA Lewis Research Center, Maxwell Technologies, and Space Systems/Loral discovered a new failure mechanism for solar arrays on communications satellites in orbit. Sustained electrical arcs, initiated by the space plasma and powered by the solar arrays themselves, were found to have destroyed solar array substrates on some Space Systems/Loral satellites, leading to array failure. The mechanism was tested at Lewis, and mitigation strategies were developed to prevent such disastrous occurrences on-orbit in the future.

Sustained arc on the EOS–AM1 solar array test article in a simulated space plasma in the Lewis Plasma Interactions Facility.

Deep Space 1 is a solar-electric-powered space mission to a comet, launched on October 24, 1998. Early in 1998, scientists at Lewis and Ballistic Missile Defense Organization (BMDO) realized that some aspects of the Deep Space 1 solar arrays were nearly identical to those that had led to the failure of solar arrays on Space Systems/Loral satellites. They decided to modify the Deep Space 1 arrays to prevent catastrophic failure in space. The arrays were suitably modified and are now performing optimally in outer space.

Finally, the Earth Observing System (EOS) AM1, scheduled for launch in mid 1999, is a NASA mission managed by the Goddard Space Flight Center. Realizing the importance of Lewis' testing on the Loral arrays, EOS–AM1 management asked Lewis scientists to test their solar arrays to show that they would not fail in the same way. The first phase of plasma testing showed that sustained arcing would occur on the unmodified EOS–AM1 arrays, so the arrays were removed from the spacecraft and fixed. Now, Lewis scientists have finished plasma testing of the modified array configuration to ensure that EOS–AM1 will have no sustained arcing problems on-orbit.

Lewis contact: Dr. Dale C. Ferguson, (216) 433–2298, Dale.C.Ferguson@grc.nasa.gov

Author: Dr. Dale C. Ferguson

Headquarters program office: OSS (ATMS)

Programs/Projects
EOS, New Millenium, GEO communications satellites, LEO satellite constellations

Lithium-Ion Polymer Rechargeable Battery Developed for Aerospace and Military Applications

A recently completed 3 1/2-year project funded by the Defense Advanced Research Projects Agency (DARPA) under the Technology Reinvestment Program has resulted in the development and scaleup of new lithium-ion polymer battery technology for military and aerospace applications. The contractors for this cost-shared project were Lockheed Martin Missiles & Space and Ultralife Batteries, Inc. The NASA Lewis Research Center provided contract management and technical oversight. The final products of the project were a portable 15-volt (V), 10-ampere-hour (A-hr) military radio battery and a 30-V, 50-A-hr marine/aerospace battery. Lewis will test the 50-A-hr battery.

The new lithium-ion polymer battery technology offers a threefold or fourfold reduction in mass and volume, relative to today's commonly used nickel-cadmium, nickel-hydrogen, and nickel-metal hydride batteries. This is of special importance for orbiting satellites. It has been determined for a particular commercial communications satellite that the replacement of 1 kg of battery mass with 1 kg of transponder mass could increase the annual revenue flow by $100 000! Since this lithium-ion polymer technology offers battery mass reductions on the order of hundreds of kilograms for some satellites, the potential revenue increases are impressive.

By the end of the project, the best high-energy formulations for the electrodes and electrolyte were providing 170 watt-hours per kilogram (W-hr/kg) specific energy and nearly 450 W-hr/liter energy density for the lithium-ion polymer cell. Battery cells have been tested to 1000 deep-discharge cycles before 20 percent of capacity has been lost. We anticipate that continued improvements in cell chemistry coupled with cycling to less than full discharge will result in the cycle lives required for low-Earth-orbit applications. Electronic circuitry has been developed to provide for charge-discharge control, cell protection, and cell rebalancing at the individual cell level. In the lithium-ion polymer cell, there is no metallic lithium, so the safety concerns associated with that metal are obviated. In a typical cell formulation, the negative electrode is a carbon material that can accept (intercalate) lithium ions at a low potential, and the positive electrode is a transition metal oxide that intercalates the ions at a potential about 4 volts higher. The two electrodes and the electrolyte structure all have as one component a thermoplastic polymeric material. Thus, the three cell elements can be independently processed using common high-speed plastic film processing technology. They can then be brought together, thermally bonded to one another, cut to the desired size and shape, activated,

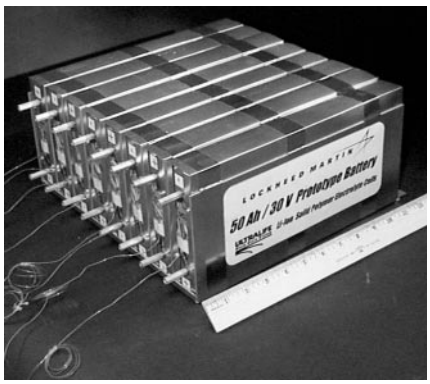

50 A-hr, 30-V lithium-ion polymer battery.

connected to form batteries, packaged, sealed, and tested. This entire process, which can be fully automated, uses inexpensive materials and offers the promise of an extremely attractive advanced technology at a low cost.

Lewis contact:
Norman H. Hagedorn, (216) 433–6157, Norman.H.Hagedorn@grc.nasa.gov

Author: Norman H. Hagedorn

Headquarters program office: OSS

Programs/Projects:
NASA/AF Lithium-ion Battery Development, NASA Aerospace Flight Battery Systems, RLV, Bantam, Future-X, LEO and GEO missions, EAPU, EMA, and in-house lithium-ion polymer battery development

Cathodes Delivered for Space Station Plasma Contactor System

The International Space Station's (ISS) power system is designed with high-voltage solar arrays that typically operate at output voltages of 140 to 160 volts (V). The ISS grounding scheme electrically ties the habitat modules, structure, and radiators to the negative tap of the solar arrays. Without some active charge control method, this electrical configuration and the plasma current balance would cause the habitat modules, structure, and radiators to float to voltages as large as –120 V with respect to the ambient space plasma.

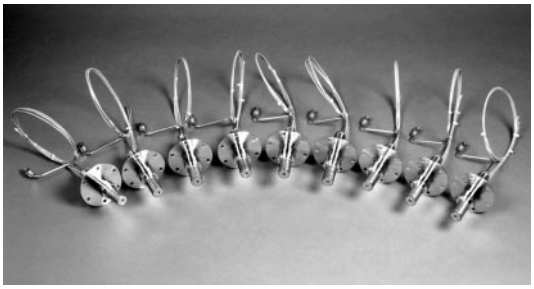

Flight-ready hollow cathode assembly units for the space station plasma contactor flight hardware (includes one qualification unit).

With such large negative floating potentials, the ISS could have deleterious interactions with the space plasma. These interactions could include arcing through insulating surfaces and sputtering of conductive surfaces as ions are accelerated by the spacecraft plasma sheath. A plasma contactor system was baselined on the ISS to prevent arcing and sputtering. The sole requirement for the system is contained within a single directive (SSP 30000, paragraph 3.1.3.2.1.8): "The Space Station structure floating potential at all points on the Space Station shall be controlled to within ±40 V of the ionospheric plasma potential using a plasma contactor." NASA is developing this plasma contactor as part of the ISS electrical power system.

For ISS, efficient and rapid emission of high electron currents is required from the plasma contactor system under conditions of variable and uncertain current demand. A hollow cathode plasma source is well suited for this application and was, therefore, selected as the design approach for the station plasma contactor system. In addition to the plasma source, which is referred to as a hollow cathode assembly, or HCA, the plasma contactor system includes two other subsystems. These are the power electronics unit and the xenon gas feed system.

The Rocketdyne Division of Boeing North American is responsible for the design, fabrication, assembly, test, and integration of the plasma contactor system. Because of technical and schedule considerations, the NASA Lewis Research Center was asked to manufacture and deliver the engineering model, the qualification model, and the flight HCA units for the plasma contactor system as government furnished equipment. To date, multiple units have been built. One cathode has demonstrated approximately 28 000-hr lifetime, two development HCA units have demonstrated over 15 000-hr lifetime, and one HCA unit has demonstrated more than 38 000 ignitions. All eight flight HCA's have been manufactured, acceptance tested, and are ready for delivery to the flight contractor.

Lewis contact:
Michael J. Patterson, (216) 977–7481, Michael.J.Patterson@grc.nasa.gov

Author: Michael J. Patterson

Headquarters program office: OSF

Programs/Projects: ISS

High-Performance Bipropellant Engine

TRW, under contract to the NASA Lewis Research Center, has successfully completed over 10 000 sec of testing of a rhenium thrust chamber manufactured via a new-generation powder metallurgy. High performance was achieved for two different propellants, N_2O_4–N_2H_4 and N_2O_4–MMH. TRW conducted 44 tests with N_2O_4–N_2H_4, accumulating 5230 sec of operating time with maximum burn times of 600 sec and a specific implulse, I_{sp}, of 333 sec. Seventeen tests were conducted with N_2O_4–MMH for an additional 4789 sec and a maximum I_{sp} of 324 sec, with a maximum firing duration of 700 sec. Together, the 61 tests totalled 10 019 sec of operating time, with the chamber remaining in excellent condition. Of these tests, 11 lasted 600 to 700 sec.

The performance of radiation-cooled rocket engines is limited by their operating temperature. For the past two to three decades, the majority of radiation-cooled rockets

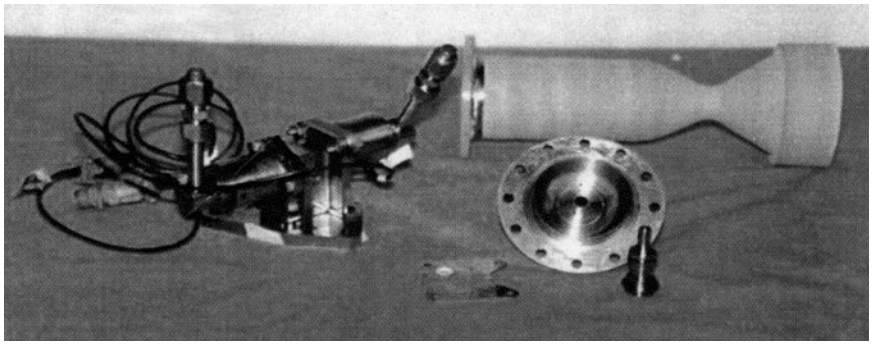

Technology demonstrator engine fabricated from rhenium.

were composed of a high-temperature niobium alloy (C103) with a disilicide oxide coating (R512) for oxidation resistance. The R512 coating practically limits the operating temperature to 1370 °C. For the Earth-storable bipropellants commonly used in satellite and spacecraft propulsion systems, a significant amount of fuel film cooling is needed. The large film-cooling requirement extracts a large penalty in performance from incomplete mixing and combustion.

A material system with a higher temperature capability has been matured to the point where engines are being readied for flight, particularly the 100-lb-thrust class engine. This system has powder rhenium (Re) as a substrate material with an iridium (Ir) oxidation-resistant coating. Again, the operating temperature is limited by the coating; however, Ir is capable of long-life operation at 2200 °C. For Earth-storable bipropellants, this allows for the virtual elimination of fuel film cooling (some film cooling is used for thermal control of the head end). This has resulted in significant increases in specific impulse performance (15 to 20 sec).

To determine the merits of a powder rhenium thrust chamber, Lewis' On-Board Propulsion Branch directed TRW (under the Space Storable Rocket Technology Program and the High Pressure Earth Storable Rocket Technology Program) to design, fabricate, and test an engineering model to serve as a technology demonstrator.

Lewis contact:
Dr. Steven J. Schneider, (216) 977–7484, Steven.J.Schneider@grc.nasa.gov

Authors: James A. Biaglow and Dr. Steven J. Schneider

Headquarters program office: OSS

Programs/Projects:
Space Storable Rocket Technology Program, High-Pressure Earth Storable Rocket Technology

Liquid Bipropellant Microrocket Concept Under Development

Fundamental research into the feasibility of microrockets for primary propulsion and attitude control for far-term micro/integrated spacecraft is being performed. These rockets would be fabricated using microelectrical and mechanical systems (MEMS) technology. The enabling technology is being developed at the Massachusetts Institute of Technology (MIT). The NASA/MIT program leverages a very large Army Research Office and Defense Advanced Research Projects Agency (DARPA) program for the development of microturbine technology. The microrocket motor is complete with regenerative cooling, turbopumps, and control valves etched onto the same chip. They would be fabricated in large numbers in parallel using semiconductor manufacturing techniques. The technology may lead to the development of microsatellites as fully integrated MEMS devices that could be mass produced at a fraction of the cost of current satellites.

This microrocket would have a specific impulse of 300 sec at a chamber pressure of 125 atm in a 15-N-thrust class engine and would use propellants such as liquid oxygen and ethanol. The motor, fabricated from silicon or silicon carbide, would have a thrust-to-weight ratio of 1500:1 compared to 15:1 for a conventional engine in this thrust range. The regeneratively cooled silicon structure is predicted to have an operating temperature less than 1400 K.

Because of the fundamental nature of the work, near-term efforts will focus on the basic feasibility issues. These include (1) MEMS fabrication technology, (2) component/propellant compatibility, (3) bonding and leakage, (4) heat transfer capabilities, (5) component life, and (6) performance.

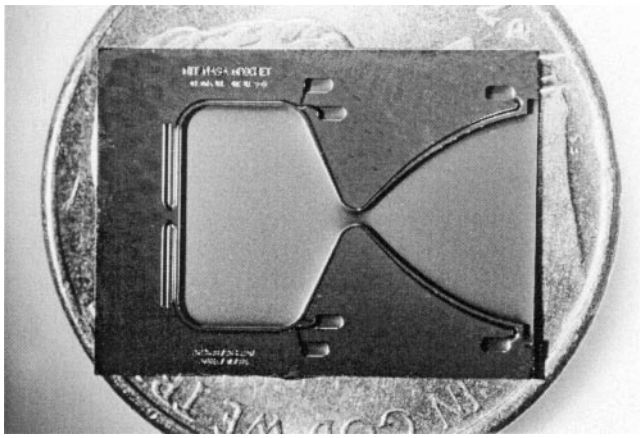

Silicon half-rocket chamber, complete with cooling channels. For scaling, this component is shown sitting atop a nickel.

Lewis contact:
Dr. Steven J. Schneider, (216) 977–7484, Steven.J.Schneider@grc.nasa.gov

Author: Dr. Steven J. Schneider

Headquarters program office:
OSS (ATMS)

Programs/Projects:
New Millenium Program, MTPE

Ion Thruster and Power Processor Developed for the Deep Space 1 Mission

The NASA Solar Electric Propulsion Technology Applications Readiness (NSTAR) Program has provided a single-string primary propulsion system to NASA's Deep Space 1 spacecraft. This spacecraft will carry about 81 kg of xenon propellant for the ion thruster, which can be throttled down from 2.3 to 0.5 kW as the spacecraft moves away from the Sun. The propellant load will provide about 20 months of propulsion at the one-half power throttle setpoint of 1.2 kW. This mission will validate the 2.5-kW ion propulsion system and will fly by the asteroid 1992 KD in 1999. If funding permits, Deep Space 1 also will encounter comets Wilson-Harrington and Borrelly in 2001.

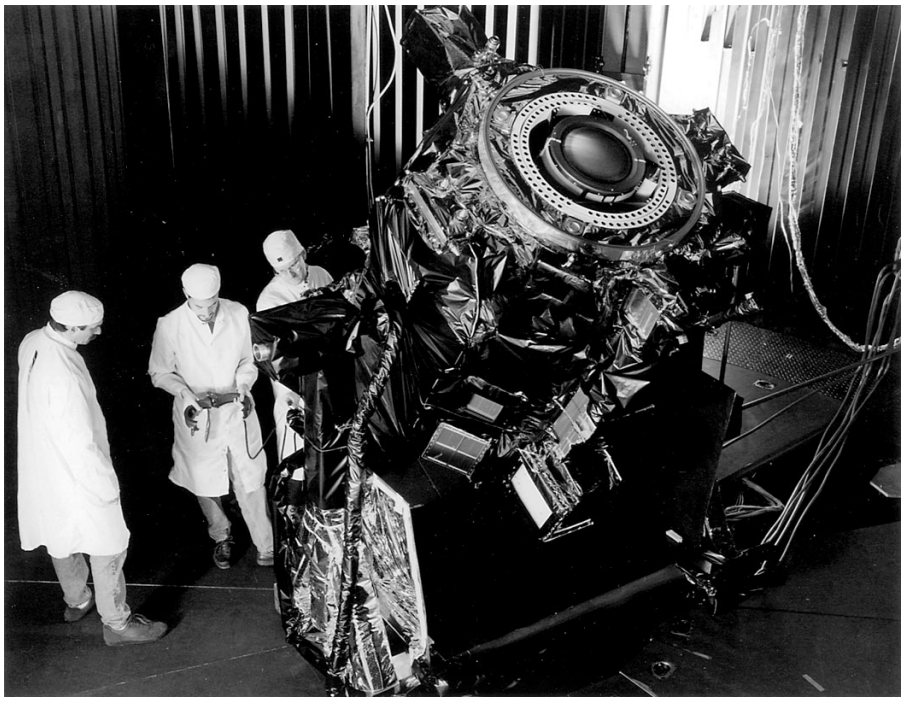

Ion thruster mounted to its gimbal ring on the Deep Space 1 spacecraft during solar thermal vacuum testing.

NASA Lewis Research Center's On-Board Propulsion Branch was responsible for the development of the 30-cm-diameter ion thruster, the 2.5-kW power processor unit (PPU), and the Digital Control and Interface Unit (DCIU) that controls the PPU/thruster/feed system and provides data and recovery from fault conditions. Lewis transferred the thruster and PPU technologies to the Hughes Electron Dynamics Division, which was selected to build two sets of flight thrusters, as well as the PPU's and DCIU's. Hughes subcontracted the DCIU development to Spectrum Astro Incorporated. The Jet Propulsion Laboratory (JPL) was primarily responsible for the NSTAR project management, thruster lifetests, the feed system, diagnostics, and the propulsion subsystem integration.

A total of four engineering model thrusters and three breadboard PPU's were built, integrated, and tested. More than 50 development

tests were conducted along with thruster design verification tests of 2000 and 1000 hours. In addition, an 8000-hr life demonstration test was successfully completed and demonstrated wear-rates consistent with full-power life-times in excess of 12 000 hours.

Because of funding and schedule constraints, the PPU's and DCIU's fabricated by Hughes Electron Dynamics Division were flight qualified at Lewis. Thrusters were acceptance tested at both Lewis and the Jet Propulsion Laboratory. All the hardware passed the qualification test program and was subsequently integrated onto the Deep Space 1 spacecraft, where the propulsion system completed a compatibility test program that included a thruster firing at full-power in the Jet Propulsion Laboratory's 25-ft space-simulation facility. Deep Space 1 was launched from Cape Canaveral Air Station on October 24, 1998, aboard a Boeing Delta 7326.

Bibliography

Sovey, J.S., et al.: Development of an Ion Thruster and Power Processor for New Millennium's Deep Space 1 Mission. AIAA Paper 97–2778, July 1997.

Rawlin, V.K., et al.: NSTAR Flight Thruster Qualification Testing. AIAA Paper 98–3936, July 1998.

Lewis contacts:
James S. Sovey, (216) 977–7454, James.S.Sovey@grc.nasa.gov; and Vincent K. Rawlin, (216) 977–7462, Vincent.K.Rawlin@grc.nasa.gov

Author: James S. Sovey

Headquarters program offices: OSS, OAT

Programs/Projects: New Millennium program, NSTAR, Deep Space 1, Deep Space 4, AST

Advanced Refrigerator/Freezer Technology Development Project

The Advanced Refrigerator/Freezer (R/F) Technology Development Project was initiated in 1994, on the basis of recommendations of a team of NASA Scientists and engineers, who assessed the need for advanced technology to support future life and biomedical sciences space flight missions. The project, which was cofunded by NASA's Office of Aero-Space Technology and Life and Biomedical Sciences & Applications Division, has two phases. In the Phase I Advanced R/F Technology Assessment, candidate technologies were identified and ranked, on the basis of a combination of their effect on system performance and their risk of developmental success. In Phase II Technology Development, the advanced technologies with the highest combined ranking, which could be accomplished within the budgetary constraints, were pursued. The effort has been mainly by contract, with a modest in-house effort at the NASA Lewis Research Center. Oceaneering Space Systems (OSS) of Houston, Texas, was selected as the prime contractor for both contract phases.

The Phase I report (ref. 1) identified nine candidate advanced technologies for development. Resource availability forced a limiting of the Phase II technology development contract effort to only the highest priority technology, rigid polymer vacuum panel multilayer insulation (MLI). Typical 3 1/2-in.-thick fiberglass insulation has an insulation value of R–11/in. or R–3.14/in. The best commercially available vacuum panel insulation has an insulation value of about R–35/in. and has an

Six-sided vacuum panel insulated box.

Stirling Orbiter Refrigerator Freezer.

expected 10-yr life with insulation value of at least R–20/in. Vacuum panel insulation tests by OSS indicated center of panel insulation values of more than R–100/in. Unfortunately, severe design compromises, made to expedite construction of the panels, yielded high conduction heat flow at the panel edges. As a result, the measured overall insulation value for a six-sided box (see the left photograph on the preceding page), constructed of these panels, was about R–11.5/in. Although this was well below the intended goal, it agreed reasonably well with the R–13.89/in. computer model prediction. OSS is confident that overall insulation values of R–60/in. to R–80/in. are achievable with optimal panel edge design. The long-term performance of these panels remains to be demonstrated. The OSS contract has been completed, and the final report has been delivered to Lewis for NASA review and editing. It should be published in early 1999.

The Stirling Orbiter Refrigerator Freezer (SOR/F), which flew as a space flight experiment on the STS–60 shuttle mission, was acquired from the NASA Johnson Space Center to serve as a test bed for in-house, advanced refrigerator/freezer technology testing at Lewis. The current effort is aimed at improving the SOR/F performance and making it more versatile. Key objectives are to (1) reduce the electrical power consumption and heat rejection, (2) reduce the rate of temperature rise with the power turned off, (3) reduce the levels of noise and vibration, and (4) extend the operating temperature range down to –80 °C. The original SOR/F operated at temperatures from 4 to –26 °C.

So that these objectives can be realized, the original double Stirling cycle cooler, built by Sunpower, Inc. of Athens, Ohio, is being replaced with two improved, higher efficiency coolers (see the photograph on the left) built by Global Cooling Manufacturing Company, under license from Sunpower. Lewis, with the aid of technology furnished by the NASA Goddard Space Flight Center, is developing controls to drive the Stirling coolers to maintain operating temperature and to minimize vibration. The new coolers use liquid cooling, which allows lower heat rejection temperature and improved cooler efficiency in comparison to the original air-cooled Sunpower coolers. Liquid cooling also eliminates the noise of a cooling fan.

The original SOR/F used heat pipes to transport heat from the storage volume to the Stirling cooler. The acetone fluid in these heat pipes limits the lower operating temperature to about –40 °C. During 1998, new heat pipes (see the photograph on the right) with propylene working fluid were designed, fabricated, and tested by Thermacore, Inc., of Lancaster, Pennsylvania, and delivered to Lewis. The new heat pipes can operate at temperatures to –100 °C. Also, they are designed to operate as thermal diodes, allowing heat to flow easily from the storage space to the cooler, but they restrict heat flow in the reverse direction, when the cooler is not operating.

For further information, check out our web page:
http://powerweb.grc.nasa.gov/stirling/DOC/adfreeze.html

Reference

1. Gaseor, T.; Hunter, R.; and Hamill, D.: Advanced Refrigerator/Freezer Technology Development Technology Assessment. NASA CR–198484, 1996.

Lewis contacts:
James E. Cairelli, (216) 433–6142, James.E.Cairelli@grc.nasa.gov; and Steven M. Geng, (216) 433–6145, Steven.M.Geng@grc.nasa.gov

Authors:
James E. Cairelli and Steven M. Geng

Headquarters program office:
OAT, OLMSA (LS)

Programs/Projects: Life and biomedical sciences spaceflight missions

Improved Stirling cooler.

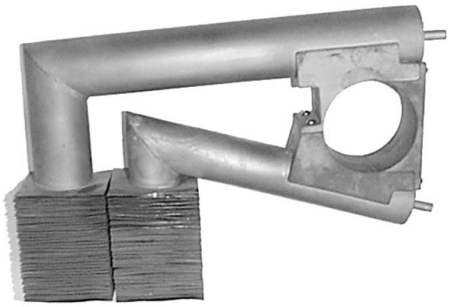

Low-temperature diode heat pipes.

Power System Optimization Codes Modified

A major modification of and addition to existing Closed Brayton Cycle (CBC) space power system optimization codes was completed. These modifications relate to the global minimum mass search driver programs containing three nested iteration loops comprising iterations on cycle temperature ratio, and three separate pressure ratio iteration loops—one loop for maximizing thermodynamic efficiency, one for minimizing radiator area, and a final loop for minimizing overall power system mass. Using the method of steepest ascent, the code sweeps through the pressure ratio space repeatedly, each time with smaller iteration step sizes, so that the three optimum pressure ratios can be obtained to any desired accuracy for each of the objective functions referred to above (i.e., maximum thermodynamic efficiency, minimum radiator area, and minimum system mass). Two separate options for the power system heat source are available:

(1) A nuclear fission reactor can be used. It is provided with a radiation shield (composed of a lithium hydride (LiH) neutron shield and tungsten (W) gamma shield). Suboptions can be used to select the type of reactor (i.e., fast spectrum liquid metal cooled or epithermal high-temperature gas reactor (HTGR)).

(2) A solar heat source can be used. This option includes a parabolic concentrator and heat receiver for raising the temperature of the recirculating working fluid.

A useful feature of the code modifications is that key cycle parameters are displayed, including the overall system specific mass in kilograms per kilowatt and the system specific power in watts per kilogram, as the results for each temperature ratio are computed. As the minimum mass temperature ratio is encountered, a message is printed out. Several levels of detailed information on cycle state points, subsystem mass results, and radiator temperature profiles are stored for this temperature ratio condition and can be displayed or printed by users.

Lewis contact:
Albert J. Juhasz, (216) 433–6134, Albert.J.Juhasz@grc.nasa.gov

Author: Albert J. Juhasz

Headquarters program office:
OSS (ATMS)

Programs/Projects:
SSP, Lunar Base Power System, Mars Base Power, multimegawatt power system for interplanetary electric propulsion systems

Lightweight Battery Charge Regulator Used to Track Solar Array Peak Power

A battery charge regulator based on the series-connected boost regulator (SCBR) technology has been developed for high-voltage spacecraft applications. The SCBR regulates the solar array power during insolation to prevent battery overcharge or undercharge conditions. It can also be used to provide regulated battery output voltage to spacecraft loads if necessary. This technology uses industry-standard dc-dc converters and a unique interconnection to provide size, weight, efficiency, fault tolerance, and modularity benefits over existing systems.

2.5-kW Series-connected boost regulator.

The high-voltage SCBR shown in the photograph has demonstrated power densities of over 1000 watts per kilogram (W/kg). Using four 150-W dc-dc converter modules, it can process 2500 W of power at 120 Vdc with a minimum input voltage of 90 Vdc. Efficiency of the SCBR was 94 to 98 percent over the entire operational range.

Internally, the unit is made of two separate SCBR's, each with its own analog control circuitry, to demonstrate the modularity of the technology. The analog controllers regulate the output current and incorporate the output voltage limit with active current sharing between the two units. They also include voltage and current telemetry, on/off control, and baseplate temperature sensors.

For peak power tracking, the SCBR was connected to a LabView-based data acquisition system for

telemetry and control. A digital control algorithm for tracking the peak power point of a solar array was developed using the principle of matching the source impedance with the load impedance for maximum energy transfer. The algorithm was successfully demonstrated in a simulated spacecraft electrical system at the Boeing PhantomWorks High Voltage Test Facility in Seattle, Washington. The system consists of a 42-string, high-voltage solar array simulator, a 77-cell, 80-ampere-hour (A-hr) nickel-hydrogen battery, and a constant power-load module. The SCBR and the LabView control algorithm successfully tracked the solar array peak power point through various load transients, including sunlight discharge transients when the total load exceeded the maximum solar array output power.

Lewis contacts:
James F. Soeder, (216) 433–5328, James.F.Soeder@grc.nasa.gov; and Robert M. Button, (216) 433–8010, Robert.M.Button@grc.nasa.gov

Authors: James F. Soeder and Robert M. Button

Headquarters program office: OSS (ATMS)

Programs/Projects: High-voltage Spacecraft; satellites powered by solar arrays; other solar array and battery applications

International Low-Earth-Orbit Spacecraft Materials Test Program Initiated for Better Prediction of Durability and Performance

Spacecraft in low Earth orbit (LEO) are subjected to many components of the environment, which can cause them to degrade much more rapidly than intended and greatly shorten their functional life. The atomic oxygen, ultraviolet radiation, and cross contamination present in LEO can affect sensitive surfaces such as thermal control paints, multilayer insulation, solar array surfaces, and optical surfaces. The LEO Spacecraft Materials Test (LEO–SMT) program is being conducted to assess the effects of simulated LEO exposure on current spacecraft materials to increase understanding of LEO degradation processes as well as to enable the prediction of in-space performance and durability. Using ground-based simulation facilities to test the durability of materials currently flying in LEO will allow researchers to compare the degradation evidenced in the ground-based facilities with that evidenced on orbit. This will allow refinement of ground laboratory test systems and the development of algorithms to predict the durability and performance of new materials in LEO from ground test results. Accurate predictions based on ground tests could reduce development costs and increase reliability.

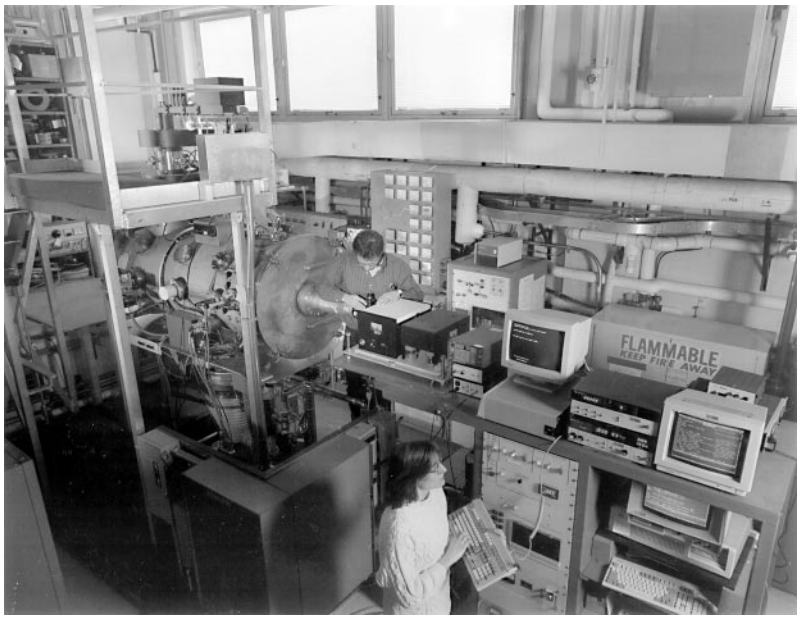

Directed atomic oxygen and synergistic vacuum ultraviolet radiation exposure facility at NASA Lewis can measure the reflectance of samples from 250 to 2500 nm while they are in the vacuum chamber.

The wide variety of national and international materials being tested represent materials being functionally used on spacecraft in LEO. The more varied the types of materials tested, the greater the probability that researchers will develop and validate predictive models for spacecraft long-term performance and durability. Organizations that are currently participating in the program are ITT Research Institute (USA), Lockheed Martin (USA), MAP (France), SOREQ Nuclear Research Center (Israel), TNO Institute of Applied Physics (The Netherlands), and UBE Industries, Ltd. (Japan). These represent some of the major suppliers of thermal control and sensor materials

currently flying in LEO. The participants provide materials that are exposed to selected levels of atomic oxygen, vacuum ultraviolet radiation, contamination, or synergistic combined environments at the NASA Lewis Research Center. Changes in characteristics that could affect mission performance or lifetime are then measured. These characteristics include changes in mass, solar absorptance, and thermal emittance. The durability of spacecraft materials from U.S. suppliers is then compared with those of materials from other participating countries. Lewis will develop and validate performance and durability prediction models using this ground data and available space data. NASA welcomes the opportunity to consider additional international participants in this program, which should greatly aid future spacecraft designers as they select materials for LEO missions.

Lewis contacts:
Bruce A. Banks, (216) 433–2308, Bruce.A.Banks@grc.nasa.gov; and Sharon K. Rutledge, (216) 433–2219, Sharon.K.Rutledge@grc.nasa.gov

Author: Sharon K. Rutledge

Headquarters program office: OSS (ATMS)

Programs/Projects: ISS, EOS

Retrieval of Mir Solar Array

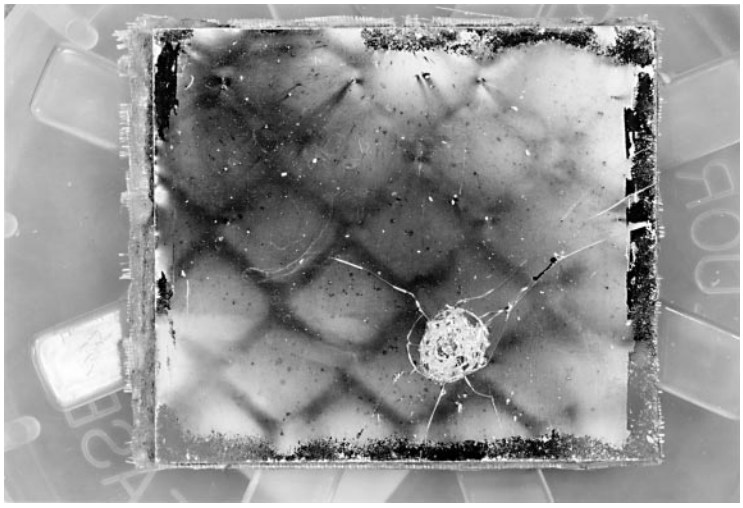

Solar reflector on the back of one of the Mir solar cells, showing a micrometeoroid impact and contamination darkening in areas not shielded by the woven mesh on the back of the array (net pattern).

A Russian solar array panel removed in November 1997 from the nonarticulating photovoltaic array on the Mir core module was returned to Earth on STS–89 in January 1998. The panel had been exposed to low Earth orbit (LEO) for 10 years prior to retrieval. The retrieval provided a unique opportunity to study the effects of the LEO environment on a functional solar array. To take advantage of this opportunity, a team composed of members from RSC–Energia (Russia), the Boeing Company, and the following NASA Centers—Johnson Space Center, Kennedy Space Center, Langley Research Center, Marshall Space Flight Center, and Lewis Research Center—was put together to analyze the array. After postretrieval inspections at the Spacehab Facility at Kennedy in Florida, the array was shipped to Lewis in Cleveland for electrical performance tests, closeup photodocumentation, and removal of selected solar cells and blanket material. With approval from RSC–Energia, five cell pairs and their accompanying blanket and mesh material, and samples of painted handrail materials were selected for removal on the basis of their ability to provide degradation information. Sites were selected that provided different sizes and shapes of micrometeoroid impacts and different levels of surface contamination. These materials were then distributed among the team for round robin testing.

A preliminary examination of the solar array panel indicated significant darkening and diffuse light scattering on the surface of the panel and structural members. By their location and appearance, the darkened surfaces appear to be silicone contamination from adhesives used to assemble the solar array panel. NASA Lewis is performing tests to look at the contamination on the array and to determine the effect of atomic oxygen and vacuum ultraviolet radiation on contaminant fixation. Two samples have been evaluated to date—a handrail section (white-painted aluminum) and a woven polymer fabric used as an overwrap tape on a handrail. Both samples had visible dark-brown contamination. Optical microscopy revealed mud-tile-like crazing patterns in the contaminated areas. Field emission microscopy showed that the contaminant layer was very thick (approximately 1.6 μm in some areas) and had spalled off in some regions. Energy-dispersive spectroscopy confirmed that the contaminant layer on both the handrail and the overwrap tape was silicon oxides (SiO_x) resulting from the oxidation of silicone.

Results are being shared with the other team members, who are each performing a different analysis, such as micrometeoroid and

debris impact measurements and electrical measurements. Degradation mechanisms described through this analysis will provide valuable information that can be used in predicting the performance of solar arrays on the International Space Station and that could prevent contamination of the level observed on the Mir array.

Lewis contacts:
Bruce A. Banks, (216) 433–2308, Bruce.A.Banks@grc.nasa.gov;
Kim K. de Groh, (216) 433–2297, Kim.K.deGroh@grc.nasa.gov; and
Sharon K. Rutledge, (216) 433–2219, Sharon.K.Rutledge@grc.nasa.gov

Authors:
Sharon K. Rutledge and Kim K. de Groh

Headquarters program office:
OSS (ATMS)

Programs/Projects: ISS

Thermal Control Replacement Materials Evaluated for Durability and Selected for the Hubble Space Telescope

During the Hubble Space Telescope (HST) second servicing mission, astronauts noticed that the outer layer of the multilayer insulation (MLI) was cracked in many locations around the telescope. The insulation's outer layer is composed of 5-mil (0.127 mm) Teflon FEP (DuPont; fluorinated ethylene propylene) with vapor-deposited aluminum (VDA) on the backside. The MLI blankets, which are used on over 80 percent of the external surface of the telescope, provide passive thermal control for equipment. Two large cracks were observed on the light shield directly above the high gain antenna. The upper light shield crack propagated from a cut placed in the blanket during installation around a handrail standoff. Two cracks propagated almost normal to each other, with the outer layer curling tightly as the cracks propagated. A second much larger vertical crack had started to curl and lift away from the telescope, as seen in the figure. MLI on the equipment bays was cracked extensively also, and in some areas it had pulled away from the bay. Continued degradation of the equipment bay insulation would potentially cause limited observations because of housekeeping boxes; for example, the data interface unit could overheat during some portions of the year, in certain sun angles.

Photograph of Hubble Space Telescope taken during the second servicing mission, showing the very large, vertical light shield cracked area and the tightly curled upper light shield cracked area.

The tightly curled, cracked FEP/VDA on the upper light shield was retrieved by astronauts and found to be severely embrittled, as witnessed by ground testing. The NASA Goddard Space Flight Center organized a Hubble Space Telescope MLI Failure Review Board, which included three members from Lewis, to (1) determine the damage mechanism of the (FEP/VDA) in the telescope's orbit environment, (2) predict the condition of the MLI at the time of the next servicing mission, and (3) recommend a replacement thermal control outer layer material to be installed on the telescope during subsequent servicing missions. The Failure Review Board chose candidate thermal control replacement materials by using a multiplicative process recommended by the NASA Lewis Research Center. Ten candidate materials were tested for environmental durability under various exposures and durations as overseen by Goddard and Lewis. Lewis conducted x-ray radiation exposure, thermal cycling under load, and large-sample thermal cycling of candidate materials. Lewis' durability testing of candi-

date replacement materials and involvement on the Failure Review Board had a direct impact on the choice of the replacement thermal control material to be placed on the Hubble Space Telescope during subsequent servicing missions in 2000 and 2003. The recommended replacement thermal control material chosen by the review board and adopted by the Hubble Space Telescope project office is 5-mil FEP/VDA bonded with a low-outgassing ultraviolet-durable adhesive to a Nomex (DuPont) scrim.

Lewis contact:
Kim K. de Groh, (216) 433–2297, Kim.K.deGroh@grc.nasa.gov

Authors:
Kim K. de Groh, Bruce A. Banks, and Patricia A. Hansen

Headquarters program office: OSS (ATMS)

Programs/Projects: HST

Effects Investigated of Ambient High-Temperature Exposure on Alumina-Titania High-Emittance Surfaces

Solar-dynamic space power systems require durable, high-emittance surfaces on a number of critical components, such as heat receiver interior surfaces and parasitic load radiator (PLR) elements. An alumina-titania coating, which has been evaluated for solar-dynamic heat receiver canister applications, has been chosen for a PLR application (an electrical sink for excess power from the turboalternator/compressor) because of its demonstrated high emittance and high-temperature durability in vacuum. Under high vacuum conditions ($\pm 10^{-6}$ torr), the alumina-titania coating was found to be durable at temperatures of 1520 °F (827 °C) for ≈2700 hours with no degradation in optical properties. This coating has been successfully applied to the 2-kW solar-dynamic ground test demonstrator at the NASA Lewis Research Center, to the 500 thermal-energy-storage containment canisters inside the heat receiver and to the PLR radiator. The solar-dynamic demonstrator has successfully operated for over 800 hours in Lewis' large thermal/vacuum space environment facility, demonstrating the feasibility of solar-dynamic power generation for space applications.

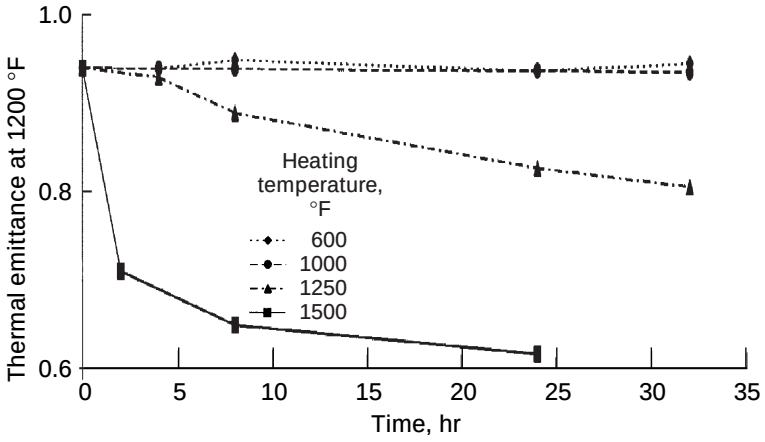

Thermal emittance (at 1200 °F) versus time of alumina-titania-coated samples that were heated in air at various temperatures.

Although the alumina-titania coating has operated successfully in the solar-dynamic ground test demonstrator system, solar-dynamic flight PLR hardware would require ambient pressure operation to verify proper system electrical function and to check out alternator control software. If operation of the PLR in air decreases the emittance, it will operate at a higher temperature than desired while on orbit. This could shorten the PLR's life, and possibly damage the elements. Therefore, a program was conducted at Lewis to test the high-temperature durability of the alumina-titania coating in air. Sixteen alumina-titania-coated Incoloy samples were prepared, and fifteen were exposed to high temperatures (316 °C (600 °F) to 816 °C (1500 °F)) for various times (2 to 32 hours). Samples were characterized prior to and after heat treatment for reflectance, solar absorptance, room temperature emittance, and emittance at 1200 °F (649 °C). Samples also were examined for physical defects and surface chemistry using optical microscopy, scanning electron microscopy operated with an energy dispersive spectroscopy (EDS) system, and x-ray photoelectron spectroscopy (XPS).

Visual examination of the heat-treated samples showed a whitening of samples exposed to temperatures of 1000 °F (538 °C) and above. Correspondingly, the optical properties of these samples were degraded. Decreases in thermal emittance at 1200 °F are shown in the graph. A sample exposed to 1500 °F (816 °C) for 24 hours appeared white, and the thermal emittance at 1200 °F had decreased from the non-heat-treated value of 0.94 to 0.62. The coating on this sample was embrittled and spalling off the substrate in several locations. On the basis of this research, we do not recommend that components with alumina-titania coatings be operated at temperatures above 600 °F (316 °C) in air because optical degradation will occur, and structure degradation of the coating may occur also. These results also indicate that components with the alumina-titania coating are likely to experience optical property degradation with atomic oxygen exposure in space. Therefore, the atomic oxygen durability of this coating needs to be assessed prior to use on surfaces directly exposed to atomic oxygen in the low-Earth-orbit space environment.

Lewis contact:
Kim K. de Groh, (216) 433–2297, Kim.K.deGroh@grc.nasa.gov

Authors:
Kim K. de Groh and Daniela C. Smith

Headquarters program office:
OSS (ATMS)

Programs/Projects:
SDFD, SD GTD, future solar dynamic power systems and systems utilizing heat received technology

Polymers Erosion and Contamination Experiment Being Developed

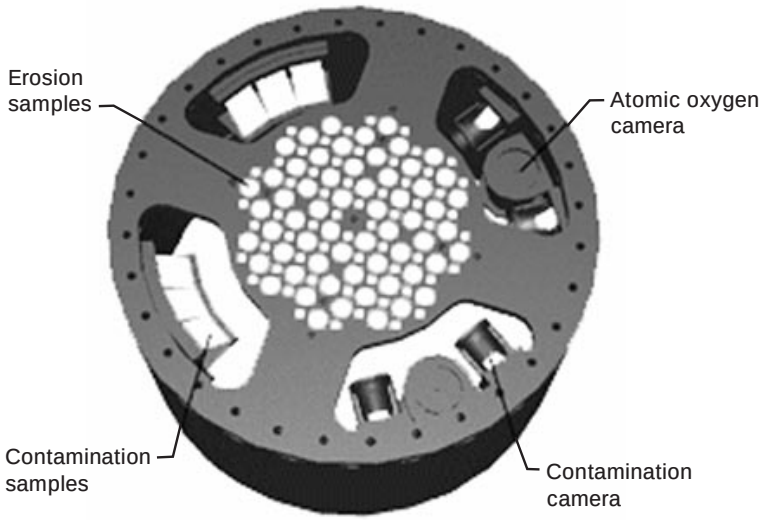

Schematic diagram of PEACE showing polymer erosion samples, silicone contamination samples, atomic oxygen pinhole cameras, and contamination pinhole cameras.

The Polymers Erosion and Contamination Experiment (PEACE) is currently being developed at the NASA Lewis Research Center by the Electro-Physics Branch in conjunction with students and faculty from Hathaway Brown School in Cleveland. The experiment is a Get Away Special Canister shuttle flight experiment sponsored by the American Chemical Society. The two goals of this experiment are (1) to measure ram atomic oxygen erosion rates of approximately 40 polymers that have potential use in space applications and (2) to validate a method for identifying sources of silicone contamination that occur in the shuttle bay. Equipment to be used in this flight experiment is shown in the schematic diagram.

Spacecraft materials subjected to attack by atomic oxygen in the space environment experience significant degradation over the span of a typical mission. Therefore, learning the rates of atomic oxygen erosion of a wide variety of polymers would be of great benefit to future missions. PEACE will use two independent techniques to determine the atomic oxygen erosion rates of polymers. Large (1-in.-diameter) samples will be used for obtaining mass loss. Preflight and postflight dehydrated masses will be obtained, and the mass lost during flight will be determined. Small (0.5-in.-diameter) samples will be protected with isolated particles (such as NaCl crystals) and then exposed to the space environment. After flight, the protective particles will be removed (washed off) and atomic force microscopy (AFM) will be used to measure the erosion depth from protected mesas. Erosion depth measurements are more sensitive than traditional mass measurements

and are very useful for materials with low erosion yields or with very low fluence missions.

PEACE will validate silicone contamination sources by using special contamination pinhole cameras with views of three different types of silicones. Six silicone samples will be viewed—three with atomic oxygen exposure and three without atomic oxygen exposure. The atomic oxygen interaction with the silicone should result in greater contamination; this can be validated with the cameras. The contamination cameras will also have a view of atomic oxygen, for atomic oxygen fixing of the contamination. Scanning ellipsometry will be used to produce an image of the source of contaminants. Using pinhole cameras to detect sources of silicone contamination will provide a model for possible use in future shuttle operations.

Three students from Hathaway Brown School spent the 1998 summer at Lewis, and five students worked during the 1998–1999 school year, designing the sample configuration, ordering samples, and learning some of the technical aspects of putting together an experiment. Members of the Electro-Physics Branch and Dynacs Engineering Co., Inc., are overseeing the development of the experiment, the faculty from Hathaway Brown School are coordinating the students' efforts, and the Space Flight Projects Branch is serving as the project manager.

Lewis contact:
Kim K. de Groh, (216) 433–2297, Kim.K.deGroh@grc.nasa.gov

Authors:
Kim K. de Groh, Bruce A. Banks, Elyse A. Baney-Barton, Edward Sechkar, and Patricia Hunt

Headquarters program office:
OSS (ATMS)

Programs/Projects: ISS, MPTE, future low-Earth-orbit satellites

Synchrotron Vacuum Ultraviolet Light and Soft X-Ray Radiation Effects on Aluminized Teflon FEP Investigated

Since the Hubble Space Telescope (HST) was deployed in low Earth orbit in April 1990, two servicing missions have been conducted to upgrade its scientific capabilities. Minor cracking of second-surface metalized Teflon FEP (DuPont; fluorinated ethylene propylene) surfaces from multilayer insulation (MLI) was first observed upon close examination of samples with high solar exposure retrieved during the first servicing mission, which was conducted 3.6 years after deployment. During the second HST servicing mission, 6.8 years after deployment, astronaut observations and photographic documentation revealed significant cracks in the Teflon FEP layer of the MLI on both the solar- and anti-solar-facing surfaces of the telescope. NASA Goddard Space Flight Center directed the efforts of the Hubble Space Telescope MLI Failure Review Board, whose goals included identifying the low-Earth-orbit environmental constituent(s) responsible for the cracking and embrittling of Teflon FEP which was observed during the second servicing mission. The NASA Lewis Research Center provided significant support to this effort.

Because soft x-ray radiation from solar flares had been considered as a possible cause for the degradation of the mechanical properties of Teflon FEP (ref. 1), the effects of soft x-ray radiation and vacuum ultraviolet light on Teflon FEP were investigated. In this Lewis-led effort, samples of Teflon FEP with a 100-nm layer of vapor-deposited aluminum (VDA) on the backside were exposed to synchrotron radiation of various vacuum ultraviolet and soft x-ray wavelengths between 18 nm (69 eV) and 0.65 nm (1900 eV). Synchrotron radiation exposures were conducted using the National Synchrotron Light Source at Brookhaven National Laboratory. Samples of FEP/VDA were exposed with the FEP surface facing the synchrotron beam. Doses and fluences were compared with those estimated for the 20-yr Hubble Space Telescope mission.

The table summarizes the results of tensile testing of synchrotron radiation-exposed FEP/VDA and gives comparisons to samples retrieved from the HST. As indicated in the table, specimens with the worst damage—those with a loss of elongation greater than 50 percent—received synchrotron exposure doses significantly in excess of HST's 20-yr lifetime estimated dose. However, these samples did not experience the complete loss of elongation shown by the samples retrieved from the telescope, which were exposed to the space environment for 6.8 years. This indicates that, at HST 6.8-yr equivalent exposure doses, using synchrotron radiation between 69 and 1900 eV, it is not possible to produce the extent of degradation observed for HST space-exposed materials. Some of the least-damaged specimens, those with less than 10-percent loss of elongation, were also exposed to radiation doses significantly in excess of the HST

SUMMARY OF TENSILE TESTING OF SYNCHROTRON-EXPOSED FEP/VDA SAMPLES AND COMPARISON TO SAMPLES RETRIEVED FROM THE HST

Energy, eV	Attenuation length,[b] μm	Fluence, J/m^2	Sample dose/ HST 20-yr x-ray dose	Loss of ultimate tensile strength UTS, percent	Loss of elongation, percent
Most damaged: >50 percent loss of elongation					
1489	2.74	95 900	1482[c]	28	83
1489	2.74	16 100	249[c]	30	67
290	.262	1 600	207[c]	26	66
700[a]	.403	1 500	136[c]		
290	.262	1 600	216[c]	27	59
700[a]	.403	1 500	137[c]		
Least damaged: <10 percent loss of elongation					
69	0.033	5 300	5638[c]	–0.2	1.5
1489	2.74	200	2.5[c]	–5.5	–7.2
1489	2.74	8 200	127[c]	–6.7	–7.7
1900	5.36	3 000	27.5[c]	–.2	–2.0
Samples retrieved from HST					
1500 to 25 000	------	225	0.32[d]	42	46
				37	68
1500 to 25 000	------	255	.36[d]	50	100
				92	100

[a]Samples were exposed sequentially to 290- and 700-eV radiation.
[b]Attenuation length for a specific energy of radiation is defined as the depth into material where radiation intensity has been reduced to 1/e times the intensity at the surface.
[c]Sample dose is that absorbed at an attenuation length of synchrotron exposure energy. The HST 20-yr x-ray dose is for x-rays in the energy range 1.5 to 12 keV absorbed within the attenuation length for the synchrotron exposure energy.
[d]Dose absorbed within the full 127-μm specimen thickness for the range of x-ray radiation energies between 1.5 and 25 keV.

20-yr estimated dose. Although exposure to synchrotron radiation in the vacuum ultraviolet and soft x-ray range of energies can degrade the mechanical properties of Teflon FEP, this radiation alone could not be the cause for the severe degradation of FEP surfaces that was observed after the 6.8-yr exposure on the Hubble Space Telescope. Other environmental factors, such as continuum x-ray radiation of energies up to 10 keV, electron and proton radiation, thermal cycling, and synergistic effects of radiation and thermal cycling, have also been investigated by NASA Lewis and NASA Goddard. Exposure to electron and proton radiation followed by thermal cycling similar to HST mission exposures caused greater degradation than exposure to radiation alone. However, further testing is required to positively identify the environmental exposure conditions responsible for the severe degradation of the FEP/VDA material retrieved after 6.8-yr exposure on the HST.

Reference

1. Milintchouk, A., et al.: Influence of X-Ray Solar Flare Radiation on Degradation of Teflon“ in Space. J. Spacecr. Rockets, vol. 34, no. 4, Jul.-Aug. 1997, pp. 542–548.

Lewis contact:
Joyce A. Dever, (216) 433–6294, Joyce.A.Dever@grc.nasa.gov

Goddard contact: Jacqueline A. Townsend, (301) 286–6685, jtownsend@pop300.gsfc.nasa.gov

Authors:
Joyce A. Dever, Jacqueline A. Townsend, Dr. James R. Gaier, and Alice I. Jalics

Headquarters program office: OSS

Programs/Projects: HST

Teflon FEP Analyzed After Retrieval From the Hubble Space Telescope

Hubble Space Telescope light shield sample retrieved during the second servicing mission; shown prior to removal.

During the Hubble Space Telescope (HST) Second Servicing Mission, 6.8 years after the telescope was deployed in low Earth orbit, degradation of unsupported Teflon FEP (DuPont; fluorinated ethylene propylene), used as the outer layer of the multilayer insulation (MLI) blankets, was evident as large cracks on the telescope light shield. A sample of the degraded outer layer (see the photograph) was retrieved during the second servicing mission and returned to Earth for ground testing and evaluation. Also retrieved was a Teflon FEP radiator surface from a cryogen vent cover that was exposed to the space environment on the aft bulkhead of the HST. NASA Goddard Space Flight Center directed the efforts of the Hubble Space Telescope MLI Failure Review Board, whose goals included determining the FEP degradation mechanisms. As part of the investigations into the degradation mechanisms, specimens retrieved from the first and second HST servicing missions, 3.6 and 6.8 years after launch, respectively, were characterized through exhaustive mechanical, optical, and chemical testing. Testing led by Goddard included scanning electron microscopy, optical microscopy, tensile testing, solar absorptance measurements, time-of-flight secondary ion mass spectroscopy (TOF–SIMS), Fourier transform infrared microscopy (μ-FTIR), attenuated total reflectance infrared microscopy (ATR/FTIR), and x-ray diffraction (XRD). The NASA Lewis Research Center contributed significantly to the analysis of the retrieved HST materials by leading efforts and providing results of bend testing, surface microhardness measurements, x-ray photoelectron spectroscopy, solid-state nuclear magnetic resonance spectroscopy, and density measurements. Other testing was conducted by Nano Instruments, Inc., and the University of Akron.

Results of mechanical properties testing of FEP specimens retrieved after 3.6 and 6.8 years of HST exposure indicated significant decrease in tensile test elongation at break and reduced tolerance to strain upon bending. Space-exposed samples also showed increased surface hardness that decreased with depth. Solar absorptance of the space-exposed FEP was slightly increased. In general, analyses showed that all of the retrieved specimens underwent chain scission. Evidence of increased crystallinity was found only in the light shield specimen from the second servicing mission, which had curled on orbit and thus experienced a significantly higher temperature than is typical for the HST light shield. Heating specimens from the first servicing mission also generated increased crystallinity. The conclusions of the Hubble Space Telescope MLI Failure Review Board were based on the combined evidence of HST damage and data uncovered in ground-based experiments. The review board concluded the following:

"The observations of HST MLI and ground testing of pristine samples indicate that thermal cycling with deep-layer damage from electron and proton radiation are necessary to cause the observed Teflon FEP embrittlement and the propagation of cracks along stress concentrations. Ground testing and analysis of retrieved MLI indicate that damage increases with the combined total dose of electrons, protons, UV, and x-rays along with thermal cycling."

Tests continue to determine the effects of the higher temperature limit that the second servicing mission MLI specimen experienced.

Lewis contacts:
Joyce A. Dever, (216) 433–6294, Joyce.A.Dever@grc.nasa.gov; and Kim K. de Groh, (216) 433–2297, Kim.K.deGroh@grc.nasa.gov

Goddard contacts:
Patricia A. Hansen, (301) 286–0564, phansen@mscmail.gsfc.nasa.gov; and Jacqueline A. Townsend, (301) 286–6685, jtownsen@pop300.gsfc.nasa.gov

Authors:
Joyce A. Dever, Kim K. de Groh, Jacqueline A. Townsend, Patricia A. Hansen, Bruce A. Banks, Len Wang, and Charles He

Headquarters program office: OSS

Programs/Projects: HST

Highly Conducting Graphite Epoxy Composite Demonstrated

Weight savings as high as 80 percent could be achieved if graphite polymer composites could replace aluminum in structures such as electromagnetic interference shielding covers and grounding planes. This could result in significant cost savings, especially for the mobile electronics found in spacecraft, aircraft, automobiles, and hand-held consumer electronics. However, such composites had not yet been fabricated with conductivity sufficient to enable these applications.

To address this lack, a partnership of the NASA Lewis Research Center, Manchester College, and Applied Sciences, Inc., fabricated nonmetallic composites with unprecedented electrical conductivity. For these composites, heat-treated, vapor-grown graphite fibers were selected which have a resistivity of about 80 μΩ-cm, more than 20 times more conductive than typical carbon fibers. These fibers were then intercalated with iodine bromide (IBr). Intercalation is the insertion of guest atoms or molecules between the carbon planes of the graphite fibers. Since the carbon planes are not highly distorted in the process, intercalation has little effect on mechanical and thermal properties. Intercalation does, however, lower the carbon fiber resistivity to less than 10 μΩ-cm, which is comparable to that of metal fibers.

Scaleup of the reaction was required since the initial intercalation experiments would be carried out on 20-mg quantities of fibers, and tens of grams of intercalated fibers would be needed to fabricate even small demonstration composites. The reaction was first optimized through a time and temperature study that yielded fibers with a resistivity of 8.7±2 μΩ-cm when exposed to IBr vapor at 114 °C for 24 hours. Stability studies indicated that the intercalated fibers rapidly lost their conductivity when exposed to temperatures as low as 40 °C in air. They were not, however, susceptible to degradation by water vapor in the manner of most graphite intercalation compounds. The 1000-fold scaleup experiments concluded that 114 °C was near the optimum temperature, but that the intercalation time needed to be lengthened by a factor of 3.

Laminar composites were hand laid up with the graphite fibers and two different resins, a room temperature epoxy and a cyanate ester resin with a cure temperature of 175 °C. The resistivity of the resulting composites was 200±25 μΩ-cm, nearly a factor of two lower than for similar composites made with intercalated pitch-based fibers. The fibers in the cyanate ester composites did not appear to lose conductivity even though the cure temperature was well above the temperature at which the fibers lost conductivity in air. Although this is the lowest resistivity composite yet fabricated, calculations indicate that it should be possible to use these fibers to make composites that are 6 to 7 times more conductive.

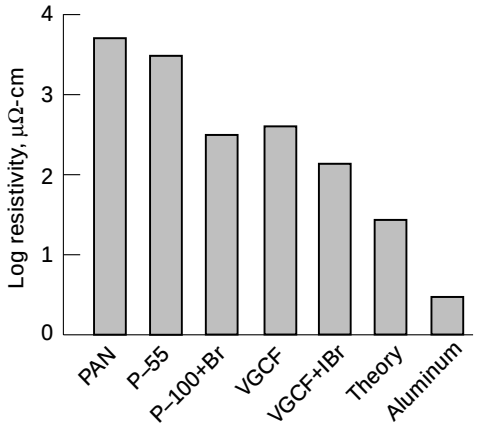

Composite resistivity of different graphite fibers.

Lewis contact: Dr. James R. Gaier, (219) 982–5075 (Feb—May, Sept—Dec); (216) 433–6686 (Jan, Jun—Aug), James.R.Gaier@grc.nasa.gov

Author: Dr. James R. Gaier

Headquarters Program Office: OSS (ATMS)

Programs/Projects: High-conductivity, low-weight applications, such as notebook computers and cell phones

Changes in the Optical Properties of Materials Are Observed After 18 Months in Low Earth Orbit

Opening the Passive Optical Sample Assembly (POSA) experiment after 18 months in low Earth orbit.

Materials located on the exterior of spacecraft in low Earth orbit are subjected to a number of environmental threats, including atomic oxygen, ultraviolet radiation, thermal cycling, and micrometeroid and debris impact. Atomic oxygen attacks materials vulnerable to oxidation. Ultraviolet radiation can break chemical bonds and cause undesirable changes in optical properties. Thermal cycling can cause cracking, and micrometeroid and debris impacts can damage protective coatings. Another threat is contamination. The outgassing of volatile chemicals can contaminate nearby surfaces, changing their thermal control properties. Contaminated surfaces may undergo further change as a result of atomic oxygen and ultraviolet radiation exposure.

The Passive Optical Sample Assembly (POSA) experiment was designed as a risk mitigation experiment for the International Space Station. Samples were characterized before launch, exposed for 18 months on the exterior of Mir, and characterized upon their return. Lessons learned from POSA about the durability of material properties can be applied to the space station and other long-duration missions.

Thirty-two Lewis samples were on POSA–2. The suitcase-sized mounting hardware, which was attached to the shuttle docking module, allowed half of the samples to face Mir and the other half of the samples to face space. Those samples facing space also faced the shuttle when it was docked to Mir.

Postflight evaluation of the samples revealed atomic oxygen erosion, changes in the optical properties of solar absorptance and infrared emittance, and contamination from at least two different sources. Dehydrated Kapton mass loss measurements identified an atomic oxygen fluence of 8.2×10^{19} atoms/cm^2 for the Mir-facing side and 2.1×10^{20} atoms/cm^2 for the space-facing side. The mass of contamination was found to be negligible.

Contamination changed some optical properties. For example, the solar absorptance of aluminum mirror samples increased in all cases, with the increase being greater for the Mir-facing samples. Such increases are undesirable because they cause unwanted heating of spacecraft surfaces. It was also observed that the infrared emittance of thermal control paint samples decreased, with the amount of decrease essentially the same for both the Mir-facing and space-facing samples. Such decreases are undesirable because they diminish the heat-rejection capability of the thermal control paint.

Chemical evaluation of several samples identified a silicon signature. The origin of the silicon is thought to be the outgassing of a silicone paint during one or more zero-eclipse orbits. The source for the other contaminant(s) is still under investigation.

Lewis contact:
Dr. Donald A. Jaworske, (216) 433–2312, Donald.A.Jaworske@grc.nasa.gov

Author: Dr. Donald A. Jaworske

Headquarters program office: OSS (ATMS)

Programs/Projects: ISS, POSA

Low-Temperature Electronic Components Being Developed

In many future NASA missions, such as deep space planetary exploration and the Next Generation Space Telescope, electrical components and systems must operate reliably and efficiently in extremely low temperature environments. Most modern electronic components cannot operate below moderately low operating temperatures (–40 to –55 °C).

The low-temperature electronics program at the NASA Lewis Research Center is focusing on the development and characterization of low-temperature components and the integration of the developed devices into demonstrable very low-temperature (–200 °C) power systems such as dc-dc converters. Such low-temperature electronics will not only tolerate hostile environments but also will reduce system size and weight by eliminating radioisotope heating units, thereby reducing launch cost, improving reliability and lifetime, and increasing energy densities.

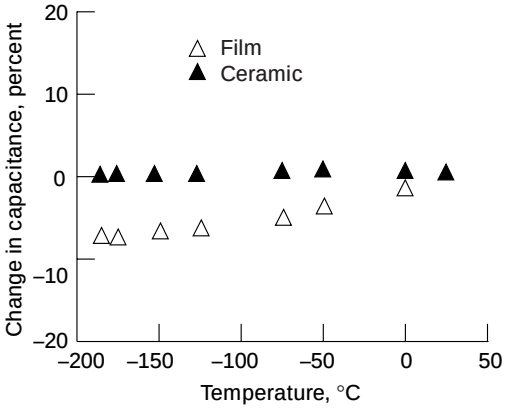

Capacitance of film and ceramic capacitors at 20-kHz versus temperature.

Low-temperature electronic components will also have a great influence on terrestrial applications such as medical instrumentation, magnetic levitation transportation systems, and arctic and antarctic exploration. Lewis researchers are now performing extensive evaluations of commercially available as well as custom-made devices. These include various types of energy storage and signal capacitors, power switching devices, magnetic and superconducting materials, and primary lithium batteries, to name a few. The following photograph shows solid tantalum and ceramic capacitors that were recently evaluated for one of our customers. The components were subjected to screening and then to comprehensive characterization of parameters such as frequency, applied bias, temperature, and multistress conditions. The graph shows the capacitance of film and ceramic capacitors as a function of temperature.

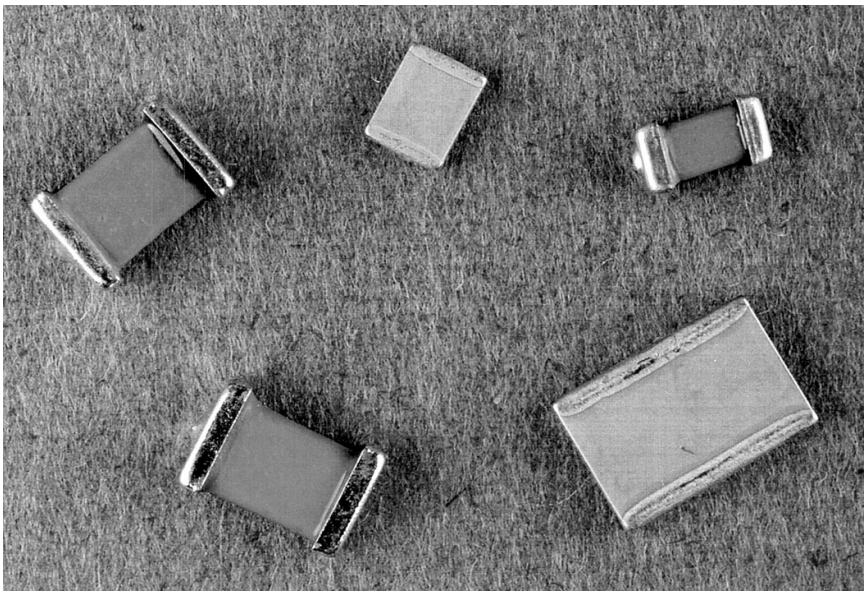

Solid tantalum (darker) and ceramic capacitors. For a color version of this photograph, see the online version of this document (http://www.grc.nasa.gov/WWW/RT1998/5000/5480patterson.htm).

These research and development efforts are being carried out through collaboration with other government agencies, industrial and aerospace companies, and academia. The Low Temperature Electronics Program supports missions and development programs at the NASA Goddard Space Flight Center and the Jet Propulsion Laboratory.

To find out more, visit us on the World Wide Web:
http://www.grc.nasa.gov/WWW/epbranch/ephome.htm (select "Low Temperature Electronics" at the bottom of the list on the left)

Lewis contact:
Richard L. Patterson, (216) 433–8166, Richard.L.Patterson@grc.nasa.gov

Authors:
Richard L. Patterson and Ahmad Hammoud

Headquarters program office:
OSS (ATMS)

Programs/Projects: X2000 (JPL), Next Generation Space Telescope (Goddard), Low Temperature Electronics

Atomic Oxygen Lamp Cleaning Facility Fabricated and Tested

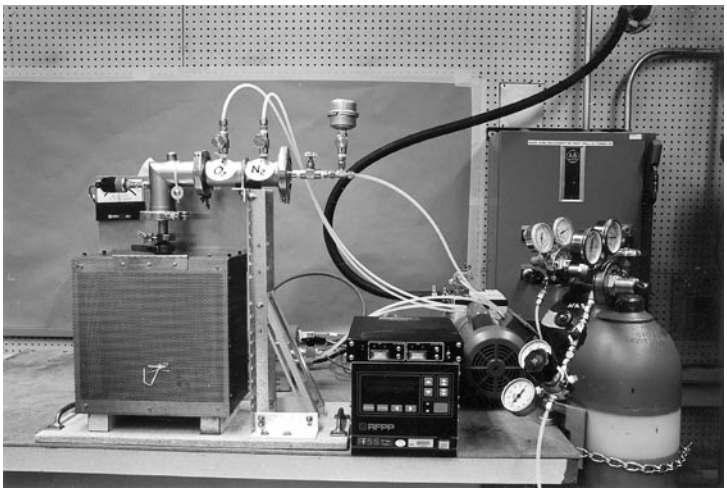

Front view of Atomic Oxygen Lamp Cleaning Facility.

NASA Lewis Research Center's Atomic Oxygen Lamp Cleaning Facility was designed to produce an atomic oxygen plasma within a metal halide lamp to remove carbon-based contamination. It is believed that these contaminants contribute to the high failure rate realized during the production of these lamps.

The facility is designed to evacuate a metal halide lamp and produce a radiofrequency-generated atomic oxygen plasma within it. Oxygen gas, with a purity of 0.9999 percent and in the pressure range of 150 to 250 mtorr, is used in the lamp for plasma generation while the lamp is being cleaned. After cleaning is complete, the lamp can be backfilled with 0.9999-percent pure nitrogen and torch sealed.

The facility comprises various vacuum components connected to a radiation-shielded box that encloses the bulb during operation. Radiofrequency power is applied to the two parallel plates of a capacitor, which are on either side of the lamp. The vacuum pump used, a Leybold Trivac Type D4B, has a pumping speed of 4-m^3/hr, has an ultimate pressure of $<8\times10^{-4}$, and is specially adapted for pure oxygen service. The electronic power supply, matching network, and controller (500-W, 13.56-MHz) used to supply the radiofrequency power were purchased from RF Power Products Inc. Initial test results revealed that this facility could remove the carbon-based contamination from within bulbs.

For more information, visit the Electro-Physics Branch on the World Wide Web:
http://www.grc.nasa.gov/WWW/epbranch/ephome.htm

Lewis contacts:
Edward A. Sechkar, (216) 433–2299, Edward.A.Sechkar@grc.nasa.gov; and Thomas J. Stueber, (216) 433–2218, Thomas.J.Stueber@grc.nasa.gov

Authors: Edward A. Sechkar and Thomas J. Stueber

Headquarters program office:
OSS (ATMS)

Programs/Projects:
Broad applicability to lamp industry—wide variety of glass bulb lamps for lighting and specific wavelength spectral source lamps; technique would assure that hydrocarbon contaminants within the lamp enclosure are not present during sealing and that the lamp function and durability would thereby be improved

Parallel Stirling Converters Being Developed for Spacecraft Onboard Power

Stirling Technology Co., as part of a NASA Lewis Research Center Phase II Small Business Innovation Research contract, has successfully demonstrated paralleling two thermodynamically independent Stirling converters. A system of four Stirling converters is being developed by NASA and the Department of Energy as an alternative high-efficiency radioisotope power source for spacecraft onboard electric power for NASA deep space missions. The high Stirling efficiency, exceeding 20 percent for this application, will greatly reduce the necessary isotope inventory in comparison to the current radioisotope thermoelectric generators (RTG's), significantly reducing mission cost and risk. Stirling is the most developed converter option of the advanced power technologies under consideration.

Previous Stirling development had focused on single converters and had not addressed how to connect multiple converters in a system. However, in most potential space applications, multiple converters are important for reliability and modularity. Thermodynamically independent converters allow one converter to fail without affecting the performance of the other. Finally, the use of multiple converters is important to controlling vibrations, a critical issue for a dynamic space power system. Synchronization of converter pairs operating in an opposed configuration provides balanced operation with minimal vibration.

Synchronization was achieved with two 350-We converters (see the photograph) operating over a wide range of conditions, including simulated degraded operation for one of the two converters. This produced a 40- to 50-fold reduction in vibrations in comparison to an unbalanced converter. Equal power generation between the two converters was shown for normal operation and simulated degradation with constant power input. Successful system operation was demonstrated with the two synchronized converters feeding a battery charger load, as would most likely be used in a radioisotope power system. Transient data taken during various connections and disconnections of the two converters showed that the converters could be synchronized reliably and rapidly. The two converters were connected electrically in parallel and mechanically through external attachments on the cold-end pressure vessels. A mechanical coupler was developed that precisely aligns the two converters and can compensate for any inherent misalignments.

This connection method for multiple converters will now be utilized to connect the prototype converters that are being developed by the Department of Energy and Stirling Technology Co. for potential use in a 150-We Stirling isotope power system.

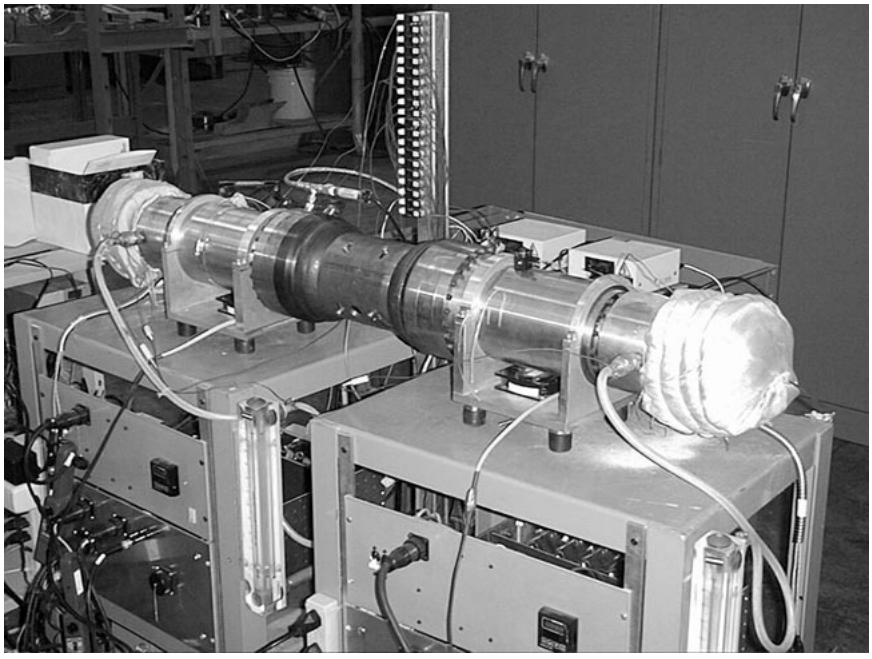

Parallel Stirling converters synchronized for system operation and low vibrations.

For further background information, visit the World Wide Web:

Research at Stirling Technology Co.:
http://www.stirlingtech.com

Research at Lewis:
http://powerweb.grc.nasa.gov/stirling/home.html

Lewis contact:
Lanny G. Thieme, (216) 433–6119,
Lanny.G.Thieme@grc.nasa.gov

Author: Lanny G. Thieme

Headquarters program office: OSS

Programs/Projects:
SBIR, advanced radioisotope power

Inflatable Solar Thermal Concentrator Delivered

Space-based solar thermal power systems are very appealing as a space power source because they generate power efficiently. However, solar thermal (dynamic) systems currently incorporate rigid concentrators that are relatively heavy and require significant packaging volume and robust deployment schemes. In many ways, these requirements make these systems less appealing than photovoltaic systems. As an alternative to solar thermal power systems with rigid concentrators, solar thermal power systems with thin-film inflation-deployed concentrators have low cost, are lightweight, and are efficiently packaged and deployed. Not only are inflatable concentrators suitable for low Earth orbit and geosynchronous orbit applications, but they can be utilized in deep space missions to concentrate solar energy to high-efficiency solar cells.

The objective of this Small Business Innovation effort with SRS Technologies, Inc., was to design, build, demonstrate, and characterize a thin-film, inflatable concentrator that has interfaces for solar thermal power systems. The actual concentrator, which was delivered to the NASA Lewis Research Center in late October 1998, is a 2.0- by 3.0-m off-axis parabolic concentrator with a 90° tilt angle and 30° half angle. The ultimate goal of this effort is to demonstrate, through testing, that inflatable concentrators for power generation are both a viable and desirable alternative to the rigid concentrator designs that are currently being used. Lewis has been working closely with the U.S. Air Force, Edwards Air Force Base, to finalize contractual agreements and test requirements to support joint testing.

The objectives of the test are to (1) quantify the thermal performance and optical performance of the test article in the simulated space environment that is provided by Lewis' Tank 6 Solar Simulator and (2) use the test data to qualify analytical computer models. This will be the first in a series of several planned space environmental tests that Lewis and the Air Force are planning as part of a technology road map for an inflation-rigidized concentrator flight experiment that is currently scheduled for 2001. During the test, thermal performance will be measured via thermocouples on the surface of the inflated concentrator and the support torus. Optical performance will be characterized via flux intensity measurements at the focal plane via a charge-coupled discharge (CCD) camera. Additional performance data will be collected on the catenary strain, torus and canopy pressure, and make-up gas requirements.

1.7- by 2.7-m inflatable concentrator designed and built by SRS Technologies, Inc.

Major activities for the Tank 6 test include

(1) Setup of the test article and test support equipment

(2) Integration of the instrumented test article with Tank 6 data collection equipment and the Thiokol inflation controller

(3) Calibration and verification of data collection, evacuation of the chamber, and thermal cycling and data collection

(4) Repressurization of the chamber, removal and storage of test articles, and restoration of Tank 6 to pretest status

(5) Data reduction

Lewis contact:
Carol M. Tolbert, (216) 433–6167, Carol.M.Tolbert@grc.nasa.gov

Author: Carol M. Tolbert

Headquarters program office: OAT

Programs/Projects:
Launch Services and Space Transportation Program Office at Lewis

Instrumentation and Controls

Acoustic Pyrometry Applied to Gas Turbines and Jet Engines

Internal gas temperature is one of the most fundamental parameters related to engine efficiency and emissions production. The most common methods for measuring gas temperature are physical probes, such as thermocouples and thermistors, and optical methods, such as Coherent Anti Stokes Raman Spectroscopy (CARS) or Rayleigh scattering. Probes are relatively easy to use, but they are intrusive, their output must be corrected for errors due to radiation and conduction, and their upper use temperature is limited. Optical methods are nonintrusive, and they measure some intrinsic property of the gas that is directly related to its temperature (e.g., lifetime or the ratio of line strengths). However, optical methods are usually difficult to use, and optical access is not always available. Lately, acoustic techniques have been receiving some interest as a way to overcome these limitations (ref. 1).

One of these techniques, acoustic pyrometry, is also nonintrusive, is simpler to use than optical pyrometry, and doesn't require optical access. To measure the mean gas temperature between two points, one places a sound (acoustic) source at one point and a microphone at a known distance from the source, then measures the time required for the signal to travel from the source to the microphone. The speed of the sound is the distance divided by the time of flight, and it is directly proportional to the square root of the absolute temperature of the gas.

Measuring gas temperature in the noisy environment of a jet engine, however, might require a very powerful sound source. Instead, an experiment was performed at the NASA Lewis Research Center in collaboration with the University of Nevada at Reno (UNR), to determine the feasibility of using the combustion noise itself as the sound source (ref. 2). The experiment consisted of installing two microphones downstream of the combustion zone of a burner rig, measuring the time of flight of the signal, and calculating the gas temperature. The setup is shown schematically in the accompanying figure. Since no signal was externally introduced at the upstream location, the time of flight had to be determined from the cross correlation of the signals from the two microphones. The upstream and downstream signals were recorded on a two-channel digital audio recorder and processed at the University of Nevada at Reno to calculate the cross correlation between signals $s(t)$ and $r(t)$ and to remove the uncorrelated noise $n(t)$ and $m(t)$, as shown in the figure (where t indicates time). The shape of the cross-correlation function indicated that the signals consisted of wideband random noise. The measured speed of sound for this particular experiment was 787 m/sec, which corresponds to 1270 °C.

Future work will include experiments to determine whether the various operating conditions of an engine have distinct acoustic signatures, raising the possibility of acoustic combustion monitoring as well as temperature measurement.

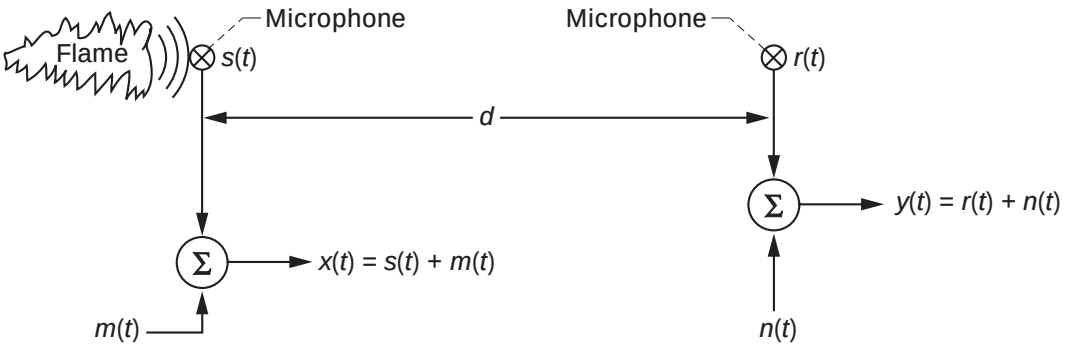

Measurement of sound speed using two microphones.

References

1. Kleppe, J.A.: High Temperature Gas Measurements Using Acoustic Pyrometry. Sens., vol. 13, no. 1, Jan. 1996, pp. 17–22.

2. Kleppe, J.; Sanches, J.; Fralick, G.: The Application of Acoustic Pyrometry to Gas Turbines and Jet Engines. AIAA Paper 98–3611, 1998.

Lewis contact:
Gustave C. Fralick, (216) 433–3645, Gustave.C.Fralick@grc.nasa.gov

Author: Gustave C. Fralick

Headquarters program office: OAT

Programs/Projects:
Propulsion Systems R&T

Scanning Mode Shock Position Sensor Invented and Demonstrated

A flow-visualizing system with a scanning optical beam offers greater advantages than the conventional approaches. In addition to a higher signal-to-noise ratio and lower source power, the scanning permits visualization of weak phenomena such as the scattering and diffraction of light on shocks. Scanning beam flow-visualization techniques were evaluated at the NASA Lewis Research Center for shock position sensing. In an effort to eliminate moving parts, a spectral scanning technique was invented and demonstrated.

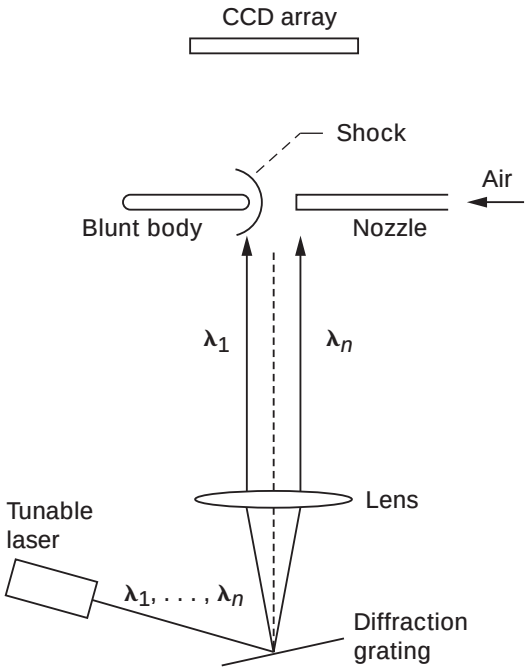

Principle of operation of a spectral scanner.

This spectral scanner consists of a tunable laser, a diffraction grating, and a lens. The tunable laser generates a narrow beam of light whose wavelength changes in a prescribed manner. When a light beam emitted by the laser interacts with the grating, the grating causes the beam to change its direction, producing a phenomenon called diffraction. The new direction depends on the wavelength. This space-wavelength scanning generates a "rainbow" in the time domain, where each "color" appears in its place at a given time. Thus, if the wavelength λ changes monotonically in time, the diffracted beam draws a cone with the apex being the point of impact of the beam on the grating. The lens is positioned so that its focal point coincides with the point of impact. It transforms the cone of light into a number of beams of different wavelengths separated from each other in time and parallel to each other in space. In other words, the lens converts an angular scanning into a linear one. When a beam encounters a shock or another type of inhomogeneity, it diffracts, splits, and forms secondary fringes and tails. The drawing shows a blunt body inserted into a stream of air. The blunt body generates the shock, and a charge-coupled discharge (CCD) camera array behind the shock observes the phenomenon. The following graphs demonstrate splitting a beam of light. At a certain wavelength (left graph) the beam strikes the shock. At a different wavelength (right graph), the light beam misses the shock and the beam shape, in this case, is not affected. This information can be used to determine the location of a shock wave.

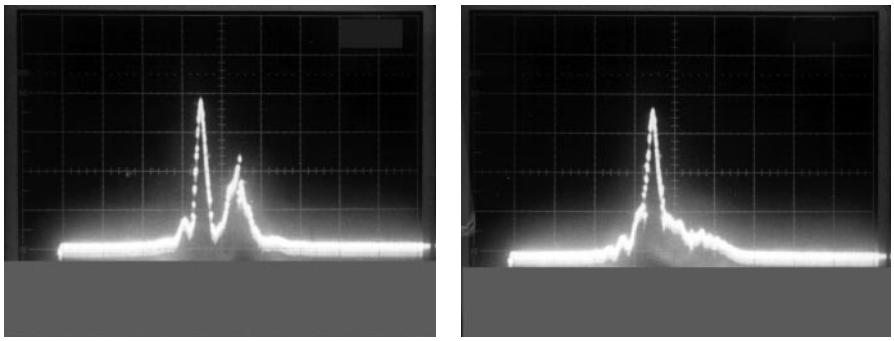

Intensity profiles observed by a CCD array at two wavelengths during the spectral scanning. Left: At the wavelength corresponding to the beam striking the shock. Right: At the wavelength corresponding to the beam missing the shock.

Bibliography

Adamovsky, G.; and Johnson, D.K.: Optical Techniques for Shock Visualization and Detection. Optical Techniques in Fluid, Thermal, and Combustion Flow. S.S. Cha and J.D. Trolinger, eds., SPIE Proceedings, Issue 2546, 1995, pp. 348–357.

Adamovsky, G.: Scanning Mode Sensor for Detection of Flow Inhomogeneities. U.S. Patent 5,715,047, Feb. 1998.

Lewis contact:
Dr. Grigory Adamovsky, (216) 433-3736, Grigory.Adamovsky@grc.nasa.gov

Author: Dr. Grigory Adamovsky

Headquarters program office: OAT

Programs/Projects:
Information Technology Base

Pressure-Sensitive Paint Applied to Ice Accretions

Aircraft icing occurs when a plane flies through a cloud of supercooled water droplets. When the droplets impinge on aircraft components, ice starts to form and accumulate. This accumulation of ice severely increases the drag and lift of the aircraft, and can ultimately lead to catastrophic failures and even loss of life. Knowledge of the air pressures on the surfaces of ice and models in wind tunnels allows researchers to better predict the effects that different icing conditions will have on the performance of real aircraft. The use of pressure-sensitive paint (PSP) has provided valuable information on similar problems in conventional wind tunnel testing.

In NASA Lewis Research Center's Icing Research Tunnel, Lewis researchers recently demonstrated the world's first application of PSP on actual ice formed on a wind tunnel model. This proof-of-concept test showed that a new paint formulation developed under a grant by the University of Washington adheres to both the ice shapes and cold aluminum models, provides a uniform coating that preserves the detailed ice shape structure, and responds to simulated pressure changes.

Three different samples of ice were acquired on a length of aerodynamic tubing attached to the ceiling of the IRT. The samples consisted of glaze ice (–0.7 °C, 30.7 °F), mixed ice (–8.1 °C, 17.4 °F) and rime ice (–15.4 °C, 4.2 °F). Prior to painting, the samples were removed from the wind tunnel and stored in the facility cold room at a temperature of –6.7 °C (20 °F). The PSP was cooled to the cold-room temperature prior to application. Then PSP was applied to the samples using a automotive type spray gun, with cooled nitrogen providing the atomization pressure. After the curing time, which was less than 5 min with this paint, finish details were noted.

A low-pressure nitrogen jet was used to determine the pressure responsiveness of the paint. The nitrogen locally displaces air and simulates a region of low pressure. PSP works on the oxygen quenching principle: in a vacuum, no quenching occurs and the intensity of the paint is at its maximum. At higher air pressures, oxygen quenches the luminescence and the normalized intensity ratio behaves in a linear fashion. The success of this test lends optimism to the final application of PSP to icing research wind tunnel testing.

Lewis contact:
Timothy J. Bencic, (216) 433–5690, Timothy.J.Bencic@grc.nasa.gov

Author: Timothy J. Bencic

Headquarters program office: OAT

Programs/Projects:
Aeronautics Base R&T

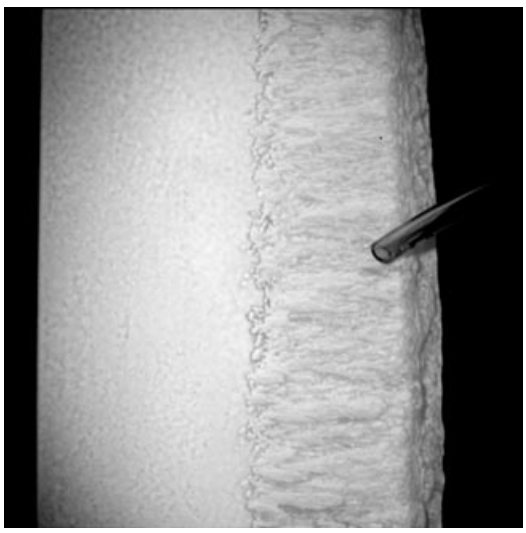

Painted rime ice and the detailed ice structures that remain after the application of the pressure-sensitive paint coating.

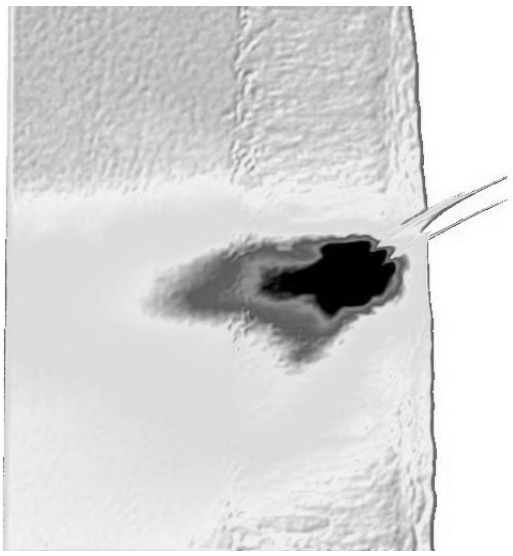

False-color reduced data image of a nitrogen jet impinging on the ice surface. These images are shown in color in the online version of this article (http://www.grc.nasa.gov/WWW/RT1998/5000/5520bencic.htm).

Neural Networks Used to Compare Designed and Measured Time-Average Patterns

Electronic time-average holograms are convenient for comparing the measured vibration modes of fan blades with those calculated by finite-element models. At the NASA Lewis Research Center, neural networks recently were trained to perform what had been a simple visual comparison of the predictions of the design models with the measurements. Finite-element models were used to train neural networks to recognize damage and strain information encoded in subtle changes in the time-average patterns of cantilevers. But, the design-grade finite element models were unable to train the neural networks to detect damage in complex blade shapes. The design-model-generated patterns simply did not agree well enough with the measured patterns. Instead, hybrid-training records, with measured time-average patterns as the input and model-generated strain information as the output, were used to effect successful training. One inspection process is outlined in the figure.

A twisted blade appears at the top left. The full time-average or characteristic pattern of the first vibration mode is shown next. The third and fourth pictures at the top show measured-region time-average patterns for undamaged and cracked blades, where a crack was induced by high-cycle fatigue. These patterns were sampled on a nonuniform finite-element-model grid (not shown). The neural networks processed the samples as often as 30 times/sec. The outputs of the neural networks, in this case, were chordwise strains.

Three kinds of neural-net training have been implemented with software. These are listed in increasing order of effectiveness.

(1) Neural networks can be model trained with model-generated time-average patterns and model-

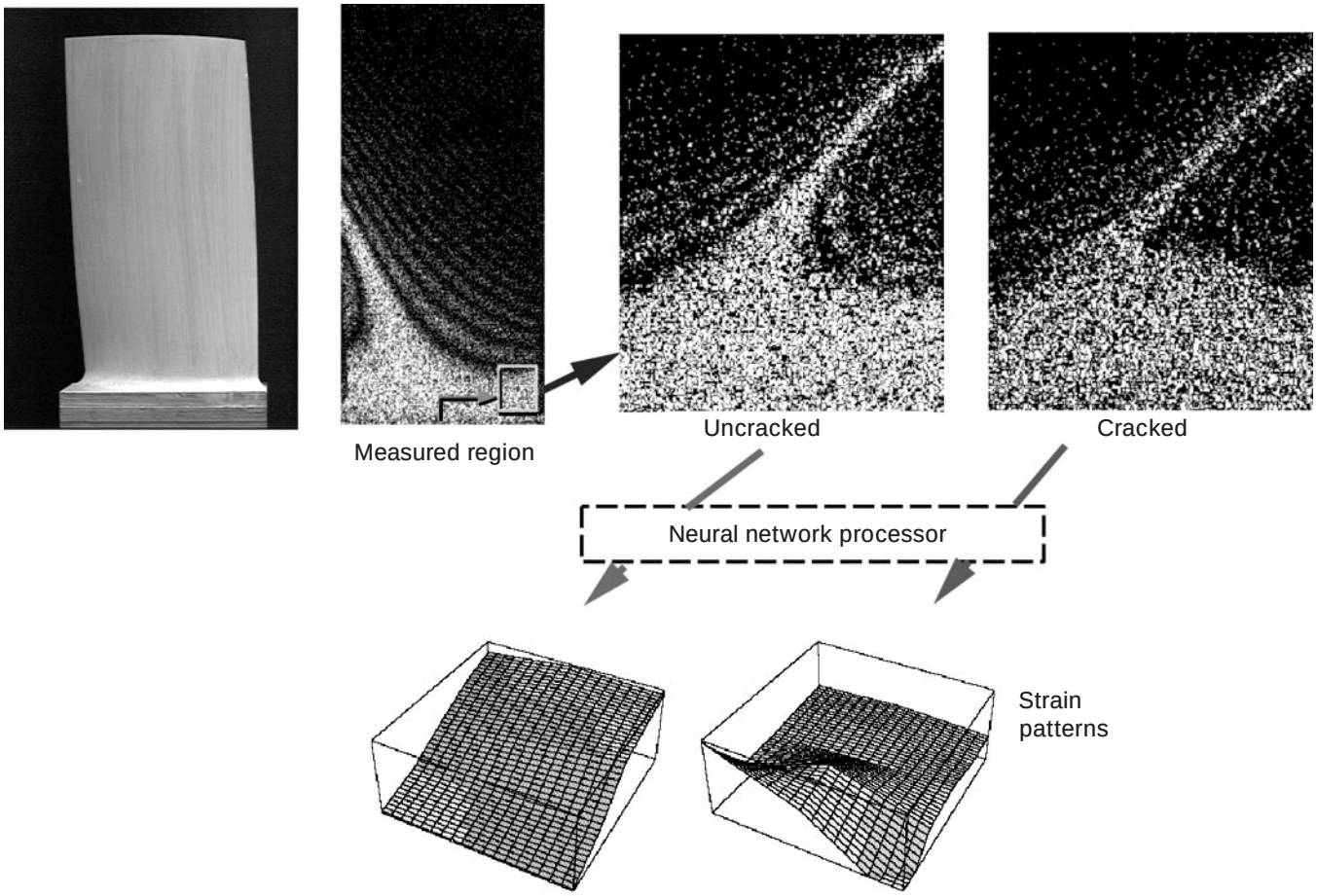

Performance of a measured-input, model-output neural network. This figure is shown in color in the online version of this article (http://www.grc.nasa.gov/WWW/RT1998/5000/5520decker.htm).

generated strain patterns. The effectiveness of this technique depends strongly on the accuracy of the models.

(2) Neural networks can be trained with measured time-average patterns and model-generated strain patterns.

(3) Neural networks can be trained very effectively to categorize measured time-average patterns. Categories can consist of damaged and undamaged fan blades, for example.

We plan to expand this work in the future from nonrotating to rotating fan blades.

Lewis contact:
Dr. Arthur J. Decker, (216) 433–3639, Arthur.J.Decker@grc.nasa.gov

Authors:
Dr. Arthur J. Decker, E. Brian Fite, Oral Mehmed, and Scott A. Thorp

Headquarters program office:
OAT, DDF

Program/Project: AST

Bibliography

Decker, A.J., et al.: Comparison of Computational-Model and Experimental-Example Trained Neural Networks for Processing Speckled Fringe Patterns. NASA TM—1998-208814 (also International Conference on Optical Technology and Image Processing in Fluid, Thermal, and Combustion Flow, Proceedings of VSJ–SPIE98, Yokohama, Japan Dec. 6–10, 1998, CD ROM format only), 1998.

Nondestructive Strain Measurement System Used to Determine Surface Strain on Fibers

Small-diameter structural fibers are being considered as reinforcements for high-temperature ceramic matrix composite materials, and thus they require characterization. At the NASA Lewis Research Center, a nondestructive optical technique was used to determine surface strain on a structural fiber, in real time, as it was pulled in a tensile test machine.

With this technique, interference or speckle patterns from the laser illuminated fiber test specimen are recorded. As the fiber is pulled, its speckle pattern shifts in proportion to the strain, translation, and rotation components of the sample deformation. Shifting speckle patterns are detected in real time by two linear charge-coupled discharge (CCD) camera arrays, and the images are processed by a hardware correlator. Surface strain is selectively detected on fibers with diameters on the order of 100 μm and can be resolved to 19 microstrain.

This system was designed to be robust and compact and generally does not require surface preparation of the structural fibers. For strain detection, two laser beams are positioned incident on the structural fiber being tested, as shown in the photograph, where the test specimen is mounted in a tensile test machine via two coupons. As the fiber is pulled, the speckle pattern produced from each laser beam is detected by one of two CCD arrays located inside the tube on the right side of the photograph.

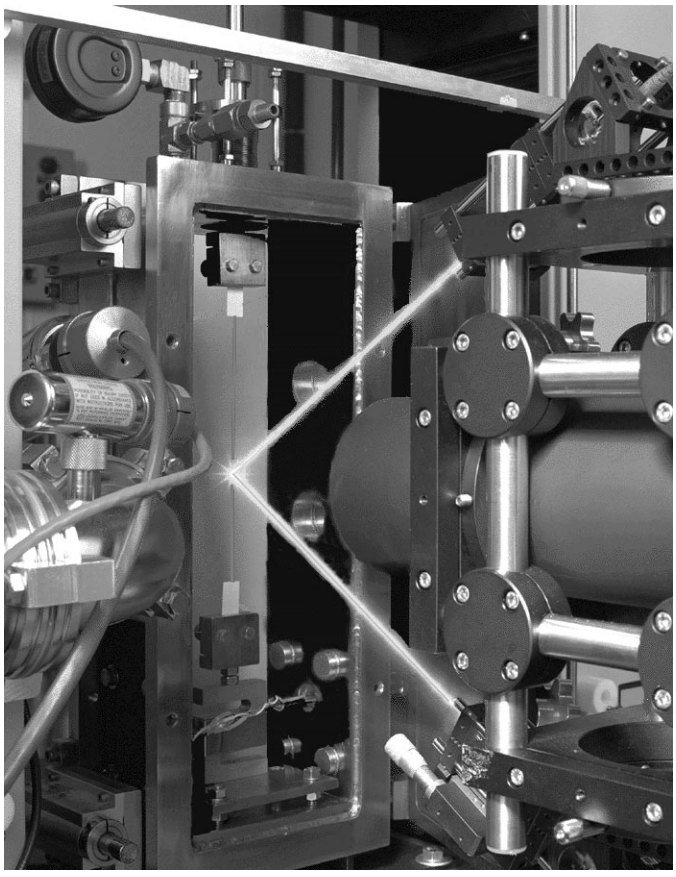

Sensor head optics of laser speckle-shift strain measurement system illuminating test specimen.

Data obtained from three standard specimens (silica, silicon carbide, and tungsten) using the real-time two-color laser speckle-shift system compared well with published values. A linear fit of the raw data was performed to determine the experimental modulus of each specimen (the slope of the stress versus the strain curve). Errors between the known and experimental values were 5.2 percent or less. Numerical results for silica, silicon carbide, and tungsten fibers are given in the following table.

COMPARISON OF EXPERIMENTAL STRAIN MEASUREMENTS TO ACCEPTED VALUES

Sample	Fiber diameter, μm	Accepted modulus, GPa	Experimental modulus, Gpa	Error, percent
Silica	142	73.1	76.9	5.2
Silicon carbide	143	410.0	418.0	2.0
Tungsten	177	380.0	389.0	2.4

The key feature of this system, which separates it from current strain detection systems, is the real-time data analysis. This allows for closed-loop system control based on the detected strain value. Some other advantages of this system follow:

(1) It is easy to use.
(2) Generally, it does not require preparation of specimen surface.
(3) It does not require post-processing.
(4) It will operate at elevated temperatures without modifications.

Because the strain of three standard structural fibers was measured successfully, this system can be used with confidence to characterize unknown samples.

Find out more about this research on the World Wide Web:
http://www.grc.nasa.gov/WWW/OptInstr/stra.html

Lewis contacts:
Dr. Margaret L. Tuma, (216) 433–8665, Margaret.L.Tuma@grc.nasa.gov; and Lawrence G. Oberle, (216) 433–3657, Lawrence.G.Oberle@grc.nasa.gov

Author: Dr. Margaret L. Tuma

Headquarters program office: OAT

Programs/Projects: HITEMP

High Reliability Engine Control Demonstrated for Aircraft Engines

For a dual redundant-control system, which is typical for short-haul aircraft, if a failure is detected in a control sensor, the engine control is transferred to a safety mode and an advisory is issued for immediate maintenance action to replace the failed sensor. The safety mode typically results in severely degraded engine performance. The goal of the High Reliability Engine Control (HREC) program was to demonstrate that the neural-network-based sensor validation technology can safely operate an engine by using the nominal closed-loop control during and after sensor failures. With this technology, engine performance could be maintained, and the sensor could be replaced as a conveniently scheduled maintenance action.

The neural network architecture used here for the sensor validation is the Auto-Associative Neural Network (AANN). This feed-forward network architecture has output data that reproduce the network input data (see the figure to the right). AANN consists of two layers, the mapping layer and the demapping layer, which are interconnected through the bottleneck layer. The mapping layer compresses the data into a reduced-order representation, eliminating redundancies and extracting the key features (principal components) in the data. Reducing the number of dimensions is the key characteristic of this

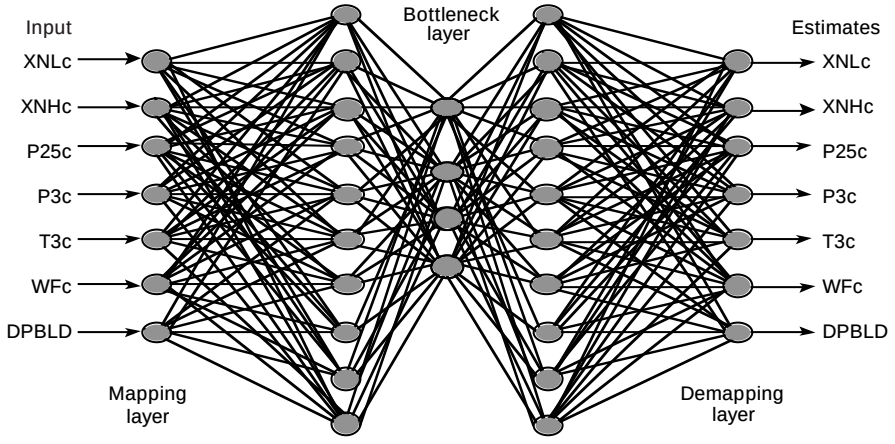

Auto-associative neural network schematic (7–10–4–10–7 network) for turbofan engine estimates.

Variable	Engine parameter
DPBLD	Delta pressure between compressor discharge and bypass duct
P25	Low-pressure compressor inlet pressure
P3	Compressor discharge pressure, burner inlet
T3	Temperature at burner inlet
WF	Fuel flow
XNL	Fan rotor speed
XNH	Core rotor speed

architecture. The demapping layer recovers the encoded information from the principal components. In addition, a fault detection logic identifies the unique sensor failure based on the pattern of the error vector of the input and output of the AANN.

In March 1998 the High Reliability Engine Control program successfully demonstrated the neural-network-based sensor failure detection and accommodation algorithm on a real-time simulation of the Allison's AE3007 engine and its Full Authority Digital Engine Controller (FADEC, ref. 1). Successful accommodation of faults for low- and high-speed rotor speed sensors was demonstrated in the closed-loop engine simulation (see the following flow diagram).

Variable	Engine parameter
ALT	Aircraft altitude
CVGMA	Compressor variable geometry command
CVGFB	Compressor variable geometry feedback
ITT	Interstage turbine temperature
MMVFB	Main metering valve feedback signal
PLA	Power lever angle (thrust command)
P2	Fan inlet pressure
T2	Fan inlet temperature
T2P5	Compressor inlet temperature
WFMA	Main metering valve command
XM	Aircraft Mach number
XNL	Fan rotor speed
XNH	Core rotor speed

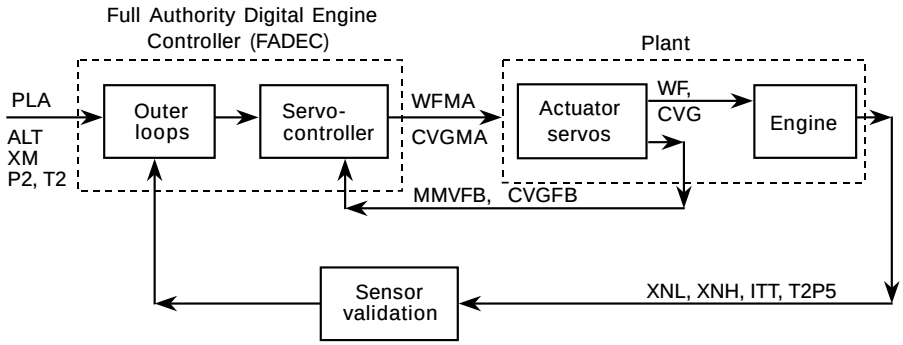

Closed-loop control with sensor validation.

Simulation results show that the neural-network-based sensor validation algorithm can identify both hard and soft sensor failures and can estimate how long the engine control will operate without degradation (ref. 2).

The High Reliability Engine Control program is a collaborative effort between NASA, the Allison Engine Company, and Scientific Monitoring Inc., a small business. In this program, NASA provided the sensor failure detection technology which included the neural network modeling, training, and detection algorithm. Allison Engine Company provided the expertise in AE3007 engine model and control, and Scientific Monitoring Inc. did the system integration and implementation. This program gave these research collaborators an opportunity to further develop and transfer NASA-developed advanced technology for sensor failure detection, isolation, and accommodation to aircraft engine industry.

References

1. Mattern, D.L., et al.: Using Neural Networks for Sensor Validation. AIAA Paper 98–3547, 1998.

2. Allison Engine Co.**:** AE 3007 High Reliability Engine Control Program. Development/Demonstration of Reliability Enhanced Control Technologies to Improve Aircraft Dispatch Reliability. NASA3–27394, Task Order 008, EDR 18549, Final Contractor Report, April 1998.

Lewis contact:
Dr. Ten-Huei Guo, (216) 433–3734, Ten-Huei.Guo@grc.nasa.gov

Author: Dr. Ten-Huei Guo

Headquarters program office: OAT

Program/Project: HREC

Distortion Tolerant Control Flight Demonstration Shown to Be Successful

Future aircraft turbine engines, both commercial and military, will have to be able to successfully accommodate expected increased levels of steady-state and dynamic engine-face distortion. Advanced tactical aircraft are likely to use thrust vectoring for enhanced aircraft maneuverability. As a result, the engines will see more extreme distortion levels than currently encountered with present-day aircraft. Also, the mixed-compression inlets needed for the High-Speed Civil Transport (HSCT) will likely encounter disturbances similar to those seen by tactical aircraft, in addition to planar pulse, inlet buzz, and high distortion levels at low flight speed and off-design operation.

The current approach of incorporating sufficient component design stall margin to tolerate these expected levels of distortion would result in significant performance penalties. The objectives of NASA's High Stability Engine Control (HISTEC) program, which has reached a highly successful conclusion, were to design, develop, and flight demonstrate an advanced, high-stability, integrated engine control system that uses measurement-based real-time estimates of distortion to enhance engine stability. The resulting distortion tolerant control adjusts the stall margin requirement online in real time. This reduces the design stall margin requirement, with a corresponding increase in performance and decrease in fuel burn.

The HISTEC approach includes two major systems: a Distortion Estimation System (DES) and Stability Management Control (SMC). The DES is an aircraft-mounted, high-speed processor that estimates the amount and type of distortion present and its effect on the engine. It uses high-response pressure measurements at the engine face to calculate indicators of the type and extent of distortion in real time. From these indicators, the DES determines the effects of the distortion on the propulsion system. In addition, the DES uses maneuver information from the flight control to anticipate high distortion conditions. The DES output consists of fan and compressor pressure ratio trim commands that

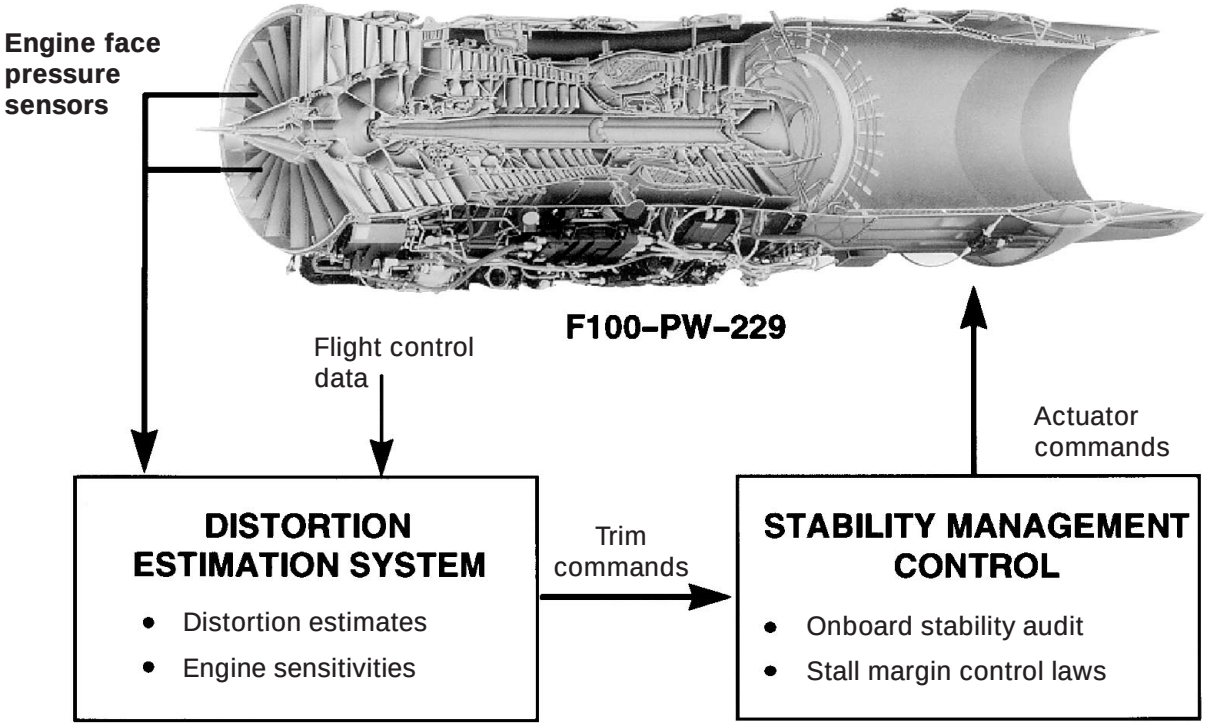

Distortion tolerant control. (Engine cutaway copyright Pratt & Whitney; used with permission.)

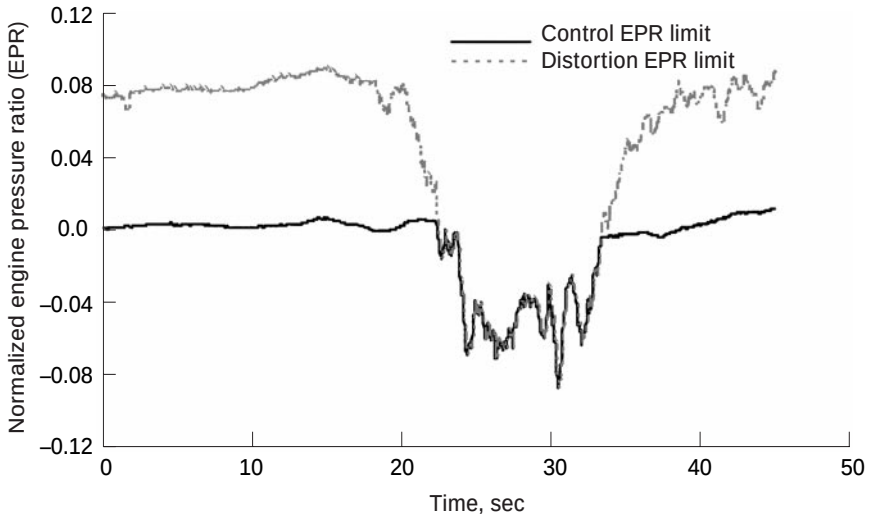

In-flight fan distortion accommodation.

are passed to the SMC. The SMC performs a stability audit online by using the trims from the DES and then accommodates the distortion through the production engine actuators.

Last year, the HISTEC distortion tolerant control system was flight tested on the NASA F–15 ACTIVE aircraft at the NASA Dryden Flight Research Center in Edwards, California. The flight demonstration showed closed-loop control operation with the engine fan and compressor stall margins being adjusted on the basis of estimated distortion. Project pilots flew the F–15 ACTIVE aircraft through a variety of maneuvers—such as high angle of attack flight, windup turns, and takeoff—which create distorted airflow conditions at the inlet. Detailed analysis of the flight test data performed this year verified that both the DES and SMC performed as designed. The system was able to successfully modify the engine pressure ratio (EPR) limit in response to high levels of distortion, thus temporarily moving the operating line to accommodate the lower stability condition.

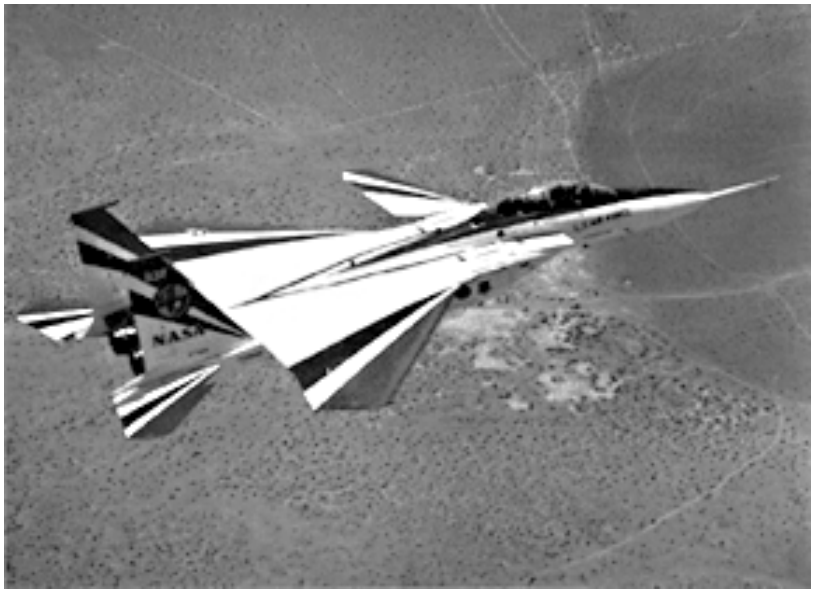

F–15 ACTIVE aircraft.

The NASA Lewis Research Center conducted the HISTEC program in partnership with the NASA Dryden Flight Research Center, Pratt & Whitney, Boeing Phantom Works (formerly McDonnell Douglas), and the U.S. Air Force.

Find out more about the High Stability Engine Control distortion tolerant control technologies on the World Wide Web:
http://www.grc.nasa.gov/WWW/cdtb/projects/histec/

Bibliography

DeLaat, J.C.; Southwick, R.D.; and Gallops, G.W.: High Stability Engine Control (HISTEC). AIAA Paper 96–2586 (NASA TM–107272), 1996. (Available online: http://gltrs.grc.nasa.gov/cgi-bin/GLTRS/browse.pl?1996/TM-107272.html)

DeLaat, J.C., et al.: The High Stability Engine Control (HISTEC) Program: Flight Demonstration Phase. AIAA Paper 98–3756 (NASA TM–1998–208482), 1998. (Available online: http://gltrs.grc.nasa.gov/cgi-bin/GLTRS/browse.pl?1998/TM-1998-208482.html)

Southwick, R.D., et al.: High Stability Engine Control (HISTEC) Flight Test Results. AIAA Paper 98–3757 (NASA TM–1998–208481), 1998. (Available online: http://gltrs.grc.nasa.gov/cgi-bin/GLTRS/browse.pl?1998/TM-1998-208481.html)

Orme, J.S., et al.: Development and Testing of a High Stability Engine Control (HISTEC) System. AIAA Paper 98–3715, 1998.

DeLaat, J.C., et al.: High Stability Engine Control (HISTEC): Flight Demonstration Results. SAE Paper 985556 (NASA TM—1998-208655), 1998.

Lewis contact:
Jonathan S. Litt, (216) 433–3748, Jonathan.S.Litt@grc.nasa.gov

Author: Jonathan S. Litt

Headquarters program office: OAT

Program/Projects:
Propulsion Systems R&T, PHSV, HISTEC

Special recognition:
1998 NASA Group Achievement Award

Combustion Instabilities Modeled

NASA Lewis Research Center's Advanced Controls and Dynamics Technology Branch is investigating active control strategies to mitigate or eliminate the combustion instabilities prevalent in lean-burning, low-emission combustors. These instabilities result from coupling between the heat-release mechanisms of the burning process and the acoustic flow field of the combustor.

Control design and implementation require a simulation capability that is both fast and accurate. It must capture the essential physics of the system, yet be as simple as possible. A quasi-one-dimensional, computational fluid dynamics (CFD) based simulation has been developed which may meet these requirements. The Euler equations of mass, momentum, and energy have been used, along with a single reactive species transport equation to simulate coupled thermoacoustic oscillations. A very simple numerical integration scheme was chosen to reduce computing time. Robust boundary condition procedures were incorporated to simulate various flow conditions (e.g., valves, open ends, and choked inflow) as well as to accommodate flow reversals that may arise during large flow-field oscillations.

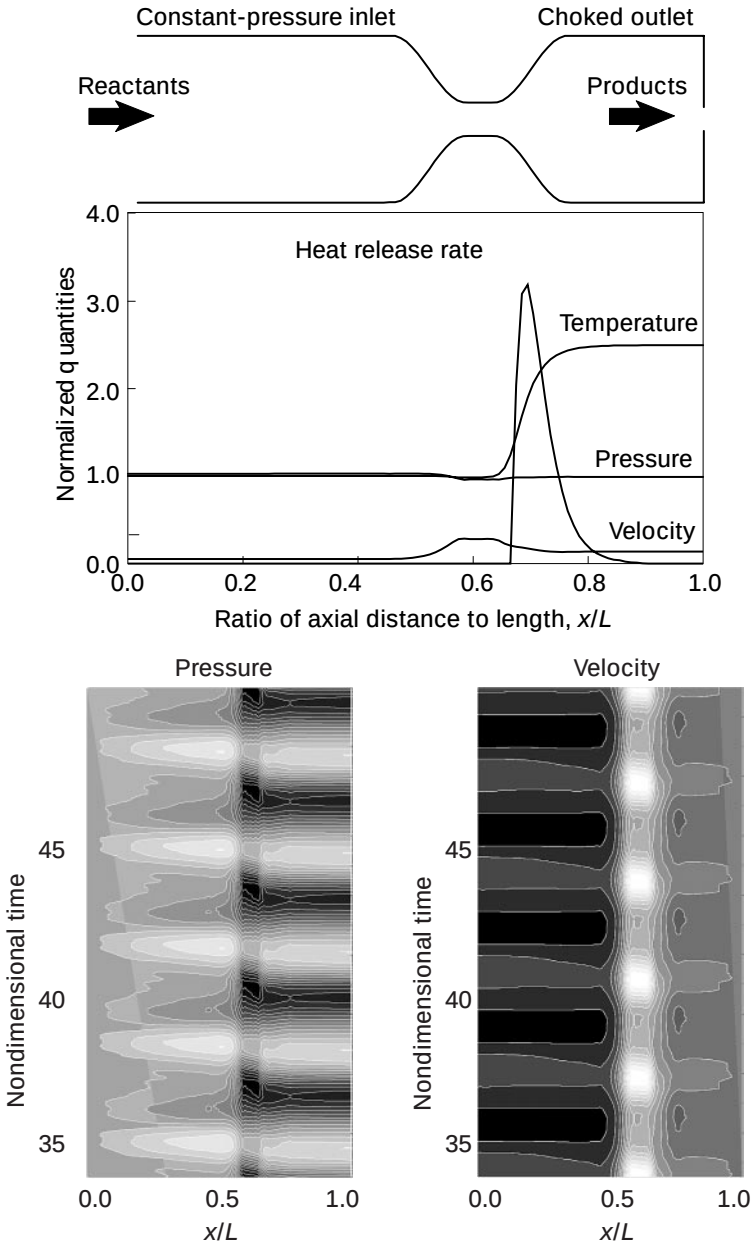

Results from a sample simulation. Top: Combustor diagram. Middle: Time-averaged pressure, temperature, velocity, and heat-release rate. Bottom: Contours of pressure and velocity showing self-sustained, coupled, thermoacoustic oscillations.

The accompanying figure shows a sample simulation result. A combustor with an open inlet, a choked outlet, and a large constriction approximately two thirds of the way down the length is shown. The middle plot shows normalized, time-averaged distributions of the relevant flow quantities, and the bottom plot illustrates the acoustic mode shape of the resulting thermoacoustic oscillation. For this simulation, the limit cycle peak-to-peak pressure fluctuations were 13 percent of the mean.

The simulation used 100 numerical cells. The total normalized simulation time was 50 units (approximately 15 oscillations), which took 26 sec on a Sun Ultra2.

Lewis contact:
Dr. Daniel E. Paxson, (216) 433–8334, Daniel.E.Paxson@grc.nasa.gov

Author: Dr. Daniel E. Paxson

Headquarters program office: OAT

Program/Project: HSCT

Communications Technology

Web Transfer Over Satellites Being Improved

Extensive research conducted by NASA Lewis Research Center's Satellite Networks and Architectures Branch and the Ohio University has demonstrated performance improvements in World Wide Web transfers over satellite-based networks. The use of a new version of the Hypertext Transfer Protocol (HTTP) reduced the time required to load web pages over a single Transmission Control Protocol (TCP) connection traversing a satellite channel. However, an older technique of simultaneously making multiple requests of a given server has been shown to provide even faster transfer time (refs. 1 to 3).

Unfortunately, the use of multiple simultaneous requests has been shown to be harmful to the network in general. Therefore, we are developing new mechanisms for the HTTP protocol which may allow a single request at any given time to perform as well as, or better than, multiple simultaneous requests (ref. 4). In the course of study, we also demonstrated that the time for web pages to load is at least as short via a satellite link as it is via a standard 28.8-kbps dialup modem channel (ref. 5). This demonstrates that satellites are a viable means of accessing the Internet.

References

1. Kruse, H., et al.: HTTP Page Transfer Rates Over Geo-Stationary Satellite Links. Proceedings of the Sixth International Conference on Telecommunication Systems, 1998, p. 518. (Available online: http://roland.grc.nasa.gov/~mallman/papers/nash98.ps)
2. Kruse, H., et al.: Performance Analysis of the HTTP Protocol on Geostationary Satellite Links. Satellite Networks: Architectures, Applications, and Technologies Workshop. NASA CP—1998-208524, 1998, pp. 65–74. (Available online: http://www.csm.ohiou.edu/kruse/Presentations/Cleve98/index.htm)
3. Kruse, H., et al.: A Comprehensive Evaluation of HTTP Over Satellite Channels. Submitted to ACM Mobile Networks and Applications Journal (Dec. 1998).
4. Kruse, H.; Allman, M.; and Mallasch, P.: Network and User-Perceived Performance of Web Page Retrievals. Proceedings of the First International Conference on Telecommunications and Electronic Commerce (ICTEC), Nov. 1998. (Available online: http://roland.grc.nasa.gov/~mallman/papers/ecom98.ps)
5. Griner, J., et al.: Internet Over a Bi-Directional Satellite Link. Satellite Networks: Architectures, Applications, and Technologies Workshop. NASA CP—1998-208524, 1998, pp. 49–50. (Available online: http://roland.grc.nasa.gov/~jgriner/papers/workshop-demo.pdf)

Find out more about this HTTP study on the World Wide Web:
http://ctd.grc.nasa.gov/5610/httpextensions.html

Lewis contact:
Mark Allman, (216) 433–6586, Mark.A.Allman@grc.nasa.gov

Author: Mark Allman

Headquarters program office: OSS

Programs/Projects:
Aeronautics Base R&T

Advances Made in the Next Generation of Satellite Networks

Because of the unique networking characteristics of communications satellites, global satellite networks are moving to the forefront in enhancing national and global information infrastructures. Simultaneously, broadband data services, which are emerging as the major market driver for future satellite and terrestrial networks, are being widely acknowledged as the foundation for an efficient global information infrastructure. In the past 2 years, various task forces and working groups around the globe have identified pivotal topics and key issues to address if we are to realize such networks in a timely fashion. In response, industry, government, and academia undertook efforts to address these topics and issues.

A workshop was organized to provide a forum to assess the current state-of-the-art, identify key issues,

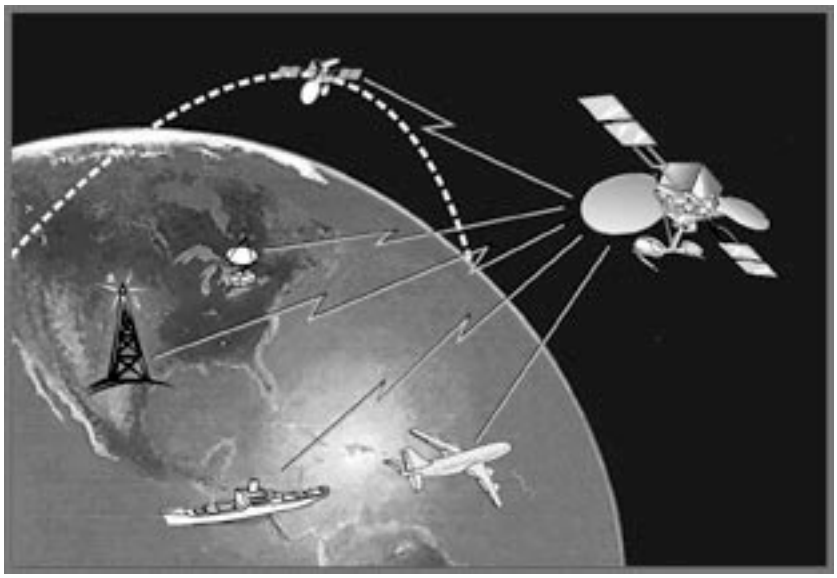

Space-based networks scenario.

and highlight the emerging trends in the next-generation architectures, data protocol development, communication interoperability, and applications. The *Satellite Networks: Architectures, Applications, and Technologies Workshop* was hosted by the Space Communication Program at the NASA Lewis Research Center in Cleveland, Ohio. Nearly 300 executives and technical experts from academia, industry, and government, representing the United States and eight other countries, attended the event (June 2 to 4, 1998). The program included seven panels and invited sessions and nine breakout sessions in which 42 speakers presented on technical topics. The proceedings (ref. 1) covers a wide range of topics: access technology and protocols, architectures and network simulations, asynchronous transfer mode (ATM) over satellite networks, Internet over satellite networks, interoperability experiments and applications, multicasting, NASA interoperability experiment programs, NASA mission applications, and Transmission Control Protocol/Internet Protocol (TCP/IP) over satellite: issues, relevance, and experience.

Reference

1. Bhasin, K.: Satellite Networks: Architectures, Applications, and Technologies, NASA/CP—1998-208524, 1998.

Lewis contact:
Dr. Kul B. Bhasin, (216) 433–3676, Kul.B.Bhasin@grc.nasa.gov

Author: Dr. Kul B. Bhasin

Headquarters program office: OSS

Programs/Projects: NII/GII

Internet Protocol Enhanced Over Satellite Networks

Extensive research conducted by the Satellite Networks and Architectures Branch of the NASA Lewis Research Center led to an experimental change to the Internet's Transmission Control Protocol (TCP) that will increase performance over satellite channels. The change raises the size of the initial burst of data TCP can send from 1 packet to 4 packets or roughly 4 kilobytes (kB), whichever is less.

TCP is used daily by everyone on the Internet for e-mail and World Wide Web access, as well as other services. TCP is one of the feature protocols used in computer communications for reliable data delivery and file transfer. Increasing TCP's initial data burst from the previously specified single segment to approximately 4 kB may improve data transfer rates by up to 27 percent for very small files. This is significant because most file transfers in wide-area networks today are small files, 4 kilobytes or less. In addition, because data transfers over geostationary satellites can take 5 to 20 times longer than over typical terrestrial connections, increasing the initial burst of data that can be sent is extremely important.

This research along with research from other institutions has led to the release of two new Request for Comments (RFC, ref. 1) from the Internet Engineering Task Force (IETF, the international body that sets Internet standards). In addition, two studies of the implications of this mechanism were also funded by NASA Lewis (refs. 2 and 3). Additional information is available in reference 4.

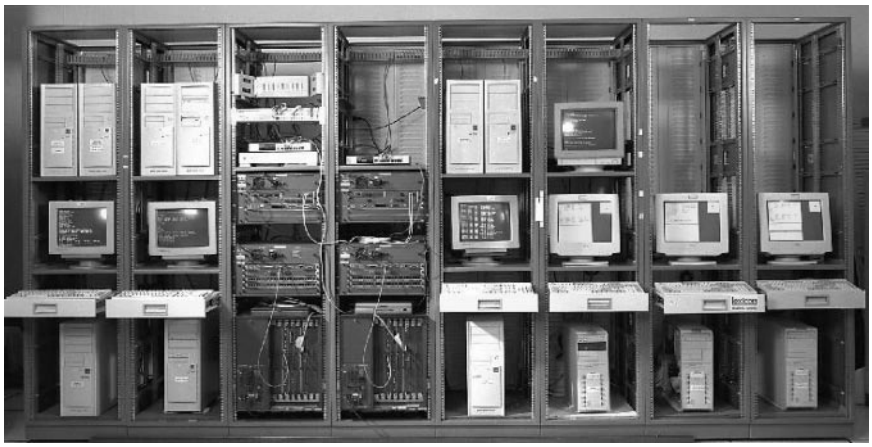

Internet Protocol Testbed.

Find out more about this research on the World Wide Web:
http://info.internet.isi.edu:80/in-notes/rfc/files/rfc2414.txt
http://info.internet.isi.edu:80/in-notes/rfc/files/rfc2416.txt
http://sulu.grc.nasa.gov/5610/inetprotocols.html

References

1. Allman, M.; Floyd, S.; and Partridge, C.: Increasing TCP's Initial Window. RFC 2414, Experimental, Sept. 1998. (Available online: http://info.internet.isi.edu:80/in-notes/rfc/files/rfc2414.txt)
2. Shepard, T.; and Partridge, C.: When TCP Starts Up With Four Packets Into Only Three Buffers. RFC 2416, Informational, BBN Technologies, Sept. 1998. (Online information: http://info.internet.isi.edu:80/in-notes/rfc/files/rfc2416.txt)
3. Allman, M.; Hayes, C.; and Ostermann, S.: An Evaluation of TCP With Larger Initial Windows. ACM SIGCOMM, vol. 28, no. 3, 1998, pp. 41–52.

Lewis contact:
William D. Ivancic, (216) 433–3494,
William.D.Ivancic@grc.nasa.gov

Author: William D. Ivancic

Headquarters program office:
OSS, OAT

Programs/Projects:
Level 1 HEDS 22 improved ground-based data networks, 64 advanced data handling; ESE 119 advanced end-to-end mission information system technologies; Level 2 3694 desktop instrument operations end-to-end protocol standards, 3700 and 2030 high-data-rate communications, 3753 communications protocols; SOMO Interoperability and Standardization 8, 9, 10; Innovative Mission Information Systems 56; and Hybrid Network Ubiquity 61, 62, 63

Satellite ATM Networks: Architectures and Guidelines Developed

An important element of satellite-supported asynchronous transfer mode (ATM) networking will involve support for the routing and rerouting of active connections. Work published under the auspices of the Telecommunications Industry Association (http://www.tiaonline.org), describes basic architectures and routing protocol issues for satellite ATM (SATATM) networks (ref. 1). The architectures and issues identified will serve as a basis for further development of technical specifications for these SATATM networks.

Three ATM network architectures for bent pipe satellites and three ATM network architectures for satellites with onboard ATM switches were developed. The architectures differ from one another in terms of required level of mobility, supported data rates, supported terrestrial interfaces, and onboard processing and switching requirements. The documentation (ref. 1) addresses low-, middle-, and geosynchronous-Earth-orbit satellite configurations.

The satellite environment may require real-time routing to support the mobility of end devices and nodes of the ATM network itself. This requires the network to be able to reroute active circuits in real time. In addition to supporting mobility, rerouting can also be used to (1) optimize network routing, (2) respond to changing quality-of-service requirements, and (3) provide a fault tolerance mechanism. Reference 1 examines the various reroute events and the time-scale in which they would occur.

Traffic management and control functions are necessary in ATM to ensure that the quality-of-service requirements associated with each connection are not violated and also to provide flow and congestion control functions. Functions related to traffic management were identified and described. Most of these traffic management functions will be supported by on-ground ATM switches, but in a hybrid terrestrial-satellite ATM network, some of the traffic management functions may have to be supported by the onboard satellite ATM switch. It is expected that the ATM traffic loading on the satellite will be high; hence, it has been proposed to transfer traffic management functions (to the degree possible) to Earth station components. This will also reduce the complexity of the satellite hardware. Future work is planned to examine the tradeoffs of placing traffic management functions onboard a satellite as opposed to implementing those functions at the Earth station components. This work was done at the NASA Lewis Research Center in collaboration with ComSat Labs.

Find out more about this research on the World Wide Web:
http://ctd.grc.nasa.gov/5610/5610.html

References

1. Satellite ATM Networks: Architectures and Guidelines, TSB91, 1998, Telecommunications Industry Association.

Lewis contact:
Thomas C. vonDeak, (216) 433–3277, fax (216) 433–8705, Thomas.C.Vondeak@grc.nasa.gov

Authors:
Thomas C. vonDeak and Ferit Yegendu

Headquarters program office: OSS

Programs/Projects: ATM research and development, SOMO, satellite communications industry

Broadband Satellite Technologies and Markets Assessed

The current usage of broadband (data rate greater than 64 kilobits per second (kbs)) for multimedia network computer applications is increasing, and the need for network communications technologies and systems to support this use is also growing. Satellite technology will likely be an important part of the National Information Infrastructure (NII) and the Global Information Infrastructure (GII) in the next decade. Several candidate communications technologies that may be used to carry a portion of the increased data traffic have been reviewed, and estimates of the future demand for satellite capacity have been made. A study was conducted by the NASA Lewis Research Center to assess the satellite addressable markets for broadband applications. This study effort included four specific milestones: (1) assess the changing nature of broadband applications and their usage, (2) assess broadband satellite and terrestrial technologies, (3) estimate the size of the global satellite addressable market from 2000 to 2010, and (4) identify how the impact of future technology developments could increase the utility of satellite-based transport to serve this market.

Lewis' approach was to assess the requirements for satellite broadband services, which are based on an understanding of user perspectives and data needs. This research effort included interviews with leading industry players and technology experts to understand the unfolding markets for broadband services and the status of terrestrial network deployments. In addition, the suitability of available and emerging terrestrial broadband technologies to compete with the newly licensed Ka-band satellite systems in providing multimedia

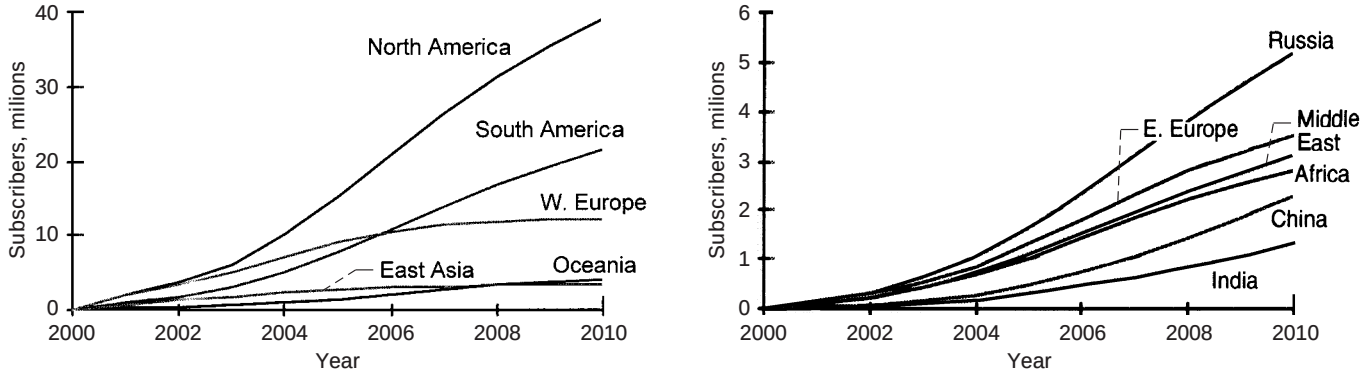

Estimated penetration of broadband into top five regional satellite markets and less developed regions. (Adapted from Booz-Allen & Hamilton analysis, ref. 1.)

services to business and consumer markets was studied. The analysis was supported by an end-to-end communications services supply-and-demand model used to make quantitative assessments. It considered relevant technical, demographic, and competitive factors including application transport requirements, user preferences, changing usage levels and application mixes, affordability by user segments and geographies, investment costs and delays for upgrades, and expansion of the terrestrial infrastructure.

We estimate that North America will have the highest number of satellite service subscribers as shown in the graph. South America is projected to be the second largest regional opportunity. In this model, the underdeveloped terrestrial networks in the region and rapidly growing gross domestic product (GDP) drive this result. Western European subscriptions could peak by 2007 and slowly decline as terrestrial buildup catches up with demand in areas not served by terrestrial technologies. In less developed regions, overall satellite service penetration is likely to be significantly lower initially than for the top five regions but to grow consistently over time. Of these, Russia is projected to be the largest single market, with over 5 million subscribers, followed by Eastern Europe, with over 3 million. We believe this result reflects the potentially underreported level of investment in terrestrial infrastructure for Russia as reported by the International Telecommunications Union (ITU). Nonetheless, Russia will most likely remain a large market for satellite services considering its large geography and low population density. A set of recommendations to improve the utility of satellite systems for delivering broadband services was developed. We expect that the methodology developed in this study will allow more quantitative assessments of specific broadband satellite technologies and markets.

References

1. Booz-Allen & Hamilton: Assessment of Broadband Satellite Technologies and Markets, Volume 2. NASA CR—1998-206595, 1998. Available from Lewis' Satellite Networks and Architectures Branch.
2. Booz-Allen & Hamilton: Assessment of Broadband Satellite Technologies and Markets, Volume 1—Executive Summary. NASA CR—1998-206596, 1998. Available from Lewis' Satellite Networks and Architectures Branch.

Lewis contact:
Dr. Thomas M. Wallett, (216) 433–3673, Thomas.M.Wallett@grc.nasa.gov

Author: Dr. Thomas M. Wallett

Headquarters program office: OSS

Programs/Projects: Space Communications, communications industry

A More Accurate and Efficient Technique to Obtain Helical Traveling-Wave Tube Interaction Impedance Using Computational Methods

The phenomenal growth of commercial communications has created a great demand for traveling-wave tube (TWT) amplifiers. Although the helix slow-wave circuit remains the mainstay of the TWT industry because of its exceptionally wide bandwidth, until recently it has been impossible to accurately analyze a helical TWT using its exact dimensions because of the complexity of its geometrical structure. For the first time, an accurate three-dimensional helical model was developed that allows accurate prediction of TWT cold-test characteristics including operating frequency, interaction impedance, and attenuation. This computational model, which was developed at the NASA Lewis Research Center, allows TWT designers to obtain a more accurate value of interaction impedance than is possible using experimental methods.

Obtaining helical slow-wave circuit interaction impedance is an important part of the design process for a TWT because it is related to the gain and efficiency of the tube. This impedance cannot be measured directly; thus, conventional methods involve perturbing a helical circuit with a cylindrical dielectric rod placed on the central axis of the circuit and obtaining the difference in resonant frequency between the perturbed and unperturbed circuits. A mathematical relationship has been derived between this frequency difference and the interaction impedance (ref. 1). However, because of the complex configuration of the helical circuit, deriving this relationship involves several approximations. In addition, this experimental procedure is time-consuming and expensive, but until recently it was widely accepted as the most accurate means of determining interaction impedance.

The advent of an accurate three-dimensional helical circuit model (ref. 2) made it possible for Lewis researchers to fully investigate standard approximations made in deriving the relationship between measured perturbation data and interaction impedance. The most prominent approximations made in the analysis were addressed and fully investigated for their accuracy by using the three-dimensional electromagnetic simulation code MAFIA (Solution of Maxwell's Equations by the Finite Integration Algorithm) (refs. 3 and 4). We found that several approximations introduced significant error (ref. 5).

To further validate the three-dimensional computational helical model, researchers duplicated the experimental perturbation method by simulating the helical circuit with a cylindrical dielectric rod of size and material properties consistent with the experimental setup. The difference in frequency between the perturbed and unperturbed circuits was obtained. Then, the interaction impedance was calculated using the previously mentioned approximate formulation relating frequency difference to interaction impedance. The following graph, which compares the results with measured values, emphasizes the accuracy of the code. The interaction impedance was calculated with the exact formula using MAFIA and is also plotted in this graph. The results calculated directly with MAFIA are consistently lower than measured results, with an average difference of 26.6 percent.

The demonstrated inaccuracy of approximations in the derived experimental impedance formula, along with the large discrepancy between these measured impedance data and direct calculations using MAFIA, verifies that a more accurate value of interaction impedance can be obtained by using three-dimensional computational methods. In addition, this implies that MAFIA will yield large savings in time and cost in comparison to expensive and time-consuming experimental cold-test measurements.

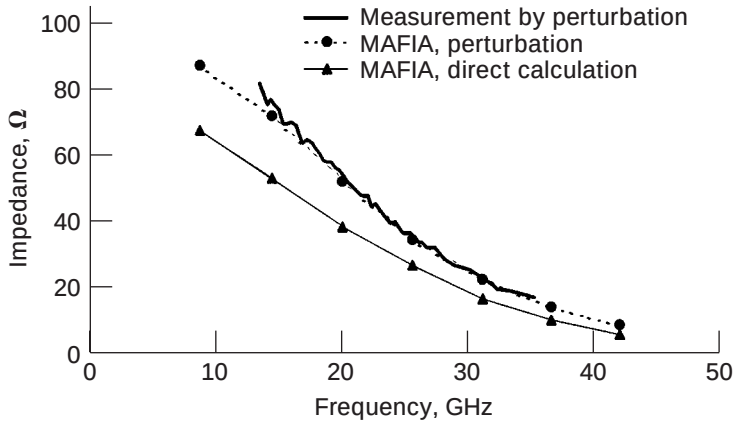

On-axis interaction impedance obtained by measurement and by using MAFIA with the perturbation method and direct calculation.

References

1. Lagerstrom, R.P.: Interaction-Impedance Measurements by Perturbation of Traveling Waves. Stanford Electronics Laboratories, Technical Report No. 7, Naval Research Contract, Nonr 225 (24), NR 373 360, Stanford University, Stanford, CA, Feb. 11, 1957.
2. Kory, C.L.; and Dayton, J.A., Jr.: Accurate Cold-Test Model of Helical TWT Slow-Wave Circuits. IEEE Trans. Electron Devices, vol. 45, no. 4, 1998, pp. 966–971.
3. Weiland, T.: On the Numerical Solution of Maxwell's Equations and Applications in the Field of Accelerator Physics. Part. Accel., vol. 15, 1984, pp. 245–292.
4. Weiland, T.: On the Unique Numerical Solution of Maxwellian Eigenvalue Problems in Three Dimensions. Part. Accel., vol. 17, 1985, pp. 227–242.
5. Kory, C.L.; and Dayton, J.A., Jr.: Computational Investigation of Experimental Interaction Impedance Obtained by Perturbation for Helical Traveling-Wave Tube Structures. IEEE Trans. Electron Devices, vol. 45, no. 9, 1998, pp. 2063–2071.

Lewis contact:
Carol L. Kory, (216) 433–3512, Carol.L.Kory@grc.nasa.gov

Author: Carol L. Kory

Headquarters program office: OSS

Programs/Projects:
CETDP; high-efficiency, high-data-rate communications systems for future missions

Diamond Analyzed by Secondary Electron Emission Spectroscopy

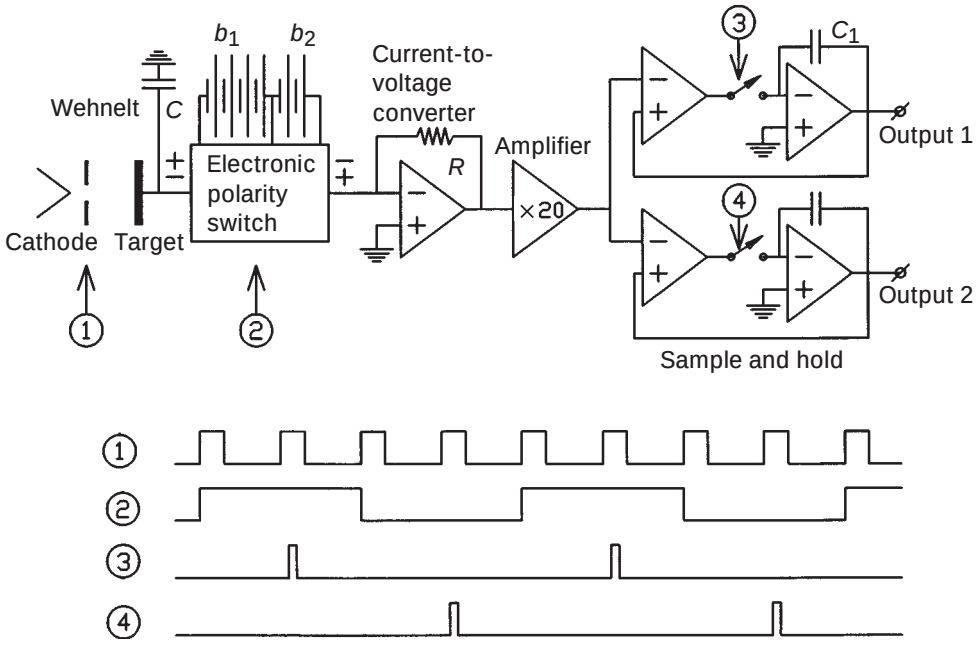

Experimental setup (b, battery; C, capacitor; R, resistor). Top: Block diagram. Bottom: Timing diagram of various voltages supplied into the top drawing.

Diamond is a promising semiconductor material for novel electronic applications because of its chemical stability and inertness, heat conduction properties, and so-called negative electron affinity (NEA). When a surface has NEA, electrons generated inside the bulk of the material are able to come out into the vacuum without any potential barrier (work function). Such a material would have an extremely high secondary electron emission coefficient σ, very high photoelectron (quantum) yield, and would probably be an efficient field emitter.

Chemical-vapor-deposited (CVD) polycrystalline diamond films have even more advantages than diamond single crystals. Their fabrication is relatively easy and inexpensive, and they can be grown with high levels of doping—consequently, they can have relatively high conductivity. Because of these properties, diamond can be used for cold cathodes and photocathodes in high-power electronics and in high-frequency and high-temperature semiconductor devices.

Using mostly secondary electron spectroscopy as a tool, the NASA Lewis Research Center conducts research on the electronic properties of both natural diamond crystals and microwave-assisted chemical-vapor-deposited thin diamond films. Whereas artificial diamond films can be made conductive, the effects occurring in natural diamond can be obscured by the undissipated charge. Because of this effect, measurements on natural diamond often have to be done in the pulse mode. The preceding block diagram shows the installation for measuring the secondary electron emission coefficient σ in such a mode, and the left graph on the next page shows measurements of σ for the (100) surface of IIb natural diamond single crystals, both saturated with hydrogen and dehydrogenated. For the dehydrogenated surface, the secondary electron yield is quite low, especially in comparison to the surface saturated with hydrogen, which has a very high secondary electron yield because of its NEA status. Hydrogen can be desorbed if the surface is heated at elevated temperatures or is exposed to an electron beam. To improve the stability of the surface under an electron beam, Lewis researchers recently studied various coatings that might preserve the NEA property of diamond surfaces. Among the materials tested for the coatings were alkali halides, such as cesium iodide (CsI). Tests showed that as a result of the exposure to the electron beam, the halogen (I in this case) desorbed into the vacuum, leaving

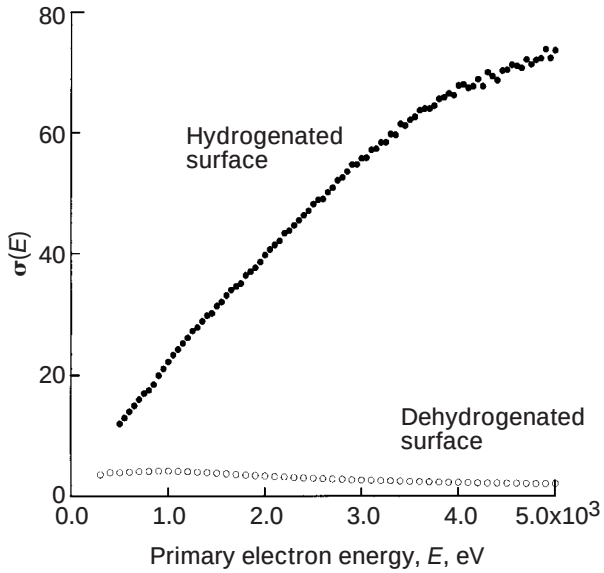

Secondary electron emission coefficient σ for (100) surface of natural IIb diamond crystal.

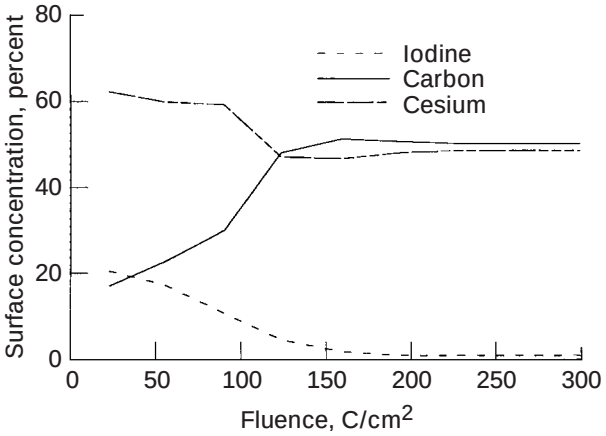

Surface concentrations versus fluence for diamond coated with 100 nm of CsI.

the surface coated with a thin layer of active ingredient. The resulting a surface was stable under the electron beam exposure and had a very high secondary electron yield, indicating that it was exhibiting NEA. The graph on the right shows an example of this effect for a thin CsI film on diamond. It can be seen that the iodine concentration at the surface diminishes with the exposure to the electron beam.

Lewis contact:
Dr. Isay L. Krainsky, (216) 433–3509, Isay.L.Krainsky@grc.nasa.gov

Author: Dr. Isay L. Krainsky

Headquarters program office: OSS

Programs/Projects:
Electron beam devices

Finite Ground Coplanar (FGC) Waveguide: Characteristics and Advantages Evaluated for Radiofrequency and Wireless Communication Circuits

Researchers in NASA Lewis Research Center's Electron Device Technology Branch are developing transmission lines for radiofrequency and wireless circuits that are more efficient, smaller, and make lower cost circuits possible. Traditionally, radiofrequency and wireless circuits have employed a microstrip or coplanar waveguide to interconnect the various electrical elements that comprise a circuit. Although a coplanar waveguide (CPW) is widely viewed as better than a microstrip for most applications, it too has problems. To solve these problems, NASA Lewis and the University of Michigan developed a new version of a coplanar waveguide with electrically narrow ground planes. This new transmission line, which we call the finite ground coplanar (FGC) waveguide, is illustrated in the following figure.

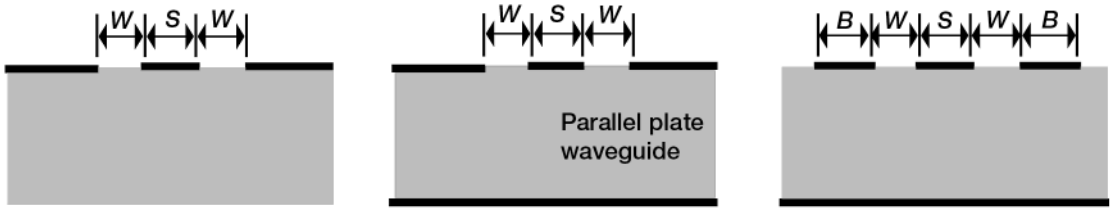

Coplanar waveguides. Waveguide width, W; center conductor width, S; ground plane width, B. Left: Conventional coplanar waveguide. Center: Waveguide with lower ground plane. Right: Finite ground coplanar waveguide.

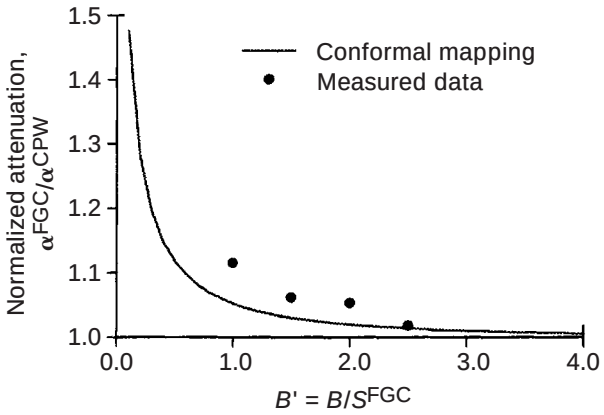

Attenuation, α, of FGC waveguide with S = W = 25 μm normalized to the attenuation of a conventional CPW with S = W = 25 μm as a function of the normalized ground plane width, B, where S is the center conductor width and W is the waveguide width.

Through extensive numerical modeling and experimental measurements, we have characterized the propagation constant of the FGC waveguide, the lumped and distributed circuit elements integrated in the FGC waveguide, and the coupling between parallel transmission lines. Although the attenuation per unit length is higher for the FGC waveguide because of higher conductor loss, the attenuation is comparable when the ground plane width is twice the center conductor width as shown in the preceding graph. An upper limit to the line width is derived from observations that when the total line width is greater than $\lambda_d/2$, spurious resonances due to the parallel plate waveguide mode are established. Thus, the ground plane width must be less than $\lambda_d/4$ where λ_d is the wavelength in the dielectric. Since the center conductor width *S* is typically less than $\lambda/10$ to maintain good transverse electromagnetic mode characteristics, it follows that a ground plane width of $B = 2S$ would also be electrically narrow. Thus, we can now treat the ground strips of the FGC waveguide the same way that the center conductor is treated.

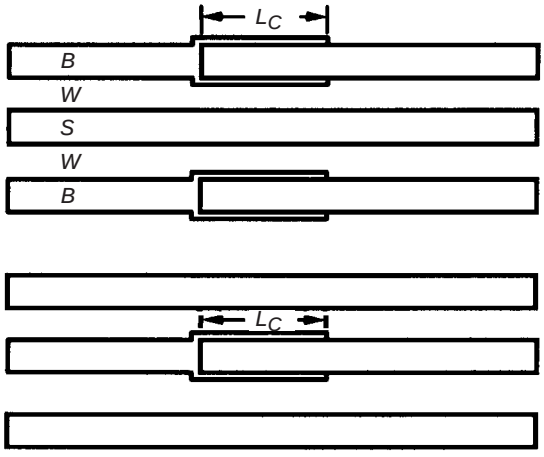

MIM capacitor. Center conductor width, S; waveguide width, W; ground plane width, B; capacitor length, L_C. Top: Integrated in ground planes. Bottom: Integrated in center conductor of the FGC waveguide.

This allows the novel integration of circuit elements in the FGC waveguide. To explore this, researchers integrated metal-insulator-metal (MIM) capacitors, inductors, and thin film resistors into the center conductor and the ground planes of the transmission line as illustrated in the final figure. Results indicate that even though the value of the parasitic reactance associated with each element is independent of the element placement, the value of the primary element value (capacitance, inductance, and resistance, respectively) does vary upon placement. Specifically, when two elements are connected in the ground planes as shown in the drawing, they add in parallel. Thus, capacitors in the ground planes can be made shorter and still provide the same capacitance as capacitors placed in the center conductor. Furthermore, since the parasitic reactance is independent of element placement, the self-resonant frequency of the capacitors in the ground planes is higher.

Lastly, coupling is reduced as the ground plane width is reduced while the distance between the center of each line is kept constant. Furthermore, the coupling between parallel transmission lines is lower for the FGC waveguide than for the conventional coplanar waveguide. In fact, even a small slot between the ground planes of the conventional coplanar waveguide can lower coupling by 10 dB.

All these results indicate that the FGC waveguide is a better transmission line than the coplanar waveguide and the microstrip for radiofrequency and wireless circuits. Further work is underway to more fully develop design rules for this new transmission line.

Bibliography

Ponchak, G.E.; Tentzeris, E.M.; and Katehi, L.P.B.: Characterization of Finite Ground Coplanar Waveguide With Narrow Ground Planes. Int. J. Microcircuits Electronic Packaging, vol. 20, no. 2, 1997, pp. 167–173.

Ponchak, G.E., et al.: Finite Width Coplanar Waveguide for Microwave and Millimeter-Wave Integrated Circuits. Proceedings of the International Symposium on Microelectronics, ISHM '96, The Microelectronics Society, Reston, VA, 1996, pp. 517–521.

Ponchak, G.E.; and Katehi, L.P.B.: Characteristics of Finite Ground Coplanar Waveguide Lumped Elements. Proceedings of the IEEE MTT–S International Microwave Symposium Digest, Vol. 2, 1997, pp. 1003–1006.

Ponchak, G.E.; and Katehi, L.P.B.: Open- and Short-Circuit Terminated Series Stubs in Finite-Width Coplanar Waveguide on Silicon. IEEE Trans. Microwave Theory Tech., vol. 45, no. 6, June 1997, pp. 970–976.

Ponchak, G.E.: Development of Passive Components for Millimeter-Wave Circuits. Ph.D. Thesis, Univ. of Michigan, 1997.

Ponchak, G.E.; Tentzeris, E.M.; and Katehi, L.P.B.: Coupling Between Adjacent Finite Ground Coplanar (FGC) Waveguides. International Symposium on Microelectronics, 1997, pp. 7–10.

Lewis contact:
Dr. George E. Ponchak, (216) 433–3504, fax (216) 433–8705, George.E.Ponchak@grc.nasa.gov

Author:
Dr. George E. Ponchak

Headquarters program office: OSS

Programs/Projects: Space communications for NASA missions

Special recognition:
IMAPS' 1997 International Symposium on Microelectronics Best Paper Award

Angular Distribution of Elastically Scattered Electrons Determined and Its Effect on Collector Performance Computed

It has been demonstrated that the suppression of secondary electron emission significantly improves the performance of electron beam collectors (ref. 1). However, a complete analysis of the effects of secondary electron emission with respect to collector performance has not been possible because of the lack of quantitative data on angular distributions of secondary electrons. Secondary electrons are emitted with energies ranging from near zero to the energy of the incident primary. For our purposes, we define elastically scattered electrons as secondary electrons within 20 percent of the incident energy. Elastically scattered electrons are of great concern because their energy allows them to follow trajectories that can carry them almost anywhere within the vacuum envelope. If these secondaries leave the collector and reenter the slow wave circuit, they can produce undesired signal distortion and oscillation.

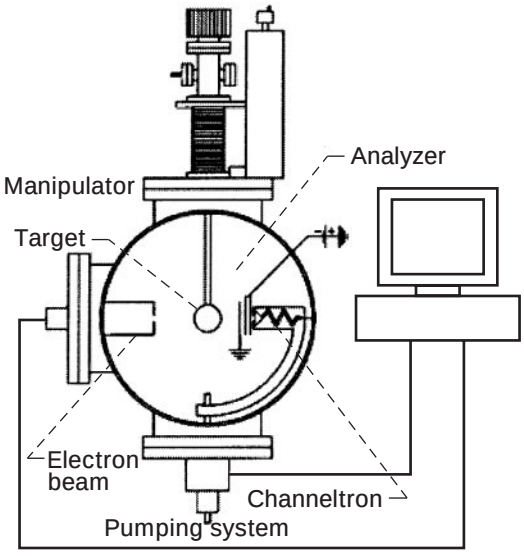

Apparatus for determining the angular distribution of secondary electrons.

This apparatus, which was built by Krainsky (ref. 2), was used at the NASA Lewis Research Center to obtain detailed measurements of the angular distributions of elastically scattered secondaries. Data were obtained for three surfaces

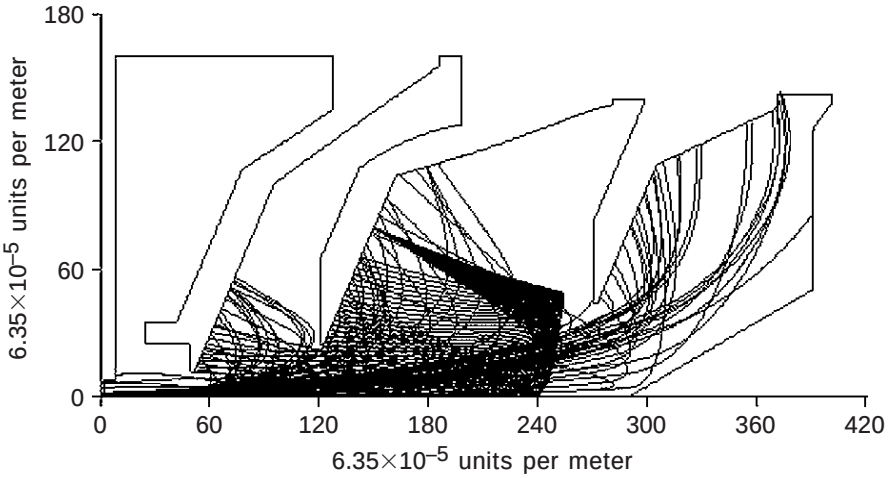

Computer model of back-scattered electrons from one impact site in the collector design for the Hughes 32-GHz traveling-wave tube proof-of-concept design for the Cassini Mission.

of significant interest to collector applications: highly polished copper, copper roughened by ion sputtering, and isotropic graphite. Lewis researchers discovered that elastically scattered electrons have a complex angular distribution that is strongly dependent on the atomic number and surface morphology of the target material, as well as the energy and angle of incidence of the primary beam. At low energies, secondary emission from polished copper in the chosen energy range is primarily directed back to the source of primary electrons (backscattering). Forward scattering increases with primary energy until, at high energies, forward scattering dominates the angular distribution. Although back-scattered secondaries dominate the distributions of the textured copper surface, the yield is substantially lower. From the standpoint of secondary emission, isotropic graphite is the most attractive material because it exhibits low yield and little back scattering.

The measured data were curve-fitted into linear combinations of Gaussian and Lorentzian functions, which were used in an interpolation routine to calculate the approximate distributions at any arbitrary primary energy and angle of incidence. The complexity of the data did not provide easy incorporation into the computational model. Furthermore, the volume of the data exceeded computational resources and software limits. However, improvements in computational power and software enhancements now allow the inclusion of the newly available data into previous models of electron beam collectors. Simulations on a collector designed for a 32-GHz traveling-wave tube (TWT) showed that forward-scattered electrons had little effect on collector performance. The angular distributions for ion-textured copper dominated by back-scattered secondaries were of more concern because those electrons are likely to reenter the slow wave circuit. However, our model of these distributions showed that approximately 1 percent of the primary beam current returned to the slow wave circuit, which is in agreement with experimental observations. The figure to the left shows a sample of such a model. These additions have brought even more accuracy and insight to previous modeling attempts.

References

1. Ramins, P.; and Ebihara, B.T.: Improvements in MDC and TWT Overall Efficiency Through Application of Carbon Electrode Surfaces. IEEE Trans. Electron Devices, vol. ED–33, no. 11, Nov. 1986, pp. 1915–1924.
2. Krainsky, I., et al.: The Angular Distribution of Elastically Scattered Electrons and Computed Impact on Collector Performance. IEEE IEDM 92–953, 1992, pp. 37.4.1–37.4.4.

Lewis contacts:
Karl R. Vaden, (216) 433–8131, Karl.R.Vaden@grc.nasa.gov; and
Dr. Isay L. Krainsky, (216) 433–3509, Isay.L.Krainsky@grc.nasa.gov

Authors:
Dr. Isay L. Krainsky and Karl R. Vaden

Headquarters program office: OSS

Programs/Projects:
Traveling-wave tubes

Thin-Film Ferroelectric Tunable Microwave Devices Being Developed

Electronically tunable microwave components have become the subject of intense research efforts in recent years. Many new communications systems would greatly benefit from these components. For example, planned low-Earth-orbiting satellite networks have a need for electronically scanned antennas. Thin ferroelectric films are one of the major technologies competing to fill these applications. When a direct-current (dc) voltage is applied to ferroelectric film, the dielectric constant of the film can be decreased by nearly an order of magnitude, changing the high-frequency wavelength in the microwave device. Recent advances in film growth have demonstrated high-quality ferroelectric thin films. This technology may allow microwave devices that have very low power and are compact, lightweight, simple, robust, planar, voltage tunable, and affordable.

The NASA Lewis Research Center has been designing, fabricating, and testing proof-of-concept tunable microwave devices. This work, which is being done in-house with funding from the Lewis Director's Discretionary Fund, is focusing on introducing better microwave designs to utilize these materials. We have demonstrated Ku- and K-band phase shifters, tunable local oscillators, tunable filters, and tunable diplexers. Many of our devices employ $SrTiO_3$ as the ferroelectric. Although it is one of the more tunable and easily grown ferroelectrics, $SrTiO_3$ must be used at cryogenic temperatures, usually below 100 K. At these temperatures, we frequently use high-temperature superconducting thin films of $YBa_2Cu_3O_{7-\delta}$ to carry the microwave signals. However, much of our recent work has concentrated on inserting room-temperature ferroelectric thin films, such as $Ba_xSr_{1-x}TiO_3$ into these devices. The $Ba_xSr_{1-x}TiO_3$ films are used in conjuction with normal metal conductors, such as gold.

The first example of ferroelectric-based components is the tunable filter, which has a compact, planar design. The metallic layer consists of a thin $YBa_2Cu_3O_{7-\delta}$ superconducting film. A 300-nm-thick $SrTiO_3$ ferroelectric film lies below the metallic layer on a $LaAlO_3$ dielectric substrate. The

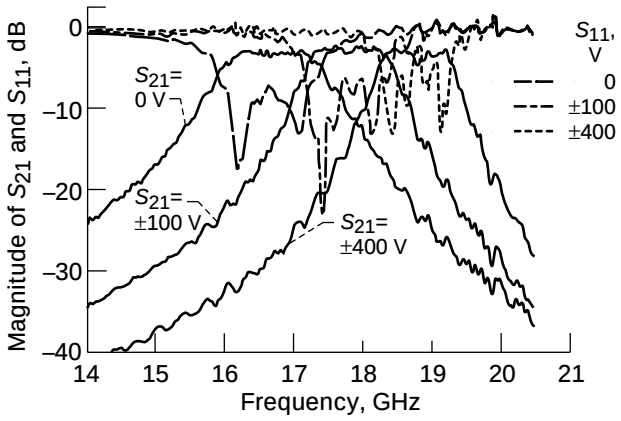

Bias dependence of transmission signal, S_{21}, and reflectance signal, S_{11}, measurements for a tunable bandpass filter at 30 K.

S-parameter transmission and reflection measurements in the graph at the bottom left indicate that filter's center frequency shifted from 16.5 GHz at no bias, to 18.8 GHz at ±400 V bias, showing a tuning range of 12 percent at 30 K. The passband losses are relatively flat, and the minimum embedded insertion loss is 1.5 dB. These results demonstrate the feasibility of using ferroelectric thin-film planar microstrip filters at Ku-band frequencies. Recent activities include fabricating and testing these tunable filters with ambient temperature ferroelectrics (e.g., $Ba_xSr_{1-x}TiO_3$).

Extensive work has gone into developing these novel ferroelectric coupled microstrip phase shifters, which were invented at Lewis. Two configurations of these phase shifters are given in the schematic at the top of the next page. The ferroelectric thin film again lies below the metallic circuit on a crystal substrate. Direct-current bias is applied between the coupled microstrips, strongly affecting the dielectric constant of the ferroelectric in the gap and causing a microwave phase shift. Larger phase shifts are obtained by placing several of these coupled microstrip sections in series. At cryogenic temperatures, these devices have shown nearly 500° of phase shift with figures of merit of 80° of phase shift per 1 dB of loss. These results are shown in the final graphs for a $YBa_2Cu_3O_{7-\delta}/SrTiO_3/LaAlO_3$ multilayer structure. On-going efforts are extending and modifying these designs to different ferroelectric films, which are being doped to reduce losses, and to different dielectric substrates.

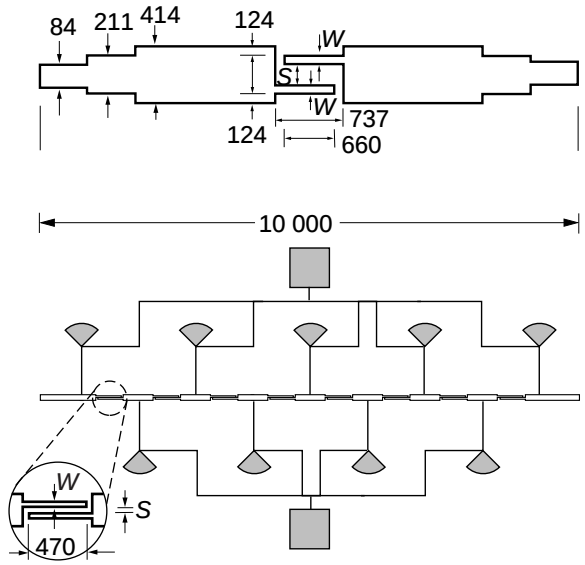

Schematic of two coupled microstrip phase shifters. All dimensions are in micrometers. Top: 25-Ω, single-element phase shifter; S = 12.7 μm, W = 76.2 μm. Bottom: 50-Ω, eight-element phase shifter; S = 7.2 μm, W = 25 μm.

In addition, proof-of-concept tunable local oscillators have been assembled from thin-film ferroelectric ring resonators combined with gallium arsenide PHEMT's (pseudomorphic high electron mobility transistors). These devices have shown apparent unloaded quality factors up to 15 000 and frequency tuning ranges of 2 GHz in the Ku-band. In addition, two tunable filters have been linked to form a tunable diplexer operating at the Ku- and K-bands. The tunable local oscillator and tunable diplexer are intended to be integrated into a discriminator-locked tunable oscillator currently under development at Lewis.

Bibliography

Van Keuls, F.W., et al.: ($YBa_2Cu_3O_{7-\delta}$, Au)/$SrTiO_3$/$LaAlO_3$ Thin Film Conductor/Ferroelectric Coupled Microstripline Phase Shifters for Phased Array Applications. Appl. Phys. Lett., vol. 71, Nov. 1997, p. 3075.

Subramanyam, G.; Van Keuls, F.; and Miranda, F.A.: A K-Band Tunable Microstrip Bandpass Filter Using a Thin Film Conductor/Ferroelectric/Dielectric Multilayer Configuration. IEEE Microwave Guided Wave Letters, vol. 8, no. 2, 1998, pp. 78–80.

Subramanyam, G.; Van Keuls, F.; and Miranda, F.A.: Novel K-Band Tunable Microstrip Bandpass Filter Using a Thin Film HTS/Ferroelectric/Dielectric Multilayer Configuration. IEEE MTT–International Microwave Symposium Digest, vol. 2 (NASA TM—1998-207940. Available online: http://gltrs.grc.nasa.gov/cgi-bin/GLTRS/browse.pl?1998/TM-1998-207940.html), 1998, pp. 1011–1014.

Romanofsky, R.R.; Van Keuls, F.W.; and Miranda, F.A.: Cryogenic GaAs PHEMT/Ferroelectric Ku-Band Tunable Oscillator. J. de Physique IV, vol. 8, no. 3 (NASA TM—1998-206967. Available online: http://gltrs.grc.nasa.gov/cgi-bin/GLTRS/browse.pl?1998/TM-1998-206967.html), 1998, pp. 171–174.

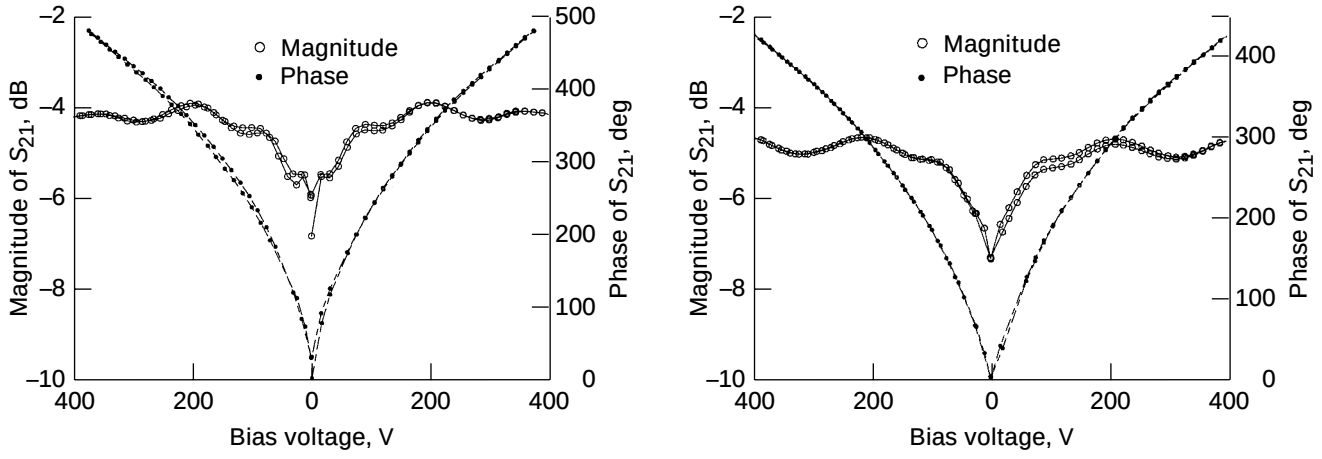

Phase shifts of 50-Ω, eight-element, $YBa_2Cu_3O_{7-\delta}$ (0.35 μm)/$SrTiO_3$ (1.0 μm)/$LaAlO_3$ (254 μm) coupled microstrip phase shifter. Left: Temperature, 40 K; frequency, 16 GHz. Right: Temperature, 77 K; frequency, 16 GHz.

Miranda, F.A., et al: Tunable Microwave Components for Ku- and K-Band Satellite Communications. Integrated Ferroelectronics, vol. 22, no. 789 (NASA TM—1998-206963. Available online: http://gltrs.grc.nasa.gov/cgi-bin/GLTRS/browse.pl?1998/TM-1998-206963.html), 1998.

Van Keuls, F.W., et al.: Influence of the Biasing Scheme on the Performance of Au/$SrTiO_3$/$LaAlO_3$ Thin Film Conductor/Ferroelectric Tunable Ring Resonators. Integrated Ferroelectrics, vol. 22, no. 883 (NASA TM—1998-206641. Available online: http://gltrs.grc.nasa.gov/cgi-bin/GLTRS/browse.pl?1998/TM-1998-206641.html), 1998.

Van Keuls, F.W.; Romanofsky, R.R.; and Miranda, F.A.: Several Microstrip-Based Conductor/ Thin Film Ferroelectric Phase Shifter Designs Using ($YBa_2Cu_3O_{7-\delta}$,Au)/$SrTiO_3$/$LaAlO_3$ Structures. Integrated Ferroelectrics, vol. 22, no. 893 (NASA TM—1998-206964. Available online: http://gltrs.grc.nasa.gov/cgi-bin/GLTRS/browse.pl?1998/TM-1998-206964.html), 1998.

Van Keuls, F.W., et al.: A Ku-Band Gold/$Ba_xSr_{1-x}TiO_3$/$LaAlO_3$ Conductor/Thin Film Ferroelectric Microstripline Phase Shifter for Room Temperature Communications Applications. Microwave and Optical Technology Letters, vol. 20, no. 1, 1999, pp. 53–56.

Lewis contacts: Dr. Frederick W. Van Keuls, (216) 433–9704, Frederick.W.Vankeuls@grc.nasa.gov; Robert R. Romanofsky, (216) 433–3507, Robert.R.Romanofsky@grc.nasa.gov; and Dr. Félix A. Miranda, (787) 850–9381, FA_MIRANDA@cuhac.upr.clu.edu, or (216) 433–6589, Felix.A.Miranda@grc.nasa.gov

Author:
Dr. Frederick W. Van Keuls

Headquarters program office:
OSS, DDF

Programs/Projects:
Low-cost tracking ground terminals, low-phase noise receivers

Technique Developed for Optimizing Traveling-Wave Tubes

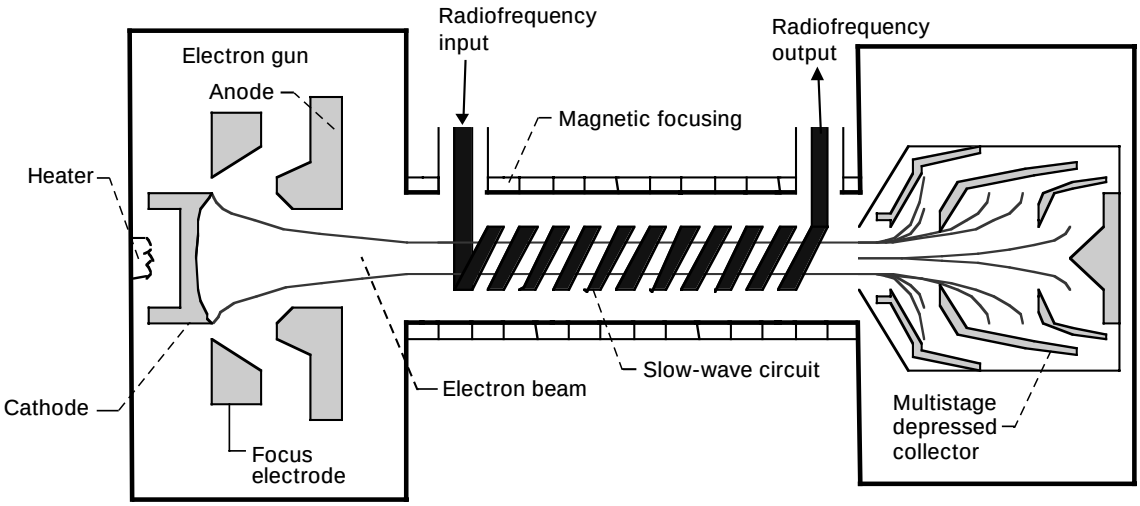

Traveling-wave tube.

A traveling-wave tube (TWT) is an electron beam device that is used to amplify electromagnetic communication waves at radio and microwave frequencies. TWT's are critical components in deep-space probes, geosynchronous communication satellites, and high-power radar systems.

Power efficiency is of paramount importance for TWT's employed in deep-space probes and communications satellites. Consequently, increasing the power efficiency of TWT's has been the primary goal of the TWT group at the NASA Lewis Research Center over the last 25 years.

An in-house effort produced a technique (ref. 1) to design TWT's for optimized power efficiency. This technique is based on simulated annealing, which has an advantage over conventional optimization techniques in that it enables the best possible solution to be obtained (ref. 2). A simulated

annealing algorithm was created and integrated into the NASA TWT computer model (ref. 3). The new technique almost doubled the computed conversion power efficiency of a TWT from 7.1 to 13.5 percent (ref. 1).

The algorithm can be readily modified so that any calculable TWT characteristic can be optimized with respect to any combination of input design parameters. This has enabled TWT's to be optimally designed for important characteristics for which there were previously no design optimization methodologies. For example, in one version, the technique has been used to design a TWT for optimized overall power efficiency, which is extremely important for TWT's used on deep-space probes and communications satellites. This design incorporates both the conversion power efficiency from the electron beam to the microwave signal and the energy collected from the "spent" beam in the multistage-depressed collector (see the illustration). In another version, the technique was used to optimize the power over a wide frequency bandwidth instead of at just a single frequency. This will substantially increase the data transmission volume capability of TWT's. In yet another version, the technique was used to design a TWT with both high conversion power efficiency and low signal distortion.

References

1. Wilson, J.D.: Simulated Annealing Algorithm for Optimizing RF Power Efficiency in Coupled-Cavity Traveling-Wave Tubes. IEEE Trans. Electron Devices, vol. 44, no. 12, Dec. 1997, pp. 2295–2299.
2. Kirkpatrick, S.: Optimization by Simulated Annealing. Science, 1983, pp. 671–680.
3. Wilson, J.D.: Revised NASA Axially Symmetric Ring Model for Coupled-Cavity Traveling-Wave Tubes. NASA TP–2675, 1987.

Lewis contact:
Dr. Jeffrey D. Wilson, (216) 433–3513, Jeffrey.D.Wilson@grc.nasa.gov

Author: Dr. Jeffrey D. Wilson

Headquarters program office: OSS

Programs/Projects:
Deep Space Network Upgrade.

Special recognition:
One of ten finalists for 1997 Rappaport Prize for the best paper published in IEEE Transactions on Electron Devices

Cassini Radio Science Experiments on Saturn and Titan Preserved Because of Lewis Analysis

The Cassini mission to Saturn is an international venture with participation from NASA, the European Space Agency, and the Italian Space Agency. The Cassini spacecraft was launched from Cape Canaveral in October 1997 and is scheduled to arrive at Saturn in July 2004. After arrival, the spacecraft will orbit Saturn about 60 times over a period of 4 years. During this time, the Cassini Radio Science Subsystem will be used to investigate the atmosphere and rings of Saturn and the atmosphere of its largest moon, Titan—which is larger than Mercury and is the only moon in our solar system with a dense atmosphere.

A critical component in Cassini's Radio Science Subsystem is a traveling-wave tube (TWT) that was designed at the NASA Lewis Research Center and built by Hughes Electronic Dynamics Division (ref. 1). This TWT will amplify downlink microwave signals at a frequency of 32 GHz for the Deep Space Network and will be involved in a number of experiments. These include occultation experiments in which the microwave signal will be beamed through rings and atmospheres toward Earth. Researchers will analyze the received signals to determine the sizes and distributions of the particles in the rings and the structure and composition of the atmospheres. The Radio Science Subsystem also will also be used to more accurately determine the mass and size of Saturn and its moons, to investigate the solar corona, and to search for gravity waves from outside the solar system.

During tests of the TWT in 1995, the Jet Propulsion Laboratory (JPL) discovered an unexpected anomalous signal at a frequency of 35 GHz. Curiously, this signal only occurred at power levels below that at which the TWT was to be operated. Mission planners were very concerned that a small change in operating conditions might

cause the spurious signal to occur at higher power levels and interfere with detection of the desired signal at 32 GHz. Because the Jet Propulsion Laboratory was unable to determine the cause of the anomalous signal experimentally, an in-house effort was initiated at Lewis to try to determine the cause of the anomalous signal with Lewis-developed computer analysis techniques.

Lewis' extensive computer analysis determined that the anomalous signal is an intermodulation product of the 32-GHz signal with a 67-GHz oscillation (ref. 2). The oscillation is induced by coupling to a second harmonic beam current, which is significantly high only at low power levels. The analysis indicated that possible changes in operating conditions would not cause the anomaly to be a problem. The analysis convinced the Jet Propulsion Laboratory to not remove the Radio Science Subsystem from the Cassini spacecraft, and the experiments will proceed as originally planned.

References

1. Curren, A.N., et al.: The Cassini Mission Ka-Band TWT. 1994 IEEE IEDM Technical Digest, 1994, pp. 783–786.
2. Dayton, J.; Wilson, J.; and Kory, C.: Computer Analysis of the Spectrum Anomaly in the 32-GHz TWT for the Cassini Mission. NASA TP—1999-208691.

Lewis contact:
Dr. Jeffrey D. Wilson, (216) 433–3513, Jeffrey.D.Wilson@grc.nasa.gov

Author: Dr. Jeffrey D. Wilson

Headquarters program office: OSS

Programs/Projects:
Cassini Mission to Saturn

Novel Low-Cost, Low-Power Miniature Thermionic Cathode Developed for Microwave/Millimeter Wave Tube and Cathode Ray Tube Applications

A low cost, small size and mass, low heater power, durable high-performance barium dispenser thermionic cathode has been developed that offers significant advancements in the design, manufacture, and performance of the electron sources used in vacuum electronic devices—such as microwave (and millimeter wave) traveling-wave tubes (TWT's)—and in display devices such as high-brightness, high-resolution cathode ray tubes (CRT's). The lower cathode heater power and the reduced size and mass of the new cathode are expected to be especially beneficial in TWT's for deep space communications, where future missions are requiring smaller spacecraft, higher data transfer rates (higher frequencies and radiofrequency output power), and greater electrical efficiency. Also expected to benefit are TWT's for commercial and government communication satellites, for both low and geosynchronous Earth orbit, with additional benefits offered by lower cost and potentially higher cathode current loading.

A particularly important TWT application is in the microwave power module (MPM), which is a hybrid microwave (or millimeter wave) amplifier consisting of a low-noise solid-state driver, a vacuum power booster (small TWT), and an electronic power conditioner integrated into a single compact package. The attributes of compactness and potentially high electrical efficiency make the MPM very attractive for many commercial and government (civilian and defense) applications in communication and radar systems. The MPM is already finding application in defense electronic systems and is under development by NASA for deep space communications. However, for the MPM to become competitive and commercially successful, a major reduction in cost must be achieved.

The new cathode is expected to make an important contribution to lowering the cost of MPM's and, in addition, offer significant improvements in the electrical efficiency and thermal management, as well as potential reductions in size and mass. Barium dispenser cathodes, with their higher emission current density capability and greater durability, offer brightness, resolution, and lifetimes superior to the alkaline-earth oxide-coated cathodes most commonly used in CRT's. Immediate applications for CRT's are in high-end monitors (such as those for medical imaging, computer-aided design (CAD), and air traffic control), in CRT-based projection displays, and in high-definition television receivers.

FDE Associates of Beaverton, Oregon, developed the miniature barium dispenser cathode under a Small Business Innovation

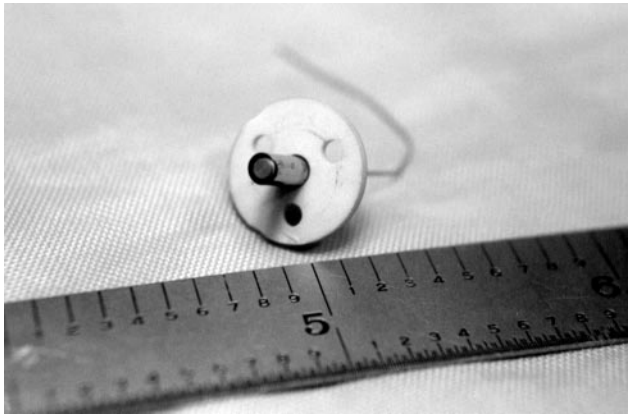

Support sleeve and ceramic disk mounting for 0.065-in. cathode scale.

Research (SBIR) contract with NASA Lewis Research Center. The design and fabrication are based on practices used in the production of CRT's, which is one of the most competitive and efficient manufacturing operations in the world today. The approach used in the design and manufacture of thermionic cathodes and electron guns for CRT's has been optimized for fully automated production, standardization of parts, and minimization of costs. In addition, this approach offers a number of potentially significant benefits for the production of similar components in microwave tubes, among which are low cost, reductions in size and mass, and significantly lower cathode heater power. Although CRT's employ primarily oxide-coated cathodes, CRT manufacturing technology is equally applicable to barium dispenser cathodes.

FDE is presently using the CRT approach to develop and produce a number of cathode sizes ranging from 0.050- to 0.0250-in. in diameter, with corresponding heater powers ranging from <1.0 to <3.5 W, respectively. In addition to miniature TWT's, the 0.050-in. cathode is applicable to high-resolution, high-performance CRT's that require a high brightness electron source. Low cathode heater power results from a highly efficient thermal design and a novel process for thinning and polishing the cathode support sleeve to reduce heat conduction and radiation losses. The barium source is a 4:1:1-impregnated, die pressed, and sintered tungsten alloy pellet for long life and enhanced electron emission (>2 A/cm^2), although other compositions, such as the osmium-coated tungsten pellet are just as feasible. Other basic design features include cylindrical mounting (for ruggedness), ceramic disk mounting (standardized drop-in mounting into electron guns), a slip-in cataphoretic-coated heater (low cost and automated production), a heater enclosure separate from the main support sleeve (for power efficiency and enhanced heater life), a nearly all-welded design with limited brazing (automatic assembly and low cost), and the use of simple shapes, drawn or stamped parts and parts joined by mechanical capture (crimping). Emphasis is on standardization of parts and the design of tooling and assembly procedures for automated production. Flexibility in manufacturing allows easy substitution of other cathode sizes.

Find out more on the World Wide Web: http://www.fdeassc.com

Lewis contact:
Edwin G. Wintucky, (216) 433–3510, Edwin.G.Wintucky@grc.nasa.gov

FDE Assoc. contact:
Bernard K. Vancil, (503) 628–0703, Bernie@fdeassc.com

Author: Edwin G. Wintucky

Headquarters program office: OSS

Programs/Projects:
Space Communications

K-Band Phased Array Developed for Low-Earth-Orbit Satellite Communications

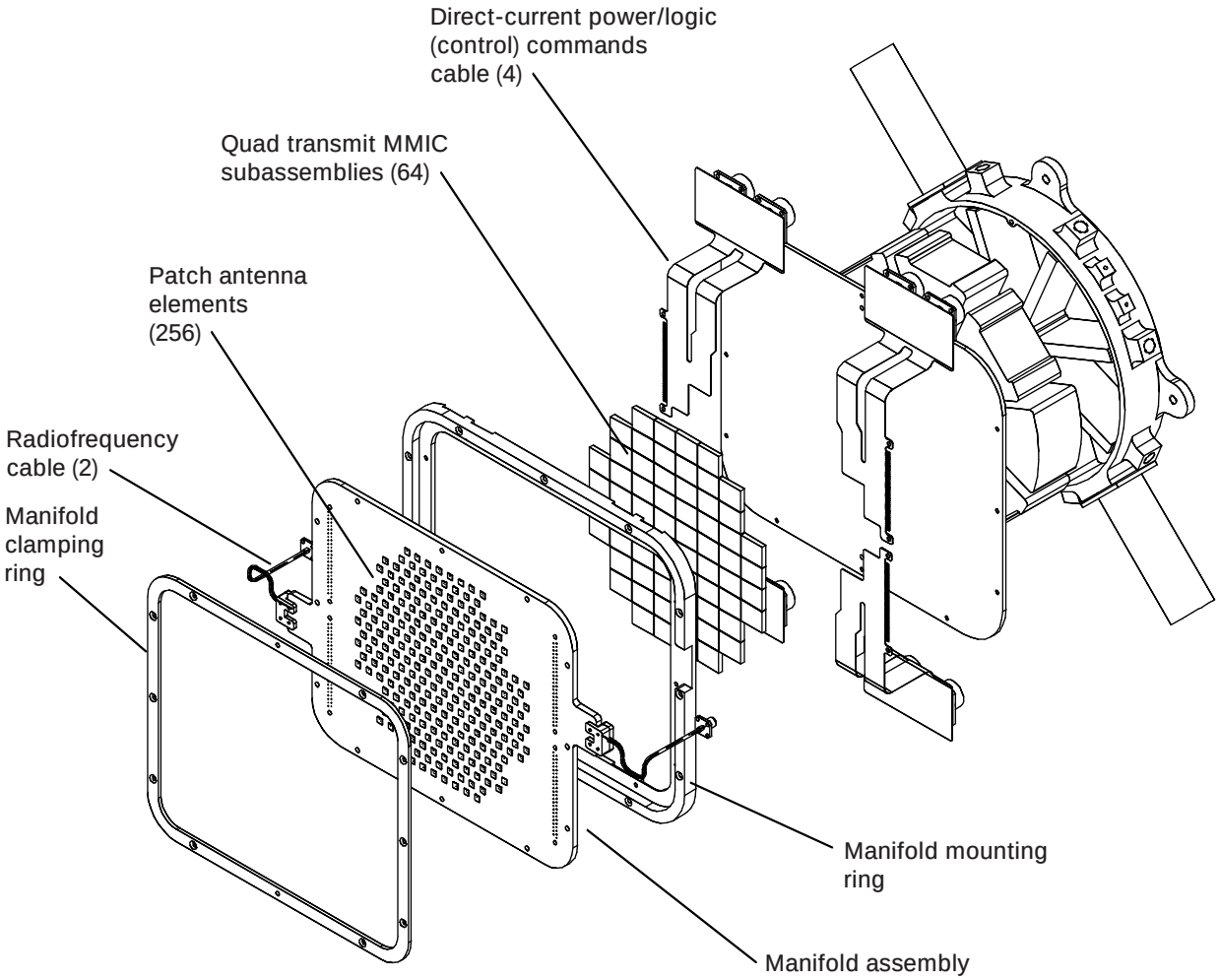

K-band phased-array antenna assembly. (Copyright Raytheon TI Systems; used with permission.)

Future rapid deployment of low- and medium-Earth-orbit satellite constellations that will offer various narrow- to wide-band wireless communications services will require phased-array antennas that feature wide-angle and superagile electronic steering of one or more antenna beams. Antennas, which employ monolithic microwave integrated circuits (MMIC), are perfectly suited for this application. Under a cooperative agreement, an MMIC-based, K-band phased-array antenna is being developed with 50/50 cost sharing by the NASA Lewis Research Center and Raytheon Systems Company. The transmitting array, which will operate at 19 gigahertz (GHz), is a state-of-the-art design that features dual, independent, electronically steerable beam operation ($\pm 42^{\circ}$), a stand-alone thermal management, and a high-density tile architecture. This array can transmit 622 megabits per second (Mbps) in each beam from Earth orbit to small Earth terminals. The weight of the total array package is expected to be less than 8 lb. The tile integration technology (flip chip MMIC tile) chosen for this project represents a major advancement in phased-array engineering and holds much promise for reducing manufacturing costs.

The transmit phased-array antenna has passed the critical design review and is being fabricated, with delivery anticipated in late 1999. Soon after the array is completed, Lewis plans to integrate it into a flight experiment to test its operation in the space environment. The array will be a critical component of the Direct Data Distribution (D^3)

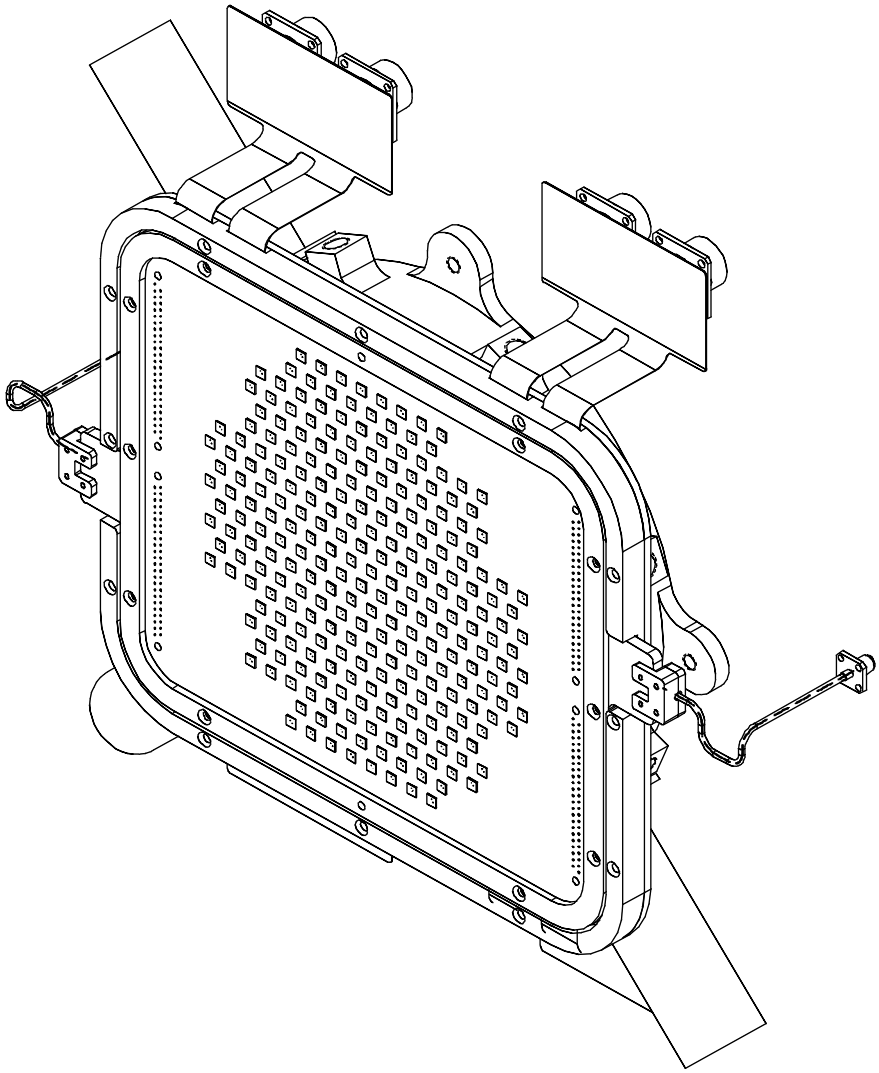

Assembled K-band phased-array antenna. (Copyright Raytheon TI Systems; used with permission.)

flight experiment on a future space shuttle mission, as early as 2001. Incorporation and proper design of significant mechanical, thermal, and control interfaces required for safe and successful operation on a shuttle mission will provide significant leverage for using the antenna in future communications spacecraft. Phased-array antennas that are capable of rapid direct downlinking of large volumes of data from various space platforms, such as the one being developed and described here, are high on the priority list.

For more information, visit Lewis' Communications Technology Division on the World Wide Web:
http://ctd.grc.nasa.gov

Lewis contact:
Godfrey Anzic, (216) 433–3570, Godfrey.Anzic@grc.nasa.gov

Author: Godfrey Anzic

Headquarters program office: OSS

Programs/Projects:
Space Communications, D^3

Conformal, Transparent Printed Antenna Developed for Communication and Navigation Systems

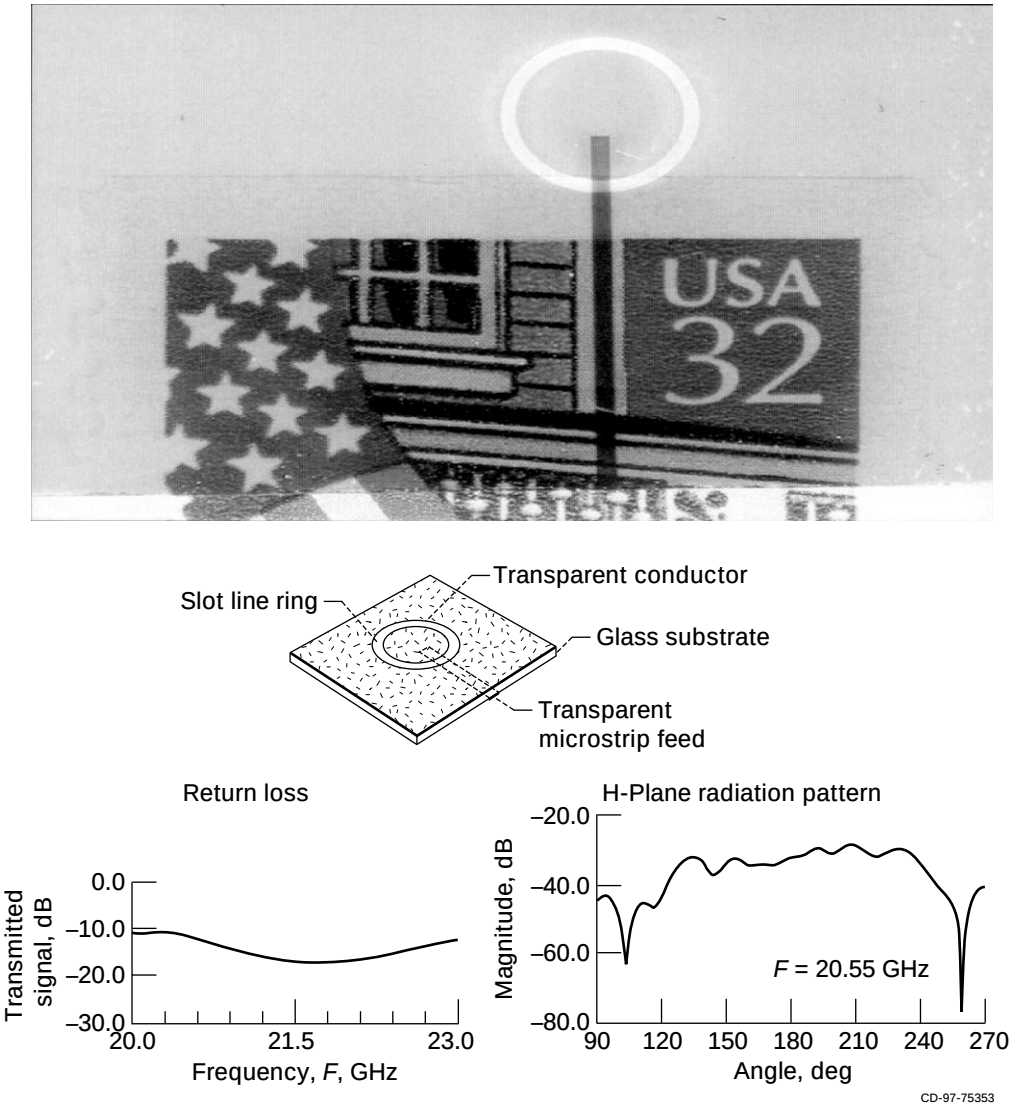

Transparent, electromagnetically coupled ring-slot optically transparent conducting (OTC) antenna. Top: Shown placed on top of a U.S. stamp. Bottom: Attachment details and performance data.

Conformal, transparent printed antennas have advantages over conventional antennas in terms of space reuse and aesthetics. Because of their compactness and thin profile, these antennas can be mounted on video displays for efficient integration in communication systems such as palmtop computers, digital telephones, and flat-panel television displays. As an array of multiple elements, the antenna subsystem may save weight by reusing space (via vertical stacking) on photovoltaic arrays or on Earth-facing sensors. Also, the antenna could go unnoticed on automobile windshields or building windows, enabling satellite uplinks and downlinks or other emerging high-frequency communications.

Recently, a class of transparent patch and slot antennas consisting of an ultrathin film of electrically conductive material deposited on glass or plastic substrates has been developed jointly by the NASA Lewis Research Center and the Federal Data Corporation. A prototype antenna has been demonstrated with the antenna fabricated

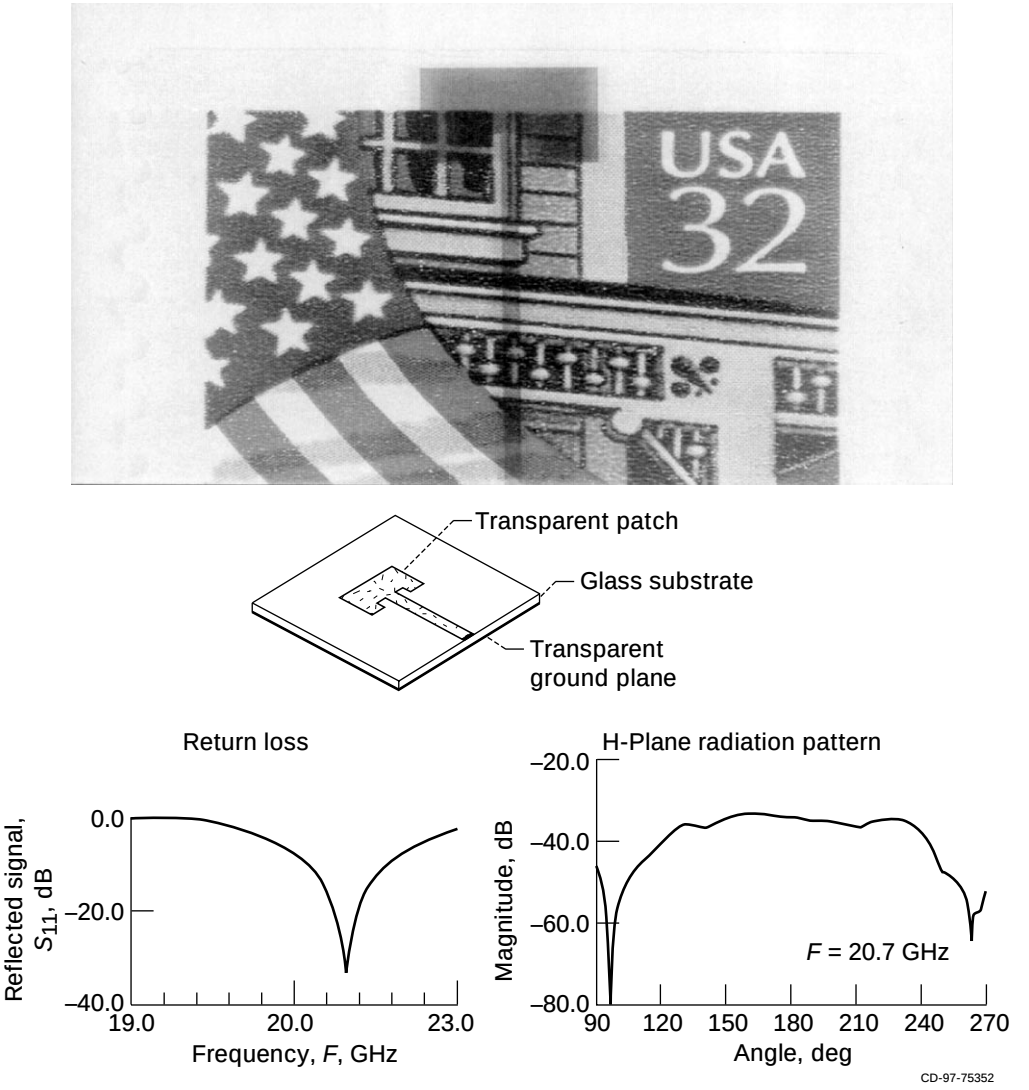

Transparent, rectangular microstrip optically transparent conducting (OTC) patch antenna. Top: Shown placed on top of a U.S. stamp. Bottom: Attachment details and performance data.

on either glass or plastic substrates. The multistep liftoff lithographic technique is used to fabricate antennas are on glass substrates. Two of the tested transparent antennas—a slot ring and a rectangular patch antenna are shown along with their performance data in the figures. The antennas have demonstrated very broadband characteristics, good impedance matching, and radiation patterns for frequencies ranging from 2 to 30 gigahertz (GHz). We believe that these antennas can be further developed to operate in the Federal Communication Commission's (FCC) newly opened, high-frequency bands above 30 GHz. Finally, a 2-by-2 array has been fabricated and is currently being characterized.

Lewis contact:
Dr. Richard Q. Lee, (216) 433–3489, Richard.Q.Lee@grc.nasa.gov

Authors: Dr. Richard Q. Lee and Dr. Rainee N. Simons

Headquarters program office:
OA (DDF)

Programs/Projects: Deep space and commercial wireless communications

Innovative, Inexpensive Etching Technique Developed for Polymer Electro-Optical Structures

Electro-optic, polymer-based integrated optic devices for high-speed communication and computing applications offer potentially significant advantages over conventional inorganic electro-optic crystals. One key area of integrated optical technology—primary processing and fabrication—may particularly benefit from the use of polymer materials. However, as efforts concentrate on the miniaturization of electro-integrated circuit pattern geometries, the ability to etch fine features and smoothly sloped sidewalls is essential to make polymers useful for electro-integrated circuit applications. There are many existing processes available to etch polymer materials, but they all yield nearly vertical sidewalls. Vertical sidewalls are too difficult to reliably cover with a metal layer, and incomplete metalization degrades microwave performance, particularly at high frequency. However, obtaining a very sloped sidewall greatly improves the deposition of metal on the sidewall, leading to low-loss characteristics, which are essential to integrating these devices in high-speed electro-optic modulators.

The NASA Lewis Research Center has developed in-house an inexpensive etching technique that uses a photolithography method followed by a simple, wet chemical etching process to etch through polymer layers. In addition to being simpler and inexpensive, this process can be used to fabricate smoothly sloped sidewalls by using a commercial nonerodible mask: Spin-On-Glass. A commercially transparent material, Spin-On-Glass, uses processes and equipment similar to that for photoresist techniques.

This new etching technique offers a simpler fabrication process and a cost-effective method of generating the moderately sized patterns typically encountered in low and medium density interconnection applications. In addition, it yields high-resolution patterns and smooth sidewalls, resulting in low optical scattering losses. With this technique, measured microwave losses have been found to be very low. The new technique offers low-loss performance comparable to that found with conventional reactive ion etching techniques, which have considerably higher costs.

Lewis contact:
Hung D. Nguyen, (216) 443–6590, Hung.D.Nguyen@grc.nasa.gov

Author: Hung D. Nguyen

Headquarters Program Office:
OSS (ATMS)

Program/Projects:
Space Communications Project

High-Performance, Low-Complexity Codes Researched for Communication Channels

NASA Lewis Research Center's Communications Technology Division has an ongoing program in the development of efficient channel coding schemes for satellite communications applications. Through a university grant, as a part of this research, the University of Toledo is investigating the performance of turbocodes, which use parallel concatenation of nonsystematic convolutional encoders with an interleaver. The error-correcting capacity of these codes is close to the Shannon limit. The research emphasis is on the development of low-complexity, but higher rate (greater than one half), turbocodes and on the iterative decoding of block codes.

Results of extensive computer simulations of higher rate turbocodes (2/3, 4/5, 5/6, 10/11, and 15/16) show that their performance is greatly affected by the proper selection of code polynomials, the puncturing pattern, and the interleaver selection. In addition, some types of turbo-codes tend to have flares or flooring in the energy-to-noise versus bit-error-rate (E_b/N_o versus BER) curve. Research shows that, for the same code polynomials selected, puncturing with the extended puncturing period exhibits significant coding gains since more diverse positions are selected. The graphs show this gain for a 5/6 turbocode. Investigations of flares (or flooring) show that there are two important parameters related to the interleaver design. The first is the degree of

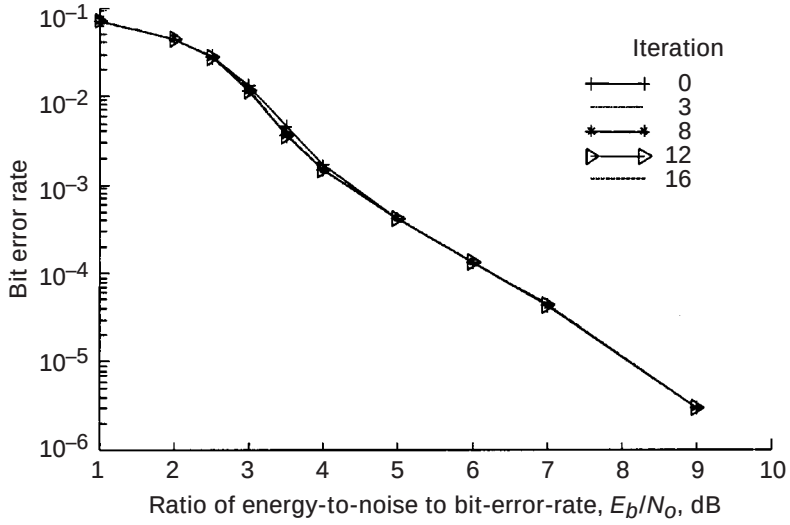

Performance of (23,31) turbocode. Rate, 5/6; conventional puncturing pattern.

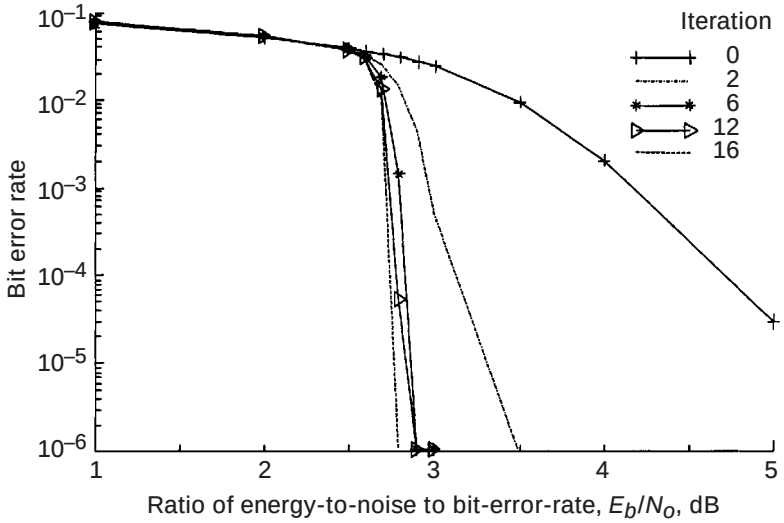

Improved performance of the turbocode with the extended puncturing period.

uniformity. A nonuniform (pseudo-random) interleaver improves performance because it can make the weight distribution of a code similar to that of a random code that has a performance close to the Shannon limit. The other aspect is the interleaver size. Results show that higher rate turbocodes with a large size random interleaver do not exhibit flare. Additional research showed that an interleaver block size of 64 by 64 is optimum for a bit error rate of 10^{-6}.

Another part of the research is on the application of the "turbo" concept to the block codes. The method of iterative decoding based on the Maximum a Posteriori Probability (MAP) algorithm, can be used to improve the performance of a simple block code to close to the theoretical limit. Results show that comparable performance with turbocodes can be achieved if a two-dimensional product code is used whose component codes are binary linear block codes such as the (15,11) extended Hamming code.

For more information, visit the Communications Technology Division on the World Wide Web:
http://ctd.grc.nasa.gov/5650/5650.html

Lewis contact:
Robert E. Jones, (216) 433–3457, Robert.E.Jones@grc.nasa.gov

Authors:
Dr. Subhash C. Kwatra and Robert E. Jones

Headquarters program office: OSS

Programs/Projects:
Space Communications

Reconfigurable Data Communications Packet-Switch Emulation Test Bed Demonstrated

The Communications Technology Division at the NASA Lewis Research Center has an ongoing program to develop advanced switching and routing technology concepts for future satellite onboard processing systems. Through a university grant as a part of this research, the Cleveland State University is using a flexible reconfigurable data communications packet switch emulation test bed to investigate packet switching techniques.

Because of the switching speed and protocol complexity, implementing a data communications network is a tremendous task. Various alternatives should be carefully studied and evaluated in the development stage so that the optimal system configuration can be obtained and implemented later. Therefore, it is desirable to predict the performance of the network before it is actually constructed. This is especially true in the case of satellite systems. In the past, theoretical analysis, software simulation, and prototyping were used to evaluate performance. However, each method has its drawback. There are basic tradeoffs among accuracy, cost, and required evaluation time. No method is completely satisfactory.

In addition to the theoretical analysis, software simulation, and prototype, there is one other possible alternative for performance evaluation—hardware emulation. Hardware emulation is similar to software simulation except that dedicated hardware modules replace software routines. The dedicated hardware can achieve much better performance and provide several orders of magnitude in increased speed over software simulation. When applied to network evaluation, it can be used to gather data for a realistic network configuration and to evaluate the performance of different schemes and protocols.

Para	Parameter	Control signal from the computer hardware
FIFO count	First in, first out count	Signal that keeps track of the number of generated data packets
Dest port	Destination port	Final destination of a generated data packet
LFSR	Linear Feedback Shift Register	Used as a uniform random number generator for generating data packets
ISA	Industry Standard Architecture	Standard hardware configuration used by 286 to 486 class IBM clone computers

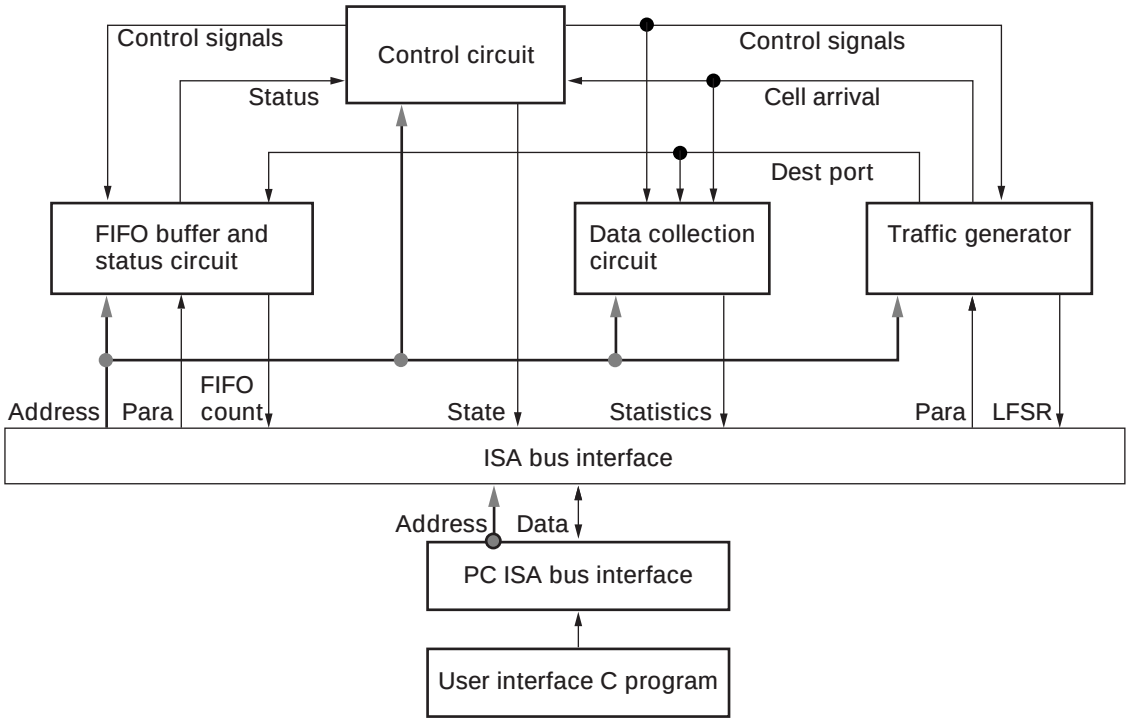

Reconfigurable packet-switch emulation test bed.

In the past, hardware emulation methods suffered the drawback of high cost and inflexibility and thus were rarely used. However, recent advances in field programmable gate array technology make it a feasible, and possibly superior, approach. The Cleveland State study investigated this approach and explored the feasibility of using hardware emulation to evaluate the performance of various asynchronous transfer mode (ATM) switch configurations and protocols. A reconfigurable test bed was developed utilizing static RAM-based (random access memory based) field programmable gate array technology. The flexible test bed, which was constructed to emulate an ATM switch, and consisted of an abstract ATM switch, a traffic generator, a data collection circuit, and a PC host interface (see the diagram). All the test bed hardware was described in industrial standard very high development language (VHDL). It was then synthesized and mapped into a field programmable gate array board. The construction and testing of the prototyping system was completed and used to evaluate several buffer management schemes. Results show that the hardware emulation was 10^2 to 10^5 times faster than software simulation.

For more information, visit the Communications Technology Division on the World Wide Web:
http://ctd.grc.nasa.gov/5650/5650.html

Lewis contact:
Robert E. Jones, (216) 433–3457, Robert.E.Jones@grc.nasa.gov

Authors:
Dr. Pong P. Chu and Robert E. Jones

Headquarters program office: OSS

Programs/Projects:
Space Communications

Bandwidth-Efficient Wireless Digital Modem Developed

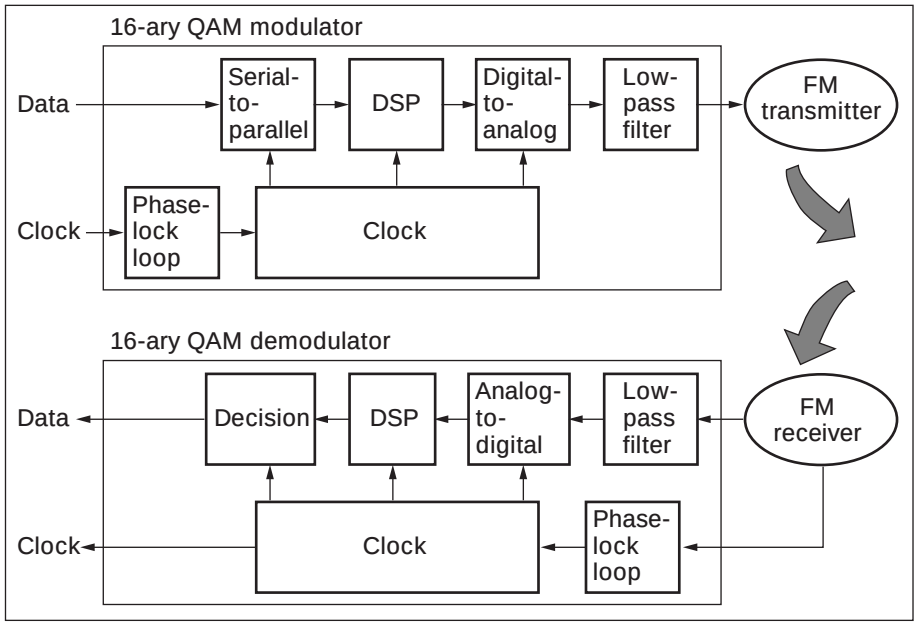

Bandwidth-efficient wireless digital modem with 16-ary quadrature amplitude modulation (QAM) and digital signal processing (DSP).

NASA Lewis Research Center has developed a digital approach for broadcasting high-fidelity audio (nearly compact disk (CD) quality sound) in the commercial frequency-modulated (FM) broadcast band. This digital approach provides a means of achieving high data transmission rates with low hardware complexity—including low mass, size, and power consumption. Lewis has completed the design and prototype development of a bandwidth-efficient digital modem (modulator and demodulator) that uses a spectrally efficient modulation scheme: 16-ary rectangular quadrature amplitude modulation, or 16-ary QAM. The digital

implementation is based strictly on inexpensive, commercial off-the-shelf digital signal processing (DSP) hardware to perform up and down conversions and pulse shaping. The digital modem transmits data at rates up to 76 kilobits per second (kbps), which is almost 3 times faster than standard 28.8-kbps telephone modems. In addition, the modem offers improved power and spectral performance, flexible operation, and low-cost implementation.

The resulting technology, digital audio broadcasting, can provide listeners with greatly enhanced, near-CD quality sound for FM radio, the consumer electronics industry with a great commercial opportunity, and radio broadcasters with the ability to provide improved sound and services to listeners. Other potential uses for this modem include digital wireless data applications (commercial, industrial, or educational), wireless transmission of point-of-sale data and hospital records, and automation of factory control signals. Its main benefits are low cost, high throughput, and small board size, comparable to that of a computer modem.

Lewis designed this bandwidth efficient digital modem under a nonreimbursable Space Act Agreement with Telos System Inc., which is based in Cleveland, Ohio. Telos Systems Inc. has explicit potential markets and applications for the modem in the commercial FM broadcast band, both in transmitting data-reduced digital signals and in broadcasting high-fidelity audio.

Lewis contact:
Muli Kifle, (216) 433–6521, Muli.Kifle@grc.nasa.gov

Author: Muli Kifle

Headquarters program office: OSS

Programs/Projects: Commercial Communications Technology

622-Mbps Orthogonal Frequency Division Multiplexing Modulator Developed

The Communications Technology Division at the NASA Lewis Research Center is developing advanced electronic technologies for the space communications and remote sensing systems of tomorrow. As part of the continuing effort to advance the state-of-the-art in satellite communications and remote sensing systems, Lewis is developing a programmable Orthogonal Frequency Division Multiplexing (OFDM) modulator card for high-data-rate communication links. The OFDM modulator is particularly suited to high-data-rate downlinks to ground terminals or direct data downlinks from near-Earth science platforms. It can support data rates up to 622 megabits per second (Mbps) and high-order modulation schemes such as 16-ary quadrature amplitude modulation (16-ary QAM) or 8-phase shift keying (8PSK). High order modulations can obtain the bandwidth efficiency over the traditional binary phase shift keying (BPSK) or quadrature phase shift keying (QPSK) modulator schemes. The OFDM modulator architecture can also be precompensated for channel disturbances and alleviate amplitude degradations caused by nonlinear transponder characteristics.

The 622-Mbps OFDM modulator contains four orthogonal 155-Mbps channels. Each channel is based on SiCOM's (Scottsdale, Arizona; see http://www.sicom.com) SMC–960A Data Encoder and Pulse Shaper ASIC (application-specific integrated circuit) chip, which is the result of Small Business Innovative Research Phase II funding from Lewis.

Find out more about Lewis' work with communications satellites on the World Wide Web:
http://sulu.grc.nasa.gov

Lewis contact:
Nam T. Nguyen, (216) 433–3425, Nam.T.Nguyen@grc.nasa.gov

Author: Nam T. Nguyen

Headquarters program office:
OSS, SBIR

Programs/Projects:
Near Earth Science, EOS, D^3

Silicon-Germanium Fast Packet Switch Developed for Communications Satellites

Emerging multimedia applications and future satellite systems will require high-speed switching networks to accommodate high data-rate traffic among thousands of potential users. This will require advanced switching devices to enable communication between satellites. The NASA Lewis Research Center has been working closely with industry to develop a state-of-the-art fast packet switch (FPS) to fulfill this requirement.

Recently, the Satellite Industry Task Force identified the need for high-capacity onboard-processing switching components as one of the "grand challenges" for the satellite industry in the 21st century. In response to this challenge, future generations of onboard processing satellites will require low power and low mass components to enable transmission of services in the 100 gigabit (10^{11} bits) per second (Gbps) range.

Lewis and Sierra Monolithics developed a state-of-the-art 10-Gbps-per-port switch. This promising silicon-germanium (SiGe) technology enables the design of high-speed circuits at very low power consumption. Some of the benefits of this state-of-the-art technology follow:

- U. S. satellite industry competitiveness will be enhanced through the development of high-throughput, low-power onboard components to support the National and Global Information Infrastructures (NII/GII).
- Satellite and terrestrial systems will become fully interoperable.
- Bandwidth efficient systems will improve capacity 100 times over existing satellite architectures for commercial applications.
- The complexity of Earth stations will be reduced.

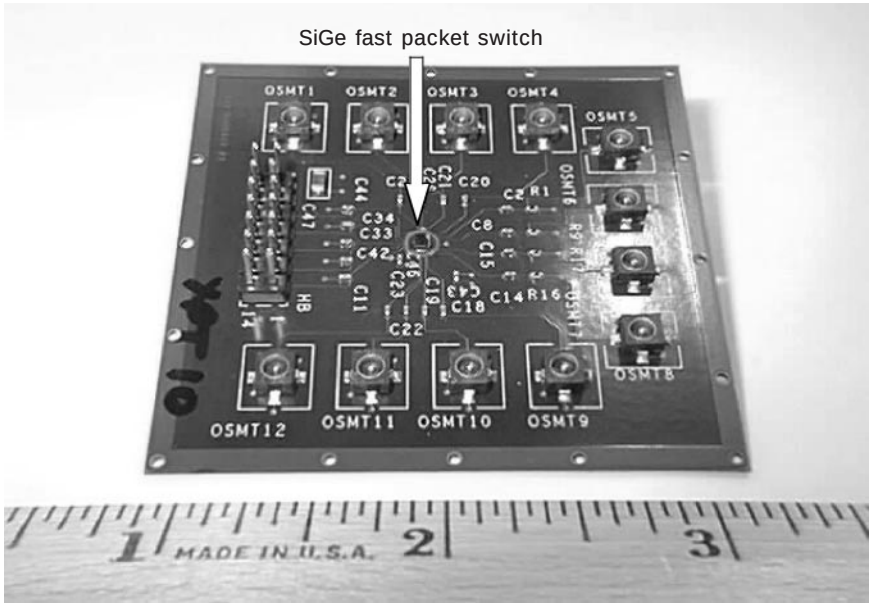

Silicon germanium fast packet switch test board.

The SiGe switch is based on a 16-input by 16-output SiGe crossbar switch that can transmit and receive data at 10 Gbps per port with very low power and weight requirements. The switch has a robust contention control that is suitable for satellite onboard processing applications.

In 1998, Sierra Monolithics simulated and tested a prototype 4-by-4 SiGe switch with favorable results. The test board, along with the fast packet switch chip, is shown in the photograph. A final 16-by-16 switch is being fabricated and will be tested and delivered to Lewis in 1999 for further evaluation. Lewis envisions this technology as suitable for next-generation satellite systems for NASA missions as well as commercial applications requiring high capacity and higher data rates.

Lewis contact:
Gene Fujikawa, (216) 433–3495, Gene.Fujikawa@grc.nasa.gov

Author: Jorge A. Quintana

Headquarters program office: OSS

Programs/Projects: NII/GII, commercial satellite and terrestrial communications systems

Turbomachinery and Propulsion Systems

Multistage Turbomachinery Flows Simulated Numerically

At the NASA Lewis Research Center, a comprehensive assessment was made of the predictive capability of the average passage flow model as applied to multistage axial-flow compressors. This model, which describes the time-averaged flow field within a typical passage of a blade row embedded in a multistage configuration, is being widely used throughout U.S. aircraft industry as an integral part of their design systems.

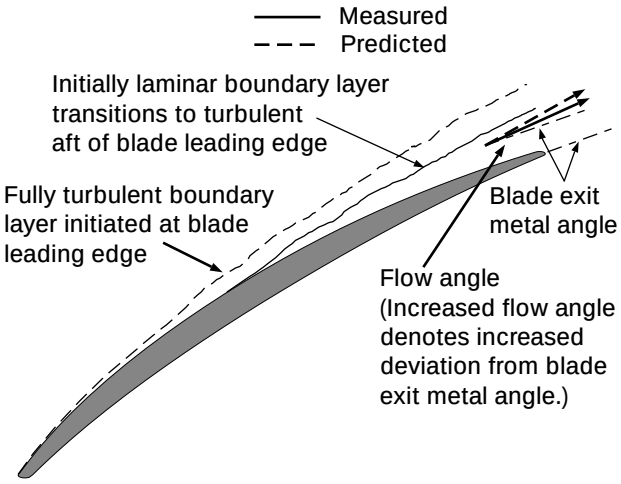

Rotor flow-angle deviation.

In this work, detailed data taken within a four and one-half stage large low-speed compressor were used to assess the weaknesses and strengths of the predictive capabilities of the average passage flow model. The low-speed compressor blading is of modern design and employs stator end-bends. Measurements were made with slow- and high-response instrumentation. The high-response measurements revealed the velocity components of both the rotor and stator wakes. From the measured wake profiles, we found that the flow exiting the rotors deviated from the rotor exit metal angle to a lesser degree than was predicted by the average passage flow model (see the top figure). This was found to be due to blade boundary layer transition, which recently has been shown to exist on multistage axial compressor rotor and stator blades (ref. 1), but was not accounted for in the average passage model. Consequently, a model that mimics the effects of blade boundary layer transition, Shih k-ε model, was incorporated into the average passage model. Simulations that incorporated this transition model showed a dramatic improvement in agreement with data (see the bottom figure). The altered model thus improved predictive capability for multistage axial-flow compressors, and this was verified by detailed experimental measurement. For more information, see references 2 and 3.

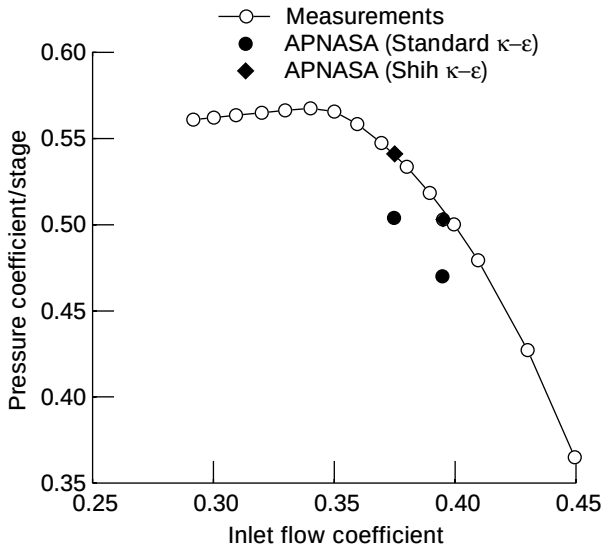

Overall pressure rise coefficient per stage.

References

1. Adamczyk, J.J., et al.: Numerical Simulation of Multistage Turbomachinery Flows. AGARD Propulsion and Energetics Panel. Tulous, France, May 1998.
2. Adamczyk, J.J., et al.: Numerical Simulation of Multistage Turbomachinery Flows. Unsteady Flows in Turbomachines, VKI–LS–1996–05, vol. 2, 1996.

3. Shih, T.-H., et al. New K-ε Eddy Viscosity Model for High Reynolds Number Turbulent Flows. Comp. Fluids, vol. 24, no. 3, 1995, pp. 227–238.

Lewis contacts:
Dr. Michael D. Hathaway, (216) 433–6250, Michael.D.Hathaway@grc.nasa.gov; and Dr. John J. Adamczyk, (216) 433–5829, John.J.Adamczyk@grc.nasa.gov

Authors: Dr. Michael D. Hathaway, Dr. John J. Adamczyk, Aamir Shabbir, and Steven R. Wellborn

Headquarters program office: OAT

Programs/Projects: Propulsion Systems R&T, P&PM, AST, HSR, SGE

Optical Flow-Field Techniques Used for Measurements in High-Speed Centrifugal Compressors

The overall performance of a centrifugal compressor depends on the performance of the impeller and diffuser as well as on the interactions occurring between these components. Accurate measurements of the flow fields in each component are needed to develop computational models that can be used in compressor design codes. These measurements must be made simultaneously over an area that covers both components so that researchers can understand the interactions occurring between the two components.

Optical measurement techniques are being used at the NASA Lewis Research Center to measure the velocity fields present in both the impeller and diffuser of a 4:1 pressure ratio centrifugal compressor operating at several conditions ranging from design flow to surge. Laser Doppler Velocimetry (LDV) was used to measure the intrablade flows present in the impeller, and the results were compared with analyses obtained from two three-dimensional viscous codes. The development of a region of low throughflow velocity fluid within this high-speed impeller was examined and compared with a similar region first observed in a large low-speed centrifugal impeller at Lewis.

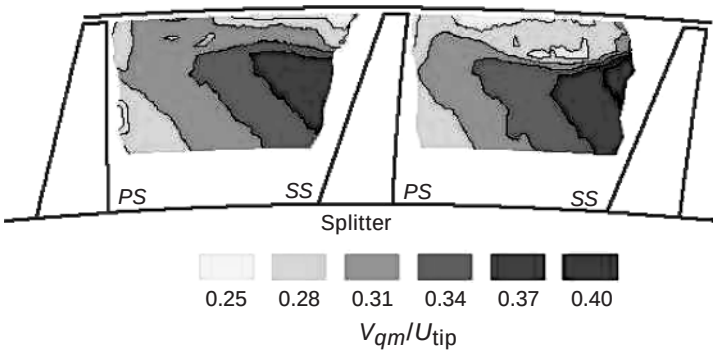

Contours of impeller throughflow velocity from LDV measurements at 70 percent of the blade chord, where V_{qm} is the quasi-meridional, or throughflow, velocity; U_{tip} is the blade tip speed at the impeller discharge; PS is the impeller blade pressure surface; and SS is the suction surface. This figure is shown in color in the online version of this article (http://www.grc.nasa.gov/WWW/RT1998/5000/5810skoch.htm).

Particle Image Velocimetry (PIV) is a relatively new technique that has been applied to measuring the diffuser flow fields. PIV can collect data rapidly in the diffuser while avoiding the light-reflection problems that are often encountered when LDV is used. The Particle Image Velocimeter employs a sheet of pulsed laser light that is introduced into the diffuser in a quasi-radial direction through an optical probe inserted near the diffuser discharge. The light sheet is positioned such that its centerline is parallel to the hub and shroud surfaces and such that it is parallel to the diffuser vane, thereby avoiding reflections from the solid surfaces. Seed particles small enough to follow the diffuser flow are introduced into the compressor at an upstream location. A high-speed charge-coupled discharge (CCD) camera is synchronized to the laser pulse rate; this allows it to capture images of seed particle position that are separated by a small increment in time. A cross-correlation of a particle's position in two consecutive images provides an estimate of flow velocity and direction. Multiple image pairs obtained in rapid succession at a particular flow condition provide enough measurements for statistical significance. PIV provides

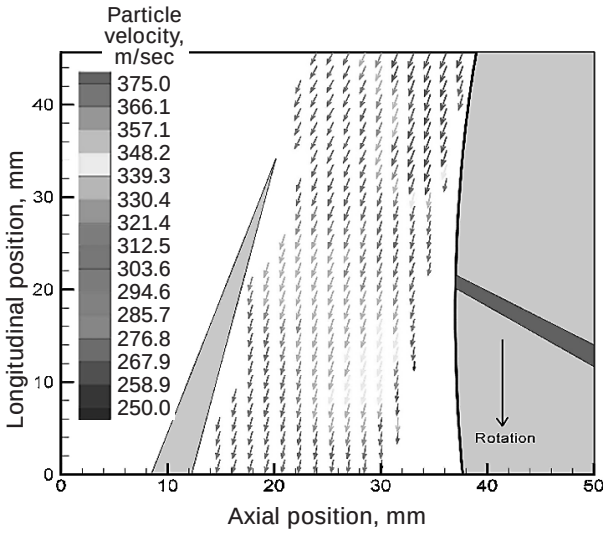

Diffuser absolute velocity field at 88 percent of the passage height obtained using Particle Image Velocimetry. This figure is shown in color in the online version of this article (http://www.grc.nasa.gov/WWW/RT1998/5000/5810skoch.htm).

simultaneous velocity measurements over the entire plane that is illuminated by the light sheet instead of at a single point, as is the case when LDV is used.

PIV has a further advantage in that the laser light pulse can be triggered by an external source such as a high-response pressure transducer. This feature will allow PIV to synchronize flow imaging to physical phenomena such as rotating stall or stall precursor waves. We hope that this technique can be used to obtain images of the flow field during and just prior to stall.

Bibliography

Skoch, G.J., et al.: Laser Anemometer Measurements of the Flow Field in a 4:1 Pressure Ratio Centrifugal Impeller. ASME Paper 97–GT–342, 1997.

Hathaway, M.D., et al.: Experimental and Computational Investigation of the NASA Low-Speed Centrifugal Compressor Flow Field. ASME J. Turbomachinery (ASME Paper 92–GT–216), vol. 115, no. 3, July 1993, pp. 527–541.

Wernet, M.P.: Digital PIV Measurements in the Diffuser of a High Speed Centrifugal Compressor. AIAA Paper 98–2777, 1998.

Lewis contacts:
Gary J. Skoch, (216) 433–3396, Gary.J.Skoch@grc.nasa.gov; and
Dr. Mark P. Wernet, (216) 433–3752, Mark.P.Wernet@grc.nasa.gov

Author: Gary J. Skoch

Headquarters program office: OAT

Programs/Projects:
Propulsion Systems R&T, P&PM

LeRC–HT: NASA Lewis Research Center General Multiblock Navier-Stokes Heat Transfer Code Developed

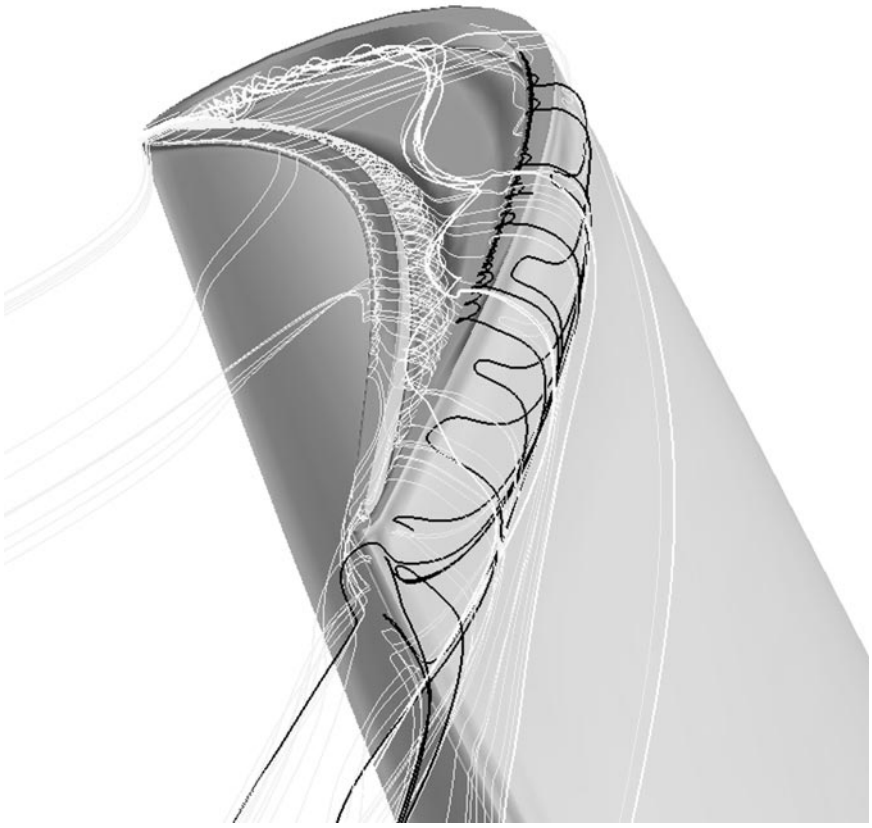

Visualization of the flow and heat transfer over the tip of a high-pressure turbine rotor blade as computed with the LeRC–HT code. Darkest areas represent undesirable high-heat-flux regions. This figure is shown in color in the online version of this article (http://www.grc.nasa.gov/RT1998/5000/5820heidmann.htm).

For the last several years, LeRC–HT, a three-dimensional computational fluid dynamics (CFD) computer code for analyzing gas turbine flow and convective heat transfer, has been evolving at the NASA Lewis Research Center. The code is unique in its ability to give a highly detailed representation of the flow field very close to solid surfaces. This is necessary for an accurate representation of fluid heat transfer and viscous shear stresses. The code has been used extensively for both internal cooling passage flows and hot gas path flows—including detailed film cooling calculations, complex tip-clearance gap flows, and heat transfer. In its current form, this code has a multiblock grid capability and has been validated for a number of turbine configurations. The code has been developed and used primarily as a research tool (at least 35 technical papers have been published relative to the code and its application), but it should be useful for detailed design analysis. We now plan to make this code available to selected users for further evaluation.

Lewis contacts:
Dr. James D. Heidmann, (216) 433–3604, James.D.Heidmann@grc.nasa.gov; and Dr. Raymond E. Gaugler, (216) 433–5882, Raymond.E.Gaugler@grc.nasa.gov

Authors:
Dr. James D. Heidmann and Dr. Raymond E. Gaugler

Headquarters program office: OAT

Programs/Projects:
Propulsion Systems R&T, AST, HSR

Research Data Acquired in World-Class, 60-atm Subsonic Combustion Rig

NASA Lewis Research Center's new, world-class, 60-atmosphere (atm) combustor research facility, the Advanced Subsonic Combustion Rig (ASCR), is in operation and producing highly unique research data. Specifically, data were acquired at high pressures and temperatures representative of future subsonic engines from a fundamental flametube configuration with an advanced fuel injector. The data acquired include exhaust emissions as well as pressure and temperature distributions. Results to date represent an improved understanding of nitrous oxide (NO_x) formation at high pressures and temperatures and include an NO_x emissions reduction greater than 70 percent with an advanced fuel injector at operating pressures to 800 pounds per square inch absolute (psia).

ASCR research is an integral part of the Advanced Subsonic Technology (AST) Propulsion Program. This program is developing critical low-emission combustion technology that will result in the next generation of gas turbine engines producing 50 to 70 percent less NO_x emissions in comparison to 1996 International Civil Aviation Organization (ICAO) limits. The results to date indicate that the AST low-emission combustor goals of reducing NO_x emissions by 50 to 70 percent are feasible.

U.S. gas turbine manufacturers have started testing the low-emissions combustors at the ASCR. This collaborative testing will enable the industry to develop low-emission combustors at the high pressure and temperature conditions of future subsonic engines.

The first stage of the flametube testing has been implemented. Four GE Aircraft Engines low-emissions fuel injector concepts, three Pratt & Whitney concepts, and two Allison concepts have been tested at Lewis' ASCR facility. Subsequently, the flametube was removed from the test stand, and the sector combustor was installed.

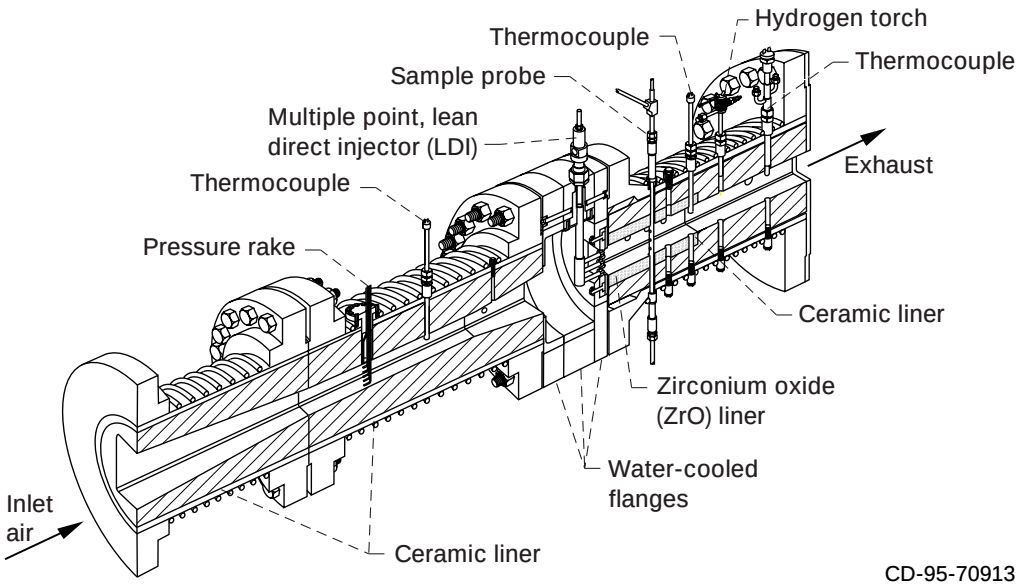

Advanced Subsonic Technology flametube combustor.

The testing of low-emissions sector has begun. Low-emission combustors developed as a result of ASCR research will enable U.S. engine manufacturers to compete on a worldwide basis by producing environmentally acceptable commercial engines.

Lewis contacts: Dr. Chi-Ming Lee, (216) 433–3413, Chi-Ming.Lee@grc.nasa.gov; and Dr. Changlie Wey, (216) 433–5379, Changlie.Wey@grc.nasa.gov

Authors: Dr. Chi-Ming Lee and Dr. Changlie Wey

Headquarters program office: OAT

Programs/Projects: AST

X–33 Combustion-Wave Ignition System Tested

The NASA Lewis Research Center, in cooperation with Rocketdyne, the Boeing Company, tested a novel rocket engine ignition system, called the combustion-wave ignition system, in its Research Combustion Laboratory. This ignition system greatly simplifies ignition in rocket engines that have a large number of combustors. The particular system tested was designed and fabricated by Rocketdyne for the national experimental spacecraft, X–33, which uses Rocketdyne's aerospike rocket engines.

The goal of the tests was to verify the system design and define its operational characteristics. Results will contribute to the eventual successful flight of X–33. Furthermore, the combustion-wave ignition system, after it is better understood and refined on the basis of the test results and, later, flight-proven onboard X–33, could become an important candidate engine ignition system for our Nation's next-generation reusable launch vehicle.

This recent test program successfully proved that the ignition system design is sound. In addition, it identified the operational characteristics of the ignition system that are important to the X–33 vehicle as well as for other future applications.

The program started in 1997, first with a subscale, prototype system that used gaseous propellants, and then with a full-scale, flightlike, prototype system that used liquid hydrogen and oxygen propellants to fully simulate the flight conditions.

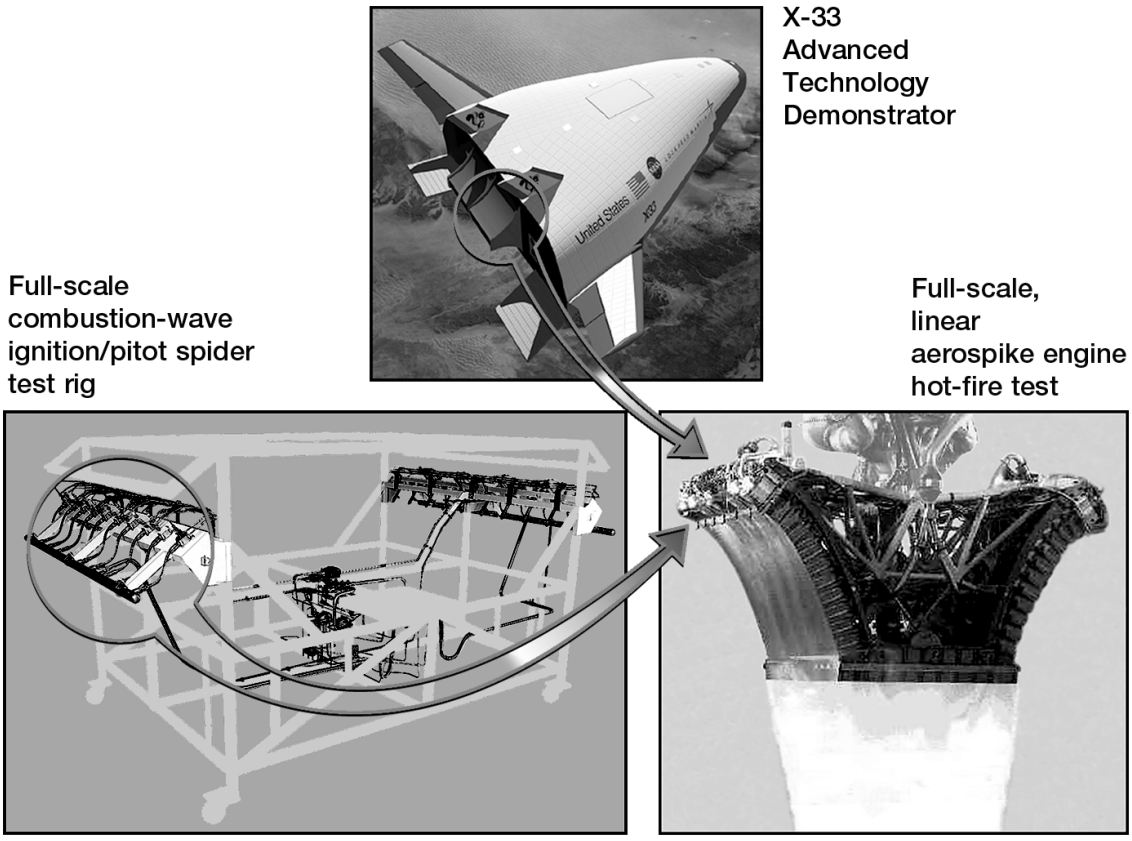

Combustion-wave ignition system testing for the X–33 demonstrator vehicle.

The general concept of the combustion-wave ignition system is that it initiates and distributes the flames of its premixed propellants so that they ignite in multiple locations. It has three basic components: a propellant premixer, an ignition device mounted to the premixer, and a number of tubes stemming from the premixer. The premixer mixes the incoming propellants as they flow into the tubes. The tubes are each terminated at a location where ignition is desired (for example, in a combustor). Several considerations need to be taken, however. First, the propellants in the ignition system should be in a gaseous state and well mixed for the flames to propagate successfully. Second, the propellant pressure in the system should be appropriate in order to avoid damage to the system upon flame initiation. Third, the timing should be optimized for propellant priming and flame initiation at the premixer for each unique application of the system.

The combustion-wave ignition system is simple to design and fabricate, and it offers weight savings, decreased electrical power consumption, and a precise and uniform timing for ignition at multiple locations.

Lewis contact:
Larry C. Liou, (216) 977–7433,
Larry.C.Liou@grc.nasa.gov

Author: Larry C. Liou

Headquarters program office: OAT

Programs/Projects: X–33 Advanced Technology Demonstrator

Use of Atomic Fuels for Rocket-Powered Launch Vehicles Analyzed

At the NASA Lewis Research Center, the launch vehicle gross lift-off weight (GLOW) was analyzed for solid particle feed systems that use high-energy density atomic propellants (ref. 1). The analyses covered several propellant combinations, including atoms of aluminum, boron, carbon, and hydrogen stored in a solid cryogenic particle, with a cryogenic liquid as the carrier fluid. Several different weight percents for the liquid carrier were investigated, and the GLOW values of vehicles using the solid particle feed systems were compared with that of a conventional oxygen/hydrogen (O_2/H_2) propellant vehicle.

Atomic propellants, such as boron, carbon, and hydrogen, have an enormous potential for high specific impulse I_{sp} operation, and their pursuit has been a topic of great interest for decades. Recent and continuing advances in the understanding of matter, the development of new technologies for simulating matter at its most basic level, and manipulations of matter through microtechnology and nanotechnology will no doubt create a bright future for atomic propellants and an exciting one for the researchers exploring this technology.

New technologies in atom isolation and in the physics of material manipulation have led to the discovery and synthesis of materials that can be used as rocket propellants (refs. 1 to 3). Solid cryogenic propellants storing atoms of aluminum, boron, carbon, or hydrogen, or other atomic additives, require a unique propulsion system design where the fuels are stored at liquid helium temperatures during ground handling and flight. Feeding atomic propellants from a propellant tank, through a feed system, to a rocket engine will be a formidable challenge.

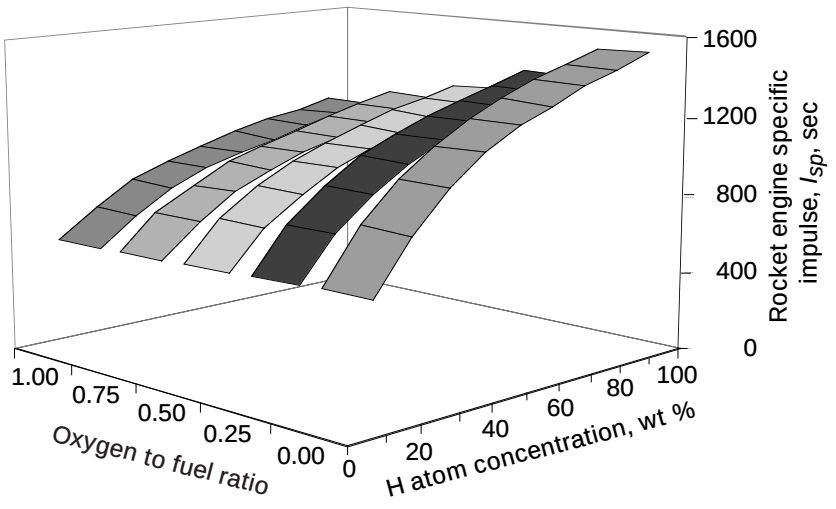

Atomic hydrogen rocket engine performance.

The performance with atomic H was the highest of any of the cases investigated, with its I_{sp} values ranging from 600 to nearly 1300 sec. As shown in this figure, the highest monopropellant performance was 1500 sec delivered at 100 weight percent (wt %) of atomic hydrogen (H). Because it is unlikely that we will be able to store 100 wt % of atomic H, the lower levels of 10, 15, and 50 wt % were investigated in these GLOW analyses.

The figure on the next page illustrates the GLOW values for atomic H. With atomic H, no GLOW reductions were possible until 15 wt % of atomic H was used. At the 10-wt % level, the atomic H GLOW was 4-percent greater than the O_2/H_2 baseline. At a 15-wt % level, the GLOW was reduced by 44 percent. With a 50-wt % atom loading, the GLOW was reduced by 78 percent.

When helium (He) was added to the flow with 10-wt % atomic H, the GLOW was 22- to 106-percent higher than for the baseline case, as shown in the previous figure. The 15-wt % atomic H cases only exceeded the baseline GLOW when 40-wt % He was added. For these cases, the GLOW ranged from a reduction of 37 percent (with a 10-wt % He addition) to an increase of 6 percent (with a 40-wt % He addition). The 50-wt % atomic H cases were almost unaffected by the He addition. The GLOW was 72-percent less than the O_2/H_2 vehicle GLOW, even with the 40-wt % He addition. In summary, with atomic H at a 10-wt % level, no reductions over O_2/H_2 vehicles were possible. At 15-wt % atomic H, there were very significant GLOW

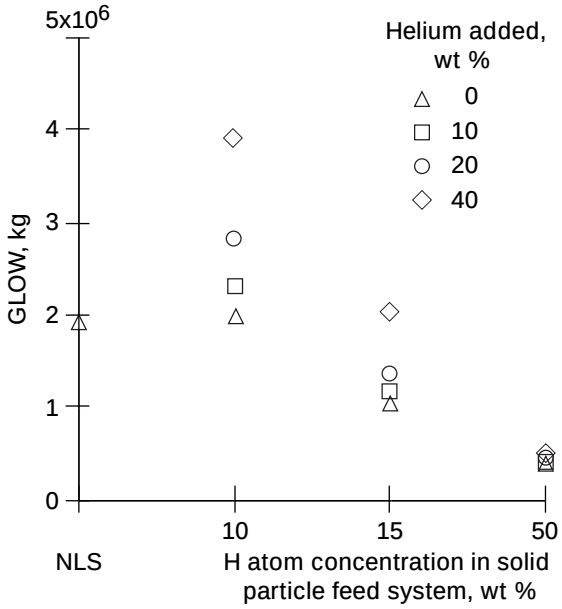

Comparison of atomic propellant launch vehicle gross lift-off weight (GLOW) for the National Launch System (NLS, a conventional O_2/H_2 vehicle) and solid particle feed systems.

reductions for all but the 40-wt % He addition case. The 50-wt % atomic H cases showed a strong insensitivity to He addition.

For more information, visit the SBIR Fuels and Space Propellants web site: http://www.grc.nasa.gov/WWW/TU/launch/foctopsb.htm

References

1. Palaszewski, B.: Launch Vehicle Performance With Solid Particle Feed Systems for Atomic Propellants. AIAA Paper 98–3736 (NASA TM—1998-208498), 1998.
2. Palaszewski, B.: Atomic Hydrogen Propellants: Historical Perspectives and Future Possibilities. AIAA Paper 93–0244 (NASA TM–106053), 1993.
3. Carrick, P.G., and Tam, S., eds.: Proceedings of the High Energy Density Materials (HEDM) Contractors' Conference. USAF Phillips Laboratory, Report Number PL–TR–95–3039, 1996.

Lewis contact: Bryan A. Palaszewski, (216) 977–7493, fax (216) 977–7545, Bryan.A.Palaszewski@grc.nasa.gov

Author: Bryan A. Palaszewski

Headquarters program office: OAT

Programs/Projects: ASTP

NASA/FAA Tailplane Icing Program Completed

Lewis' Twin Otter icing research aircraft.

The NASA/Federal Aviation Administration (FAA) Tailplane Icing Program (TIP) resulted from a concern about aircraft incidents and accidents due to ice-contaminated tailplane stall (ICTS). At least 16 accidents resulting in 139 fatalities have been attributed to such stall. The objectives of this program were to improve understanding of iced tailplane aeroperformance and aircraft aerodynamics and to develop training aids and design tools to expand the awareness of ICTS.

TIP was a 4-yr research program that employed a combination of facilities. These included NASA Lewis Research Center's Icing Research Tunnel to generate actual ice shapes, the Ohio State University's 7×10 ft Low Speed Wind Tunnel to provide tailplane aeroperformance data, and finally Lewis' icing research aircraft, a modified DeHavilland DHC–6 Twin Otter, for tailplane aeroperformance and aircraft aerodynamics measurements. The highlighted accomplishments to date follow:

Twin Otter tailplane with artificial ice shape and flow probes. The ice shapes were cast from ice generated in Lewis' Icing Research Tunnel.

- Development of a comprehensive database on tailplane aeroperformance
- Identification of dominant drivers that lead to tailplane stall
- Demonstration of an effective tailplane stall recovery procedure
- Provision of in-flight demonstrations to guest pilots
- Production and distribution of an educational video for pilots

At the conclusion of the flight tests, we felt that TIP had gathered enough new information that it should be shared. A Guest Pilot Workshop was developed to demonstrate first hand the unique flying qualities of an aircraft with an ice-contaminated tailplane. An international group representing various facets of the aviation industry—aviation regulatory agencies, aircraft manufacturers, and aviation media pilots and reporters—were invited. In total, 15 guest pilots and engineers flew the Twin Otter with the tailplane ice shape attached. This demonstration program provided a mutually beneficial forum for the exchange of information between NASA and the user community. Feedback from the guest pilots has been very positive. Each indicated a greater appreciation of ICTS as a result of this guest pilot workshop. In addition, a 23-min video, *Tailplane Icing*, was produced and distributed. The target audience is primarily pilots who might encounter in-flight icing. It has been enthusiastically received.

TIP and the Guest Pilot Workshop are excellent examples of NASA's response to flight safety initiatives and quick release of information to the user community. TIP is now complete, but a follow-on program, TIP 2, has begun to look at other tailplane configurations and subscale test methods. Learjet and The Wichita State University are partners in the continued activity.

Find out more about this research in the Icing Branch's document archive:
http://icebox.grc.nasa.gov/DocArchive.html

Lewis contacts:
Thomas P. Ratvasky, (216) 433–3905, Thomas.P.Ratvasky@grc.nasa.gov; and Judith Foss Van Zante, (216) 433–3587, Judith.K.VanZante@grc.nasa.gov

Authors:
Thomas P. Ratvasky and Judith Foss Van Zante

Headquarters program office: OAT

Programs/Projects: AOS

Special recognition: Six articles in aviation magazines including *Aviation Week*, *Flying*, and *Airline Pilot*

National Transportation Safety Board Aircraft Accident Investigation Supported

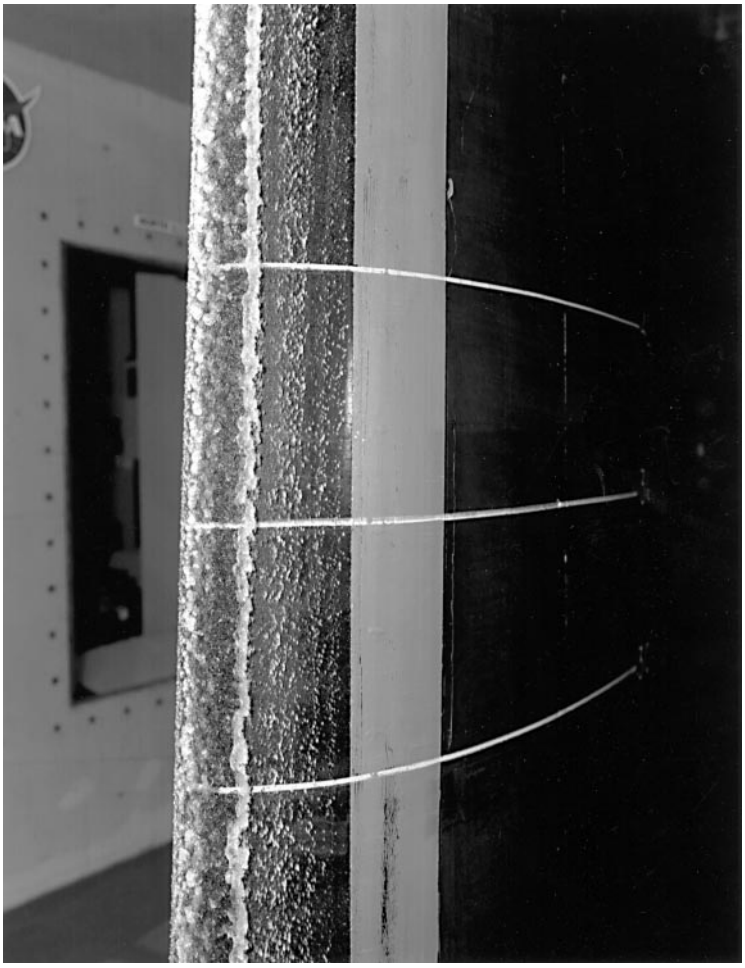

Ice accreted during the testing of the EMB–120 wing in Lewis' Icing Research Tunnel.

The main purpose of this investigation was for NASA to help the National Transportation Safety Board (NTSB) gain better understanding of the events that led to the loss of Comair Flight 3272 over Monroe, Michigan, on January 9, 1997. In-flight icing was suspected as being the primary cause of this accident. Of particular interest to the Safety Board was what NASA could learn about the potential performance degradation of the wing of the Embraer EMB–120 twin-turboprop commuter aircraft with various levels of ice contamination.

NASA agreed to undertake (1) ice-accretion prediction computations with NASA's LEWICE program to bound the kind of contaminations that the vehicle may have developed, (2) testing in the NASA Lewis Research Center's Icing Research Tunnel to verify and refine the ice shapes developed by LEWICE, (3) a two-dimensional Navier-Stokes analysis to determine the performance degradation that those ice shapes could have caused, and (4) an examination using three-dimensional Navier-Stokes codes to study the three-dimensional effects of ice contamination.

The experimental and two-dimensional Navier-Stokes study showed a possible scenario of what may have happened during the accident. Several of the ice shapes accreted in the Icing Research Tunnel had a rough-leading-edge ice accretion with a prominent ridge. The most significant finding of the analysis was that the ridged ice shape produced lift and drag degradations that could have caused the kind of control disruption recorded in Flight 3272.

The National Transportation Safety Board presented its findings in a public meeting on August 27,1998. One of the conclusions was that ice formation played a significant role in the accident. Among the safety recommendations, two were directed to NASA. The first recommended that NASA continue its efforts to develop training tools to educate the flying community regarding the hazards of in-flight icing. The second advised NASA to conduct additional research to define realistic ice shapes and understand their effect on aerodynamics to help in defining future certification and training requirements.

Find out more on the World Wide Web: http://icebox.grc.nasa.gov/

Lewis contacts:
Andrew L. Reehorst, (216) 433–3938, Andrew.L.Reehorst@grc.nasa.gov; and Dr. Mark G. Potapczuk, (216) 433–3919, Mark.G.Potapczuk@grc.nasa.gov

Author: Andrew L. Reehorst

Headquarters program office: OAT

Programs/Projects: AOS

Microelectrical Mechanical Systems Flow Control Used to Manage Engine Face Distortion in Compact Inlet Systems

Turbofan engine-face flow distortion is one of the most troublesome and least understood problems for designers of modern engine inlet systems (refs. 1 and 2). One concern is that there are numerous sources of flow-field distortion that are ingested by the inlet or generated within the inlet duct itself. Among these are (1) flow separation at the cowl lip during in-flight maneuvering, (2) flow separation on the compression surfaces due to shock-wave/boundary layer interactions, (3) spillage of the fuselage boundary layer into the inlet duct, (4) ingestion of aircraft vortices and wakes emanating from upstream disturbances, and (5) strong secondary flow gradients and flow separation induced by wall curvature within the inlet duct itself. Most developing aircraft (including the B70, F–111, F–14, Mig–25, Tornado, and Airbus A300) have experienced one or more of these types of problems, particularly at high Mach numbers and/or extreme maneuver conditions when flow distortion at the engine face exceeded the allowable limits of the engine.

Using vane vortex generators to "locally" control the effects of separation has been the most common method of flow control in inlet ducts. Low- and high-momentum regions are mixed locally in the flow to effectively spread out the lower momentum fluid and suppress flow separation from the wall. However, in advanced, inlet serpentine S-duct configurations, this method often does not achieve significant control and reduction in engine face distortion. Furthermore, locally used vortex generators can control separation at one flow condition only (usually the cruise condition)—all other flow conditions are off-design.

In this study at the NASA Lewis Research Center, vortex generators were used in an entirely different manner. They were used to "globally" restructure secondary flow to increase inlet total pressure recovery and decrease engine face distortion (as first proposed in refs. 3 and 4). Such vortex generator installations can be optimized for optimum system levels of the inlet total pressure recovery and engine face distortion level over a wide range of inlet operating conditions. Thus, flow separation is not prevented unless this improves the overall inlet system as measured by engine face flow characteristics. With this global method, computational fluid dynamics (CFD) and design of experiments (DOE) optimization procedures can be used to design vortex generator installations that encompass a wide variety of inlet operating conditions.

Work done under the NASA/MOD cooperative Joint Aeronautical Program (refs. 5 and 6) led to an equivalency-of-flow principle: It does not matter how vorticity is produced; all that matters is the overall vorticity strength and distribution and how it interacts with the inlet secondary flow field. Consequently, inlet flow-control research shifted from concerns for vane generator geometry and preventing flow separation to establishing the proper overall vorticity signature to maximize inlet total pressure recovery and minimize engine face distortion. This equivalency principle simplifies the modeling of vortex generators by full Navier-Stokes CFD analyses, and it gives excellent performance comparisons with experimental data even for coarse grid calculations (ref. 7).

The current development strategy for combat aircraft emphasizes reducing life-cycle cost without compromising aircraft performance and survivability. Because this strategy has been extended to the component level, advanced S-duct inlet configurations are being made more compact (or shorter) to reduce weight and volume (and life-cycle cost). However, these compact S-ducts are typified by high distortion and low pressure recovery because of the extreme wall curvature and strong secondary flow gradients. Flow-control methods are being developed for these compact ducts to improve their performance. In addition, microelectrical mechanical systems (or MEMS-based) actuators are being evaluated as minimally intrusive, lightweight, controllable flow-control effectors to replace fixed-vane vortex generators. However, before MEMS technology can manage inlet flow fields successfully, much basic and applied aerodynamic research must be done.

This study used a full Navier-Stokes analysis to examine MEMS flow control of compact inlets, focusing on developing a workable installation. Instead of examining a particular MEMS device, it defined a device that could manage the entire inlet flow field effectively. This reference MEMS device has a vane height between 2 and 4 mm above the duct walls (about the height of the boundary layer momentum thickness). The objectives of this study were to

(1) Enable the MEMS reference vane generator installations to manage the entire inlet flow field by controlling the secondary flow in the thin layer adjacent to the wall.

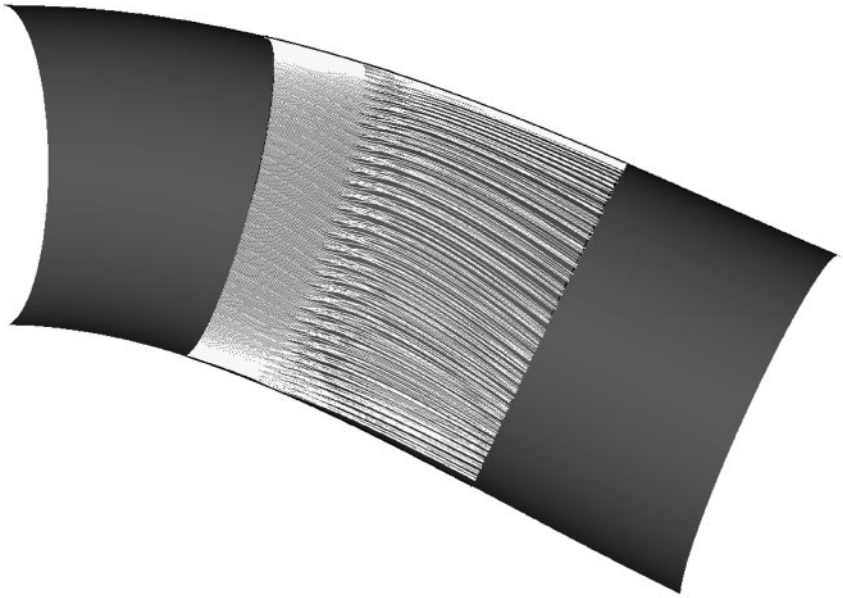

Particle traces showing the secondary flow field induced by the MEMS-scale reference generator installation.

(2) Use DOE procedures and full Navier-Stokes analysis to determine design rules for the MEMS installations, where the grid defines the individual vanes.

(3) Validate that CFD modeling can be used effectively to design MEMS installations by using a full Navier-Stokes analysis to repeat the DOE design matrix, where the individual vanes are modeled.

These CFD experiments were conducted using the Defense Evaluation Research Agency DERA/M2129 inlet S-duct (ref. 8) and the Lockheed Martin Tactical Aircraft Systems (LMTAS) full Navier-Stokes FALCON code (ref. 7), which includes a vortex generator model. In part, this study, which is part of The Technical Cooperative Program (TTCP), is a validation of the vortex generator model in the FALCON code.

The figure shows particle traces emanating just below the height of the MEMS reference vane generator installation, a co-rotating installation. Co-rotating installations interact to create vortices that merge quickly to form an overall single secondary flow pattern that remains in the wall boundary layer. This induced flow pattern prevents pairs of counter-rotating vortices from forming in the S-duct and, consequently, prevents the damaging effects of vortex lift-off (separation) on engine face distortion.

References

1. Advisory Group for Aerospace Research and Development (AGARD): Engine Response to Distorted Inflow Conditions. AGARD CP–400, 1987.
2. E.L. Goldsmith and J. Seddon, eds.: Practical Intake Aerodynamic Design. Blackwell Scientific Publications, Oxford, 1993.
3. Anderson, B.H., et al.: Study of Vortex Flow Control of Inlet Distortion. J. Propuls. Pow., vol. 8, no. 6, Nov.—Dec. 1992, pp. 1266–1272.
4. Anderson, B.H.; and Gibb, J.: Study on Vortex Generator Flow Control for the Management of Inlet Distortion. J. Propuls. Pow., vol. 9, no. 3, May—June 1993, pp. 420–430.
5. Anderson, B.; and Gibb, J.: Vortex-Generator Installation Studies on Steady-State and Dynamic Distortion. AIAA Paper 96–3279, 1996.
6. Gibb, J.; and Anderson, B.H.: Vortex Flow Control Applied to Aircraft Intake Ducts. Proceedings of the High Lift and Separation Control Conference, Royal Aeronautical Society, U.K., 1995, pp. 14.1 to 14.11.
7. Bender, E.E.; Anderson, B.H.; and Yagle, P.T: Vortex Generator Modeling for Navier-Stokes Codes. Symposium on Flow Control of Wall Bounded and Free Shear Flow, 1999 Joint ASME/JSME Fluids Engineering Conference, ASME Paper FEDSM99–6919, 1999.
8. Willmer, A.C.; Brown, T.W.; and Goldsmith, E.L.: Effects of Intake Geometry on Circular Pitot Intake Performance at Zero and Low Forward Speeds. Aerodynamics of Power Plant Installation, AGARD CP–301, Paper 5, 1981, pp. 51–56.

Lewis contact:
Bernhard H. Anderson, (216) 433–5822, Bernhard.H.Anderson@grc.nasa.gov

Authors:
Bernhard H. Anderson and
Daniel N. Miller

Headquarters program office: OAT

Programs/Projects:
Propulsion Systems R&T, TTCP

Two-Dimensional Bifurcated Inlet/Engine Tests Completed in 10- by 10-Foot Supersonic Wind Tunnel

A Two-Dimensional Bifurcated (2DB) Inlet was successfully tested in NASA Lewis Research Center's 10- by 10-Foot Supersonic Wind Tunnel. These tests were the culmination of a collaborative effort between the Boeing Company, General Electric, Pratt & Whitney, and Lewis. Extensive support in-house at Lewis contributed significantly to the progress and accomplishment of this test. The results, which met or exceeded many of the High-Speed Research (HSR) Program goals, were used to revise system studies within the HSR Program. The HSR Program is focused on developing low-noise, low-polluting, high-efficiency supersonic commercial aircraft. A supersonic inlet is an important component of an efficient, low-noise vehicle.

The Two-Dimensional Bifurcated (2DB) Inlet model is a mixed-compression inlet that was designed to efficiently and reliably convert the high supersonic airflow of a High-Speed Civil Transport (HSCT) into high-pressure, subsonic flow for a jet engine. This inlet concept is different from the external compression inlets used on most supersonic fighter aircraft. Testing began in October 1996 with a "cold-pipe" test. A cold pipe is a large valve used as a simple simulation of a jet engine. A year later, the cold-pipe hardware was replaced with a J85 turbojet engine. Recent tests characterized the operability and dynamics of the inlet installed in front of the J85 Engine. Testing was conducted over a range of supersonic Mach numbers as well as at some subsonic flow conditions.

When compared with an external compression inlet, a mixed-compression inlet has generally better efficiency but greater natural flow instability. This potential instability can be controlled through the proper choice of variable geometry. Features of this model included remotely variable ramp geometry, multiple bleed compartments, and bypass valves. Therefore, variable geometry features were needed to develop a robust control for this mixed-compression inlet over the entire High-Speed Civil Transport flight regime. Operation across variations in normal shock location, inlet unstart/restart, and angle of attack was demonstrated both with and without the J85 Engine installed.

This program is an example of a successful industry/NASA partnership. The test series was responsive to the needs of the HSR program. The end result was a test that brought efficient, robust mixed-compression inlet concepts one step closer to reality.

Find out more on the World Wide Web:
http://www.grc.nasa.gov/WWW/HSR
http://www.grc.nasa.gov/WWW/inlet

Lewis contacts:
John D. (Dave) Saunders, (216) 433–6278, John.D.Saunders@grc.nasa.gov; and David J. Arend, (216) 433–2387, David.J.Arend@grc.nasa.gov

Author: John D. Saunders

Headquarters program office: OAT

Programs/Projects: HSR, HSCT

Two-Dimensional Bifurcated Inlet and J85 Engine installed in Lewis' 10- by 10-Foot Supersonic Wind Tunnel.

Back end of installation showing the nozzle leaves of the J85 Engine.

WIND Flow Solver Released

The WIND code is a general-purpose, structured, multizone, compressible flow solver that can be used to analyze steady or unsteady flow for a wide range of geometric configurations and over a wide range of flow conditions. WIND is the latest product of the NPARC Alliance, a formal partnership between the NASA Lewis Research Center and the Air Force Arnold Engineering Development Center (AEDC). WIND Version 1.0 was released in February 1998, and Version 2.0 will be released in February 1999.

The NPARC (National Program for Applications-Oriented Research in CFD) Alliance was established in 1992 with the goal of providing an applications-oriented computational fluid dynamics (CFD) system, primarily for aerospace flow simulation. This alliance is committed to the long-range maintenance and improvement of this capability, with teams focused on user support, code development, and validation. The unique talents and capabilities of its partners, plus the experience and insight of its government, industrial, and academic customers, are used to ensure that the alliance's efforts are cost-effective and responsive to users' needs.

The WIND code represents a merger of the capabilities of three existing computational fluid dynamics codes—NPARC (the original NPARC Alliance flow solver), NXAIR (an Air Force code used primarily for unsteady store separation problems), and NASTD (the primary flow solver at McDonnell Douglas, now part of Boeing). The development effort began in early 1997 using the NASTD code as the basis, and was carried out jointly between Lewis, AEDC, and Boeing. Recently, the Air Force Research Laboratory joined the effort. Funding for the work has been provided by NASA's High-Speed Research (HSR) Program, by AEDC, by Boeing, and by the Air Force's High Performance Computing Modernization Program.

A variety of physical models are available in the WIND code, allowing users to choose those appropriate to the problem being analyzed. These include

- Navier-Stokes, thin-layer Navier-Stokes, parabolized Navier-Stokes, or Euler equations
- Algebraic, one-equation, and two-equation turbulence models
- Perfect gas, frozen chemistry, equilibrium air, and finite rate chemistry models
- Abutting and/or overlapping grid zones

In addition, a variety of numerical models are available, including

- Explicit, scalar implicit, or block implicit solution operators
- Central, Coakley upwind, Roe upwind, and physical upwind explicit differencing—first to fifth order
- Implicit and explicit boundary conditions

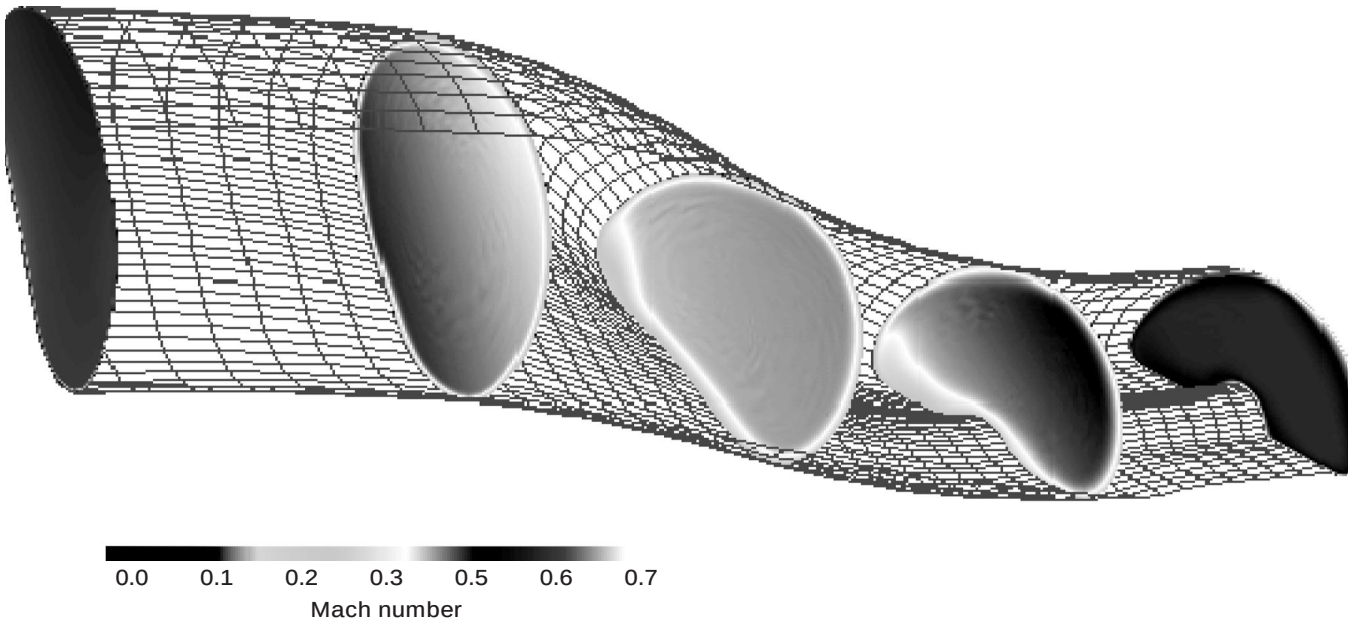

Mach number contours for flow through a subsonic diffuser with turning. This figure is shown in color in the online version of this document (http://www.grc.nasa.gov/WWW/RT1998/5000/5850towne.htm).

- Second- and fourth-order explicit smoothing, boundary damping, and TVD[a] flux limiting
- Time step specification via a CFL[b] number, Global Newton iteration, and Runge-Kutta schemes
- Convergence acceleration using grid sequencing, local CFL numbers, and ramped CFL numbers

The WIND code is available to all U.S.-owned companies, public and private universities, and Government agencies. However, only U.S. citizens and resident aliens may access the software. Instructions for obtaining the code are available on the NPARC Alliance home page on the World Wide Web or from the NPARC Alliance User Support team.

[a]Total Variation Diminishing.
[b]Courant-Friedrichs and Lewy.

Additional information about the NPARC Alliance and the WIND code is available at the following WWW sites:
NPARC Alliance: http://www.arnold.af.mil/nparc
WIND documentation: http://www.grc.nasa.gov/WWW/winddocs
WIND validation: http://www.grc.nasa.gov/WWW/wind/valid/validation.html

Lewis contact:
Dr. Charles E. Towne, (216) 433–5851, Charles.E.Towne@grc.nasa.gov

AEDC contact: NPARC Alliance User Support, (931) 454–7455, nparc-support@info.arnold.af.mil

Author: Dr. Charles E. Towne

Headquarters program office: OAT

Programs/Projects: HSR, AST, HPCCP, Propulsion Systems Base R&T

Results of Liquid Motion Experiment Analyzed

About half of all scientific and commercial spacecraft spin during some part of their mission. Although spinning has many benefits (increasing stability, controlling the location of liquid propellants, and distributing solar heat loads), it also creates problems because a precession (or wobble) motion is unavoidable. For modern spacecraft, by far the largest source of wobble is energy dissipation in the liquid of partially filled tanks. The liquid's energy dissipation cannot, however, be quantified adequately by any ground test. Current analytical models are also inadequate because fundamental data on fluid motion in low gravity are needed to validate them. Consequently, spacecraft attitude-control systems are designed and operated very conservatively. Nonetheless, spacecraft often still perform poorly in orbit, and some have been lost because of a rapid increase of the wobble rate. The Liquid Motion Experiment (LME) was designed to provide spacecraft designers accurate data on the wobble dynamics of spacecraft that contain large quantities of mobile liquids. LME, which was flown on the space shuttle mission STS–84, was built under contract to the NASA Lewis Research Center by the Southwest Research Institute of San Antonio, Texas. Major accomplishments for 1998 include reduction of the flight data and publication of the experimental results.

LME was essentially a spin table that created a realistic nutation motion of scale-model tanks containing liquid. Two spherical and two cylindrical transparent tanks were tested simultaneously, and three sets of such tanks were employed to vary liquid viscosity, fill level, and propellant management device (PMD) design. All the tanks were approximately 4.5 in. in diameter. The primary test measurements were the radial and tangential torques exerted on the tanks by the liquid. These torques could not be measured on the ground because of the masking effects of gravity.

Liquid resonant frequencies and viscous damping coefficients were determined by sine sweep tests. The observed resonance frequencies for cylindrical tanks depended on the fill level. These frequencies were in the range of 0.73 to 0.78 times the spin rate for resonances about the radial axis and were in the range of 0.55 to 75 times the spin rate for resonances about the tangential axis. The available analytical model predicted only one resonance for a given fill level, and this prediction agreed rather closely with the tangential axis resonance frequencies observed in the tests. The resonances for the spherical tanks, which were in the range of 0.74 to 77 times the spin rate, did not vary significantly between the tangential and radial axes. The PMD's sometimes enhanced the resonances and

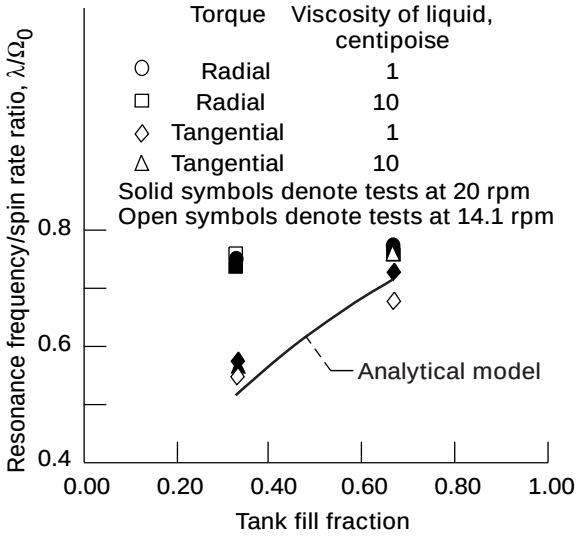

Resonant frequencies for bare cylindrical tanks at high spin rates (20 and 14.1 rpm spin).

energy dissipation rates and sometimes decreased them. This inconsistency points out our need to better understand the effects of PMD on liquid motion as a function of PMD and tank design. Energy dissipation rates were determined by sine dwell tests. The LME energy dissipation rates varied from 0.3 to 0.5 times the estimates obtained from previous ground tests and spacecraft flight data.

Find out more on the World Wide Web: http://space-power.grc.nasa.gov/ppo/lme/lme.html

Bibliography

Chato, D.J., et al.: Liquid Motion Experiment Flight Test Results. NASA TM—1998-208479, 1998.

Deffenbaugh, D.M.; Dodge, F.T.; and Green, S.T.: Liquid Motion in a Rotating Tank Experiment (LME). NASA CR—1998-208667, 1998.

Lewis contact:
David J. Chato, (216) 977–7488, David.Chato@grc.nasa.gov

Author: David J. Chato

Headquarters program office: OSS

Programs/Projects:
Microgravity Science, HEDS, In-STEP, Space Transportation R&T

Rapid Chill and Fill of a Liquid Hydrogen Tank Demonstrated

The NASA Lewis Research Center, in conjunction with Boeing North American, has been supporting the High Energy Upper Stage (HEUS) program by performing feasibility studies at Lewis' Supplemental Multilayer Insulation Research Facility (SMIRF). These tests were performed to demonstrate the feasibility of chilling and filling a tank with liquid hydrogen in under 5 minutes.

The goal of the HEUS program is to release a satellite from the shuttle cargo bay and then use a cryogenic (high-energy) upper stage to allow the satellite to achieve final orbit. Because of safety considerations, the propellant tanks for the upper stage will be launched warm and dry. They will be filled from the shuttle's external tank during the mission phase after the solid rocket boosters have jettisoned and prior to jettison of the external tank. Data from previous shuttle missions have been analyzed to ensure that sufficient propellant would be available in the external tank to fill the propellant tank of the proposed vehicle upper stage. Because of mission time-line considerations, the propellant tanks for the upper stage will have to be chilled down and filled in approximately 5 minutes.

An existing uninsulated flight weight test tank was installed inside the vacuum chamber at SMIRF, and the chamber was evacuated to the 10^{-5} torr range to simulate space vacuum conditions in the cargo bay with the doors open. During prerun operations, the facility liquid hydrogen (LH_2) supply piping was prechilled with the vent gas bypassing the test article. The liquid hydrogen supply dewar was saturated at local ambient pressure and then pressurized with ambient temperature gaseous helium to the test pressure. A control system was used to ensure that the liquid hydrogen supply pressure was maintained at the test pressure.

During the initial phase of the test, the test tank vent valve was open. Despite the open valve, pressure in the test article rose rapidly until it approached the supply dewar pressure. During this initial pressure rise, the warm test tank walls were sprayed with liquid. As the

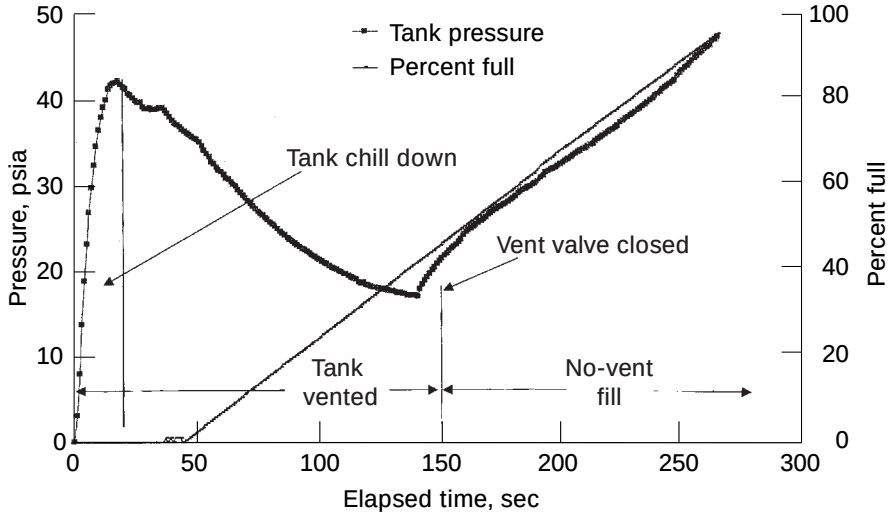

Typical tank pressure and liquid level versus elapsed time.

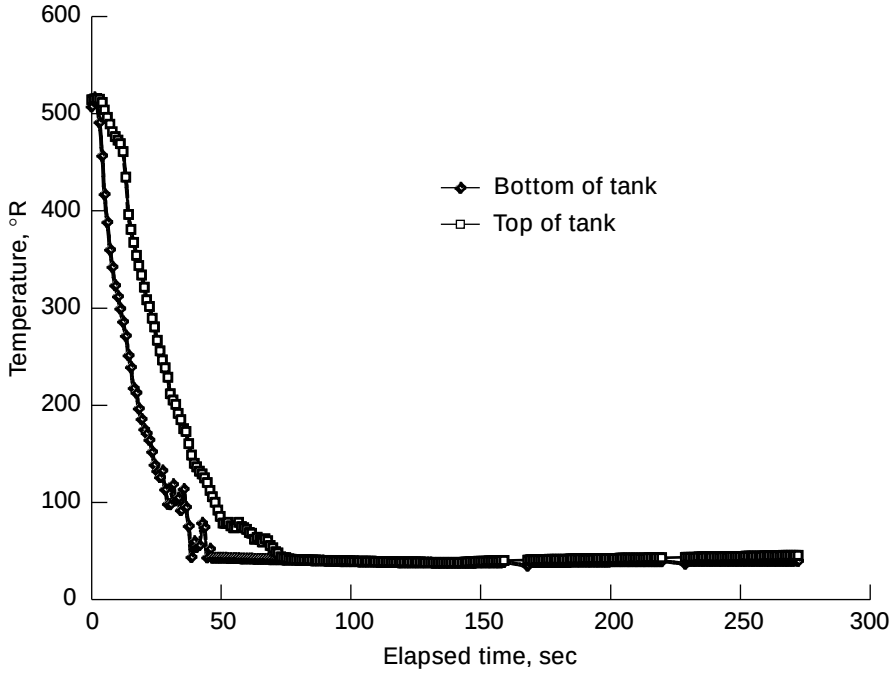

Typical tank temperatures versus elapsed time.

walls reached near liquid temperatures, the quantity of gas evolved began to decrease and test tank pressure began to drop. When the test tank pressure had fallen close to atmospheric pressure, the tank vent valve was closed and the fill process was allowed to continue. The purpose of closing the vent valve was to demonstrate the no-vent fill process, which conserves propellant and yields a pressurized propellant tank when the fill is complete. See the graphs for the pressure, fill level, and temperature traces for a typical test.

Four demonstrations of the rapid chill and fill process were completed at the SMIRF facility. All tests resulted in greater than 85-percent fills obtained in under 5 minutes. Some parametric studies were performed to provide a relationship between the liquid hydrogen supply dewar pressure and the fill efficiency. The timing of the test tank vent-valve closure was also studied. Testing at the SMIRF facility demonstrated the feasibility of the rapid chill and fill technique and reduced the technology risks for the High Energy Upper Stage program.

Lewis contact:
Maureen T. Kudlac, (216) 977–7476, Maureen.T.Kudlac@grc.nasa.gov

Author: Maureen T. Kudlac

Headquarters program office: OSF

Programs/Projects: HEUS

Zero Boiloff Storage of Cryogenic Propellants Achieved at Lewis' Supplemental Multilayer Insulation Research Facility

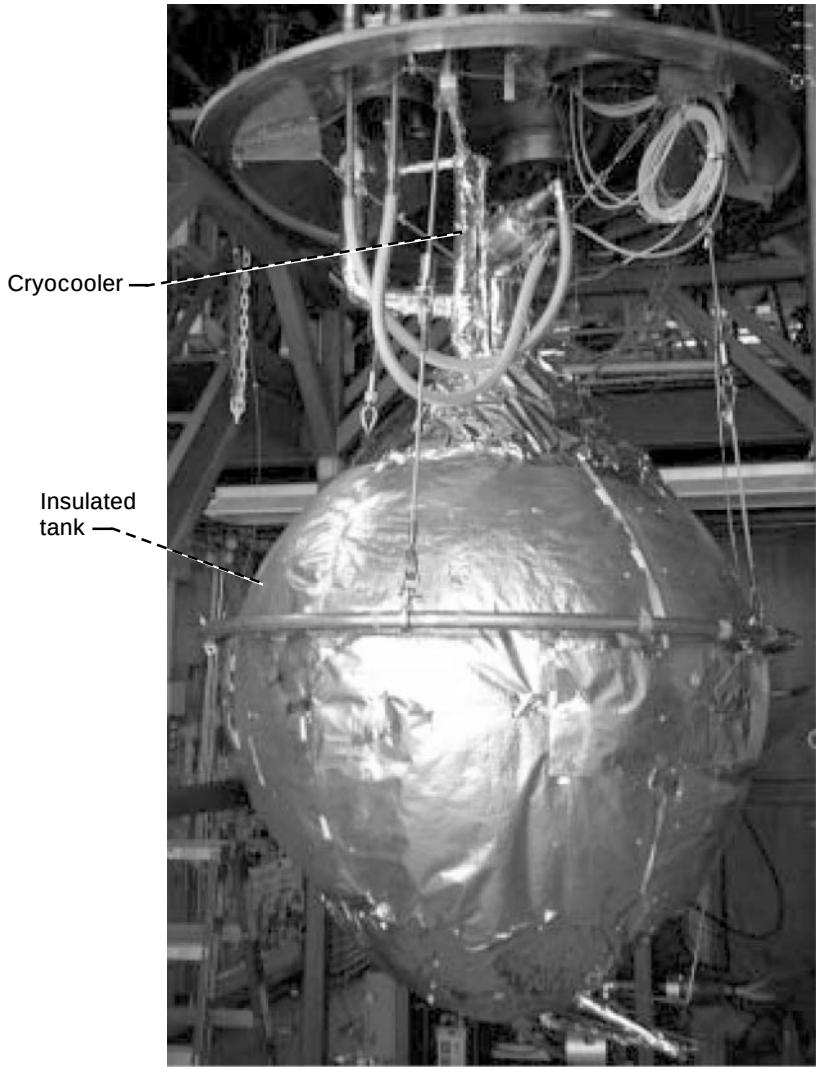

Test article prior to installation into the vacuum chamber. Mated to the cryocooler is a condenser (not shown) which was designed to transmit heat entering the tank by condensing hydrogen vapor. This extended into the ullage of the liquid hydrogen tank.

Tests conducted at the NASA Lewis Research Center's Supplemental Multilayer Insulation Research Facility (SMIRF) demonstrated that a hybrid thermal control system could eliminate boiloff of cryogenic propellants. This is significant because of the substantial mass and cost savings that could be achieved for any long-duration space mission that requires cryogenic propellants.

With long-duration cryogenic storage, propellants will boil off because of the environmental heating of the tank. To accommodate these losses, extra propellant is required along with larger propellant tanks. Analysis of Mars mission scenarios using space-transfer cryogenic stages showed that significant savings in propellant mass and tank size could be achieved if it were possible to eliminate or significantly reduce propellant boiloff.

Engineers and technicians at NASA Lewis designed, built, and tested a hybrid thermal control system to eliminate or significantly reduce cryogenic propellant boiloff. The system consists of an active cryocooling system using a cryocooler in addition to the traditional passive thermal insulation, as shown in the photo.

Testing conducted over the summer of 1998 compared the performance of the hybrid system to that of the traditional passive-only insulation solution. The hardware consisted of a pressurized 50-ft^3 tank insulated with 34 layers of multilayer insulation (MLI), a condenser, and a Gifford/McMahon Cryocooler that has a cooling capacity of 15 to 17.5 watt (W). Liquid hydrogen was the test fluid. The test tank was installed into a vacuum chamber, simulating space vacuum.

First, the passive insulation system was tested to determine the boiloff under steady-state conditions. The measured steady-state boiloff rate was approximately 0.12 kg/hr, equating to a heating rate of approximately 14.5 W, slightly higher than the prediction of 13 W and the historic data of 11.5 W (1978 tests). Even so, the heating rate was less than the cryocooler capacity (15 to 17.5 W).

Next, a series of tests was conducted with the cryocooler in operation. Late into these tests, after the chamber vacuum pressure finally inched upward to approximately 8.5×10^{-5} torr, which was still a full one-half decade worse

than that of our previous test, we achieved zero boiloff (0.00 kg/hr). At this time, the test tank pressure and temperatures decreased. This tank pressure decrease was approximately 0.07 psi/hr, and the condenser temperature decrease was approximately 0.12 K/hr. The testing was terminated when the tank pressure dropped near atmospheric pressure. This was to prevent air from being accidentally drawn into the tank.

These tests confirmed that it is possible to achieve zero boiloff with cryogenic propellant storage using a hybrid thermal control system, and they provided the foundation for the more detailed analysis and testing needed to support future long-duration space missions.

Lewis contact:
David W. Plachta, (216) 977–7126, David.W.Plachta@grc.nasa.gov

Author: David W. Plachta

Headquarters program office: OSF (Advanced Projects), AST at MSFC

Programs/Projects:
Propulsion Systems R&T, AST

Engineering Application Integration Architecture Devised

Researchers at the NASA Lewis Research Center have devised an object-oriented architecture for integrating engineering application software. The architecture provides an environment in which the complete engineering design and analysis process can be conducted. It eliminates the need to repeatedly adapt graphical user interfaces (and other tools) to various experimental and analytical information sources, and it brings those sources into a common domain to facilitate the easy (and, eventually, automatic) sharing of engineering content. This architecture has been implemented in the C++ language, and a graphical user interface interacting with the architecture has been developed with a portable tool kit.

The structure, depicted in the figure, consists of an application object (labeled *PacAppl* in the figure) from which emanates (1) a tree of data identifications (the *Pid* items to the right), (2) a tree of data configurations (the *PacCfg* items extending toward the lower left), and (3) a map of available operations (the *Op* items to the upper left). The structure of the data is revealed by the structure of the identification tree, eliminating the need to replicate data within configurations merely to reveal structure. Missing data elements of a configuration are then inherited from the most immediate precursor. Encapsulated operations, as well as data identifications, operate within the context of a current data configuration and, thus, are able to refuse operations not supported by the state of the data.

All the object classes of the architecture derive from a common

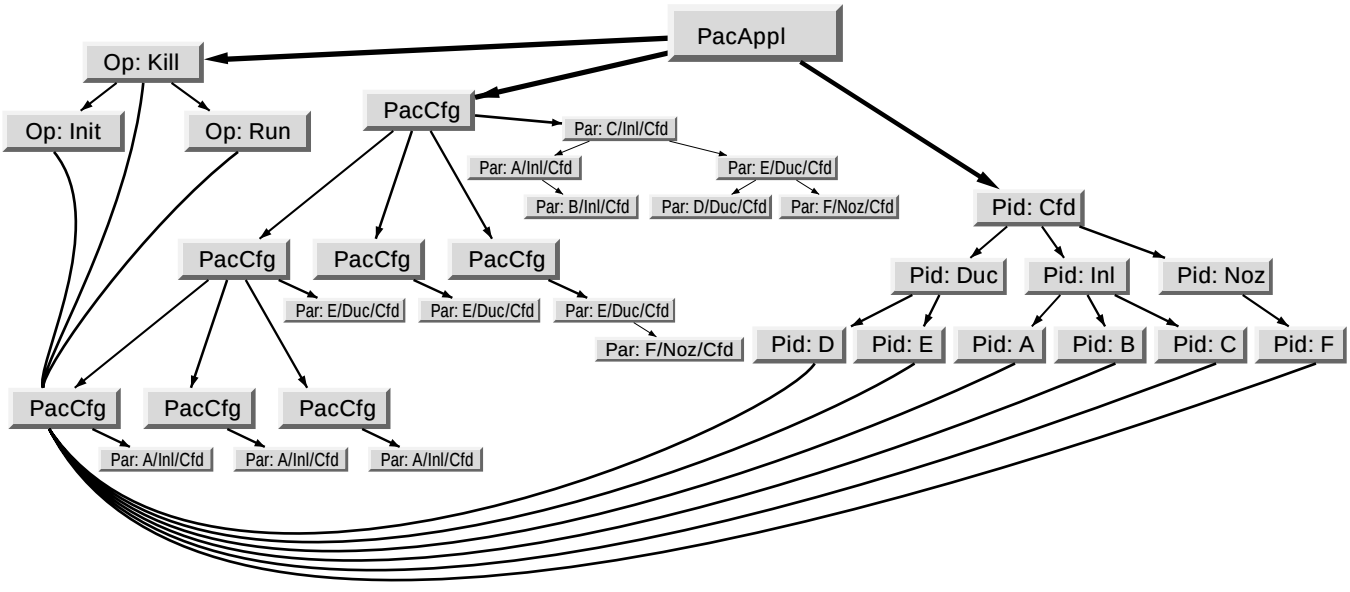

Generic engineering application integration architecture.

base class that can provide descriptions of the objects when desired. Names, units, annotations, access controls, and the like can be attached on an object-by-object basis. Key among these is automatic value change histories and a text description, which can be used as a basis for engineering journals.

More information about the engineering application integration architecture is available on the World Wide Web: http://www.grc.nasa.gov/WWW/price000/

Lewis contact:
Dr. William H. Jones, (216) 433–5862, William.H.Jones@grc.nasa.gov

Author: Dr. William H. Jones

Headquarters program office: OAT

Programs/Projects:
Information Systems Base R&T

Space-Time Conservation Element and Solution Element Method Being Developed

The engineering research and design requirements of today pose great computer-simulation challenges to engineers and scientists who are called on to analyze phenomena in continuum mechanics. The future will bring even more daunting challenges, when increasingly complex phenomena must be analyzed with increased accuracy. Traditionally used numerical simulation methods have evolved to their present state by repeated incremental extensions to broaden their scope. They are reaching the limits of their applicability and will need to be radically revised, at the very least, to meet future simulation challenges.

At the NASA Lewis Research Center, researchers have been developing a new numerical framework for solving conservation laws in continuum mechanics, namely, the Space-Time Conservation Element and Solution Element Method, or the CE/SE method. This method has been built from fundamentals and is not a modification of any previously existing method. It has been designed with generality, simplicity, robustness, and accuracy as cornerstones.

The CE/SE method has thus far been applied in the fields of computational fluid dynamics, computational aeroacoustics, and computational electromagnetics. Computer programs based on the CE/SE method have been developed for calculating flows in one, two, and three spatial dimensions. Results have been obtained for numerous problems and phenomena, including various shock-tube problems, ZND detonation waves, an implosion and explosion problem, shocks over a forward-facing step, a blast wave discharging from a nozzle, various acoustic waves, and shock/acoustic-wave interactions. The method can clearly resolve shock/acoustic-wave interactions, wherein the difference of the magnitude between the acoustic wave and shock could be up to six orders. In two-dimensional flows, the reflected shock is as crisp as the leading shock. CE/SE schemes are currently being used for advanced applications to jet and fan noise prediction and to chemically reacting flows.

Key features and advantages of the CE/SE method follow.

• Space and time are treated in a unified fashion. The space-time domain is discretized into Solution Elements (SE's), within which the numerical approximation is a simple (linear, for example) function of space and time. Conservation Elements (CE's) that fill the space-time domain without overlap are also defined.

• The main emphasis is on solving the integral form of the conservation law in the space-time domain, although the differential form is also considered. Conservation of space-time flux is enforced for each CE. Because the CE's fill space-time without overlap, and because the flux through any face of a CE is uniquely defined, this local conservation of flux ensures that space-time flux is conserved globally in the space-time domain.

• The method is very simple. It uses only the simplest of approximation techniques. In addition, no knowledge of the properties of the solution, such as the characteristics or the shock-wave profile, is used.

• The flux-based nature of the method leads to the use of flux-based boundary conditions. The nonreflecting boundary conditions needed for practical computations on unbounded spatial domains are remarkable for their simplicity, needing only a few lines in the computer program. These conditions allow even shock waves to pass out of the domain with no noticeable reflection at the boundary.

• The CE/SE method is genuinely multidimensional; that is, no directional splitting is employed in modeling multidimensional problems.

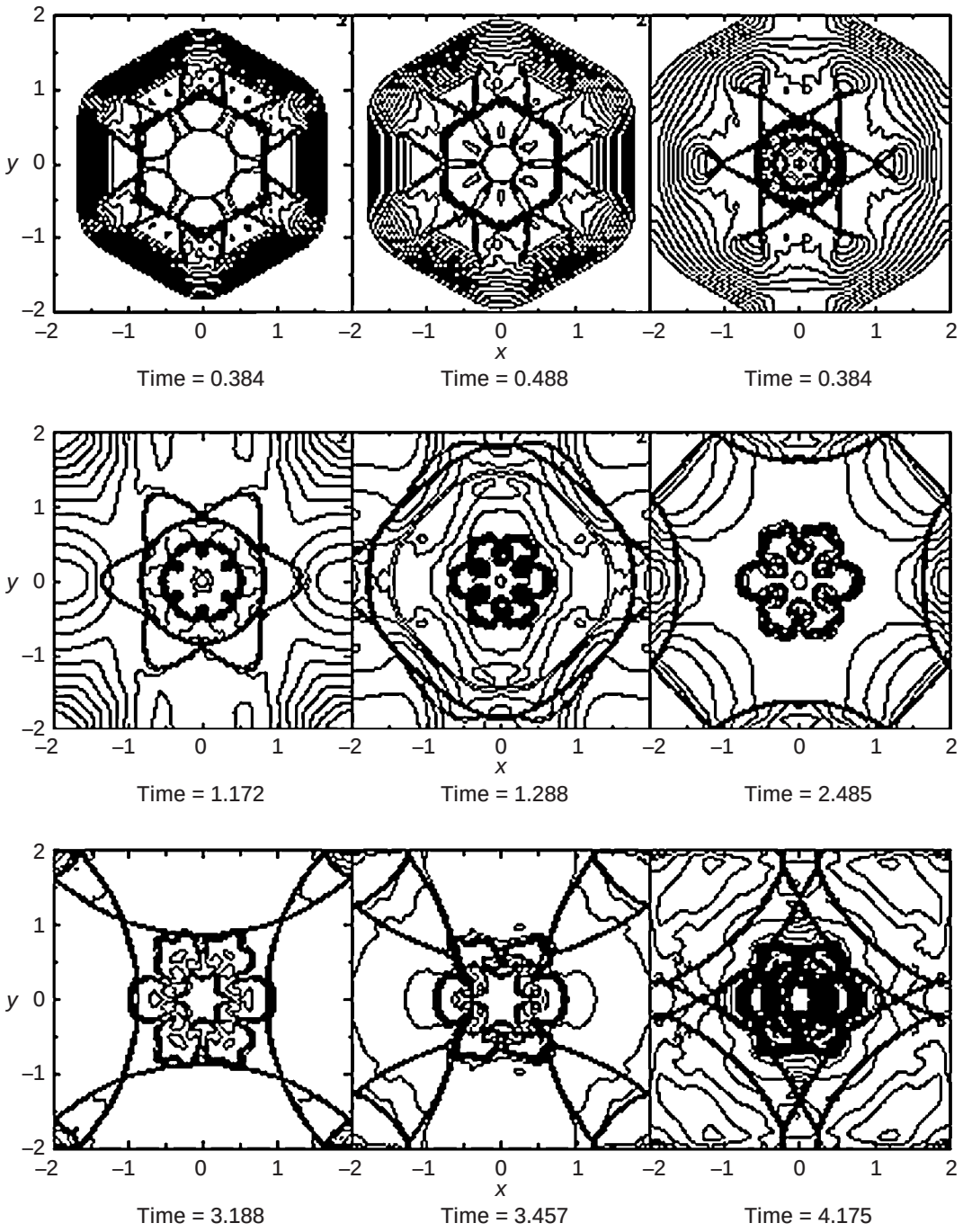

Snapshots in time (nondimensionalized) of the implosion/explosion of a hexagonal shock in a square box. Pressure ratio, 10.

• The two- and three-dimensional spatial meshes employed by the present method are built from triangles and tetrahedrons, respectively. Triangles and tetrahedrons, respectively, are also the simplest building blocks for two- and three-dimensional unstructured meshes. Thus, the multidimensional schemes can be directly applied on unstructured meshes, which are the only efficient way to deal with complex geometries.

• The simplicity of the CE/SE schemes makes the computer programs easy to vectorize and parallelize.

Find out more about this research on the World Wide Web:
http://www.grc.nasa.gov/WWW/microbus/

Bibliography

Chang, S.C., et al.: The Method of Space-Time Conservation Element and Solution Element—A New Paradigm for Numerical Solution of Conservation

Laws. To appear in Computational Fluid Dynamics Review, M.M. Hafez and K. Oshima, eds., John Wiley and Sons, West Sussex, U.K.

Chang, S.-C.: The Method of Space-Time Conservation Element and Solution Element—A New Approach for Solving the Navier-Stokes and Euler Equations. J. Comput. Phys., vol. 119, 1995, pp. 295–324.

Lewis contact:
Dr. Philip C.E. Jorgenson, (216) 433–5386, Philip.C.Jorgenson@grc.nasa.gov

Authors: Dr. Sin-Chung Chang, Dr. Ananda Himansu, Dr. Philip C.E. Jorgenson, Dr. Ching-Yuen Loh, Dr. Xiao-Yen Wang, and Dr. Sheng-Tao Yu

Headquarters program office: OAT

Programs/Projects: Propulsion Systems R&T, AST

Structures and Acoustics Division

Nondestructive Evaluation Correlated With Finite Element Analysis

Advanced materials are being developed for use in high-temperature gas turbine applications. For these new materials to be fully utilized, their deformation properties, their nondestructive evaluation (NDE) quality and material durability, and their creep and fatigue fracture characteristics need to be determined by suitable experiments. The experimental findings must be analyzed, characterized, modeled and translated into constitutive equations for stress analysis and life prediction. Only when these ingredients—together with the appropriate computational tools—are available, can durability analysis be performed in the design stage, long before the component is built.

For example, for NDE information to be useful in structural characterization and modeling, the NDE data format must be compatible with microstructural and structural models currently being developed (refs. 1 and 2). In addition, qualitative and quantitative computer analysis tools based on NDE imaging modalities must be developed to enhance the usefulness of NDE applications. Qualitative tools include two- and three-dimensional visualization methods. Quantitative tools include segmentation methods that can send output to commercial finite element, micromechanical, and/or continuum damage model software (refs. 3 and 4) for evaluation of composite materials and components. Linking NDE data with engineering analysis methods will provide the engineering community the great ability to do a complete structural analysis on as-manufactured or as-inspected components rather than solely on as-designed components. With this capability, extensive effect-of-defect studies can be performed to determine the effect of manufacturing anomalies or in-service component degradation on part performance. This will provide an NDE capability for engineering structures and condition-based maintenance.

One of the many structural components being evaluated by the NDE group at the NASA Lewis Research Center is the flywheel system. It is being considered as an energy storage device for advanced space vehicles. Such devices offer advantages over electrochemical batteries in situations demanding high power delivery and high energy storage per unit weight. In addition, flywheels have potentially higher efficiency and longer lifetimes with proper motor-generator and rotor design (ref. 5). Flywheels made of fiber-reinforced polymer composite material show great promise for energy applications because of the high energy and power densities that they can achieve (ref. 6) along with a burst failure mode that is relatively benign in comparison to those of flywheels made of metallic materials (ref. 7).

However, the big challenge of developing materials for high-energy flywheel systems that can withstand the stresses caused by high rotational speeds remains eminent. For example, a typical 16-in. steel or titanium flywheel can shatter at 20 000 rpm. However, flywheels made out of composites show good promise since they can store 20 to 30 times more power per unit/weight than lead-acid batteries, can be recharged repeatedly, and can handle a wide range of temperature variations. They can also be respun thousands of times to regain their stored energy.

Therefore, to help improve durability and reduce structural uncertainties, we are developing a comprehensive analytical approach to predict the reliability and life of these components under these harsh loading conditions. The combination of NDE and two- and three-dimensional finite element analyses (e.g., stress analyses and fracture mechanics) is expected to set a standardized procedure to accurately assess the applicability of using various composite materials to design a suitable rotor/flywheel assembly. Following the figures is a brief description of some preliminary analytical results.

The figures represent typical NDE-finite element results. The top left figure shows a computed tomography (CT) scan for a rotor made of polymer matrix composite. This scan illustrates the defects in the rotor due to centrifugal loading (spun at 34 000 rpm); a crack along the circumferential direction is very obvious. The bottom left figure shows the finite element models for the rotor assembly. This assembly consists of the composite rotor (Hexel's IM–7 and AS4D) and an aluminum hub (7075–T6). Two and three-dimensional models were generated (ref. 8) because of analysis requirements. Results obtained via finite element analyses (ref. 9) are shown in the figures

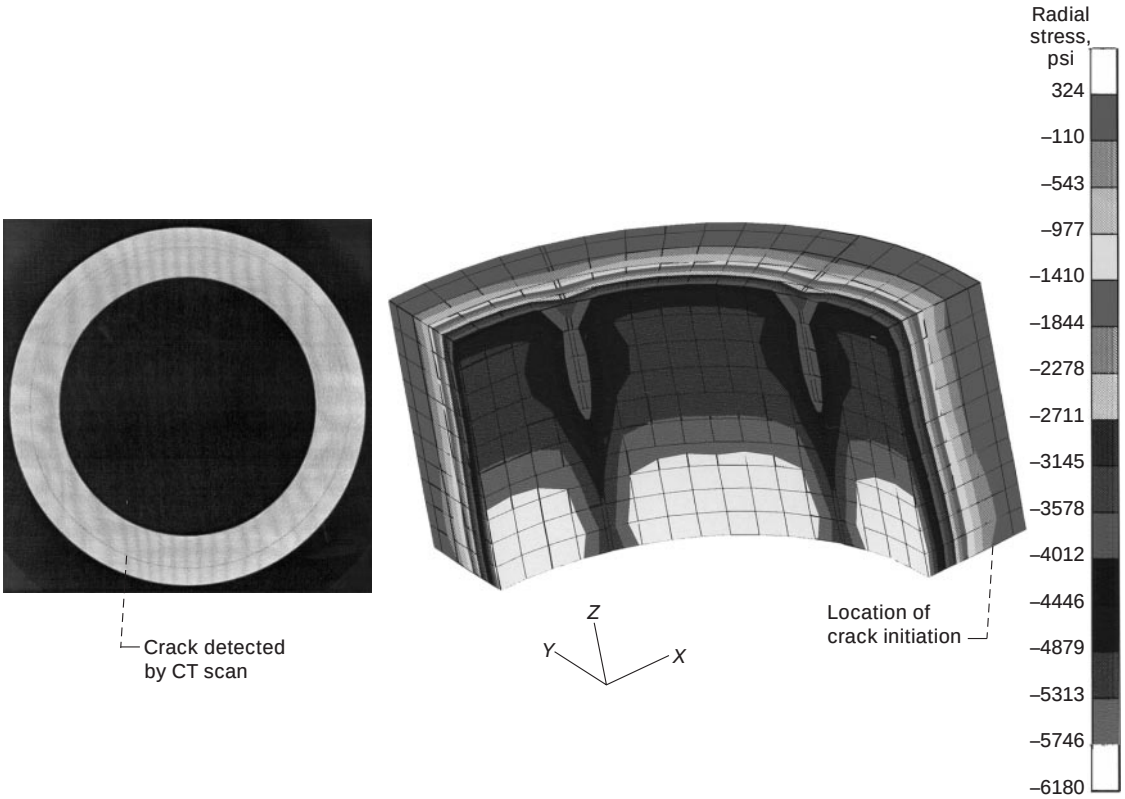

Left: Computer tomograph (CT) of a flywheel. Right: Radial stresses in a rotor.

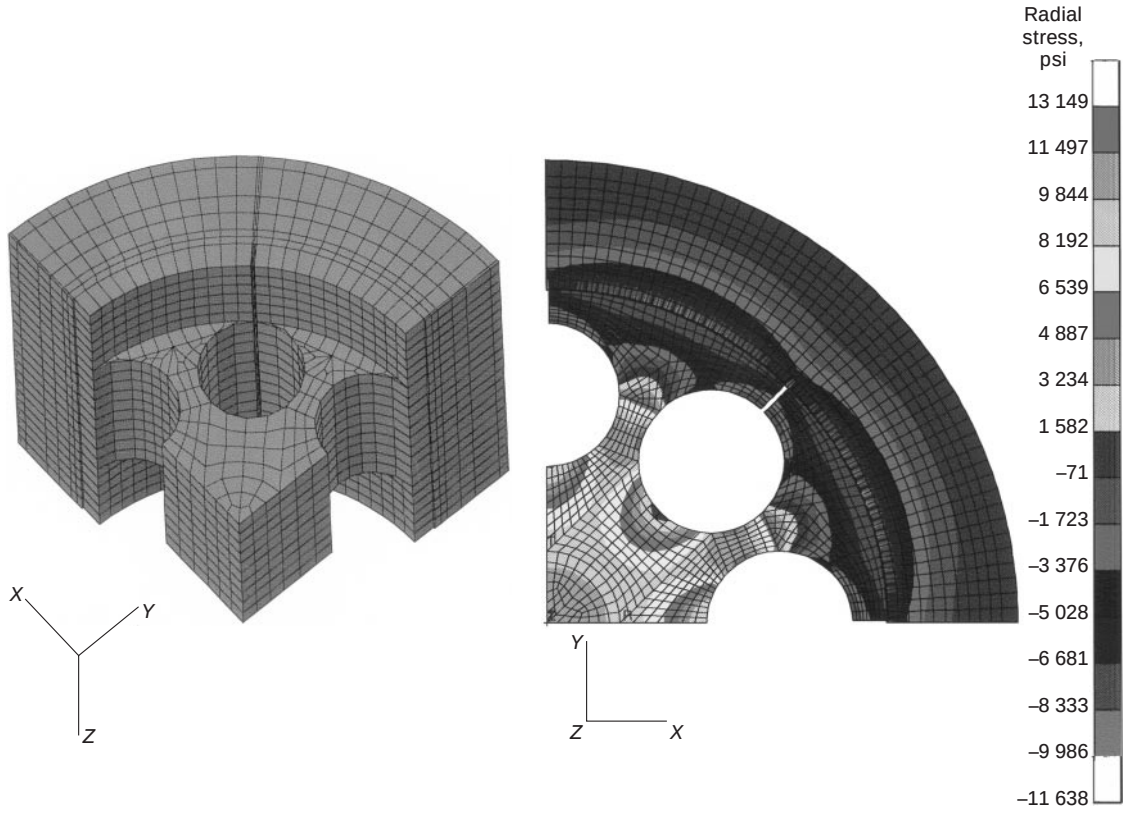

Left: Three-dimensional finite element model; 6747 nodes, 5424 hexagonal elements. Right: Radial stresses in a rotor-hub assembly. These figures are shown in color in the online version of this article (http://www.grc.nasa.gov/WWW/RT1998/5000/5920aziz.htm).

on the right, where the stress levels depend on the applied loading. Furthermore, the bottom right figure illustrates the radial stress distribution in the rotor whereby the tensile stresses near the middle indicate the presence of the crack as detected by the computed tomography scanning shown in the top figure. Although these results are considered to be preliminary, they reflect a step forward in correlating NDE findings with finite element analysis.

For more information, visit Lewis' Life Prediction Branch on the World Wide Web: http://www.grc.nasa.gov/WWW/LPB/

References

1. Baaklini, G.Y., et al.: Structural Characterization of Metal Matrix Composites Using NDE Data. HITEMP Review 1997, NASA CP–10192, Vol. II, 1997, paper no. 41, pp. 1–15. (Available from NASA Lewis' Subsonic Systems Office.)
2. Baaklini, G.Y., et al.: Nondestructive Evaluation of Titanium Alloy MMC Rings for Gas Turbine Engines. MMC Life System Development (Phase I)—A NASA/Pratt & Whitney Life Prediction Cooperative Program. E.V. Zaretsky, ed., NASA RP–1361, 1996, pp. 61–73.
3. Wilt, T.E.: Arnold, S.M.; and Goldberg, R.: Micromechanics Analysis Code, MAC Features and Applications. HITEMP Review 1997, NASA CP–10192, Vol. II, 1997, paper no. 30, pp. 1–13. (Available from NASA Lewis' Subsonic Systems Office.)
4. Arnold, S.M.; and Wilt, T.E.: Deformation and Life Prediction of Circumferentially Reinforced SCS–6/Ti–15–3 Ring. MMC Life System Development (Phase I)—A NASA/Pratt & Whitney Life Prediction Cooperative Program. E.V. Zaretsky, ed., NASA RP–1361, 1996, pp. 51–60.
5. Ashley, S.: Flywheels Put a New Spin on Electric Vehicles. Mech. Engrg., vol. 115, no. 10, Oct. 1993, pp. 44–51.
6. Olszewski, M.; et al.: On the Fly or Under Pressure. Mech. Engrg., vol. 110, no. 6, Jun. 1988, pp. 50–58.
7. Coppa. A.P.: Flywheel Containment and Safety Considerations. An Assessment of Integrated Flywheel System Technology. NASA CP–2346, 1984, pp. 243–264.
8. The MacNeal-Schwendler Corporation: MSC/PATRAN Graphics and Finite Element Package. Vols. I and II, MacNeal-Schwendler, Costa Mesa, CA, 1997.
9. MARC Analysis Research Corporation: MARC General Purposes Finite Element Analysis program. Vol. A: User Information manual, and Vol. F: Theoretical Manual. MARC Analysis Research Corporation, Palo Alto, CA, 1996.

Lewis contact:
Ali Abdul-Aziz, (216) 433–6729, Ali.Abdul-Aziz@grc.nasa.gov

Authors:
Ali Abdul-Aziz and George Y. Baaklini

Headquarters program office: OAT

Programs/Projects:
Aeronautics Base R&T, HITEMP, ACESE

Deformation Behaviors of HIPped Foil Compared With Those of Sheet Titanium Alloys

Micromechanics-based modeling of composite material behaviors requires an accurate assessment of the constituent properties and behaviors. For the specific case of continuous-fiber-reinforced metal matrix composites (MMC's) manufactured from a foil/fiber/foil process, much emphasis has been placed on characterizing foil-based matrix materials that have been fabricated in the same way as the composite. Such materials are believed to yield mechanical properties and behaviors that are representative of the matrix constituent within the composite (in situ matrix). Therefore, these materials are desired for micromechanics modeling input. Unfortunately, such foils are extremely expensive to fabricate and procure because of the labor-intensive rolling process needed to produce them. As a potential solution to this problem that would maintain appropriately representative in situ properties, the matrix constituent could be characterized with sheet-based materials, which are considerably less expensive to manufacture than foils, are more readily procured, and result in fewer plies to obtain a desired panel thickness. The critical question is, however, does the consolidated sheet material exhibit the same properties and behaviors as do the consolidated foils? Researchers at NASA Lewis Research Center's Life Prediction Branch completed a detailed experimental investigation to answer this question for three titanium alloys commonly used in metal matrix composite form.

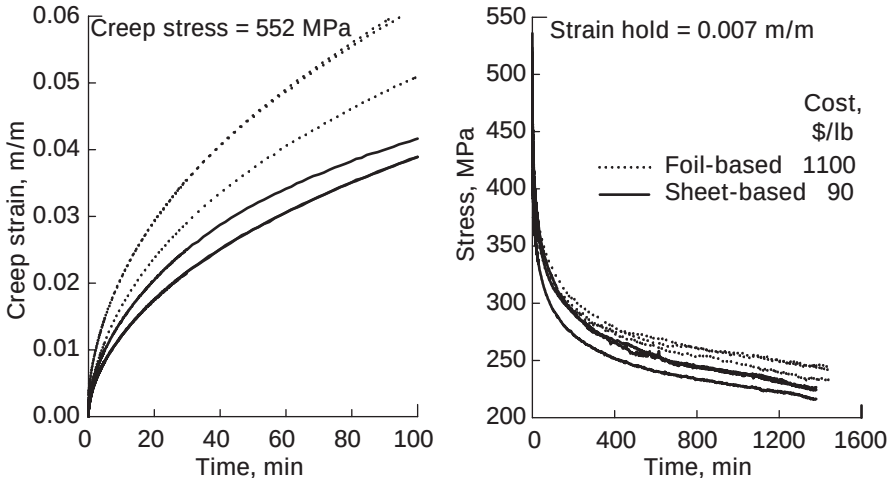

Creep and stress relaxation behavior of HIPped foil and sheet Ti-6-4 matrix at 427 °C (800 °F).

The experimental investigation compared the 427 °C (800 °F) mechanical properties and deformation behaviors of three HIPped (Hot Isostatic Pressed) foil and HIPped sheet titanium matrix materials commonly used in silicon-carbide- (SiC-) reinforced titanium composites. The alloys investigated were Ti-15V-3Cr-3Al-3Sn (Ti-15-3), Ti-15Mo-3Nb-3Al-0.2Si (Ti-21S), and Ti-6Al-4V (Ti-6-4). Elastic properties, creep deformation, and stress relaxation were examined along with the microstructural features before and after deformation. Differences in behavior were judged on the basis of statistical significance, where both a univariate analysis of variance (ANOVA) and a multivariate analysis of variance (MANOVA) were used and a two-parameter Norton-Bailey power law relationship was employed. In general, the HIPped foil and sheet were found to be significantly different in creep and stress relaxation at the 95-percent confidence level, with the only exceptions being Ti-15-3 in creep and Ti-21S in stress relaxation. Influencing this conclusion was the fact that the behaviors for any one alloy/product-form combination tended to be tightly grouped and exhibited relatively low sample-to-sample functional deviations. Of the three alloys, only the Ti-15-3 differed significantly within the microstructure in comparison to the foil and sheet forms. Furthermore, this was the only alloy to exhibit differences between the pre- and post-deformation states. This resulted from the metastable condition of the Ti-15-3 (even after a stabilization heat treatment). At 427 °C (800 °F), this alloy tends to experience a notable degree of deformation-assisted α-Ti precipitation within the β matrix. Although the strictly interpreted statistical analysis indicated that the foils and sheets exhibited significantly different behaviors, often a more practical engineering assessment and interpretation of the behaviors suggested that the sheet material could, in fact, be substituted for the foil, depending on the intended application of the data.

Lewis contacts:
Michael G. Castelli, (216) 433–8464, Michael.G.Castelli@grc.nasa.gov; and Dr. Bradley A. Lerch, (216) 433–5522, Bradley.A.Lerch@grc.nasa.gov

Author: Michael G. Castelli

Headquarters program office: OAT

Programs/Projects:
Propulsion Systems R&T, HITEMP

Thermomechanical Fatigue Durability of T650–35/PMR–15 Sheet-Molding Compound Evaluated

High-performance polymer matrix composites (PMC's) continue to be the focus of a number of research efforts aimed at developing cost-effective, lightweight material alternatives for advanced aerospace and aeropropulsion applications. These materials not only offer significant advantages in specific stiffness and strength over their current metal counterparts, but they can be designed and manufactured to eliminate joints and fasteners by combining individual components into integral subassemblies, thus making them extremely attractive for commercial applications. With much emphasis on the low-cost manufacturing aspects of advanced composite structures, there is heightened interest in high-performance sheet-molding compounds (SMC's). SMC's effectively reduce the costs associated with component production that uses prepregs, where variable costs are generally associated with labor, secondary processes, and scrap. With compression molding, SMC's can be fabricated into complex shapes facilitating the use of simple charge patterns, part consolidation, and molded-in inserts, which reduce labor, equipment, and operation costs for preparatory and secondary processes.

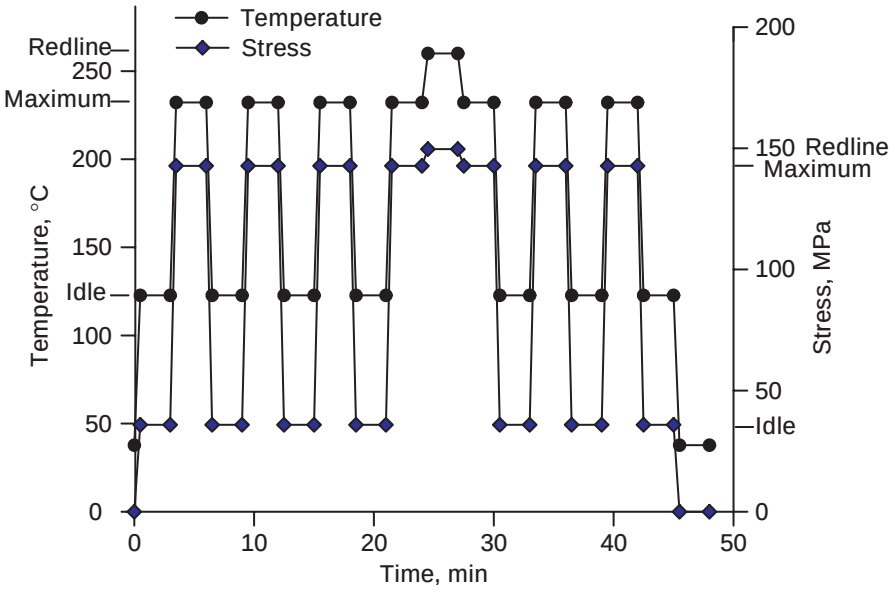

Thermomechanical fatigue mission cycle used for the T650–35/PMR–15 SMC inner-vane endwall application, showing idle, maximum, and redline (overload) conditions for temperature and stress.

Researchers at the NASA Lewis Research Center, in cooperation with the Allison Advanced Development Company, completed an investigation examining the use of T650–35/PMR–15 SMC for a midstage inner-vane endwall application within a gas turbine engine compressor. This component resides in the engine flow path and is subjected not only to high airflow rates, but also to elevated temperatures and pressures. This application is unique in that it represents a very aggressive use of high-performance SMC's, raising obvious concerns related to durability and property retention in the presence of microstructural damage. Therefore, it was necessary to evaluate the fatigue behavior and damage tolerance of this material subjected to a representative thermomechanical fatigue (TMF) mission-cycle loading spectrum.

Damage progression was tracked through changes in the macroscopic deformation and elastic stiffness in the loading direction. Additional properties, such as the glass transition temperature and dynamic mechanical response also were examined. The fiber distribution orientation was characterized through a detailed quantitative image analysis, and material durability and damage tolerance were quantified on the basis of residual static tensile properties after a prescribed number of TMF missions. Detailed microstructural examinations used optical and scanning electron microscopy to characterize the local damage.

Results indicate that the imposed TMF missions had only a modest effect on material durability as measured by the mechanical properties. Some microstructural damage was observed subsequent to 100 hours of TMF cycling. It consisted primarily of fiber debonding and transverse cracking local to predominantly transverse fiber bundles. No statistically significant degradation occurred in the residual tensile properties. Some of the more aggressive TMF scenarios examined, however, did promote notable creep damage and excessive strain accumulation that led to rupture. In some cases this creep behavior occurred at temperatures in excess of 150 °C below commonly cited values for the glass transition temperature. As a result, thermomechanical exploratory creep tests were conducted. These revealed that the SMC was subject to time-dependent deformation at stress/temperature thresholds of 150 MPa/230 °C and 170 MPa/180 °C.

Bibliography

Castelli, M.G.; Sutter, J.K.; and Benson, D.: Durability and Damage Tolerance of a Polyimide/Chopped Fiber Composite Subjected to Thermomechanical Fatigue Missions and Creep Loadings. Time Dependent and Nonlinear Effects in Polymers and Composites. ASTM STP–1357, R.A. Schapery and C.T. Sun, eds., American Society for Testing and Materials, 1999.

Lewis contacts:
Michael G. Castelli, (216) 433-8464, Michael.G.Castelli@grc.nasa.gov; and Dr. James K. Sutter, (216) 433-3226, James.K.Sutter@grc.nasa.gov

Author: Michael G. Castelli

Headquarters program office: OAT

Programs/Projects:
Propulsion Systems R&T, HITEMP

“Ultra”-Fast Fracture Strength of Advanced Structural Ceramic Materials Studied at Elevated Temperatures

The accurate determination of inert strength is important in reliable life prediction of structural ceramic components. At ambient temperature, the inert strength of a brittle material is typically regarded as free of the effects of slow crack growth due to stress corrosion. Therefore, the inert strength can be determined either by eliminating active species, especially moisture, with an appropriate inert medium, or by using a very high test rate.

However, at elevated temperatures, the concept or definition of the inert strength of brittle ceramic materials is not clear, since temperature itself is a degrading environment, resulting in strength degradation through slow crack growth and/or creep. Since the mechanism to control strength is rate-dependent viscous flow, the only conceivable way to determine the inert strength at elevated temperatures is to utilize a very fast test rate that either minimizes the time for or eliminates slow crack growth. Few experimental studies have measured the elevated-temperature, inert (or “ultra”-fast fracture) strength of advanced ceramics. This is, in part, because conventional test frames are incapable of very high rate testing. In addition, data acquisition systems are inadequate, and there are safety concerns. Commonly, a maximum test rate of about 30 MPa/sec has been used to determine the elevated-temperature strength of ceramic materials. The strength that is determined at this test rate has been called the fast-fracture strength, implying that it is the maximum attainable, or ultimate, strength of the material at the temperature.

At the NASA Lewis Research Center, an experimental study was initiated to better understand the “ultra”-fast fracture strength behavior of advanced ceramics at elevated temperatures. Fourteen advanced ceramics—one alumina, eleven silicon nitrides, and two silicon carbides—have been tested to date using constant stress-rate (dynamic fatigue) testing in flexure with a series of stress rates including the “ultra”-fast stress rate of 33 000 MPa/sec with digitally controlled test frames. The experimental results for these 14 advanced ceramics indicate that, notwithstanding possible changes in flaw populations as well as in flaw configurations because of elevated temperatures, the strength at 33 000 MPa/sec approached the room-temperature strength or reached a higher value than that determined at the conventional test rate of 30 MPa/sec. The graphs summarize the test results for the 14 ceramics, where the reduced strength is an elevated-temperature strength normalized with respect to the corresponding room-temperature strength. On the basis of the experimental data, it can be stated that the elevated-temperature, inert strength of an advanced ceramic material can be defined as the strength where no

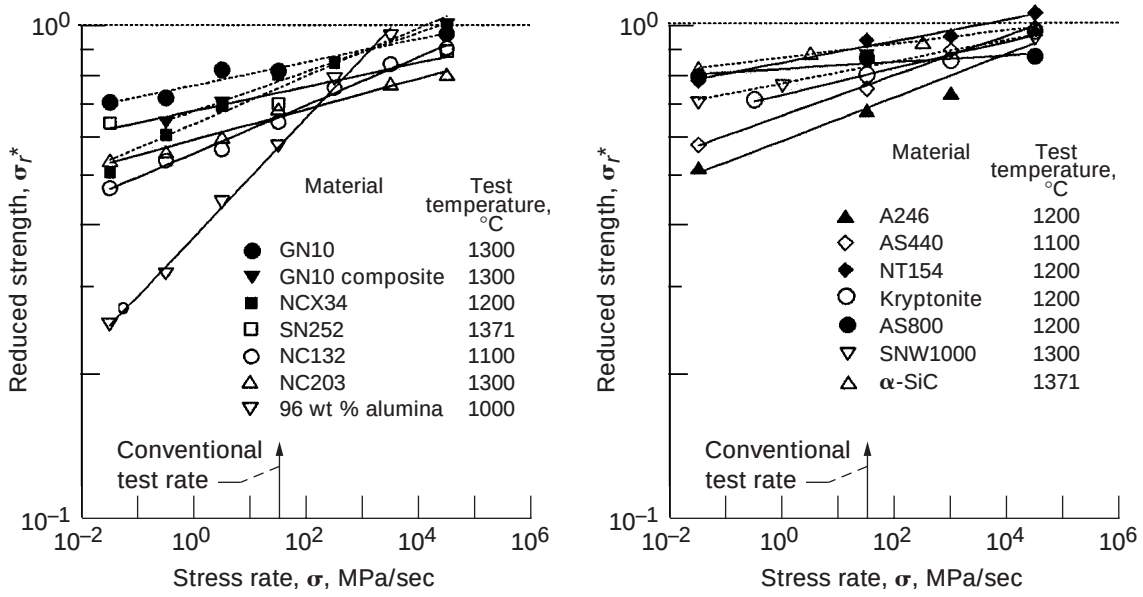

Summary of reduced strength as a function of stress rate for 14 advanced ceramics. Left: GN10, GN10 composite, NCX34, SN252 and NC132 silicon nitrides, NC203 silicon carbide, and 96 wt % alumina; Right: A2Y6, AS440, NT154, “Kryptonite” composite, AS800 and SNW1000 silicon nitrides, and α-silicon carbide.

slow crack growth takes place at the temperature. Specifically, the elevated-temperature inert strength is close to its room-temperature counterpart and can be obtained via a series of "ultra"-fast stress rates, including 33 000 MPa/sec in many cases. The strength determined at 33 000 MPa/sec must be used as an inert strength to determine the required life prediction parameters of the material.

Bibliography

Choi, S.R.; and Gyekenyesi, J.P.: Elevated-Temperature, 'Ultra'-Fast Fracture Strength of Advanced Ceramics: An Approach to Elevated-Temperature Inert Strength. ASME Paper 98–GT–479, 1998.

Choi, S.R.; and Gyekenyesi, J.P.: Elevated Temperature 'Ultra'-fast Fracture Strength Behavior of Advanced Structural Ceramics. Ceramic Materials and Components for Engines, K. Niihara, et al., eds., Technoplaza Co., Japan, 1998, pp. 689–694.

Choi, S.R.; and Salem, J.A.: 'Ultra'-Fast Fracture Strength of Advanced Ceramics at Elevated Temperature. Mater. Sci. Eng., A242, 1998, pp. 129–136.

Lewis contacts:
Dr. Sung R. Choi, (216) 433–8366, Sung.R.Choi@grc.nasa.gov; and Dr. John P. Gyekenyesi, (216) 433–3210, John.P.Gyekenyesi@grc.nasa.gov

Authors:
Dr. Sung R. Choi and Dr. John P. Gyekenyesi

Headquarters program office: OAT

Programs/Projects: HITEMP, P&PM

Viscoplastic Constitutive Theory Demonstrated for Monolithic Ceramic Materials

Development of accurate three-dimensional (multiaxial) inelastic stress-strain models is critical in utilizing advanced ceramics for challenging 21st century high-temperature structural applications. The current state of the art uses elastic stress fields as a basis for both subcritical crack growth and creep life prediction efforts aimed at predicting the time-dependent reliability response of ceramic components subjected to elevated service temperatures. However, to successfully design components that will meet tomorrow's challenging requirements, design engineers must recognize that elastic predictions are inaccurate for these materials when subjected to high-temperature service conditions such as those encountered in advanced heat engine components. Analytical life prediction methodologies developed for advanced ceramics and other brittle materials must employ accurate constitutive models that capture the inelastic response exhibited by these materials at elevated service temperatures.

A constitutive model recently developed at the NASA Lewis Research Center helps address this issue by accounting for the time-dependent (inelastic) material deformation phenomena (e.g., creep, rate sensitivity, and stress relaxation) exhibited by monolithic ceramics exposed to high-temperature service conditions. In addition, the proposed formulation is based on a threshold function that is sensitive to hydrostatic stress and allows different behavior in tension and compression, reflecting experimental observations obtained for these material systems.

The objective of this effort was to demonstrate the capabilities and inherent features of the mathematical formulation of the constitutive theory. In this regard, the viscoplastic constitutive equations formulated for the flow law (i.e., the strain rate) and the evolutionary law were incorporated into computer algorithms for predicting the multiaxial inelastic (creep) response of a given homogeneous state of stress. For the solution of a full multiaxial creep problem, 12 coupled differential equations had to be integrated. These represent the constitutive law: that is, six equations from the flow law (i.e., strain rate) and six from the evolutionary law.

Examples have been simulated numerically to illustrate the model's ability to qualitatively capture the time-dependent phenomena suggested here. For an imposed service (load) history, the computer algorithm can generate creep curves and viscoplastic flow surfaces that demonstrate its ability to capture the inelastic creep deformation response. No attempt was made to assess the accuracy of the model in comparison to the experiment. A quantitative assessment has been reserved for a later date—after the material constants have been suitably characterized for a specific ceramic material. Creep rupture is not considered in the model, although incorporating damage mechanics concepts into the present theory could yield a workable creep rupture model. This task also has been reserved for a future enhancement.

Bibliography
Janosik, L.A.; and Duffy, S.F.: A Viscoplastic Constitutive Theory for Monolithic Ceramics—I. J. Engrg. Gas Turb. Power (ASME Paper 96–GT–368) vol. 120, no. 1, Jan. 1998, pp. 155–161.

Lewis contact:
Lesley A. Janosik, (216) 433–5160, Lesley.A.Janosik@grc.nasa.gov

Author: Lesley A. Janosik

Headquarters program office: OAT

Programs/Projects:
Propulsion Systems R&T, P&PM

Resistance of Titanium Aluminide to Domestic Object Damage Assessed

A team consisting of GE Aircraft Engines, Precision Cast Parts, Oremet, and Chromalloy were awarded a NASA-sponsored Aerospace Industry Technology Program (AITP) to develop a design and manufacturing capability that will lead to the engine test demonstration and eventual implementation of a γ-Ti-47Al-2Nb-2Cr (at. %) titanium aluminide (TiAl) low-pressure turbine blade into commercial service. One of the main technical risks of implementing TiAl low-pressure turbine blades is the poor impact resistance of TiAl in comparison to the currently used nickel-based superalloy. The impact resistance of TiAl is being investigated at the NASA Lewis Research Center as part of the Aerospace Industry Technology Program and the Advanced High Temperature Engine Materials Program (HITEMP).

The overall objective of this work is to determine the influence of impact damage on the high cycle fatigue life of TiAl-simulated low-pressure turbine blades. To this end, impact specimens were cast to size in a dog-bone configuration and given a typical processing sequence followed by an exposure to 650 °C for 20 hours to simulate embrittlement at service conditions. Then, the specimens were impacted at 260 °C under a 69-MPa load. Steel projectiles with diameters 1.6 and 3.2 mm were used to impact the specimens at 90° to the leading edge. Two different impact energies (0.74 and 1.5 joules) were used to simulate fairly severe domestic object damage on a low-pressure turbine blade.

Fatigue tests were performed at 650 °C and at a frequency of 100 Hz. In addition, three different loading ratios, *R*, were used to assess the effect of mean stresses. As expected, the specimens impacted at the higher energy levels failed at lower fatigue stresses because of the larger "defect" associated with the impact. Both energy levels resulted in fatigue strengths that were significantly lower, yet predictable, than for the smooth bars (i.e., nonimpacted specimens). In addition, a Goodman mean stress approach could be used to accurately model the fatigue data for all impacted specimens.

The industry-NASA team is using the results of this study to minimize the technical risks associated with impact issues. The actual damage tolerable for a low-pressure turbine blade application will be determined by a combination of fatigue testing and consideration of actual engine conditions. The current evaluations indicate that Ti-47Al-2Nb-2Cr possesses the level of damage tolerance required for implementation into service.

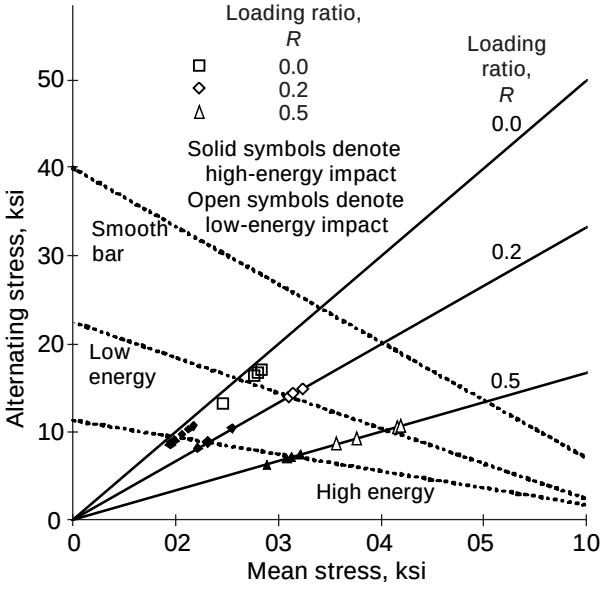

Goodman diagram for γ-TiAl specimens tested at 650 °C.

Bibliography
Draper, S.L.: Pereira, J.M.; and Nathal, M.V.: Impact Resistance of γ-Ti-48Al-2Nb-2Cr. HITEMP Review 1997, NASA CP–10192, Vol. II, 1997, paper no. 25, pp. 1–13. (Available from NASA Lewis' Subsonic Systems Office.)

Lewis contact:
Dr. Bradley A. Lerch, (216) 433–5522, Bradley.A.Lerch@grc.nasa.gov

Authors:
Dr. Bradley A. Lerch, Susan L. Draper, Dr. J. Michael Pereira, Dr. Michael V. Nathal, and Curt Austin

Headquarters program office: OAT

Programs and projects:
Aeronautics Base R&T, HITEMP, AITP

Multiaxial Experiments Conducted to Aid in the Development of Viscoplastic Models

Aeropropulsion components, such as disks, blades, and shafts, are commonly subjected to multiaxial stress states at elevated temperatures. Experimental results from loadings as complex as those experienced in service are needed to help guide the development of accurate viscoplastic, multiaxial deformation models that can be used to improve the design of these components. Typically, past studies investigated model materials, concentrating, for experimental simplicity, on room temperature. This study provides first-of-a-kind data by conducting axial-torsional tests at service-related temperatures on a popular aeropropulsion material, namely INCONEL 718 (IN–718, Inco Alloys International, Inc., Huntington, West Virginia). The data from this type of study can be used to develop the evolution equations necessary for this and similar engineering materials.

Yield loci were determined for aged IN–718 at 650 °C. This was done using experimental procedures developed over the past several years in a cooperative program between Penn State University and the NASA Lewis Research Center. This program represents an ongoing effort to develop test methods necessary for the validation of viscoplastic models. The von Mises (J_2) yield criterion was found to not fit the data well because of a strength differential in tension and compression. That is, the initial yield strength in compression was greater than it was in tension. The strength differential was present for the entire range of loading (up to at least strains of ±1 percent), but it decreased as plastic flow increased. In addition, the strength differential increased as the temperature increased in the range of 20 to 650 °C.

Yield surfaces also were obtained after preloading the material to various levels. After applying an axial-shear prestrain to an equivalent inelastic strain of 500 microstrain, the yield surface translated in the direction of the prestrain (see the figure). In addition, the yield surface elongated in the direction of prestraining and flattened on the back side. Thus, there is a component of distortional hardening that needs to be accounted for in the theoretical evolution equations.

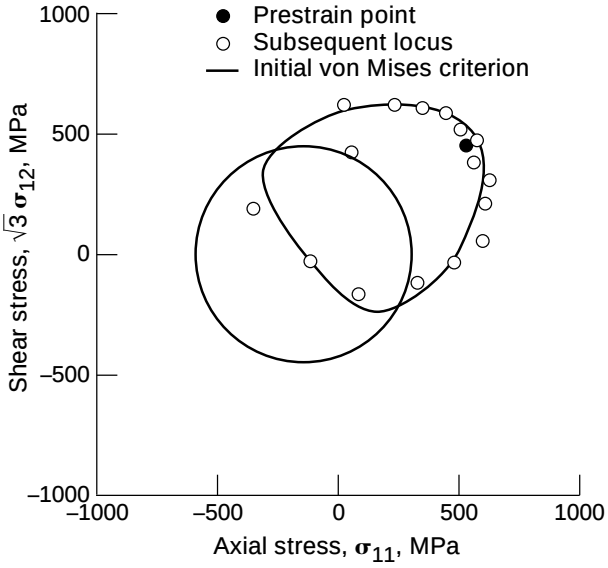

Yield locus subsequent to an axial-shear inelastic prestrain of 500-microstrain for IN–718 aged at 650 °C. Offset for individual probes, ε^{off}, 30 microstrain.

We are presently developing techniques to transform the yield surface data to flow surfaces, which are similar to yield surfaces except that they are rate-dependent, and thus more meaningful for viscoplastic models. Since the von Mises yield criterion was inadequate for IN–718, experiments and associated modeling work are planned to determine the dependence of initial yielding on the stress invariants (I_1, J_2, and J_3) and to establish the importance of these invariants. In addition, we plan to examine load path dependence for the evolution of state and compare these results with predictions from viscoplastic models.

Bibliography

Gil, C.M.; Lissenden, C.J.; and Lerch, B.A.: Determination of Yield in Inconel 718 for Axial-Torsional Loading at Temperatures up to 649 °C. NASA TM—1998-208658, 1998.

Gil, C.M.; Lissenden, C.J.; and Lerch, B.A.: Investigation of Anomalous Behavior in Metallic-Based Materials Under Compressive Loading. NASA TM—1998-206640, 1998.

Lissenden, C.J., et al.: Robinson: Experimental Determination of Yield and Flow Surfaces Under Axial-Torsional Loading. Multiaxial Fatigue and Deformation Testing Techniques. ASTM STP–1280, S. Kalluri and P.J. Bonacuse, eds., 1997, pp. 92–112.

Lewis contact: Dr. Bradley A. Lerch, (216) 433–5522, Bradley.A.Lerch@grc.nasa.gov

Authors: Dr. Bradley A. Lerch, Prof. Clifford J. Lissenden, and Christopher Gil

Headquarters program office: OAT

Programs/Projects: HITEMP

Multidisciplinary Probabilistic Heat Transfer/Structural Analysis Code Developed—NESTEM

High-Speed Civil Transport (HSCT) engine combustor liners are subjected to complex thermal environments and have to endure these for thousands of hours with assured reliability. In the past, several deterministic analyses have been performed, including detailed heat transfer analyses to obtain thermal profiles and deterministic stress analyses to identify critical locations of high stresses. Actual rig tests also have been performed for segments by simulating these loading situations as closely as possible. However, it is well known that many uncertainties exist in loading (primarily thermal loads due to heat transfer), boundary conditions (end fixity unknowns), and material properties (moduli, thermal-expansion coefficients, and conductivities). The present in-house effort at the NASA Lewis Research Center is directed toward accounting for these in a formal way to assess the performance of liner components under complex and uncertain loading conditions as well as subject to other geometry- and material-related uncertainties.

Under the sponsorship of the Enabling Propulsion Materials (EPM) project, Lewis' Structures and Acoustics Division recently developed a computational capability, NESTEM (see the figures),

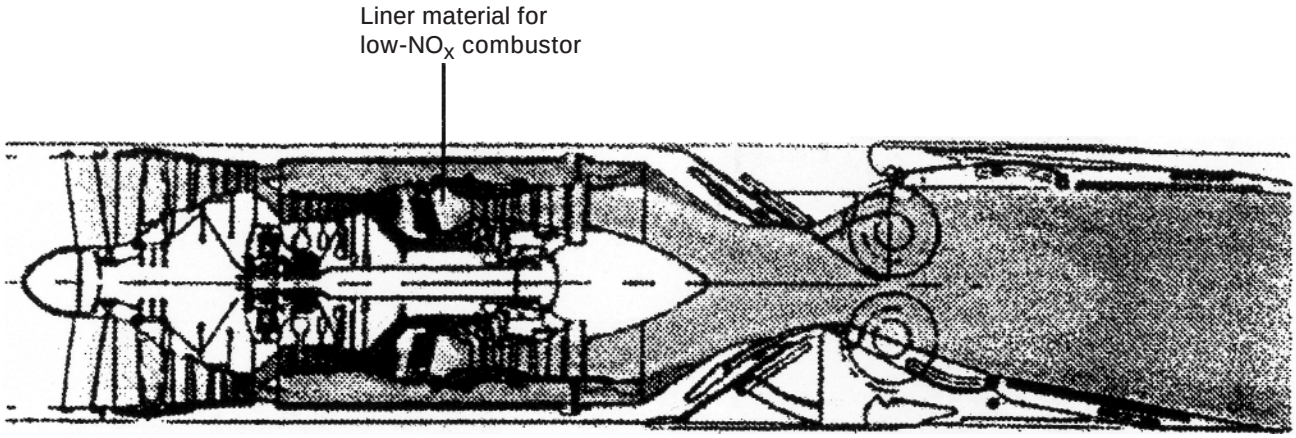

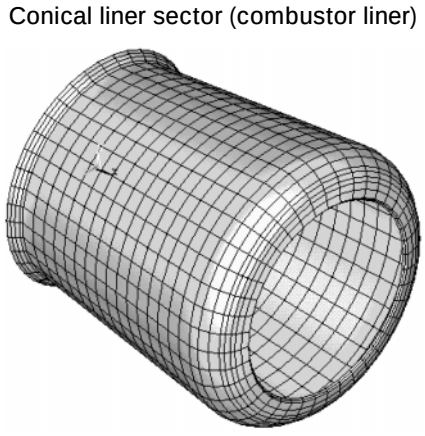

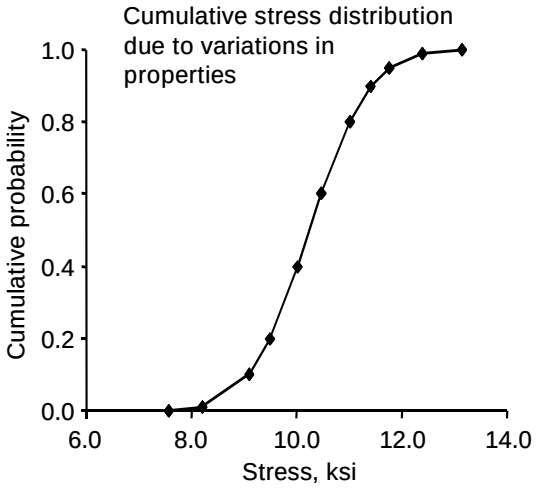

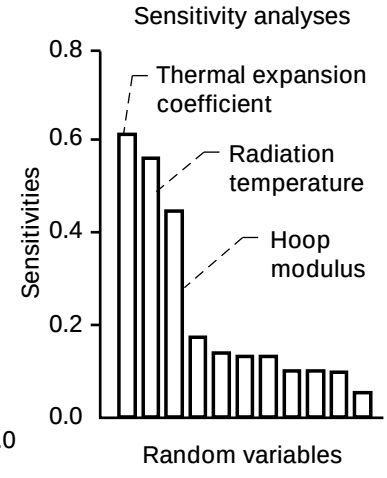

Sample output from NESTEM for a conical ceramic-matrix-composite liner segment.

through a contract to Modern Technologies Corporation. NESTEM is a computer code that combines the heat transfer analysis capability of the EPM backbone computer code CSTEM (Coupled Structural, Thermal and Electro-Magnetic Tailoring) with Lewis' in-house probabilistic structural analysis code NESSUS (Numerical Evaluation of Stochastic Structures Under Stress). The code can now analyze and assess the complex combustor thermal environment with uncertainties, as well as its effects on the overall ceramic matrix composite (CMC) liner response. It enables us to formally assess the uncertainties in loads, material property variations, and geometric imperfections on the overall structural behavior (such as stability, frequencies, and stresses). Typical output of the code is probabilistic stress distributions at the hot spots, probabilistic frequencies, and buckling loads. This information allows designers to make more informed judgments regarding the preliminary design of the liner components without resorting to overly conservative deterministic approaches with ad hoc knockdown factors. The information also permits more accurate calculation of the reliability and life of such components. In addition, the code provides information on the sensitivities of the various uncertainties and ranks them in the order of importance as a byproduct. The accompanying figures show a sample output for a conical ceramic-matrix-composite liner segment.

NESTEM's features include

- Automatic geometry and finite element mesh generation
- Finite element property card generation for arbitrary composite layups
- Uncertainties in heat-transfer-related variables, combustor temperatures, geometry, material properties, and boundary conditions
- Heat transfer and structural analysis in the same run
- Cumulative distribution functions of response, including temperatures, stresses, natural frequencies, buckling loads, and displacements
- Sensitivities of variables with uncertainties at various probability levels

Lewis contacts:
Dr. Pappu L.N. Murthy, (216) 433–3332, Pappu.L.Murthy@grc.nasa.gov; and Dr. Shantaram S. Pai, (216) 433–3255, Shantaram.S.Pai@grc.nasa.gov

Authors:
Dr. Pappu L.N. Murthy and Dr. Shantaram S. Pai

Headquarters program office: OAT

Programs/Projects: HSR, EPM

Special recognition:
Team Achievement Award

Design Tool Developed for Probabilistic Modeling of Ceramic Matrix Composite Strength

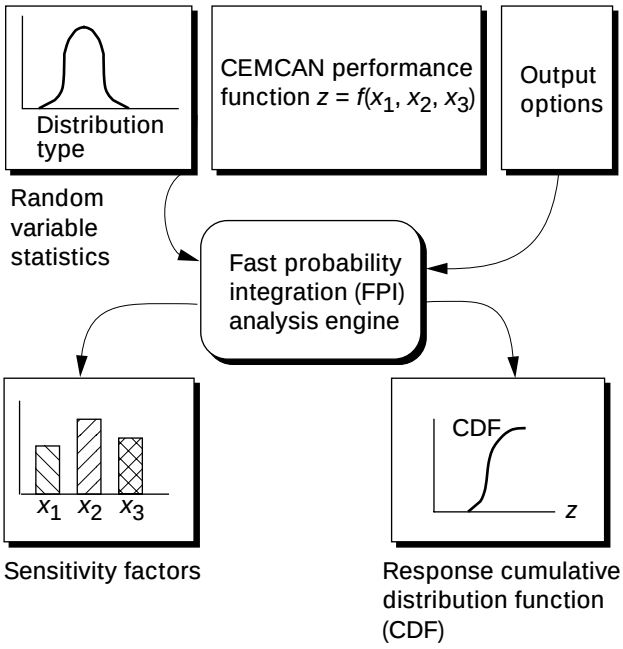

Fast probability integration input and output.

Ceramic matrix composites are being evaluated as candidate materials for many high-temperature applications such as engine combustor liners for the High-Speed Civil Transport (HSCT). They are required to have an assured life of several thousand hours. Estimating the reliability of these components is quite a complex process and requires knowledge of the uncertainties that occur at various scales. The properties of ceramic matrix composites (CMC) are known to display a considerable amount of scatter due to variations in fiber/matrix properties, interphase/coating properties, bonding, amount of matrix voids, and many geometry- and fabrication-related parameters such as ply thickness and ply orientations. The objective

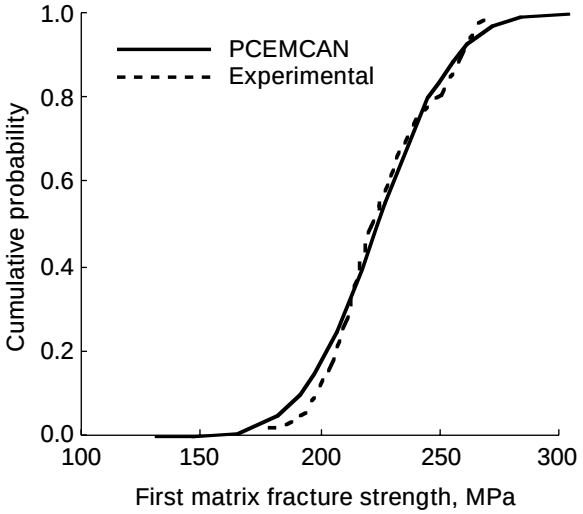

Comparison of the first matrix cracking strength cumulative-distribution-function simulation (PCEMCAN, Probabilistic Ceramic Matrix Composite Analyzer) with the experimental data for a $[0]_8$ SCS–6/RBSN composite laminate.

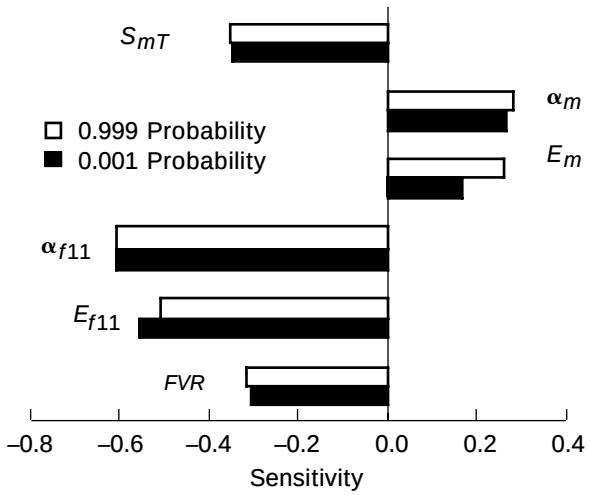

Sensitivity of the first matrix cracking strength to the primitive random variables of a $[0]_8$ SCS–6/RBSN composite laminate. Matrix tensile strength, S_{mT}; fiber coefficient of thermal expansion, α_{f11}; fiber longitudinal modulus, E_{f11}; fiber volume ratio, FVR.

of this research effort is to account for these uncertainties in a formal way by probabilistically analyzing both the stiffness- and strength-related properties of CMC's. In current deterministic approaches, uncertainties are usually accounted for by safety factors. This approach often yields overly conservative designs, thereby reducing the potential of many advanced composite materials.

Work is underway at the NASA Lewis Research Center to incorporate the probabilistic distribution of material-behavior and fabrication-related parameters into the micromechanics and macromechanics of CMC's. The primary objective of this work was to develop an efficient computational design tool that could account for all the uncertainties in a more rigorous and formal manner, providing overall composite properties and their probabilistic distributions.

Therefore, we combined the CMC analysis embedded in the CEMCAN (Ceramic Matrix Composite Analyzer) computer code with the fast probability integration (FPI) techniques available in the NESSUS (Numerical Evaluation of Stochastic Structures Under Stress) code. CEMCAN provides functional relationships that tie the constituent properties and other geometry- and fabrication-related parameters to the overall composite properties. Fast probability integration is used to perform probabilistic analyses by utilizing the properties generated by CEMCAN. The results are cumulative distribution functions (CDF's) and probability density functions (PDF's) for the ply and laminate properties of the CMC. This technique is more efficient than a standard Monte-Carlo technique, where a large number of simulations are needed to generate a cumulative distribution function. The probabilistic sensitivities of the output variables with respect to inherent scatter in basic variables are obtained as a byproduct of the fast probability integration analyses. This provides very useful information to design and test engineers in evaluating the importance of variables that control the scatter in an overall property. The accompanying figures show sample results from the analyses.

Lewis contact:
Dr. Pappu L.N. Murthy, (216) 433–3332, Pappu.L.Murthy@grc.nasa.gov

University of Toledo contact:
Subodh K. Mital, (216) 433–3261, Subodh.K.Mital@grc.nasa.gov

Authors:
Dr. Pappu L.N. Murthy, Subodh K. Mital, and Ashwin R. Shah

Headquarters program office: OAT

Programs/Projects: HITEMP

CARES/*Life* Ceramics Durability Evaluation Software Enhanced for Cyclic Fatigue

The CARES/*Life* computer program predicts the probability of a monolithic ceramic component's failure as a function of time in service. The program has many features and options for materials evaluation and component design. It couples commercial finite element programs—which resolve a component's temperature and stress distribution—to reliability evaluation and fracture mechanics routines for modeling strength-limiting defects. The capability, flexibility, and uniqueness of CARES/*Life* have attracted many users representing a broad range of interests and has resulted in numerous awards for technological achievements and technology transfer.

Recent work with CARES/*Life* was directed at enhancing the program's capabilities with regards to cyclic fatigue. Only in the last few years have ceramics been recognized to be susceptible to enhanced degradation from cyclic loading. To account for cyclic loads, researchers at the NASA Lewis Research Center developed a crack growth model that combines the Power Law (time-dependent) and the Walker Law (cycle-dependent) crack growth models. This combined model has the characteristics of Power Law behavior (decreased damage) at high *R* ratios (minimum load/maximum load) and of Walker law behavior (increased damage) at low *R* ratios. In addition, a parameter estimation methodology for constant-amplitude, steady-state cyclic fatigue experiments was developed using nonlinear least squares and a modified Levenberg-Marquardt algorithm. This methodology is used to give best estimates of parameter values from cyclic fatigue specimen rupture data (usually tensile or flexure bar specimens) for a relatively small number of specimens. Methodology to account for runout data (unfailed specimens over the duration of the experiment) was also included.

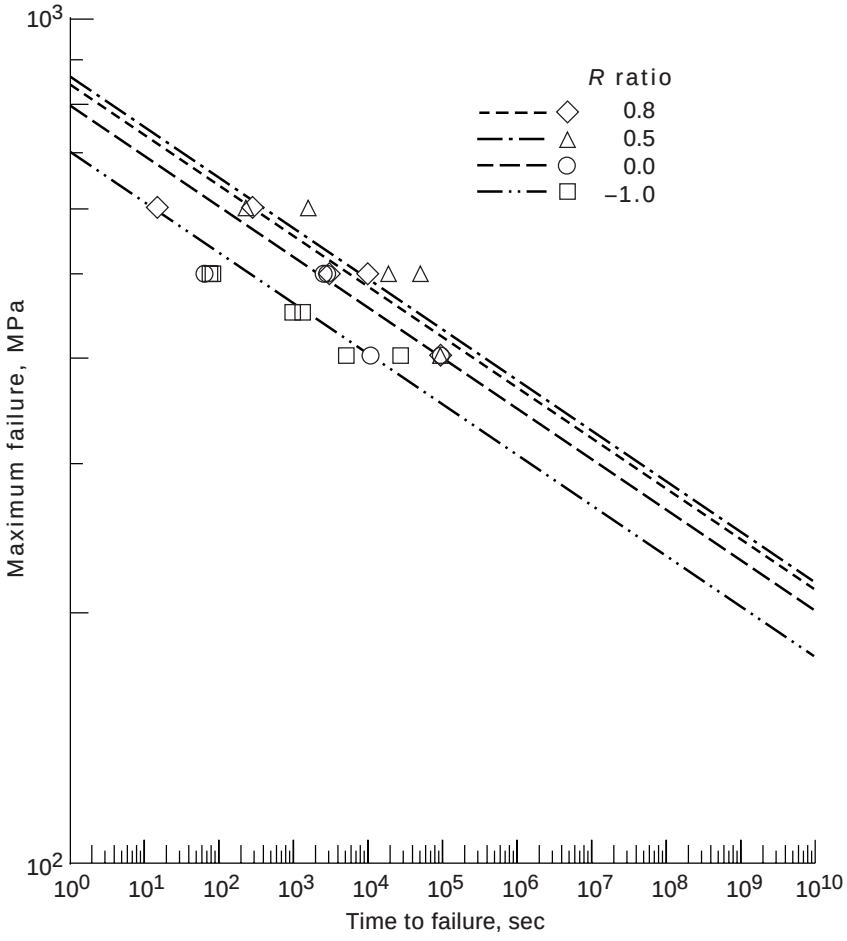

Median regression lines for partially stabilized zirconia tensile specimens with various R-ratios (combined law model).

The graph shows an example of this regression technique for tensile specimen data for partially stabilized zirconia. Data for various *R* ratios and their corresponding median regression lines are shown for the combined fatigue law model. Note that at lower *R* ratios (0 and –1) the combined law predicted increased material strength degradation, whereas at higher *R* ratios (0.5 and 0.8) this trend was reversed.

Find out more on the World Wide Web: http://www.grc.nasa.gov/WWW/LPB/cares/life/software.html

Bibliography

Nemeth, N.N., et al.: Designing Ceramic Components for Durability. Advanced Ceramic Matrix Composite—Design Approaches, Testing and Life Prediction Methods, E.R. Generazio, ed., Technomic Publishing Company, Lancaster, PA, 1996, pp. 3–16.

Nemeth, N.N., et al.: Durability Evaluation of Ceramic Components Using CARES/*Life*. ASME J. Engrg. Gas Turb. Power, vol. 118, Jan. 1996, pp. 150–158.

Rahman, S.; Nemeth, N.N.; and Gyekenyesi, J. P.: Life Prediction and Reliability Analysis of Ceramic Structures Under Combined Static and Cyclic Fatigue. ASME Paper 98–GT–569, 1998.

Lewis contacts:
Noel N. Nemeth, (216) 433–3215, Noel.N.Nemeth@grc.nasa.gov;
Lynn M. Powers, (216) 433–8374, Lynn.M.Powers@grc.nasa.gov; and
Lesley A. Janosik, (216) 433–5160, Lesley.A.Janosik@grc.nasa.gov

Authors: Noel N. Nemeth, Lynn M. Powers, and Lesley A. Janosik

Headquarters program office: OAT

Programs/Projects: P&PM, broad range of propulsion technology

Special recognition:
Numerous awards including 1998 EDI Innovation Award (Enterprise Development Inc.) given to Lewis for the development of CARES

Novel Method Used to Inspect Curved and Tubular Structural Materials

At the NASA Lewis Research Center, a technique for the ultrasonic characterization of plates has been extended to tubes and to curved structures in general. In this technique, one performs measurements that yield a thickness-independent value of the local through-the-thickness speed of sound in a specimen. From such measurements at numerous locations across the specimen, one can construct a map of velocity as a function of location. The gradients of velocity indicated by such a map indicate local through-the-thickness-averaged microstructural parameters that affect the speed of sound. Such parameters include the pore volume fraction, mass density, fiber volume fraction (in the case of a composite material), and chemical composition. Apparatus was designed to apply the technique to tubular and other curved specimens.

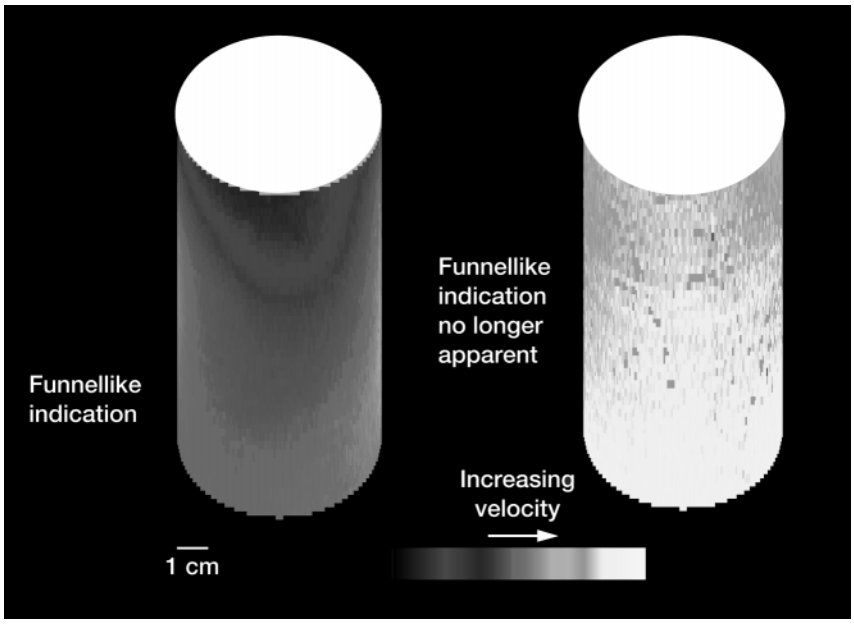

Apparent and thickness-independent velocity images of silicon nitride tube as decaled onto tubular models. Baseline orientation. Left: Apparent velocity image. Right: Thickness-independent velocity image.

The specimen was mounted on a horizontal turntable in a water tank, with its axis vertical and coincident with the turntable axis. A machined metal reflector plate narrow enough to fit within the inner diameter of the specimen was suspended vertically from above and positioned inside the specimen about 1 cm from the inner tube wall. A horizontally oriented ultrasonic transducer was positioned outside the specimen, facing the reflector plate. Then, pulse/echo measurements were taken in basically the same manner as for the plate specimens. The transducer was translated vertically to obtain measurements at various axial positions (e.g., increments of 1 mm), and the turntable was rotated to obtain measurements at various azimuthal positions (e.g., increments of 1°).

The technique has been demonstrated in experiments on tubular specimens of mullite (silica/alumina), a polymer-matrix composite, a composite of SiC fibers in an SiC matrix, and a high-temperature structural grade of silicon nitride. Although the turntable, specimen, reflector plate, and transducer should be aligned as nearly perfectly as possible and

the specimen should approximate a perfect round tube, it was observed that, in general, some misalignment and out of roundness can be tolerated. This is an advantage over peak-amplitude-based ultrasonic techniques in which measurements are altered drastically by refractive effects associated with out of roundness. The present technique made it possible to eliminate most of the effects of variations in tube-wall thicknesses upon velocity maps (through-the-thickness velocities as functions of axial and azimuthal positions). However, edge effects associated with discontinuous changes in thickness were not eliminated completely. In the case of the silicon nitride tube, differences between velocities at different locations were found to be correlated with differences between densities and pore volume fractions revealed by x-radiography and destructive metallographic analysis at those locations. The illustration shows the apparent (without thickness variation subtracted) and thickness-independent velocity images of the silicon nitride tube as decaled onto tubular models.

For more information about this research, visit us on the World Wide Web:
http://www.grc.nasa.gov/WWW/LPB/tiui/

Lewis contact:
Dr. Don J. Roth, (216) 433–6017, don.j.roth@grc.nasa.gov

Authors:
Dr. Don J. Roth, George Y. Baaklini, Dorothy V. Carney, James R. Bodis, and Richard W. Rauser

Headquarters program office: OAT

Programs/Projects: HITEMP, P&PM

Special recognition: Part of the effort that received an R&D100 award and the Federal Laboratory Consortium Excellence in Technology Transfer Award; to be featured on the cover of the *International Journal of Materials Evaluation* in 1998

Composite Nozzle/Thrust Chambers Analyzed for Low-Cost Boosters

The Low Cost Booster Technology Program is an initiative to minimize the cost of future liquid engines by using advanced materials and innovative designs, and by reducing engine complexity. NASA Marshall Space Flight Center's 60K FASTRAC Engine is one example where these design philosophies have been put into practice. This engine burns a liquid kerosene/oxygen mixture. It uses a one-piece, polymer composite thrust chamber/nozzle that is constructed of a tape-wrapped silica phenolic liner, a metallic injector interface ring, and a filament-wound epoxy overwrap (figure on the left). This integral chamber/nozzle design minimizes engine operations costs because it simplifies engine refurbishment procedures.

A cooperative effort between NASA Lewis Research Center's Structures Division and Marshall is underway to perform a finite element analysis of the FASTRAC chamber/nozzle under all the loading and environmental conditions that it will experience during its lifetime. The chamber/nozzle is a complex composite structure. Of its three different materials, the two composite components have distinctly different fiber architectures and, consequently, require separate material model descriptions. Since the liner is tape wrapped, it is orthotropic in the nozzle global coordinates; and since the overwrap is filament wound, it is treated as a monoclinic material. Furthermore, the wind angle on the overwrap (figure on the right) varies continuously along the length of the chamber/nozzle.

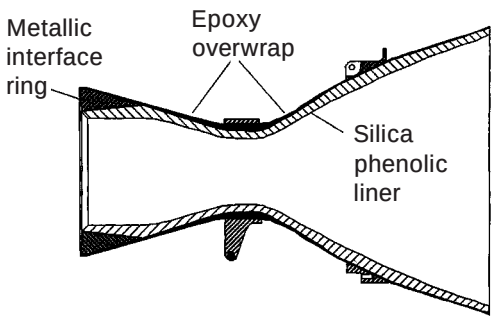

Thrust chamber/nozzle of 60K FASTRAC Engine.

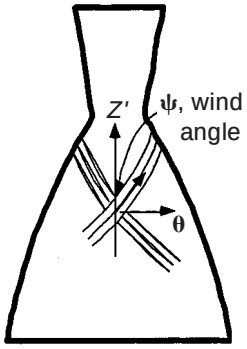

Thrust chamber/nozzle showing filament wind angles.

The angle is very shallow in the throat region and becomes steep toward the ends.

During early fabrication attempts, cracking of the liner posed a significant problem. The cracking was the result of residual stresses that developed during processing because of the large differences between the thermal expansion coefficients of the silica phenolic and the epoxy overwrap. The final figure shows the tangential thermal expansion coefficient as a function of the axial position for both the liner and the overwrap. Although the liner tangential thermal expansion coefficient is constant with position, the overwrap thermal coefficient varies considerably along the length because of the varying wind angle.

A finite element analysis of the chamber/nozzle was performed under processing conditions. The results were instrumental in resolving the residual-stress cracking problem and helped to establish a representative analog using straight cylinders. The analyses verified that cylindrical analogs will duplicate the highest stress states in the nozzle, which occur at the nozzle throat. Furthermore, they helped to identify large discrepancies between the material strengths measured using the traditional dogbone configuration and the strengths measured in a cylindrical configuration.

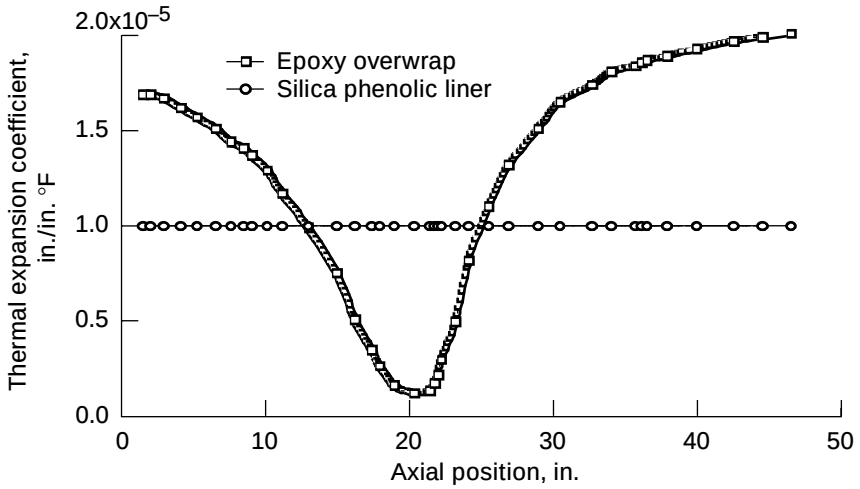

Tangential thermal expansion coefficient versus axial position.

Future analyses of the chamber/nozzle are planned to determine the residual stress levels for a variety of possible material systems, nozzle designs, and fiber architectures. The objective is to choose the optimal material system to minimize residual stresses. Furthermore, we plan to perform finite element analyses for all the loading and temperature conditions that the chamber/nozzle will experience during 60K FASTRAC Engine operation.

Lewis contact:
Roy M. Sullivan, (216) 433–3249, Roy.M.Sullivan@grc.nasa.gov

Author: Roy M. Sullivan

Headquarters program office: OAT

Programs/Projects: ASTP, LCBT

Flutter Version of Propulsion Aeroelasticity Code Completed

NASA's Advanced Subsonic Technology (AST) Program seeks to develop new technologies to increase the fuel efficiency of commercial aircraft engines, improve the safety of engine operation, and reduce emissions and engine noise. For new designs of ducted fans, compressors, and turbines to achieve these goals, a basic aeroelastic requirement is that there should be no flutter or high resonant blade stresses in the operating regime. For verifying the aeroelastic soundness of the design, an accurate prediction/analysis code is required. Such a three-dimensional viscous propulsion aeroelastic code, named TURBO–AE, is being developed at the NASA Lewis Research Center. The development and verification of the flutter version of the TURBO–AE code (version 4) has been completed. Validation of the code is partially complete.

The TURBO–AE aeroelastic code is based on a three-dimensional unsteady aerodynamic Euler/Navier-Stokes turbomachinery code TURBO, developed previously under a grant from Lewis. This code can model viscous flow effects, which play an important role in certain aeroelastic problems such as flutter with flow separation, flutter at high loading conditions near the stall line (stall flutter), and

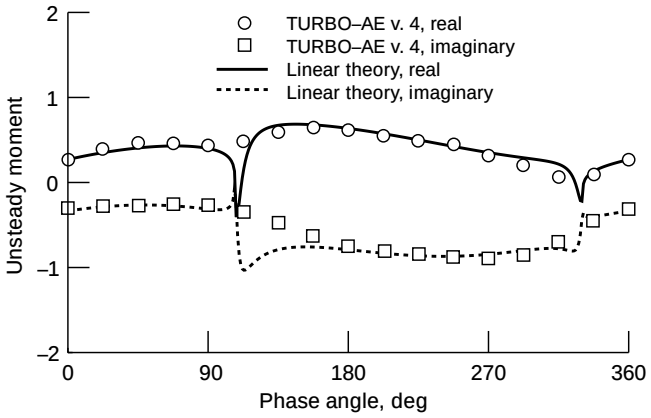

Unsteady moment for the torsional blade vibrations of a helical fan.

flutter in the presence of shock and boundary-layer interaction. In the TURBO–AE code, the structural dynamics representation of the blade is based on a normal mode representation. Any finite-element analysis code can be used to calculate in-vacuum vibration modes and the associated natural frequency. As an alternative, experimental measurements of these vibration characteristics can be used.

A work-per-cycle approach is used to determine aeroelastic stability (flutter). With this approach, the motion of the blade is prescribed to be a harmonic vibration in a specified in-vacuum normal mode. The work done by aerodynamic forces on the vibrating blade during a cycle of vibration is calculated. If this work is positive, the blade is dynamically unstable, because it will extract energy from the flow, leading to an increase in the amplitude of the blade's oscillation.

As part of the verification of the TURBO–AE code, calculations were performed for a helical fan test configuration. This configuration was used to compare the code to two-dimensional linear potential (classical linear/flat plate) theory. Results from the midspan of the blade undergoing torsional vibrations were compared with linear theory results for the pitching motion of a flat plate cascade. Excellent agreement was observed for this test case, providing a fundamental verification of the TURBO–AE code.

TURBO–AE code will provide a useful aeroelastic prediction/analysis capability for engine manufacturers. It will reduce design cycle times by allowing new blade designs to be verified for aeroelastic soundness before blades are built and tested. Using this prediction capability, it will be possible to build thinner, lighter, and faster rotating blades without encountering aeroelastic problems like stall flutter and high-cycle fatigue due to forced vibrations.

Bibliography

Bakhle, M.A., et al.: Aeroelastic Calculations Based on Three-Dimensional Euler Analysis. AIAA Paper 98–3295, July 1998.

Lewis contacts:
Milind A. Bakhle, (216) 433–6037, Milind.A.Bakhle@grc.nasa.gov; Rakesh Srivastava, (216) 433–6045, Rakesh.Srivastava@grc.nasa.gov; and George L. Stefko, (216) 433–3920, George.L.Stefko@grc.nasa.gov

Author: Milind A. Bakhle

Headquarters program office: OAT

Program/Project: AST, TURBO–AE

Stability of the Tilt Modes of an Actively Controlled Flywheel Analyzed

Applications of strongly gyroscopic rotors are becoming important, including flywheels for terrestrial and space energy storage and various attitude control devices for spacecraft. Some of these applications, especially the higher speed ones for energy storage, will have actively controlled magnetic bearings. These bearings will be required where speeds are too high for conventional bearings, where adequate lubrication is undesirable or impossible, or where bearing losses must be minimized for efficient energy storage.

Flywheel rotors are highly gyroscopic, and above some speed that depends on the bandwidth of the feedback system, they always become unstable in an actively controlled magnetic bearing system. To assess ways to prevent instability until speeds well above the desired operating range, researchers at the NASA Lewis Research Center used a commercial controls code to calculate the eigenvalues of the tilt modes of a rigid gyroscopic rotor supported by active magnetic bearings. The real part of the eigenvalue is the negative of the damping of the mode, and the imaginary part is approximately equal to the mode's frequency.

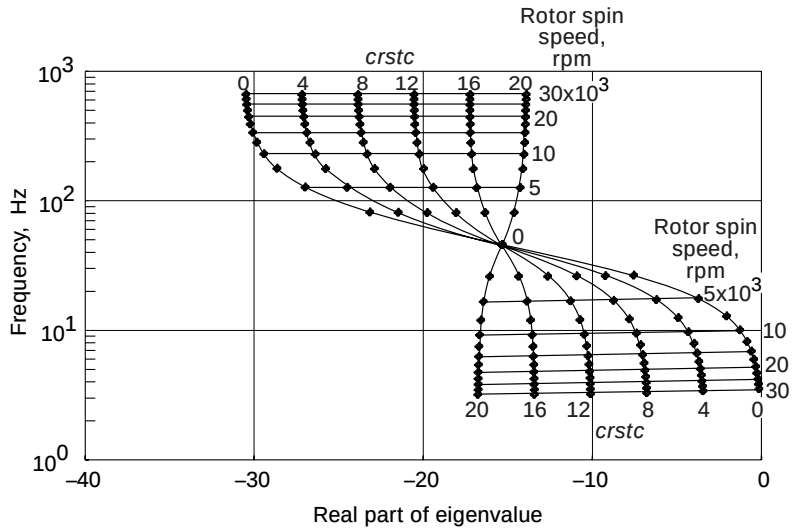

Effect of position cross coupling with Ω factor; five corners at 50 kHz.

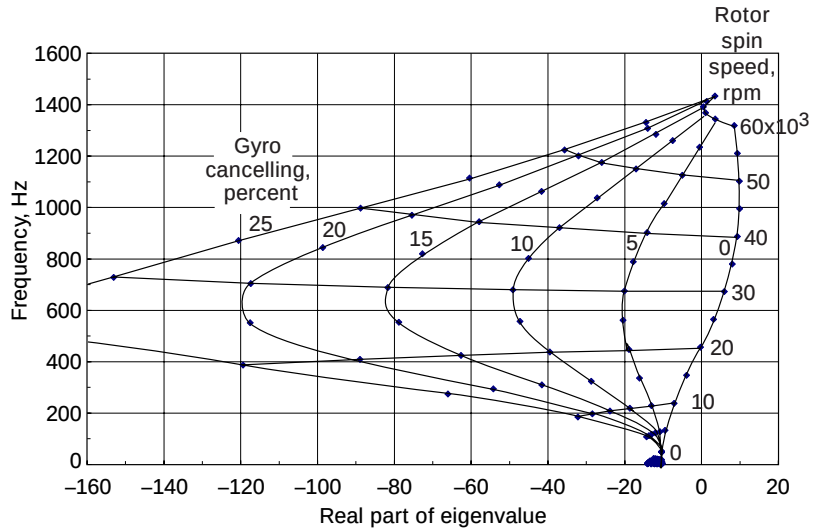

Effect of small-percent gyro canceling with position cross coupling; five corners at 2 kHz; crstc, 12.

A modal controller was presumed in which the pure translation and pure tilt modes were separated. We addressed only the tilt modes. The controller included simple proportional-derivative (PD) gains for each tilt angle and proportional and derivative cross-coupling gains. Bandwidths were imposed in the control loop to represent the various phase lags of a magnetic bearing system. The effects of bandwidths, cross-axis proportional gain, and cross-axis derivative gain (gyroscopic canceling) were considered individually and in combination to show the qualitative and quantitative effects of each. Both cross-axis gains were “scheduled” by being multiplied by the rotor spin speed Ω since they were needed only to counteract the effects of gyroscopic torques.

The tilt mode of a nonspinning rotor becomes two modes under rotation: one mode (called the forward whirl mode) goes up in frequency with the rotor speed; the other (called the backward whirl mode) goes down. We found that cross-axis proportional gain, *crstc*, increases the damping of the backward whirl mode, which is otherwise a poorly damped, low-frequency mode at high rotor spin speed (see the top figure, which was calculated with high bandwidth). The point common to all curves is for zero rpm. Damping increases toward the left. This gain (*crstc*) decreases the damping of the forward whirl mode, which is otherwise better damped, but which could be subject to strong forcing by rotor unbalance as rotor speed increases (see the top figure). Cross-axis derivative gain (also called gyroscopic cancelling) can improve the forward whirl mode damping but has little effect on the backward whirl mode. An appropriate combination of these cross-axis gains can result in a closed-loop system that is stable over a wide speed range without additional gain scheduling, as shown in the bottom figure, which was calculated with more realistic bandwidths. Again, the point common to all curves is for zero rpm. Modes to the right of the vertical axis are unstable; modes to the left are progressively more stable as damping increases. Note that with 10-percent gyroscopic canceling, for example, the flywheel would be stable to nearly 60 000 rpm.

Lewis contacts:
Dr. Gerald V. Brown, (216) 433–6047, Gerald.V.Brown@grc.nasa.gov; and Albert F. Kascak, (216) 433–6024, Albert.F.Kascak@grc.nasa.gov

Authors:
Dr. Gerald V. Brown and Albert F. Kascak

Headquarters program office: OAT

Program/Project: Magnetic bearings for flywheels for energy storage and space attitude control, ACESE

Dual-Laser Probe for Measuring Blade-Tip Clearance Tested

A dual-probe, integrated fiber-optic laser system for measuring blade tip clearance in rotating turbomachinery was developed cooperatively with Integrated Fiber Optic Systems, Inc., and tested at the NASA Lewis Research Center. Because the probes are nearly flush with the casing inner lining, there is minimal flow disturbance. The two probes are closely spaced in a circumferential plane and are slanted at an angle relative to each other so that the time it takes the blade tip to traverse the space between the two beams varies with the tip radius, making it possible to determine the tip clearance at rotor operating conditions. The tip clearance can be obtained for all the blades in a rotor with a single system, provided there are no synchronous vibrations present at a particular operating condition.

The two probes for the laser system were installed in two holders. For one, the included angle between the probes was 20°, and for the other, it was 40°. The two configurations were calibrated in a vacuum spin-rig facility that can reproduce realistic blade-tip speeds. A specially designed, nondeflecting rotor was used to calibrate the probes. This rotor consisted of a tapered titanium bar with three teeth on each end, the thickness of which was representative of a typical blade-tip thickness. The bar and measuring teeth were in a horizontal plane in the spin rig, and the axis of rotation was vertical. To set the clearances, we used a remotely controlled optical stage that could be traversed vertically.

The 40° probe system also was used to measure the tip clearance during an engine fan prototype test in a wind tunnel. Using the spin-rig calibrations, we estimated the accuracy of the tip-clearance measurement in the test to be 0.005 in. This program is ongoing.

Bibliography

Dhadwal, H.S.; and Kurkov, A.P.: Dual-Laser Probe Measurements of Blade-Tip Clearance. ASME Paper 98–GT–183, 1998.

Lewis contact:
Dr. Anatole P. Kurkov, (216) 433–5695, Anatole.P.Kurkov@grc.nasa.gov

Authors:
Dr. Harbans S. Dhadwal and
Dr. Anatole P. Kurkov

Headquarters program office: OAT

Program/Project: AST

Time-Shifted Boundary Conditions Used for Navier-Stokes Aeroelastic Solver

Under the Advanced Subsonic Technology (AST) Program, an aeroelastic analysis code (TURBO–AE) based on Navier-Stokes equations is currently under development at NASA Lewis Research Center's Machine Dynamics Branch. For a blade row, aeroelastic instability can occur in any of the possible interblade phase angles (IBPA's). Analyzing small IBPA's is very computationally expensive because a large number of blade passages must be simulated. To reduce the computational cost of these analyses, we used time-shifted, or phase-lagged, boundary conditions in the TURBO–AE code. These conditions can be used to reduce the computational domain to a single blade passage by requiring the boundary conditions across the passage to be lagged depending on the IBPA being analyzed. The time-shifted boundary conditions currently

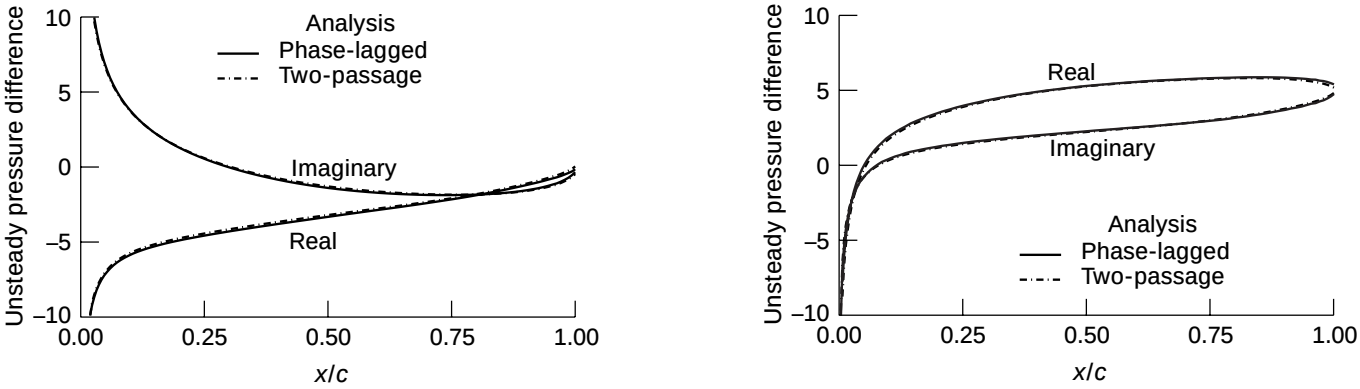

Comparison of the unsteady pressure difference variation at midspan for 180^{O} IBPA oscillations; distance along chord from leading edge, x; chord, c. Left: Pitching. Right: Plunging.

implemented are based on the direct-store method. This method requires large amounts of data to be stored over a period of the oscillation cycle. On CRAY computers this is not a major problem because solid-state devices can be used for fast input and output to read and write the data onto a disk instead of storing it in core memory.

In aeroelastic analyses using TURBO–AE, the unsteady aerodynamic loads are obtained by solving the Reynolds-averaged Navier-Stokes equations. The aerodynamic equations are solved via a finite volume scheme. Flux vector splitting is used to evaluate the flux Jacobians on the left side, and a higher order Total Variation Diminishing (TVD) scheme based on Roe's flux vector splitting is used to discretize the fluxes on the right side. Newton subiterations are used at each time step to maintain higher accuracy. Then, symmetric Gauss-Sidel iterations are applied to the discretized equations, and a dynamic grid deformation technique is used to simulate the blade motions. TURBO–AE updates the grid at each time step by recalculating it using linear interpolation and by assuming the far field to be fixed. It determines the aeroelastic characteristics of the blade row by calculating the energy exchange between the vibrating blade and its surrounding fluid for all possible frequencies and IBPA's of interest. Positive work on the blade indicates instability.

To verify and validate the time-shifted analysis, we used a flat-plate, helical-fan geometry. The helical fan consisted of 24 flat-plate blades with zero thickness. The inflow conditions and stagger angle were set to induce an inflow with a relative Mach number of 0.7 at an incidence of zero at the midspan. The results were obtained for several IBPA's and compared with those of the analysis using multiple blade passages. Only a few typical results are shown here; for more detail please refer to the reference. The graphs on the preceeding page show the unsteady pressure difference for the 180° IBPA pitching and plunging cases. The time-shifted results were compared with results from a two-passage analysis. A very good comparison was obtained in both cases, indicating that the time-shifted boundary condition was properly implemented and reproduced the results of the multiple-passage analysis.

In the graph on the left, the rate of convergence for the time-shifted analysis for –90° IBPA pitching is compared with that of the multiple-passage analysis. From this figure, it can be seen that the work-per-cycle for the four-passage analysis converged within four to five oscillation cycles, whereas roughly seven to eight cycles were required for the time-shifted analysis. Even though approximately 40-percent more cycles were required for convergence, the computational time was reduced by almost 60 percent. This is because only one blade passage was needed in the time-shifted analysis. We also found that the convergence rate for the time-shifted analysis was independent of the IBPA analyzed (see the graph on the right).

Bibliography

Srivastava, R., et al.: Application of Time-Shifted Boundary Conditions to a 3D Euler/Navier-Stokes Aeroelastic Code. ASME Paper 98–GT–42, 1998.

Lewis contacts:
Rakesh Srivastava, (216) 433–6045, Rakesh.Srivastava@grc.nasa.gov; Milind A. Bakhle, (216) 433–6037, Milind.A.Bakhle@grc.nasa.gov; and George L. Stefko (216) 433–3920, George.L.Stefko@grc.nasa.gov

Author: Rakesh Srivastava

Headquarters program office: OAT

Program/Project: AST, TURBO–AE

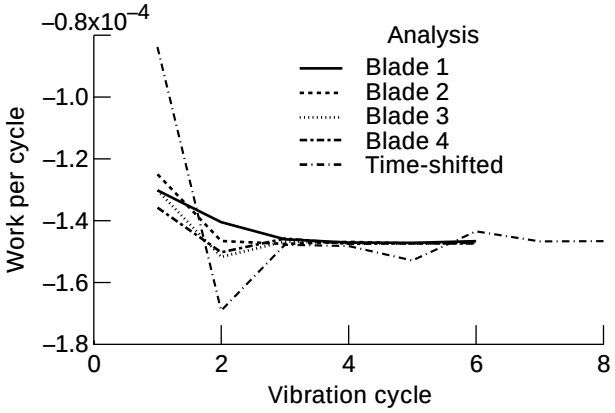

Comparison of the work-per-cycle convergence for a time-shifted analysis with multiple passages.

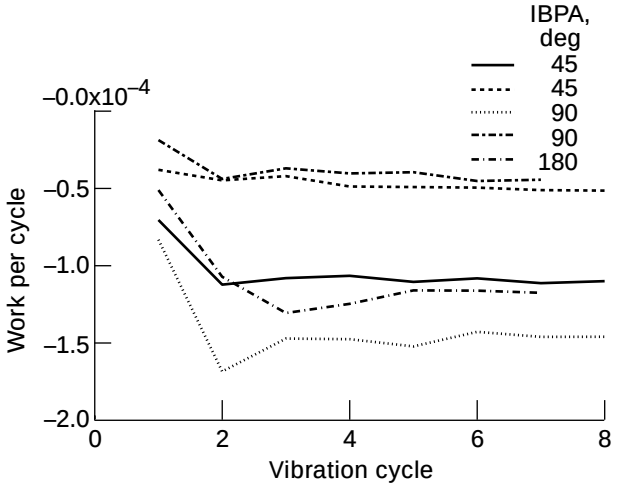

Comparison of the work-per-cycle convergence history for various interblade-phase-angle pitching oscillations.

Low-Noise Potential of Advanced Fan Stage Stator Vane Designs Verified in NASA Lewis Wind Tunnel Test

NASA/Allison Engine Company Low Noise Fan test in Lewis' 9- by 15-Foot Low-Speed Wind Tunnel.

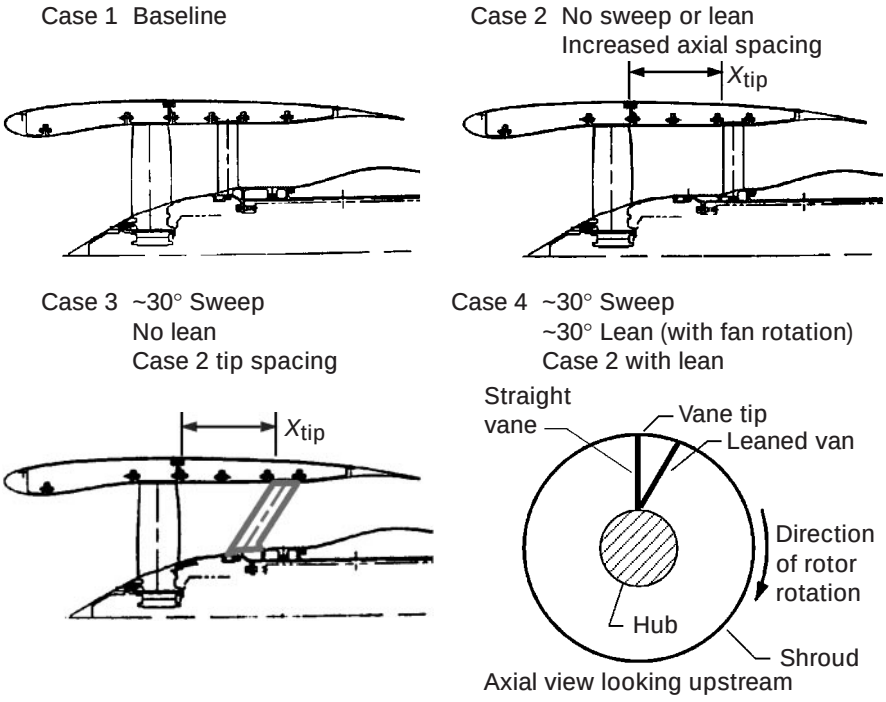

NASA/Allison Low Noise Fan test; stator vane sweep and lean.

With the advent of new, more stringent noise regulations in the next century, aircraft engine manufacturers are investigating new technologies to make the current generation of aircraft engines as well as the next generation of advanced engines quieter without sacrificing operating performance. A current NASA initiative called the Advanced Subsonic Technology (AST) Program has set as a goal a 6–EPNdB (effective perceived noise) reduction in aircraft engine noise relative to 1992 technology levels by the year 2000. As part of this noise program, and in cooperation with the Allison Engine Company, an advanced, low-noise, high-bypass-ratio fan stage design and several advanced technology stator vane designs were recently tested in NASA Lewis Research Center's 9- by 15-Foot Low-Speed Wind Tunnel (an anechoic facility). The project was called the NASA/Allison Low Noise Fan (see the figures).

A bypass fan stage consists of a fan and a stator vane assembly. The advanced technology bypass fan stage for this project was 22 in. in diameter and consisted of a low-pressure ratio, 18-bladed fan and an integral, 42-bladed stator vane assembly. The testing used an air turbine propulsion simulator to power the model fan stage across a wide range of operating conditions from idle to full takeoff power at a wind tunnel velocity of Mach 0.10, or about 67 knots. The main objective of the project was to evaluate the noise reduction potential of a series of advanced stator vane designs. Variations in stator vane geometry that were introduced include increasing the spacing between the fan and the stator vanes, incorporating sweep into

the stator vanes (similar to aircraft wing sweep), and finally leaning the swept stator vanes over in the fan direction of rotation. During testing, the acoustic characteristics of each fan and stator vane assembly combination were measured using fixed and traversing microphones inside the wind tunnel. The aerodynamic performance of each fan/stator vane combination was also measured using pressure/temperature rakes and force balances to determine what effect the new low-noise stator vanes would have on the fan stage efficiency.

The research results generated as part of this project allowed a major interim milestone, to demonstrate a 3–EPNdB reduction in noise by 1997**,** to be reached for the Advanced Subsonic Technology Program. Test results will be used to create a data base that engineers can draw upon for comparison with computer predictions of the effect of fan stage geometry on aircraft engine noise. In addition, aircraft manufacturers will be able to use these results to influence the design of the next generation of advanced technology aircraft engines or the next growth version of current technology engines.

Lewis contacts: Christopher E. Hughes, (216) 433–3924, Christopher.E.Hughes@grc.nasa.gov; and Richard P. Woodward, (216) 433–3923, Richard.P.Woodward@grc.nasa.gov

Author: Christopher E. Hughes

Headquarters program office: OAT

Programs/Projects:
AST (Noise Reduction Element)

NASA Space Mechanisms Handbook—Lessons Learned Documented

The need to improve space mechanism reliability is underscored by a long history of flight failures and anomalies caused by malfunctioning mechanisms on spacecraft and launch vehicles. Some examples of these failures are listed in the table. Mechanism anomalies continue to occur and to be a cause of catastrophic mission failures. Several factors cause problems for space system mechanisms. The space environment produces wide temperature ranges, thermal gradients, and rapid changes in temperature, which can bind the moving parts of mechanisms. Ultraviolet radiation and vacuum cause the properties of many materials to degrade to unacceptable levels or to behave differently in space than on Earth, making it difficult to simulate operation during ground tests. The lack of gravity in space causes mechanisms to operate differently than on the ground. Sometimes the effects of zero gravity can be simulated to some degree in ground testing, such as by offloading the weight of a deployable appendage. Other effects, such as lubricant migration, cannot be simulated and must be considered in the design. Finally, the launch environment imposes severe dynamic loads on mechanisms and can cause structural damage, loosen fasteners, and damage delicate surfaces.

Given these complexities, it is not surprising that it is not always possible to uncover and correct all the hidden problems with mechanisms prior to launch. Fortunately, there are ways to reduce the number of failures involving mechanisms and/or mitigate the effects of a failure of a component. In many cases, failures were caused by design problems that have caused similar failures in the past, and thus could have been avoided had the designers been aware of the past mistakes. Because much experience has been gained over the years, many specialized design practices have evolved and many unsatisfactory design approaches have been identified. In many cases, however, this knowledge has remained with the individual mechanism designer and has not been widely shared.

To alleviate this situation, NASA and the NASA Lewis Research Center conducted a Lessons Learned Study (refs. 1 and 2) and wrote a handbook to document what has been learned in the past. The primary goals of the handbook were to identify desirable and undesirable design practices for space mechanisms and to reduce the number of failures caused by the repetition of past design errors. Another goal was to identify a variety of design approaches for specific applications and to provide the associated considerations and caveats for each approach in an effort to help designers choose the approach most suitable for each application. The handbook also provides some design principles. These principles, which can be applied to any mechanism to avoid common failure modes, can be particularly useful for the esoteric mechanism configurations that

SUMMARY OF SPACECRAFT MECHANISM FAILURES

Program	Date	Problem	Cause
Program 461	1964	Solar array failed to deploy fully	Mishandling during stowage
STP 67–2 (OV2–5)	1968	Solar array booms failed to deploy fully	Field modification problem
777	1970	Omni antenna latch broke during spin-up	Attitude control instability
Program A	1971	Antenna failed to deploy fully	Wire harness binding
Program B	1971	Solar array deployed late	Silicon rubber sticking
STP 71–5	1972	Boom failed to deploy	Dynamic clearance problem
Skylab	1973	Solar array failed to deploy	Interference with cabling or thermal blankets
Transit	1975	Solar array failed to deploy fully; cable hung up	Anomalous flat trajectory caused high heating rates
Viking	1975	Sampling arm failed to deploy	Debris in gear train
STP 74–1 (Solrad)	1976	Solar panel failed to deploy	Release mechanism binding
DMSP F–1	1976	Solar array failed to deploy fully	Excessive wire harness stiffness
DMSP F–2	1977	Solar array delayed release	Friction welding
		Science boom failed to deploy fully	Microswitch failed
Voyager	1977	Science boom failed to deploy fully	Microswitch failed
		Scan platform gearbox seized	Lubricant failed
		Magnetometer boom misaligned	Unknown
Seasat	1978	Spacecraft power failed	Slip ring debris between power and ground rings
Apple	1981	Solar array failed to deploy	Failure of deployment device
DE	1981	Sensing antenna failed to deploy	Unknown
Insat 1	1982	Solar sail failed to deploy	Unknown
ERBS	1982	Solar array failed to deploy	Unknown
GLOMR	1985	Spacecraft failed to separate from orbiter	Canister door did not open fully
VUE	1988	Telescope failed to rotate about azimuth	Inadequate torque margin on azimuth caging arm
Galileo	1989	High-gain antenna failed to deploy	Cold welding in ball and socket joint
		Instrument cover jettisoned late	Thermal binding
Magellan	1989	Solar array failed to latch at end of travel	Microswitch misadjusted
Macsat	1990	Gravity gradient boom failed to deploy	Inadequate force margin
CRRES	1990	Magnetometer boom failed to orient fully	Interference between thermal blanket Velcro and wiring harness
Ulysses	1990	Spin-stabilized spacecraft wobbled	Antenna boom thermal distortion caused spacecraft center-of-gravity offset
Hubble	1990	Solar array booms jittered as telescope went between sun and shade	Thermal gradient across boom diameter
ANIK E2	1991	C-band antenna failed to fully deploy	Thermal blanket interference
Unknown		Sampling arm failed to deploy	Screw backed out and wedged against housing
Tether Satellite System	1993	Reel-out mechanism jammed	Screw added for structural margin interfered with reel-out mechanism
GOES 10	1997	Solar Array Drive malfunctioned	Under investigation

dwell on topics that are not unique to space applications, it does cite references, where appropriate, for additional information or more indepth discussion of specific topics.

The handbook is divided into six parts. Part I, *Introduction to Space Mechanisms*, starts with an overview of various types of spacecraft mechanisms. It then discusses the requirements that are typically imposed on space mechanisms, their implications, and what steps can be taken to ensure that the requirements are met. The discussion concludes with a description of a typical mechanism design process and addresses how the design evolves from concept to fabrication. Part II, *Design Considerations for Space Mechanisms*, provides guidelines for recommended design practices for most spacecraft mechanisms. It also contains subsequent chapters that are devoted to guidelines applicable to specific types of mechanisms. Part III, *Space Mechanism Components*, proceeds to the next level of detail and discusses design considerations for mechanisms. This part is divided into general design guidelines that are applicable to the various components of spacecraft mechanisms. Part IV delves into two areas of testing, environmental testing and tribological testing of space mechanisms. Part V lists expert areas and the names and addresses of individuals who are experts in those areas of testing. Finally, Part VI lists testing laboratories and the individuals involved in the testing programs.

We anticipate that this handbook will be useful to a variety of readers. By studying the numerous guidelines presented in this handbook, entry-level design engineers will be able to quickly gather practical information on how to avoid common pitfalls. Experienced mechanical design engineers who are new to space mechanism applications will benefit from learning the unique requirements created by the space and launch environments. Also, users who need to evaluate their suppliers' products, but have little personal experience in the design of mechanisms, can find useful information on identifying key performance, risk, and cost drivers for most space mechanisms and components. The Space Mechanisms Handbook is available from Lewis' Mechanical Components Branch.

References

1. Shapiro, W., et al.: Space Mechanisms Lessons Learned Study, Volume I—Summary. NASA TM–107046, 1995.
2. Shapiro, W., et al.: Space Mechanisms Lessons Learned Study, Volume II—Literature Review. NASA TM–107047, 1995.

Lewis contact:
Robert L. Fusaro, (216) 433–6080, Robert.L.Fusaro@grc.nasa.gov

Author: Robert L. Fusaro

Headquarters program office:
OA (Chief Engineer)

Programs/Projects:
Safety and Mission Assurance

Metrology Evaluation of Superfinished Gears Completed

Gears, bearings, and similar mechanical elements transmit loads through the surfaces that are in contact with one another. Thus, the fatigue lives of gears can be improved by providing smoother tooth surfaces. At the NASA Lewis Research Center, we completed a metrology evaluation of one method for making gears with a highly polished, mirrorlike surface (see the following photo). The polished gears were measured carefully. The measurement data showed that the polishing process did, indeed, reduce the surface roughness but did not change the overall tooth shape in any harmful way.

Highly polished surface of superfinished gears.

This work was done as a partnership of NASA, the U.S. Army, and the University of Wales. NASA provided conventionally ground gear specimens and has begun testing to determine the fatigue lives of the superfinished gears. Under contract, the University of Wales superfinished the gears and inspected them before and after the superfinishing operation. The U.S. Army European Research Office provided the funds and procured the contract with the University of Wales.

For gears, the rate of fatigue is greatly affected by the ratio of the oil film thickness to the roughness of the contacting surfaces. In this work we are seeking to improve fatigue lives by reducing the surface roughness. Conventionally ground, aerospace quality gears were manufactured, and their geometry was inspected. Next, the gears were superfinished by placing them in a vibrating bath consisting of water, detergent, abrasive powder, and small pieces of zinc. Upon removal from the bath, the surfaces were highly polished (see the preceding photo). The gears were then again inspected, and the measurements of the gears before and after the superfinishing operation were compared. Typical inspection data are provided in the plots on the following page. The grinding marks are clearly evident in the figure on the left. Superfinishing removed the peaks of the grinding marks and left a much smoother surface

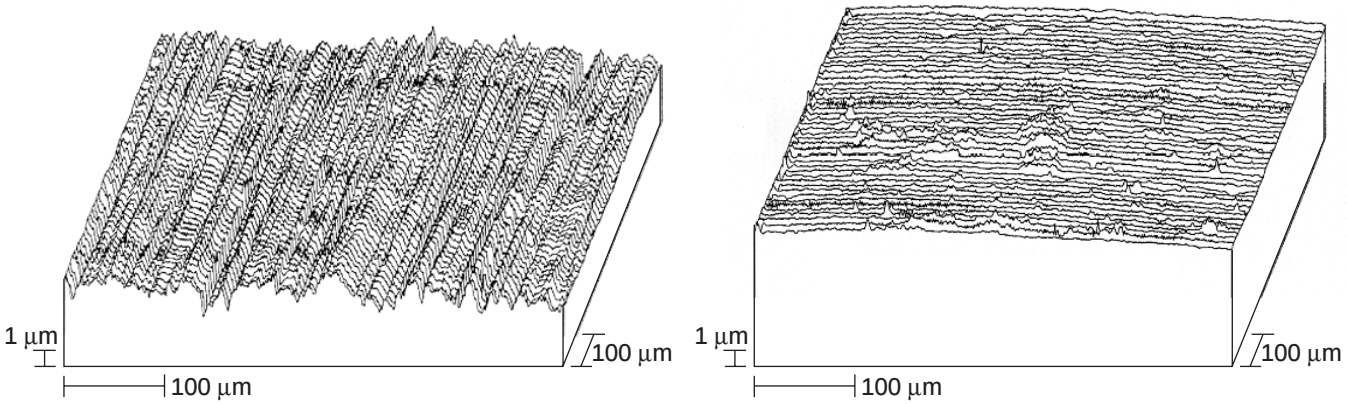

Profile of tooth surfaces. Left: Ground. Right: Superfinished.

as is evident in the figure on the right. Profile and spacing checks proved that the overall gear tooth shape was not affected in any harmful way. Superfinishing uniformly removed approximately 2.5 μm from each surface. See reference 1 for a complete report.

Reference

1. Snidle, R.W.; Evans, H.P.; and Alanou, M.P.: The Effect of Superfinishing on Gear Tooth Profile. Report AD–A327916, June 1997. (Available from the Defense Technical Information Center (DTIC) (http://www.dtic.mil/) or the National Technical Information Service (NTIS) (http://www.ntis.gov/), or the Center for AeroSpace Information (http://www.sti.nasa.gov/rselect/FAQ.html#docorder).

Lewis contact:
Timothy L. Krantz, (216) 433–3580, Timothy.L.Krantz@grc.nasa.gov

Author: Timothy L. Krantz

Headquarters program office: OAT

Programs/Projects:
Rotorcraft Base Program

Three-Dimensional Gear Crack Propagation Studied

Gears used in current helicopters and turboprops are designed for light weight, high margins of safety, and high reliability. However, unexpected gear failures may occur even with adequate tooth design. To design an extremely safe system, the designer must ask and address the question, “What happens when a failure occurs?” With gear-tooth bending fatigue, tooth or rim fractures may occur. A crack that propagates through a rim will be catastrophic, leading to disengagement of the rotor or propeller, loss of an aircraft, and possible fatalities. This failure mode should be avoided. A crack that propagates through a tooth may or may not be catastrophic, depending on the design and operating conditions. Also, early warning of this failure mode may be possible because of advances in modern diagnostic systems.

One concept proposed to address bending fatigue fracture from a safety aspect is a split-tooth gear design (ref. 1). The prime objective of this design would be to control crack propagation in a desired direction such that at least half of the tooth would remain operational should a bending failure occur. A study at the NASA Lewis Research Center analytically validated the crack-propagation failsafe characteristics of a split-tooth gear (ref. 2). It used a specially developed three-dimensional crack analysis program that was based on boundary element modeling and principles of linear elastic fracture mechanics. Crack shapes as well as the crack-propagation life were predicted on the basis of the calculated stress intensity factors, mixed-mode crack-propagation trajectory theories, and fatigue crack-growth theories.

The following figures show the effect of the location of initial cracks on crack propagation. Initial cracks in the fillet of the teeth produced stress intensity factors of greater magnitude (and thus, greater crack growth rates) than those in the root or groove areas of the teeth. Crack growth was simulated in a case study to evaluate crack-propagation paths (see the final figure). Tooth fracture was

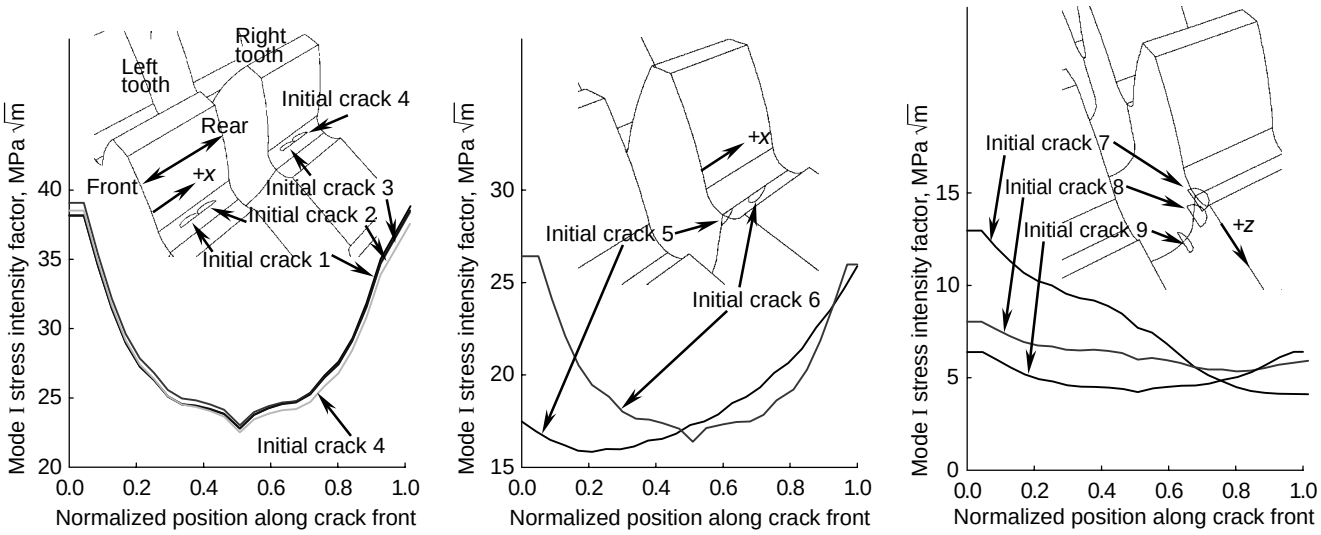

Effect of initial crack location on mode I stress intensity factors. Left: Tooth fillet locations. Center: Tooth foot locations. Right: Tooth groove locations.

predicted from the crack-growth simulation for an initial crack in the tooth fillet region. This was the desired failure mode for an ultrasafe design. Lastly, tooth loads on the uncracked mesh of the split-tooth design were up to five times greater than those on the cracked mesh if equal deflections of the cracked and uncracked teeth were considered. This effect needs to be considered in the design of a split-tooth configuration.

This work was done in-house at Lewis in support of the National Rotorcraft Technology Center project, Ultra-Safe Gear Design, with the Boeing Defense and Space Group. The crack-propagation package was developed by the Cornell Fracture Group at Cornell University. The reported results, which are the initial findings of Lewis' gear-crack-propagation research for the Rotorcraft Base Program, will be further investigated to develop generalized gear design guidelines.

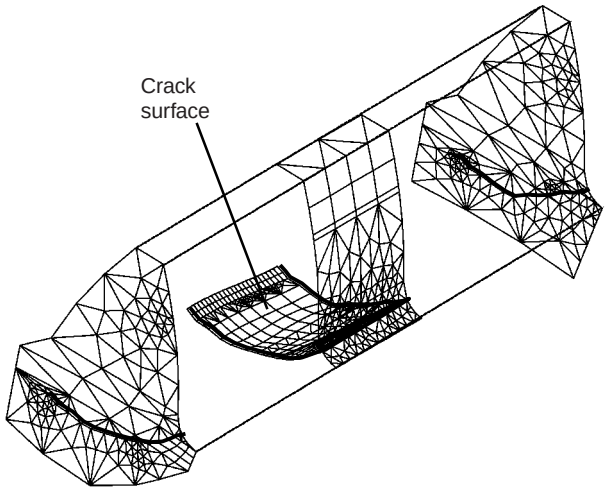

Exploded gear tooth view of predicted crack growth after 15 steps.

References

1. Drago, R.J.; Sane, A.D.; and Brown, F.W.: UltraSafe Gear Systems for Critical Applications—Initial Development. AGMA TP–97FTM10, 1997.
2. Lewicki, D.G., et al.: Three-Dimensional Gear Crack Propagation Studies. NASA TM—1999-208827, 1999.

Lewis contact:
Dr. David G. Lewicki, (216) 433–3970, David.G.Lewicki@grc.nasa.gov

Author: Dr. David G. Lewicki

Headquarters program office: OAT

Programs/Projects:
Rotorcraft Base Program

NASA Lewis Thermal Barrier Feasibility Investigated for Use in Space Shuttle Solid-Rocket Motor Nozzle-to-Case Joints

Assembly joints of modern solid-rocket motor cases are usually sealed with conventional O-ring seals. The 5500 °F combustion gases produced by rocket motors are kept a safe distance away from the seals by thick layers of insulation and by special compounds that fill assembly splitlines in the insulation. On limited occasions, NASA has observed charring of the primary O-rings of the space shuttle solid-rocket nozzle-assembly joints due to parasitic leakage paths opening up in the gap-fill compounds during rocket operation. Thus, solid-rocket motor manufacturer Thiokol approached the NASA Lewis Research Center about the possibility of applying Lewis' braided-fiber preform seal as a thermal barrier to protect the O-ring seals. This thermal barrier would be placed upstream of the primary O-rings in the nozzle-to-case joints to prevent hot gases from impinging on the O-ring seals (see the following illustration). The illustration also shows joints 1 through 5, which are potential sites where the thermal barrier could be used.

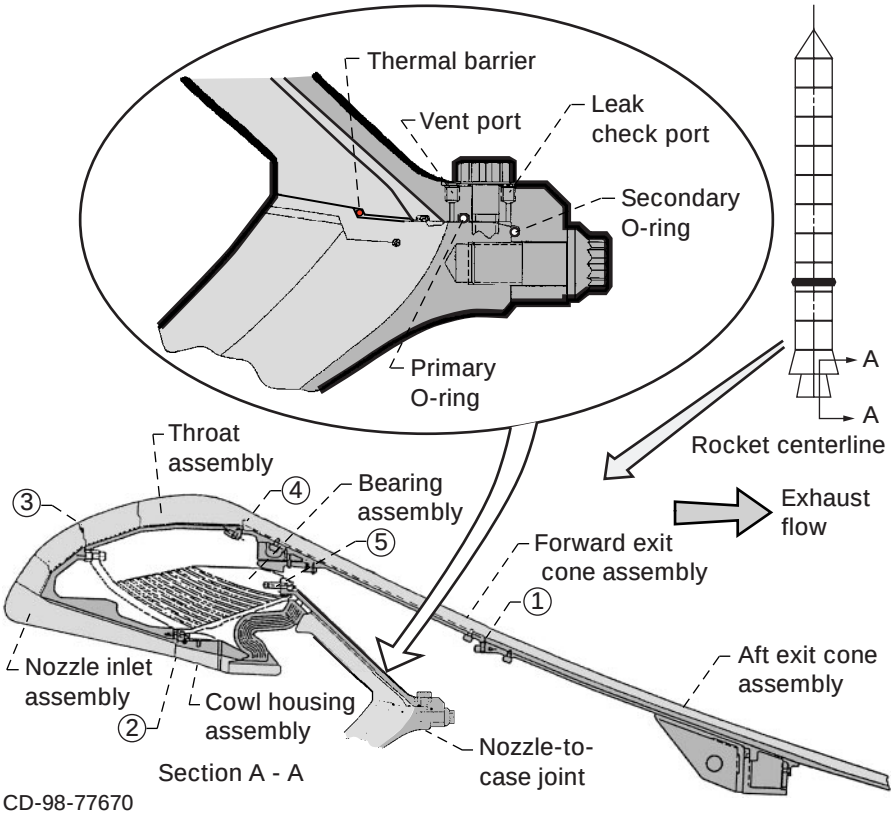

Potential shuttle solid-rocket motor joint locations (circled numbers) for candidate thermal barrier. Top: Enlarged view of nozzle-to-case joint showing primary and secondary pressure O-rings, leak-check part, and proposed thermal barrier location. Bottom: Overall nozzle cross section (half view).

Burn tests at temperatures representative of the rocket thermal environment were used to evaluate the thermal resistance of braided rope thermal barriers made of different materials. Thermal barriers were placed in the hottest part of the flame of an oxyacetylene torch at 5500 °F, and the amount of time to completely cut through them was measured. A 0.125-in.-diameter stainless steel rod was cut through in 5 sec, whereas 0.125-in.-diameter thermal barriers of braided ceramic and superalloy materials lasted less than 15 sec. In contrast, 0.125-in.-diameter thermal barriers of braided carbon fibers lasted over 2 min. Carbon-fiber thermal barriers with diameters of 0.200 and 0.260 in. lasted over 6.5 and 8.5 min., respectively, before they were cut through (see the photo on the following page). As a point of reference, the solid-rocket motors of the space shuttle only burn for 2 and 4 sec, much shorter than the burn-through times of the carbon-fiber thermal barriers. On the basis of these results, the decision was made to use carbon fibers to braid the thermal barriers.

Flow tests performed on the thermal barriers showed that they blocked hot gas flow but were permeable enough to allow leak checks of the primary/secondary O-ring system. The barriers also were resilient enough to accommodate flange movements in the solid-rocket motor. To simulate a rocket environment, Thiokol performed subscale rocket "char" motor tests in which the thermal barrier was subjected to hot gases that flowed through an intentional 0.060-in. circumferential gap defect both upstream and downstream of

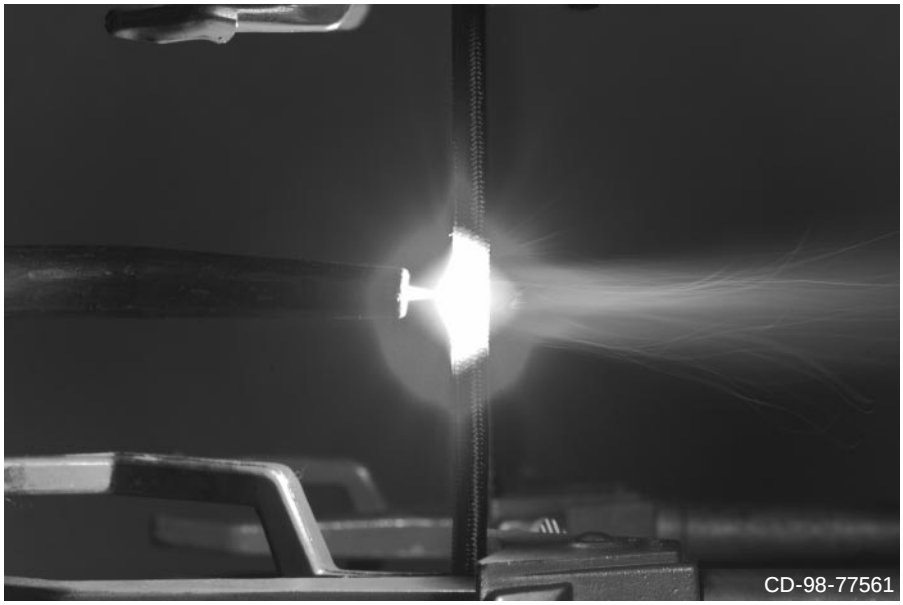

Candidate thermal barrier (0.2-in. diameter) for shuttle solid-rocket motor in 5500 °F oxyacetylene burn test. Time for burn through, 6.5 min.

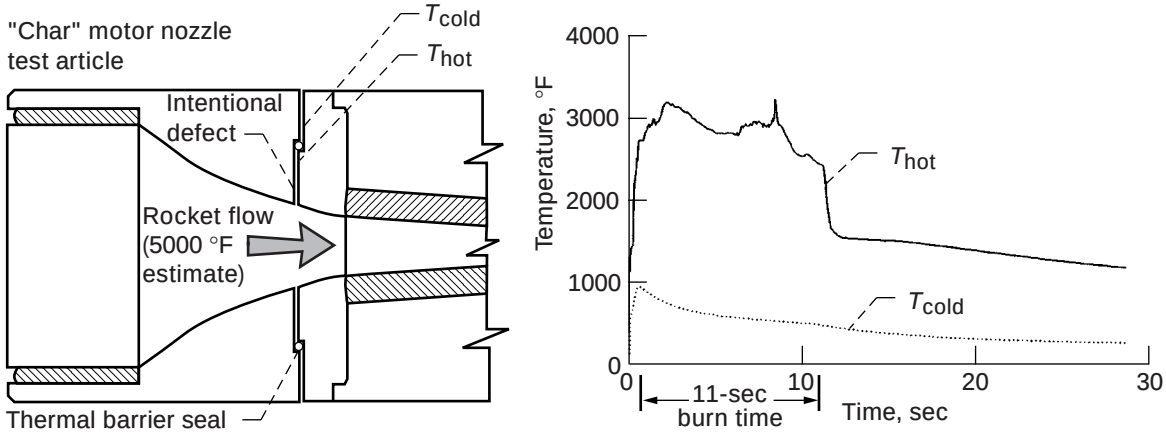

Preliminary subscale (70-lbf thrust) "char" motor tests examining thermal barrier effectiveness. Left: Test configuration: thermal barrier (0.125-in. diameter) filling an intentional joint defect. Right: Temperature data: upstream (T_{hot}) and downstream (T_{cold}) sides of thermal barrier. (Copyright Thiokol Corp.; used with permission.)

the thermal barrier. During the 11-sec rocket firing, temperatures over 3200 °F were measured on the hot side of the 0.260-in.-diameter thermal barrier, whereas temperatures on the cold side were about 950 °F, for a temperature drop of over 2200 °F across the thermal barrier (see the graphs).

On the basis of these results, additional mechanical and thermal testing is planned at Lewis to help further characterize the thermal barrier. Thiokol is planning to test the thermal barrier in a subscale solid-rocket motor, where it would be installed first in its undamaged state and then with an intentional defect (Spring and Fall 1999). If all planned tests show success, the Lewis-developed thermal barrier would be prepared for Full Scale RSRM static tests in November 2000 (no-joint defect) and May 2002 (with joint defect); it would be subsequently qualified for flight.

Find out more on the World Wide Web:
http://www.grc.nasa.gov/WWW/TU/InventYr/1996Inv_Yr.htm

Bibliography

Steinetz, B.M.; and Dunlap, P.H.: Feasibility Assessment of Thermal Barrier Seals for Extreme Transient Temperatures. AIAA Paper 98-3288 (NASA TM—1998-208484) 1998.

Lewis contact:
Dr. Bruce M. Steinetz, (216) 433–3302, Bruce.M.Steinetz@grc.nasa.gov

Modern Technologies Corp. contact:
Patrick H. Dunlap, Jr., (216) 433–6374, Patrick.H.Dunlap@grc.nasa.gov

Authors:
Dr. Bruce M. Steinetz and
Patrick H. Dunlap, Jr.

Headquarters program office: OAT

Programs/Projects: HITEMP,
High Temperature Seal Development

Special recognition: 1996 NASA Invention of the Year awarded to the fiber preform seal, precursor to the thermal barrier seal

Space

Space Communications

Advanced Communications Technology Satellite Now Operating in an Inclined Orbit

The Advanced Communications Technology Satellite (ACTS) system has been modified to support operation in an inclined orbit that is virtually transparent to users, and plans are to continue this final phase of its operation through September 2000. The next 2 years of ACTS will provide a new opportunity for using the technologies that this system brought online over 5 years ago and that are still being used to resolve the technical issues that face NASA and the satellite industry in the area of seamless networking and interoperability with terrestrial systems.

New goals for ACTS have been defined that align the program with recent changes in NASA and industry. ACTS will be used as a testbed to

(1) Show how NASA and other Government agencies can use commercial systems for future support of their operations

(2) Test, characterize, and resolve technical issues in using advanced communications protocols such as asynchronous transfer mode (ATM) and transmission control protocol/Internet protocol (TCP/IP) over long latency links as found when interoperating satellites with terrestrial systems

(3) Evaluate narrow-spot-beam Ka-band satellite operation in an inclined orbit

(4) Verify Ka-band satellite technologies since no other Ka-band system is yet available in the United States

On July 9, 1998, the final north/south stationkeeping was performed on ACTS. Inclined-orbit operations technically began when the spacecraft left its original north/south limits of $\pm 0.05°$ on August 8, 1998. The spacecraft will be maintained at 100° W longitude throughout the remaining life of the program. At the program's completion, a final sequence of burns will superorbit the satellite into a higher orbit where the payload and spacecraft will be shut down.

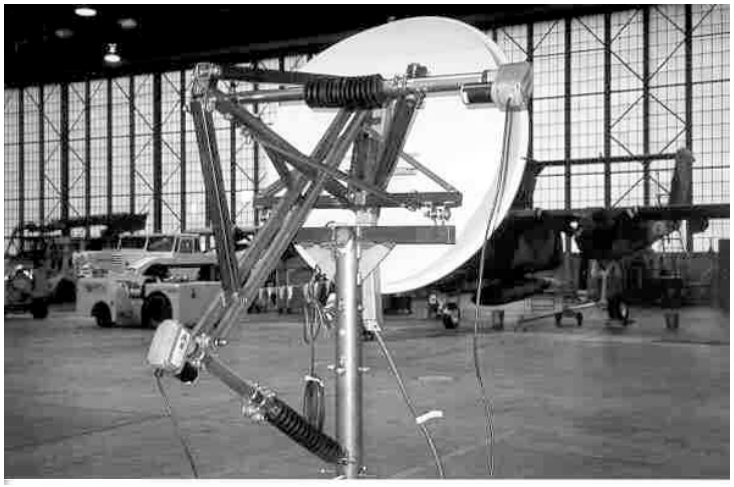

Tracking modifications to a 1.2-m T1VSAT.

Preparation for inclined-orbit operations involved reviewing all aspects of the communications link that could be affected by the spacecraft no longer being stationary. Changes were made to onboard software and operations procedures to maintain the pointing accuracy of the narrow 0.3° spot beams so that the coverage pattern would not change. With the spacecraft increasing in north/south drift by 0.78° per year, inclined-orbit operations will be limited to about 2.5 years, or 30 months.

The ground segment was modified in-house at the NASA Lewis Research Center to track the satellite. The four major components modified with tracking hardware were the T1VSAT's,[a] Gigabit Earth Stations, USAT's,[b] and the Link Evaluation Terminal. The Master Ground Station at Lewis was originally designed with a tracking system for its 5.5-m antenna, so no further modifications were needed.

Inclined-orbit operations offer the ACTS program a final opportunity to affect the design of the next generation of communications satellites. To encourage new experiments and announce the ongoing opportunity to use ACTS, Lewis

[a]T1 Very Small Aperture Terminal—an Earth station that operates at the telephony standard data rate of T1 or 1.544 Mbps and uses a 1.2-m-diameter reflector.
[b]Ultra Small Aperture Terminal—a small Earth station that uses a 0.6-m-diameter reflector and supports data rates of up to T1 for transmissions while receiving at up to 40 Mbps.

released an experiment opportunity guide (http://kronos.grc.nasa.gov/acts/eoa/guide.html) in March 1998.

A set of in-house technical experiments is planned as the core set of experiments for operations. Other experiments hosted by Lewis' Space Communications Program include "High Data Rate Interoperability," "Internet Protocol Performance and Coding Effects," "Hybrid Networking Using Digital Imaging and Communications in Medicine (DICOM)/Telemammography," and "Advanced Air Transportation Technology." Experiments are currently planned by the Air Force Research Laboratory (Rome Labs), Carnegie Mellon University, Lockheed Martin Western Development Laboratory, Savannah State University, and Intelsat. Over 20 organizations have expressed interest in using ACTS during inclined-orbit operations, including the Boeing Company, Southwest Research Institute, Texas Medical Center, and the Naval Research Laboratory. The next 2 years hold promise for new experiment plans as ACTS continues to be an important resource for resolving issues in satellite communications.

Find out more about this research on the World Wide Web:
http://acts.grc.nasa.gov

Lewis contact:
Robert A. Bauer, (216) 433–3431, Robert.A.Bauer@grc.nasa.gov

Author: Robert A. Bauer

Headquarters program office: OSF

Programs/Projects:
ACTS, SOMO, NII/GII, CSOC

Microgravity Science

DARTFire Sees Microgravity Fires in a New Light—Large Data Base of Images Obtained

The recently completed DARTFire sounding rocket microgravity combustion experiment launched a new era in the imaging of flames in microgravity. DARTFire stands for "Diffusive and Radiative Transport in Fires," which perfectly describes the two primary variables—diffusive flow and radiation effects—that were studied in the four launches of this program (June 1996 to September 1997). During each launch, two experiments, which were conducted simultaneously during the 6 min of microgravity, obtained results as the rocket briefly exited the Earth's atmosphere.

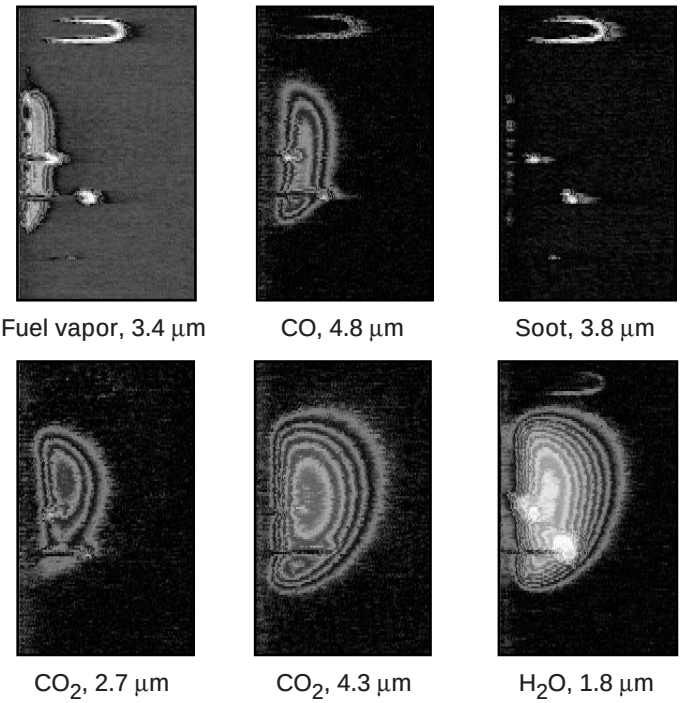

Filtered infrared multispectral images of a microgravity flame were obtained during a DARTFire sounding rocket experiment. This figure is shown in color in the online version of this article (http://www.grc.nasa.gov/www/RT1998/6000/6711olson.htm)

Within the rocket, mirror-image flow tunnels supported low-speed oxidizer flow through each tunnel. An infrared laser diode was mounted in the ceiling of one of the two tunnels to provide external radiant heating onto the black polymethyl-methacrylate (PMMA, an acrylic plastic) fuel surface. Controlled external radiant heating compensated for inherent heat losses such as those from surface radiation. The walls of the tunnels had windows for ultraviolet-visible and infrared imaging of the flame. DARTFire was the first combustion experiment to image flames in these wavelengths, producing unique images of microgravity flames as they have never been seen before.

Infrared emissions from the gaseous combustion products were monitored in real time during the DARTFire experiment. An infrared camera was modified to include an internal rotating filter wheel that holds six different filters so that it can look at radiant emissions from six different infrared bands as the filter wheel rotates in front of the camera. The images in the preceding figure were obtained simultaneously with six different infrared filters, including a fuel vapor image, a carbon monoxide (CO) image, a soot image, two different wavelengths of carbon dioxide (CO_2), and a water vapor (H_2O) image. This infrared imaging provided immense quantities of data regarding the species fields in the experiment. A blackbody calibration of each filter provided effective blackbody temperature distributions for each image, and numerical predictions of the temperature and species fields were used to calculate the radiation distribution. The radiation distribution could then be compared directly with these calibrated images to test our understanding of the experiment.

A multispectral intensified array video camera was also used to image the flame in the ultraviolet and visible wavelength ranges. As with the infrared camera, six filters were used to obtain intensified images of the dim flames in different wavelengths, as shown in the following figure. Color images were obtained by combining red, green, and blue filtered images to obtain a 24-bit RGB color composite image of the flame. So that the combustion intermediate (free radical) species could be imaged directly, filters were used to capture the ultraviolet chemiluminescence of the methyl (CH*) and hydroxyl (OH*) excited-state free radicals in the reaction zone of the flames. The color images are what astronauts would see with their eyes.

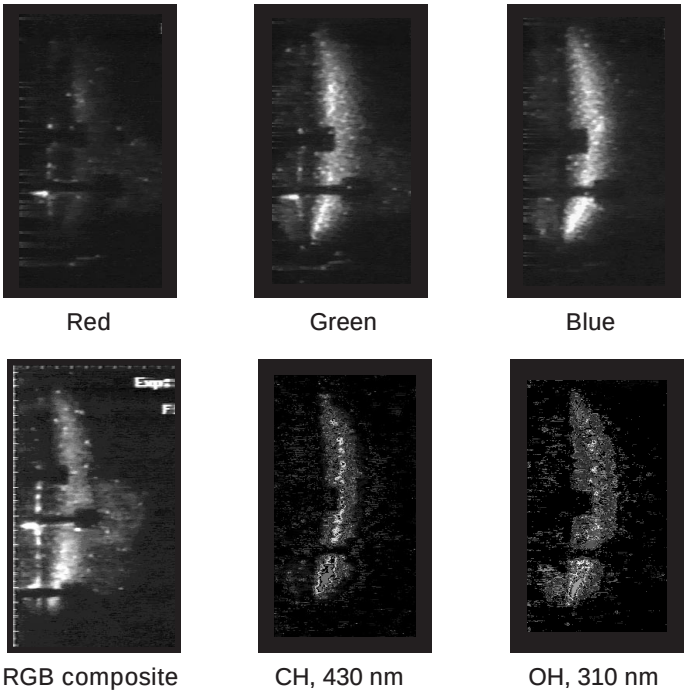

Ultraviolet and visible light (intensified) multispectral images of a microgravity flame obtained during a DARTFire sounding rocket experiment. This figure is shown in color in the online version of this article (http://www.grc.nasa.gov/WWW/RT1998/6000/6711olson.htm).

The size, shape, and color of the visible flame can be compared with the large normal-gravity flame data base. The chemilumiscent images allow an extended view into the heart of the reaction zone, where detailed chemistry models of the combustion process are sorely lacking experimental data.

The DARTFire experiment provided the first comprehensive spectral imaging of microgravity combustion flames. The effects of the flow and external radiant heating on the flame are well captured by this nonintrusive imaging. This large data base of information is a wealth of information for researchers interested in the spectral emissions of microgravity flames. The DARTFire hardware was built by the NASA Lewis Research Center, and the image analysis was supported by Lewis' Graphics Visualization Laboratory.

Find out more on the World Wide Web: http://zeta.grc.nasa.gov/expr3/combust.htm

Bibliography

Olson, S.L., et al.: Diffusive and Radiative Transport in Fires Experiment: DARTFire. Proceedings of the Fourth International Microgravity Combustion Workshop. NASA CP–10194, 1997.

Lewis contact:
Sandra L. Olson, (216) 433–2859, Sandra.L.Olson@grc.nasa.gov

Authors:
Sandra.L. Olson, Uday Hegde, Robert A. Altenkirch, and Subrata Bhatacharjee

Headquarters program office: OLMSA

Programs/Projects: Microgravity Combustion Science, DARTFire

Special recognition:
Special Act and Service Awards presented to the DARTFire team

Solid Surface Combustion Experiment Yields Significant Observations

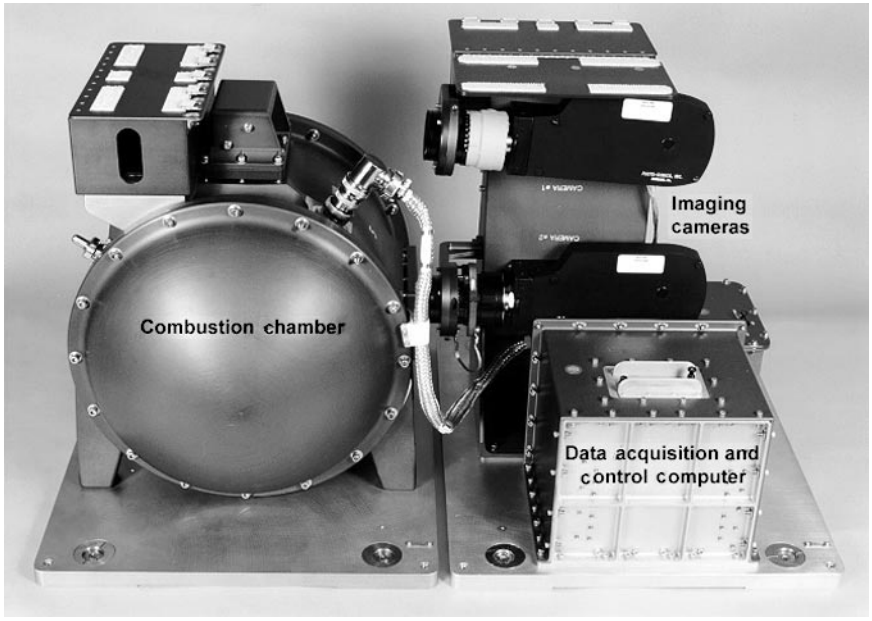

Solid Surface Combustion Experiment hardware, including the chamber module and camera module.

The spread of a flame over solid fuel is not only a fundamental textbook combustion phenomenon, but also the central element of destructive fires that cause tragic loss of life and property each year. Throughout history, practical measures to prevent and fight fires have been developed, but these have often been based on lessons learned in a costly fire. Since the 1960's, scientists and engineers have employed powerful tools of scientific research to understand the details of flame spread and how a material can be rendered nonflammable. High-speed computers have enabled complex flame simulations, and lasers have provided measurements of the chemical composition, temperature, and air velocities inside flames. The microgravity environment has emerged as the third great tool for these studies.

Spreading flames are complex combinations of chemical reactions and several physical processes including the transport of oxygen and fuel vapor to the flame and the transfer of heat from the flame to fresh fuel and to the surroundings. Depending on its speed, air motion in the vicinity of the flame can affect the flame in substantially different ways. For example, consider the difference between blowing on a campfire and blowing out a match. On Earth, gravity induces air motion because of buoyancy (the familiar rising hot gases); this process cannot be controlled experimentally. For theoreticians, buoyant air motion complicates the modeling of flame spread beyond the capacity of modern computers to simulate. The microgravity environment provides experimental control of air motion near spreading flames, with results that can be compared with detailed theory.

The Solid Surface Combustion Experiment (SSCE) was designed to obtain benchmark flame spreading data in quiescent test atmospheres—the limiting case of flames spreading. Professor Robert Altenkirch, Vice President for Research at Mississippi State University, proposed the experiment concept, and the NASA Lewis Research Center designed, built, and tested the SSCE hardware. It was the first microgravity science experiment built by Lewis for the space shuttle and the first combustion science experiment flown in space.

Hardware for SSCE consisted of a sealed chamber module containing the test samples, ashless filter paper or polymethylmethacrylate (PMMA, an acrylic plastic), and a test atmosphere of 35- to 70-percent oxygen mixed with nitrogen. The samples were instrumented with thermocouples. A second module contained cameras, a computer, and a battery.

SSCE has flown 10 times on the space shuttle, with the final flight, STS–91, occurring during 1998. In each experiment, the samples ignited successfully. The resulting flames were recorded on film and video; thermocouple temperatures were recorded digitally.

Several scientifically significant observations have emerged from the SSCE tests. Steady flame spread occurs over thin samples, even in quiescent atmospheres. Thicker PMMA samples burn unsteadily and finally self-extinguish, but they require as long as 9 min (e.g., the STS–85 test) to quench.

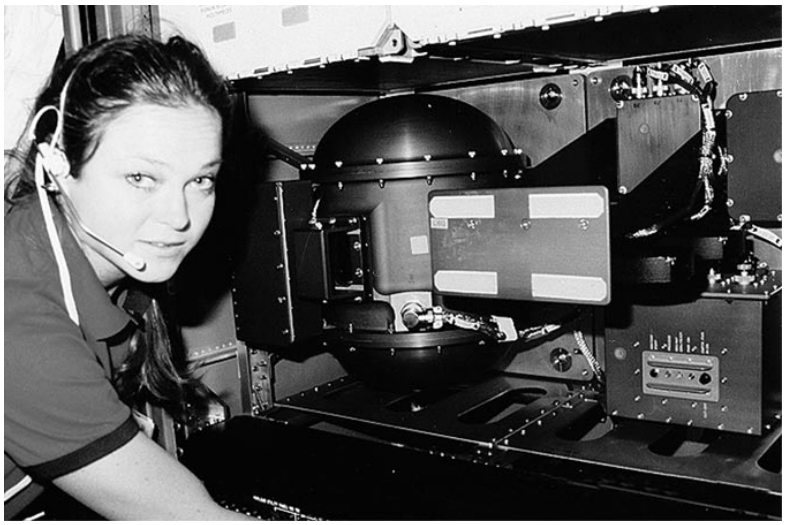

Astronaut Tamara Jernigan performing the Solid Surface Combustion Experiment in the Space Shuttle Columbia during STS–40.

Comparisons of flight data with Professor Altenkirch's numerical simulations indicate that (unlike in normal gravity) radiative heat transfer is a dominating influence in flame spread in quiescent atmospheres. In summary, these experiments demonstrate that the controlling mechanisms for material flammability and flame spread are quite different in microgravity and normal Earth gravity. Results of the SSCE experiment will help spacecraft designers and Earth-bound fire safety technologists to improve fire safety, through enhanced fire prevention, detection, and mitigation techniques.

Lewis contact: Kurt. R. Sacksteder, (216) 433–2857, Kurt.R.Sacksteder@grc.nasa.gov

Authors: Kurt R. Sacksteder, John M. Koudelka, and Franklin Vergilii

Headquarters program office: OLMSA

Programs/Projects: Microgravity Science, SSCE

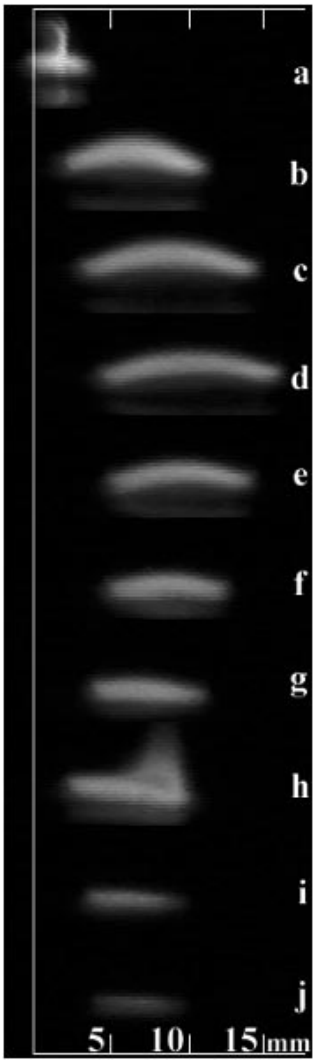

Side-view image of unsteady flame spread over a flat sample of PMMA in a test atmosphere of 50-percent oxygen/50-percent nitrogen at 1 atm of pressure. The flame advanced nearly 2 cm from the ignitor, then regressed and finally extinguished, requiring nearly 9 min to quench.

Stability of Enclosed Laminar Flames Studied in Microgravity

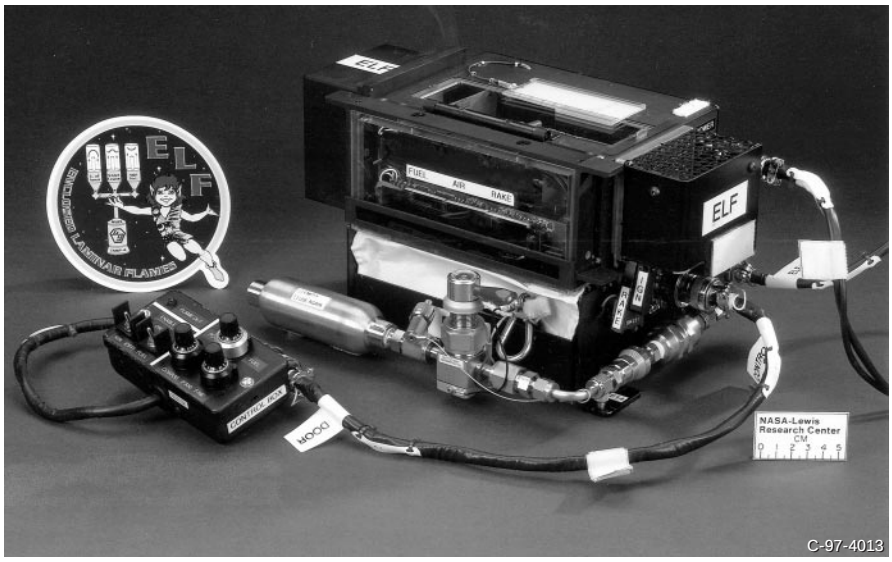

ELF flight hardware assembled for testing.

In practical combustion systems, the flame is often anchored at the inlet where the fuel is injected into an air duct. This type of system is found in powerplant combustors, gas turbine combustors, and the jet engine afterburner. Despite its successful use, this configuration is vulnerable to adverse flow conditions that can cause the flame to literally lift off from the inlet or even blowout. Poor flame stability is, of course, unwanted, especially where safety has a high priority. Our understanding of the mechanisms that control flame stability is incomplete in part because the interaction of buoyant (i.e., gravity-induced) convection makes it difficult to interpret normal-gravity results. However, a comparison of normal-gravity and microgravity results can provide a clear indication of the influence of forced and buoyant flows on flame stability. Therefore, a joint microgravity study on the stability of Enclosed Laminar Flames (ELF) was carried out by researchers at The University of Iowa and the NASA Lewis Research Center. The microgravity tests were conducted in the Microgravity Glovebox (MGBX), during the STS–87 space shuttle mission in late 1997, using hardware designed and produced at Lewis and shown in the photo to the left.

The primary objective of the ELF investigation was to determine the mechanisms controlling the stability of round, laminar, gas-jet diffusion flames in a coflow air duct. The study specifically focused on the effect of buoyancy on the flame characteristics and velocities at the lift-off, reattachment, and blowout of the flame. When the

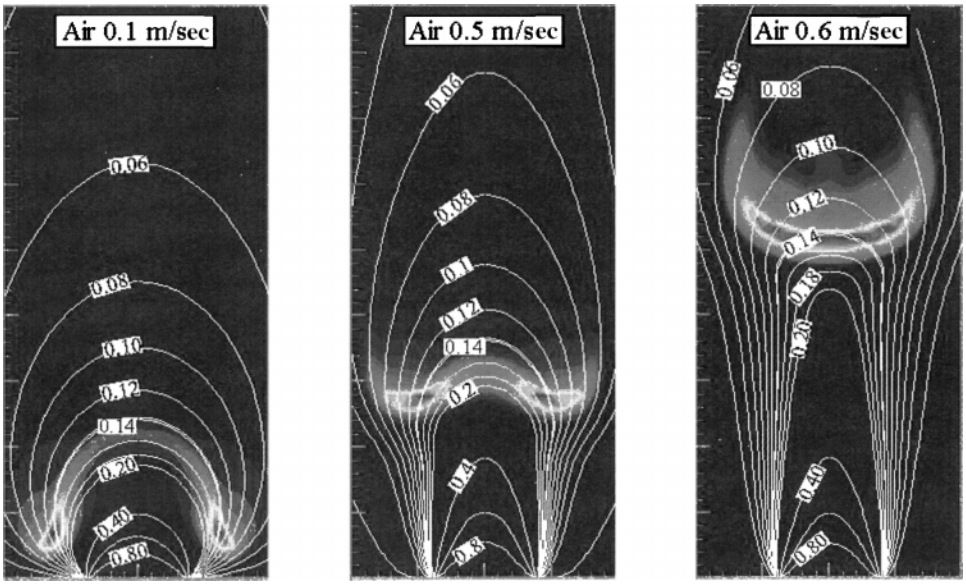

Numerical predictions of flame lifting and shape change with increasing air velocity. Heat release rate and mixture fraction for attached (left), lifted (center), and near blowout (right) condition. Fuel-jet velocity, 0.2 m/sec.

fuel or air velocity is increased to a critical value, the flame base abruptly jumps downstream, and the flame is said to have reached its lift-off condition. Flow conditions are such that the flame cannot be maintained at the burner rim despite the presence of both fuel and oxygen. When the velocity is further increased, the flame eventually extinguishes at its blowout condition. In contrast, if the velocity is reduced, the flame base eventually returns to anchor at the burner rim, at a velocity lower than that of lift-off, indicating a hysteresis effect.

During the STS–87 shuttle mission, approximately 50 tests were conducted using a 50/50 mixture (by volume) of methane and nitrogen as the fuel. Stable lifted flames were observed in microgravity, except at high fuel flows where the microgravity flames blew out immediately after lift-off. The experimental results verify the hypothesis that substantially greater velocities are required to destabilize a flame in microgravity because of the absence of buoyant acceleration in the flow. Preliminary results reveal that the increase in air velocity required to induce lift-off in microgravity (in comparison to normal gravity) was nearly equal to the increase required to induce blowout. Furthermore, the air velocity increase was relatively independent of the fuel flow, except at low fuel flows. Preliminary numerical predictions are in qualitative agreement with the experimental results; an example is shown in the bottom figure on the preceding page. Further analysis is underway, and on the basis of ELF's success on STS–87, a ground-based proposal has been approved, offering ELF researchers the opportunity to compete for a reflight on the space shuttle.

Enclosed Laminar Flames (ELF) is described on the World Wide Web:
http://zeta.grc.nasa.gov/expr/elf.htm

Lewis contact:
Dennis P. Stocker, (216) 433–2166, Dennis.P.Stocker@grc.nasa.gov

Author: Dennis P. Stocker

Headquarters program office: OLMSA

Programs/Projects: HEDS, Microgravity Science, STS–87, USMP–4, MGBX, ELF

Unlocking the Keys to Vortex/Flame Interactions in Turbulent Gas-Jet Diffusion Flames—Dynamic Behavior Explored on the Space Shuttle

Most combustion processes in industrial applications (e.g., furnaces and engines) and in nature (e.g., forest fires) are turbulent. A better understanding of turbulent combustion could lead to improved combustor design, with enhanced efficiency and reduced emissions. Despite its importance, turbulent combustion is poorly understood because of its complexity. The rapidly changing and random behavior of such flames currently prevents detailed analysis, whether experimentally or computationally. However, it is possible to learn about the fundamental behavior of turbulent flames by exploring the controlled interaction of steady laminar flames and artificially induced flow vortices. These interactions are an inherent part of turbulent flames, and understanding them is essential to the characterization of turbulent combustion. Well-controlled and defined experiments of vortex interaction with laminar flames are not possible in normal gravity because of the interference of buoyancy- (i.e., gravity) induced vortices. Therefore, a joint microgravity study was established by researchers from the Science and Technology Development Corp. and the NASA Lewis Research Center. The experimental study culminated in the conduct of the Turbulent Gas-Jet Diffusion Flames (TGDF) Experiment on the STS–87 space shuttle mission in November 1997. The fully automated hardware, shown in photo, was designed and built at Lewis. During the mission, the experiment was housed in a Get Away Special (GAS) canister in the cargo bay.

In the TGDF experiment, toroidal flow vortices were generated by sinusoidally varying the open diameter of an iris around the base of a propane flame, thereby causing large-scale fluctuations in the entrained airflow. The iris frequency, which was varied to be 1.5, 3.0, and 5.0 Hz, was the experiment's key variable. TGDF's primary objective was to gain an understanding of the dynamic behavior of the vortex/flame interaction, including possible vortex breakup or merging, and the interaction's effect on the time-averaged values of flame temperature, radiation, and shape. In addition, the experiment has provided insights into the development and extinction of microgravity flames. The experimental results were compared with a comprehensive

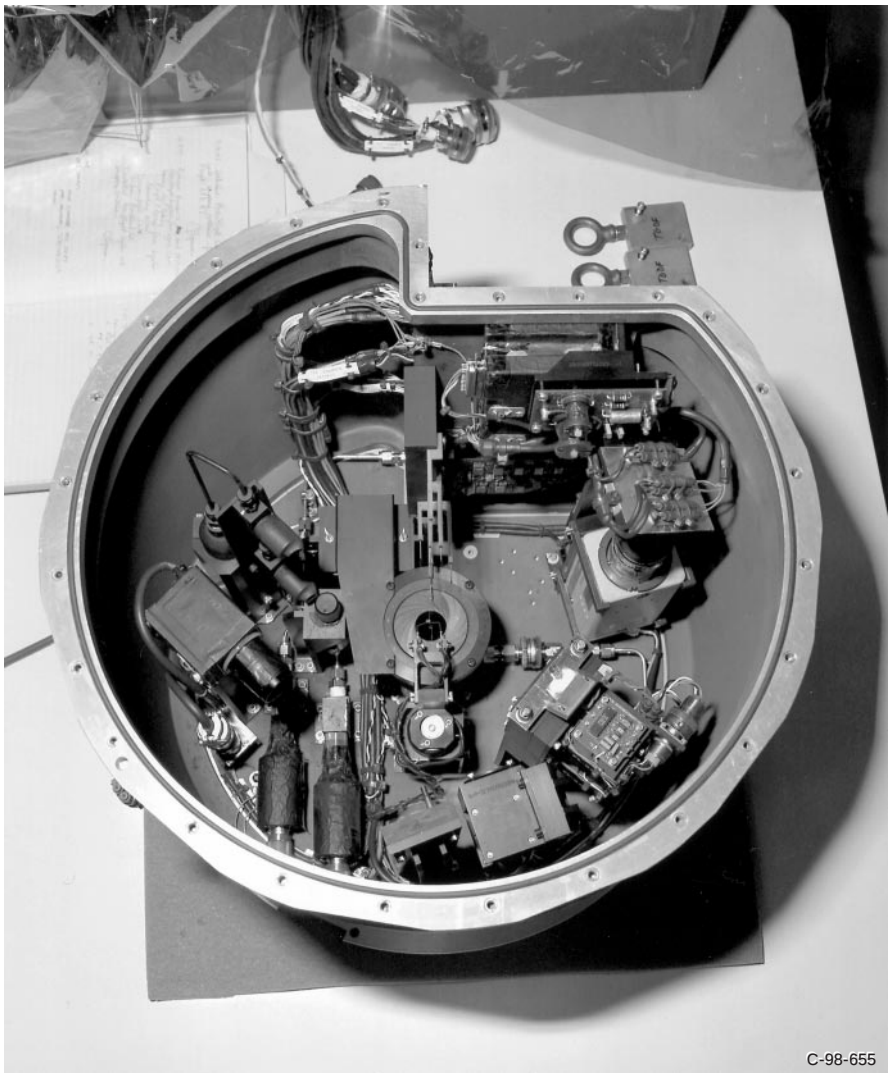

Interior of the TGDF combustion chamber, with the innovative vortex generation mechanism visible in the center.

numerical model of the pulsed flame to validate the accuracy of the model and verify our understanding of the flame behavior.

Analysis of the results revealed that the microgravity flame possesses three axially spaced zones of vortex interaction. In the lower portion of the flame, there is a significant transfer of energy from the mean field to the oscillations. In the numerical simulation, the vortex dissipation rate and the kinetic energy of the oscillations both peak in the lower part of the flame. In the central region, the energy transfer is from the primary oscillation to its harmonic and/or the mean field. In the upper portion of the flame, the oscillations decay, and there is no significant transfer of energy between the oscillations and the mean flow, or between oscillations. In contrast, the oscillations grow in the upper portion of buoyant normal-gravity flames. Radiation measurements also indicate that the core of the upper zone receives energy from the flame and the mean flow at the flame base. Thus, the temperature (and combustion) in the upper zone is enhanced by the vortex interaction. This has been confirmed by numerical computation and is in agreement with observations of pulsation-induced flame-tip closure in supporting ground-based studies of microgravity flames. Further analysis is underway, and a TGDF reflight proposal, based on the successful STS–87 results, will be submitted.

The TGDF Experiment is described on the World Wide Web: http://zeta.grc.nasa.gov/expr2/gjdfe.htm

Lewis contact:
Dennis P. Stocker, (216) 433–2166, Dennis.P.Stocker@grc.nasa.gov

Author: Dennis P. Stocker

Headquarters program office: OLMSA

Programs/Projects: HEDS, Microgravity Science, STS–87, GAS, TGDF

Crystal Growth Using MEPHISTO

The shuttle flight experiment "In Situ Monitoring of Crystal Growth Using MEPHISTO" was accomplished during STS–87 as part of the fourth flight of the United States Microgravity Payload (USMP–4), which was flown from November 19 to December 5, 1997. The data returned from that flight are just now beginning to yield quantitative results. This project is an international collaboration: the furnace system known as MEPHISTO was built in France by CNES (French National Space Agency) and CEA (French Atomic Energy Commission); the principal investigator, Prof. Reza Abbaschian, is from the University of Florida at Gainesville; and numerical and analytical modeling support includes collaborators from the University of New South Wales, Australia, the University of Wisconsin at Milwaukee, the National Institute of Standards and Technology, and the NASA Lewis Research Center. MEPHISTO is a French acronym that translates into English as *Materials for the Study of Interesting Phenomena of Solidification on Earth and in Orbit*. Since this was the fourth flight of the MEPHISTO furnace, the experiment is referred to as MEPHISTO–4.

MEPHISTO–4 was a directional solidification experiment that studied the liquid-to-solid transformation of bismuth alloyed with tin. Directional solidification is a freezing technique common to the processing of the electronic materials used in integrated circuits and detectors, such as silicon and germanium. When liquids are frozen on Earth, they must be cooled. The cooling causes stirring because of density variations in the liquid (ref. 1). This stirring, known as natural convection, influences the quality of the resulting solid. During freezing, regions of high and low concentrations of tin are created. This introduces another important phenomenon: diffusion, or the movement by molecular action of matter from regions of high concentration to regions of lower concentration. In MEPHISTO–4, it is tin that diffuses from the high-concentration region in front of the solid-liquid interface to more distant low-concentration regions. Finally, the concentration gradients of tin also cause density variations, and hence are another source of stirring of the liquid on Earth. The interplay among temperature, concentration, convection, diffusion, and solidification becomes extremely complex, and a complete understanding of solidification is beyond the present state of the art.

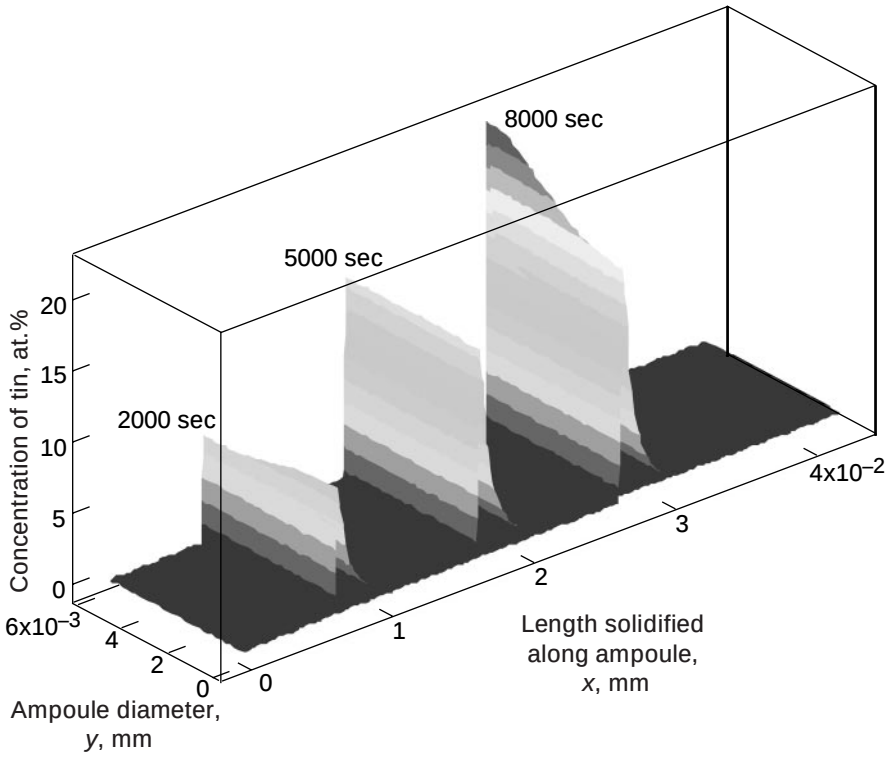

Length solidified along the ampoule, x, versus the ampoule diameter from bottom to top, y, and concentration of tin. No radial segregation is shown after 5000 sec of growth, indicating diffusion dominance; radial segregation is shown after 8000 sec because of solutal convection.

In MEPHISTO-4 the microgravity environment is being used to greatly reduce convection effects in the solidification process. In this way, preliminary theories describing solidification in terms of diffusion-only can be examined, and the effects of diffusion can be more readily assessed than is possible on Earth, where natural convection swamps the more delicate diffusion phenomena. When theories that include only diffusion have been tested using the flight data, more advanced theories that include both diffusion and convection can be developed and tested using both flight and Earth-based data.

All pertinent aspects of the MEPHISTO–4 experiment were monitored and controlled remotely

through NASA's Payload Operations Control Center located at the NASA Marshall Space Flight Center. To monitor all the parameters needed for the study of solidification, three samples were processed identically and simultaneously in the MEPHISTO furnace: one used the Seebeck technique (refs. 2 and 3) to measure the temperature at the interface between the solid and liquid; the second employed a pulse of electricity to mark the shape of the solid/liquid interface; and the third measured the rate of solidification by monitoring the electrical resistance of the sample. This third sample was also quenched at the end of the experiment to freeze the concentration gradients built up in the liquid near the solid/liquid interface. As part of the analysis of the flight sample, this quenched concentration profile will be measured and used to calculate a diffusion coefficient for tin in liquid bismuth. The diffusion coefficient is an important parameter in the analyses and theories of solidification. In the MEPHISTO furnace, several experiments can be done through the repeated melting, solidifying, and remelting of the samples. Due in part to the results of the numerical modeling teams (refs. 4 and 5), MEPHISTO–4 operations were extended and continued through nearly the entire 16-day mission. The flexible and responsive performance of the furnace, the optimization through numerical modeling of the experiment, and the dedication of the principal investigator's teams enabled about twice the number of experiments to be accomplished during flight than were originally planned.

An example of the numerical modeling results is shown in the figure (ref. 6). The modeling enabled the team to estimate the level and effects of convection during flight. It also determined how long we needed to wait between solidification runs for the high concentrations of tin at the solid/liquid interface to be reduced to low levels by diffusion and convection, thereby allowing our mission time to be optimized.

After the USMP–4 mission, the MEPHISTO hardware was shipped to the French support contractor SEP (Société Européenne de Propulsion) for checkout and removal of the samples. The samples and flight data are now being analyzed by the University of Florida team. MEPHISTO–4 is scheduled to be completed, with its final report given to NASA, by April 1999. Mission and flight data results were recently summarized (ref. 7) and include measurement of the average diffusion coefficient of tin in liquid bismuth of 3.5×10^{-5} cm^2/sec.

Find out more on the World Wide Web:
http://zeta.grc.nasa.gov/expr/insitu.htm
http://cml.grc.nasa.gov/degroh/
http://cfd.mech.unsw.edu.au/
http://www.uwm.edu/Dept/ECL/garimella.htm

References

1. de Groh, H.C., III; and Lindstrom, T.: Interface Shape and Convection During Solidification and Melting of Succinonitrile. NASA TM–106487, 1994.
2. Abbaschian, R., et al.: A Study of Directional Solidification of Faceted Bi-Sn Alloys in Microgravity. AIAA Paper 95–0608, 1995.
3. Alvarez, J.; Peteves, S.D.; and Abbaschian, G.J.: Thermoelectric Effects Across Solid-Liquid Gallium Interface. Thin Films and Interfaces II. J.E.E. Baglin, D.R. Campbell, and W.K. Chu, eds. MRS Symposium Proceedings, vol. 25, 1984, pp. 345–350.
4. Chen, P., et al.: Rehomogenization—Diffusion and Correction in Microgravity. AIAA Paper 98–0740, 1998.
5. Yao, M.; de Groh, H.C., III; and Abbaschian, R.: Numerical Modeling of Solidification in Space with MEPHISTO–4 (Part I). AIAA Paper 97–0449, 1997.
6. Timchenko, V., et al.: Directional Solidification in Microgravity. Heat Transfer 1998, Proceedings of 11th IHTC, Kyongju, Korea, Taylor & Francis, vol. 7, pp. 515–520, 1998.
7. Cambon, G., et al.: MEPHISTO/USMP–4/STS–87, In-Situ Monitoring of Crystal Growth Using MEPHISTO, Preliminary Flight Results. IAF/IAA–98–J.3.04, 49th International Astronautical Congress, 1998.

Lewis contact:
Henry C. de Groh III, (216) 433–5025, Henry.C.deGroh@grc.nasa.gov

Author: Henry C. de Groh III

Headquarters program office: OLMSA

Programs/Projects: Microgravity Materials Science Program, USMP–4

Special recognition: Best poster in session, 11th International Heat Transfer Conference, Korea, 1998

Effects of g-Jitter on Diffusion in Binary Liquids

The microgravity environment offers the potential to measure the binary diffusion coefficients in liquids without the masking effects introduced by buoyancy-induced flows due to Earth's gravity. However, the background g-jitter (vibrations from the shuttle, onboard machinery, and crew) normally encountered in many shuttle experiments may alter the benefits of the microgravity environment and introduce vibrations that could offset its intrinsic advantages. An experiment during STS–85 (August 1997) used the Microgravity Vibration Isolation Mount (MIM) to isolate and introduce controlled vibrations to two miscible liquids inside a cavity to study the effects of g-jitter on liquid diffusion.

Diffusion in a nonhomogeneous liquid system is caused by a nonequilibrium condition that results in the transport of mass (dispersion of the different kinds of liquid molecules) to approach equilibrium. The dynamic state of the system tends toward equilibrium such that the system becomes homogeneous. An everyday example is the mixing of cream and coffee (a nonhomogeneous system) via stirring. The cream diffuses into the coffee, thus forming a homogeneous system. At equilibrium the system is said to be mixed. However, during stirring, simple observations show complex flow field dynamics—stretching and folding of material interfaces, thinning of striation thickness, self-similar patterns, and so on. This example illustrates that, even though mixing occurs via mass diffusion, stirring to enhance transport plays a major role. Stirring can be induced either by mechanical means (spoon or plastic stirrer) or via buoyancy-induced forces caused by Earth's gravity. Accurate measurements of binary diffusion coefficients are often inhibited by buoyancy-induced flows. The microgravity environment minimizes the effect of buoyancy-induced flows and allows the true diffusion limit to be achieved. One goal of this experiment was to show that the microgravity environment suppresses buoyancy-induced convection, thereby mass diffusion becomes the dominant mechanism for transport. Since g-jitter transmitted by the shuttle to the experiment can potentially excite buoyancy-induced flows, we also studied the effects of controlled vibrations on the system.

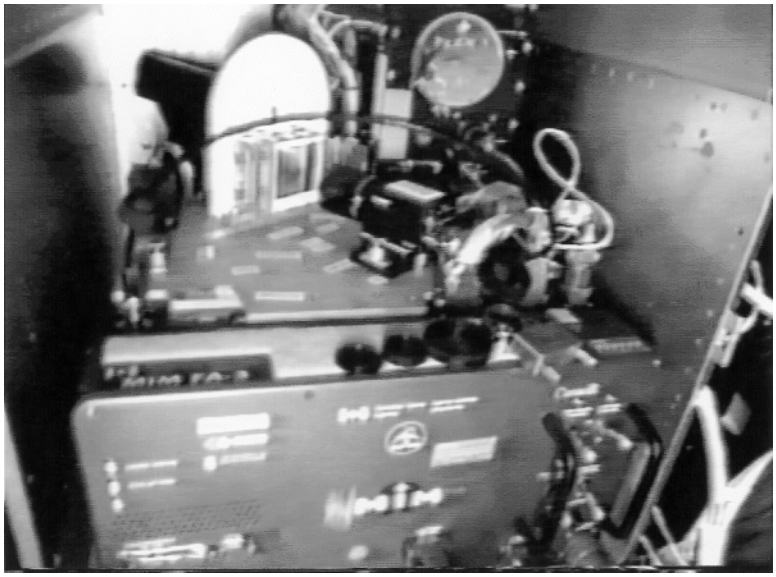

Experiment mounted on the MIM platform on STS–85

The physics of the interface behavior of two miscible liquids subjected to steady and oscillatory body forces was predicted, and the results were documented in a series of publications (refs. 1 to 4). The experiment was conceived and designed by W.M.B. Duval at the NASA Lewis Research Center. However, because an important finding of the theoretical prediction was the presence of standing waves due to oscillatory body forces (refs. 1 and 3), a special experimental apparatus was needed. Showing the existence of standing waves required the use of a platform that could both isolate the experiment from vibrations and input known vibration sources to it. These requirements were fulfilled by the use of the Microgravity Vibration Isolation Mount (MIM), designed by B.V. Tryggvason through an international collaboration with the Canadian Space Agency. The experimental setup flown on STS–85 is shown in the photo to the left. Hardware consisted of the mixing cell, a light source, a motor to remove the shim, and a black & white camera that was mounted on the MIM platform. Experiments on the MIM were performed in two different modes: (1) an isolation mode to damp out background g-jitter and (2) an active mode to input known vibration sources to the experiment.

On the next page, the top and bottom photos, respectively, show ground-based and microgravity results. Because of the large size of the mixing cell, 5-cm high by 5-cm wide by 1-cm deep, it was extremely challenging to damp

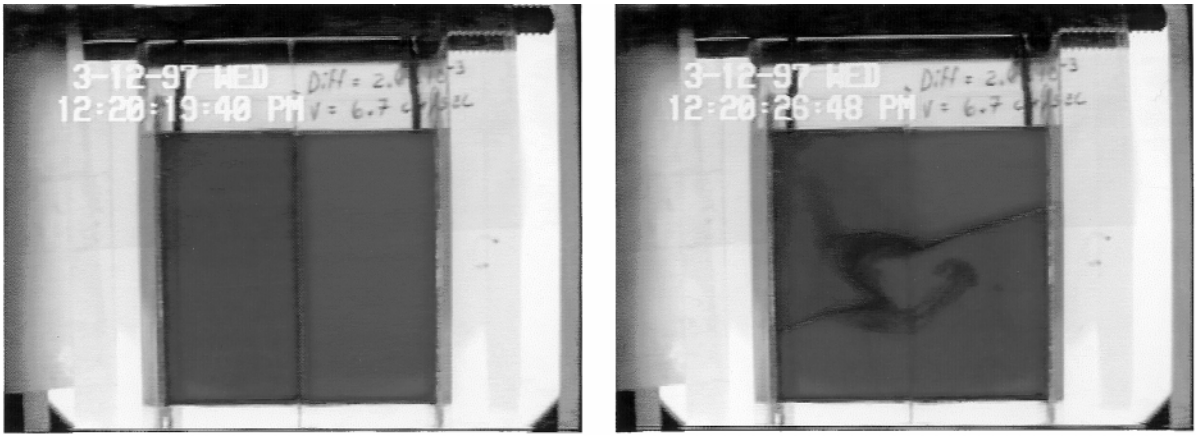

Ground-based experiment. Left: Initial condition of two miscible liquids at time zero. Fluid on the left side of the photo is 2.2-vol % deuterium oxide with deionized water and blue dye; fluid on the right side of the photo is 100-vol % deionized water with red dye—a specific gravity difference of 0.0026. Right: Configuration of the interface after removal of the shim showing an internal breakwave after approximately 7 sec.

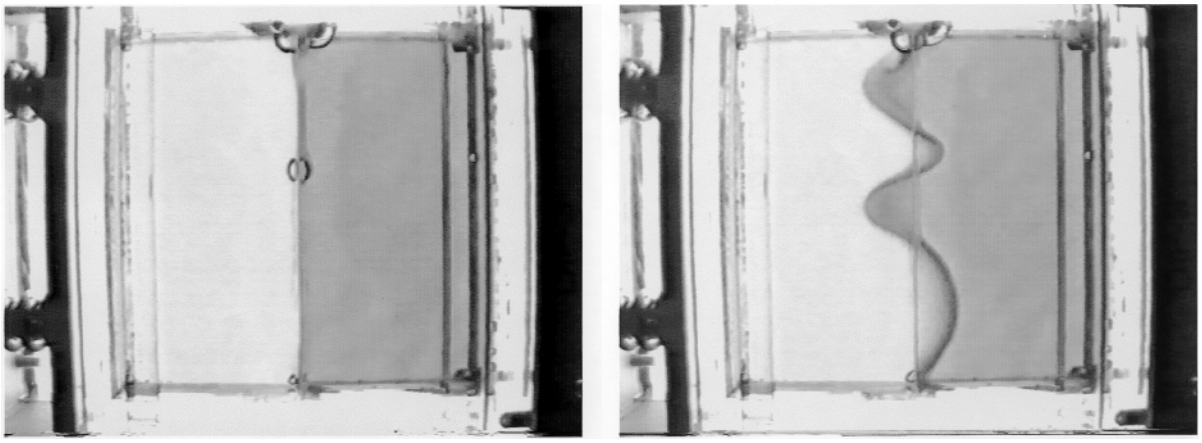

Microgravity experiments. Left: Isolation mode 17 sec after removal of the shim, showing a stationary interface (fluid on the left side of the photo contains 20-vol % ethylene-glycol with water and blue dye; fluid on the right side of the photo contains 100-vol % deionized water with red dye—a specific gravity difference of 0.028). Right: Forcing mode at a frequency of 1 Hz and an amplitude of 0.02g, showing a four-mode standing wave.

out buoyancy-induced forces, which can stretch and fold the interface. The top photos capture a typical scenario showing the effect of a steady body force on the ground. The initial condition at time zero consists of two miscible liquids separated by a thin shim, as in the top left photo. Once the shim is pulled, the hydrostatic pressure imbalance between the two liquids causes an overturning motion that stretches and folds the interface. The top right photo shows the evolution of an internal breakwave after approximately 7 sec.

In contrast, the microgravity result in the bottom left photo shows a stationary interface after 17 sec. The MIM was operating in isolation mode; the background acceleration was nearly steady on the order of a micro-g (10^{-6}g). This result illustrates the effectiveness of the microgravity environment in damping buoyancy-induced flows, thus permitting liquids to mix via mass diffusion. Note that the presence of any residual buoyancy-induced force would cause the interface to deform. Mass diffusion over a long time scale would cause the two fluids to mix while the interface remained stationary in the vertical configuration. Given that the interface can remain stationary over a time interval, the MIM was operated in the excitation mode with a frequency of 1 Hz and an amplitude of 0.02g with a sinusoidal input. The bottom right photo shows that the interface becomes unstable against Kelvin-Helmholtz instability and produces a four-mode standing wave. In this case, the instability of the interface enhances local mass transport.

The analysis of the vibration data input by the MIM on the experiment is ongoing. Recent computational results in fiscal year 1998 agreed with the experimental findings of the four-mode standing wave; however, subtleties of the experimental findings are being addressed. These results are expected to shed light on the use of isolation systems for the International Space Station.

Visit Lewis on the World Wide Web: http://www.grc.nasa.gov

References

1. Duval, W.M.B.; and Jacqmin, D.A.: Interfacial Dynamics of Two Liquids Under an Oscillating Gravitational Field. AIAA J., vol. 28, Nov. 1990, pp. 1933–1941.
2. Duval, W.M.B.: Numerical Study of Mixing of Two Fluids Under Low Gravity. NASA TM–105865, 1992.
3. Duval, W.M.B.: The Kinematics of Buoyancy Induced Mixing. Proceedings of the 8th European Symposium on Materials and Fluid Sciences in Microgravity, ESA–SP–333, Vol. 2, 1992, pp. 855–861.
4. Duval, W.M.B.: Flow Field Topology of Buoyancy Induced Mixing. AIAA Paper 96–0253, 1996.

Lewis contact:
Walter M.B. Duval, (216) 433–5023, Walter.M.Duval@grc.nasa.gov

Author: Walter M.B. Duval

Headquarters program office:
OLMSA (UG)

Programs/Projects:
Microgravity Science

Special recognition:
Superior Accomplishment Award given in 1998 for space flight experiment conducted on STS–85 in August 1997

Viscosity of Xenon Examined in Microgravity

Why does water flow faster than honey? The short answer, that honey has a greater viscosity, merely rephrases the question. The fundamental answer is that viscosity originates in the interactions between a fluid's molecules. These interactions are so complicated that, except for low-density gases, the viscosity of a fluid cannot be accurately predicted. Progress in understanding viscosity has been made by studying moderately dense gases and, more recently, fluids near the critical point. Modern theories predict a universal behavior for all pure fluids near the liquid-vapor critical point, and they relate the increase in viscosity to spontaneous fluctuations in density near this point. The Critical Viscosity of Xenon (CVX) experiment tested these theories with unprecedented precision when it flew aboard the Space Shuttle Discovery (STS–85) in August 1997.

Near the critical point, xenon is a billion times more compressible than water, yet it has about the same density. Because the fluid is so "soft," it collapses under its own weight when exposed to the force of Earth's gravity—much like a very soft spring. Because the CVX experiment is conducted in microgravity, it achieves a very uniform fluid density even very close to the critical point. The accompanying graph reveals the dramatic difference between Earth-based measurements and the data obtained in microgravity.

At the heart of the CVX experiment is a novel viscometer built around a small nickel screen. An oscillating electric field forces the screen to oscillate between pairs of electrodes. Viscosity, which dampens the oscillations, can be calculated by measuring the screen motion and the force applied to the screen. So that the fluid's delicate state near the critical point will not be disrupted, the screen oscillations are set to be both slow and small.

CVX is the culmination of a series of Earth-based viscosity measurements near critical points. Robert F. Berg and Michael R. Moldover of the National Institute of Standards and Technology are the principal investigators, and Gregory Zimmerli of Lewis and the National Center for Microgravity Research is the project scientist. NASA funded both the Earth-based and flight experiments through Lewis' Microgravity Science Division. NASA Lewis science contractors, NYMA, ADF, and Sverdrup, developed and built the flight instrument.

Since the flight, the principal investigators have analyzed the flight data in great detail. The data show that the viscosity increases as the critical point is approached and that it agrees with the theoretical prediction. CVX also measured low-frequency viscoelasticity in a pure fluid for the first time. Viscoelasticity is a partly elastic response to shear stress. It is common in polymers, foams, and other complex fluids, but has never been observed in a simple fluid such as xenon. A journal publication describing the scientific findings has been published (ref. 1).

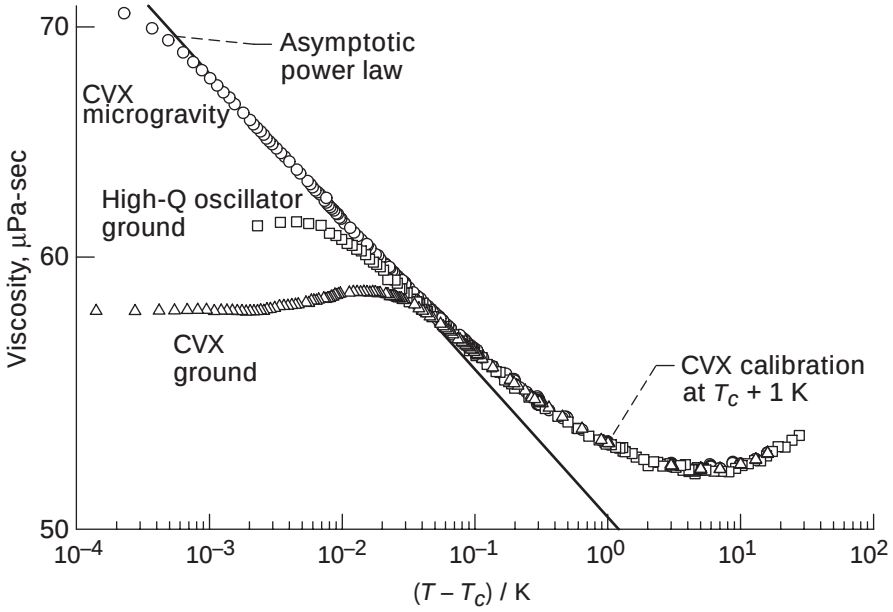

Ground-based and microgravity measurements of the viscosity of xenon near the critical point. In microgravity, the increase of viscosity is measured 100 times closer to the critical temperature, T_c, and much more accurately than on Earth. The asymptotic power law characterizes the universal behavior of viscosity in all pure fluids near the critical point. Temperature of sample, T; quality factor, Q. (High-Q indicates weak damping.)

As an extension to this very successful flight experiment, the principal investigators are preparing a second flight experiment, CVX–2. This experiment, which will measure the shear thinning of viscosity near the critical point of xenon, will be the first experiment of its kind to measure shear thinning in a simple fluid. A quantitative understanding of shear thinning near the critical point will lead to a better understanding of shear thinning in more complex fluids, such as polymers and emulsions, and thus may have broad applications in science and industry.

Reference

1. Berg, R.F.; Moldover, M.R.; and Zimmerli, G.A.: Viscoelasticity of Xenon near the critical point. Phys. Rev. Lett., vol. 82, Feb. 1, 1999, pp. 920–923.

Lewis contacts:
Richard W. Lauver, (216) 433–2860, Richard.W.Lauver@grc.nasa.gov;
Gregory A. Zimmerli, (216) 433–6577, Gregory.A.Zimmerli@grc.nasa.gov;
Dr. Bhim S. Singh, (216) 433–5396, Bhim.S.Singh@grc.nasa.gov; and
Susan M. Motil, (216) 433–8589, Susan.M.Motil@grc.nasa.gov

Authors: Gregory A. Zimmerli, Robert F. Berg, and Michael R. Moldover

Headquarters program office:
OLMSA (UG)

Programs/Projects:
Microgravity Science

Laser Light Scattering With Multiple Scattering Suppression Used to Measure Particle Sizes

Laser light scattering is the technique of choice for noninvasively sizing particles in a fluid. The members of the Advanced Technology Development (ATD) project in laser light scattering at the NASA Lewis Research Center have invented, tested, and recently enhanced a simple and elegant way to extend the concentration range of this standard laboratory particle-sizing technique by several orders of magnitude. With this technique, particles from 3 nm to 3 μm can be measured in a solution. But, until recently, it was difficult at best to look into the depths of fluids that are not as clear as water. With higher concentrations of particles, the large increase in multiple scattering would corrupt the data.

Recently, laser light scattering evolved to successfully size particles in both clear solutions and concentrated milky-white solutions. The enhanced technique uses the property of light that causes it to form tall interference patterns at right angles to the scattering plane (perpendicular to the laser beam) when it is scattered from a narrow laser beam. Such multiple-scattered light forms a broad fuzzy halo around the focused beam, which, in turn, forms short interference patterns. By placing two fiber optics on top of each other and perpendicular to the laser beam (see the drawing), and then cross-correlating the signals they produce, only the tall interference patterns formed by singly scattered light are detected. To restate this, unless the two fiber optics see the same interference pattern, the

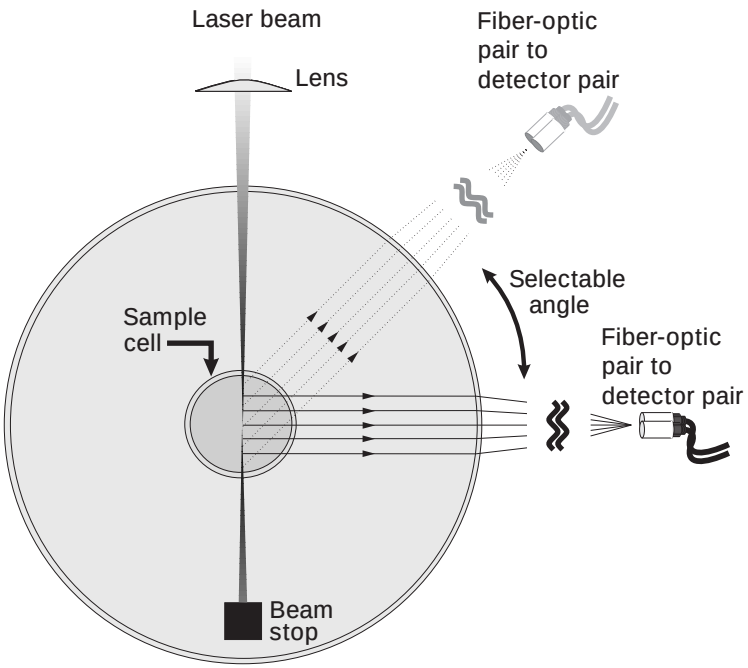

Diagram of multiangle laser-light-scattering instrument with multiple-scattering suppression using single-color cross-correlation. Both fibers are stacked perpendicular to the scattering plane.

scattered light is not incorporated into the signal. With this technique, only singly scattered light is seen (multiple-scattered light is rejected) because only singly scattered light has an interference pattern tall enough to span both of the fiber-optic pickups. This technique is simple to use, easy to align, and works at any angle. Placing a vertical slit in front of the signal collection fibers enhanced this approach. The slit serves as an optical mask, and it significantly shortens the time needed to collect good data by selectively masking out much of the unwanted light before cross-correlation is applied.

Different scattering angles and polarizations can be used to extract additional information from the samples—information that was previously unavailable and not theoretically interpreted. Both of these concerns are being addressed, and we believe that this will have a significant impact in the particle-sizing community.

In addition, the Advanced Technology Development light-scattering group at Lewis is extending the capabilities of laser light scattering by using fiber optics to overcome the problems of stray light (which until now could corrupt the interpretation of otherwise good data). Launching the laser beam used to probe the particles both into the solution and into a fiber optic that is coupled to the signal-receiving fiber will introduce a local oscillator at the detector. This overcomes the problems introduced by a small amount of stray light. It also provides significant (homodyne) gain for the signal and eliminates many of the cross-terms that would otherwise make data analysis more complicated. Although bulk-optic homodyne instruments have been used in the past, alignment problems made these difficult, onerous beasts (especially when multiple-angle measurements were being made). With fiber optics, homodyning is much easier. Mixing the scattered light signal and the laser beam in polarization maintains monomode fiber optics and is 100-percent efficient because of the wavefront matching imposed by the fiber-optic couplers.

Lewis' light-scattering group is continuing to provide new laser-light-scattering technologies and techniques that help answer fundamental science questions—questions that can be answered by studying colloid particle interactions and fluid-crystal-glass phase transitions in space (where gravity does not destroy the study with conventional effects). These studies serve as a good model for atomic interactions and crystal formation and have led to a number of pleasant surprises and advances. The commercial biotechnology community is also asking Lewis' light-scattering group about using light scattering to study proteins. Further interest is surfacing in the computer industry, where polishing compounds grind themselves up when they are used to make computer chips. Here, constant monitoring of the particle grit size is needed to increase silicon wafer production yield. Other opportunities are also being addressed.

Lewis contact:
William V. Meyer, (216) 433–5011, William.V.Meyer@grc.nasa.gov

Authors:
William V. Meyer, Padetha Tin, James A. Lock, David S. Cannell, Anthony E. Smart, and Thomas W. Taylor

Headquarters program office:
OLMSA (UG)

Programs/Projects:
Microgravity Science, NCMR, ATD

Phase-Shifted Laser Feedback Interferometry

Phase-shifted, laser feedback interferometry is a new diagnostic tool developed at the NASA Lewis Research Center under the Advanced Technology Development (ATD) Program directed by NASA Headquarters' Microgravity Research Division. It combines the principles of phase-shifting interferometry (PSI) and laser-feedback interferometry (LFI) to produce an instrument that can quantify both optical path length changes and sample reflectivity variations. In a homogenous medium, the optical path length between two points is the product of the index of refraction and the geometric distance between the two points. LFI differs from other forms of interferometry by using the laser as both the source and the phase detector. In LFI, coherent feedback of the incident light either reflected directly from a surface or reflected after transmission through a region of interest will modulate the output intensity of the laser. The combination of PSI and LFI has produced a robust instrument, based on a low-power helium-neon (HeNe) gas laser, with a high dynamic range that can be used to measure either static or oscillatory changes of the optical path length. Small changes in optical path length are limited by the fraction of a fringe that can be measured; we can measure nonoscillatory changes with a root mean square (rms) error of the wavelength/1000 without averaging.

The photograph on the left shows the phase-shifted, laser feedback interferometer installed in a replica of the "glovebox" that was used aboard the space shuttle. The laser can be observed just behind the center panel (which was intentionally left open). To the left of the laser is a photodetector, and to the right is the electro-optic modulator (gold box) used to introduce the phase shifts. To achieve higher spatial resolution, we coupled the interferometer with a high numerical aperture objective and placed the sample to be scanned at the focus of the objective. The glovebox was suspended from elastic cords to isolate the apparatus from vibrations. The photograph on the right shows an expanded view of the electro-optic modulator, the corner cube used to bend the laser beam, and the microscope objective. A demonstration of this apparatus was recently provided at the Third Microgravity Fluid Physics Conference, and changes in the optical path length as small as 5 nanometers (nm) were readily achieved even during times of heavy pedestrian traffic.

We also combined the phase-shifted, laser feedback interferometer with a reflecting light microscope and obtained images of contours of static fluid drops on

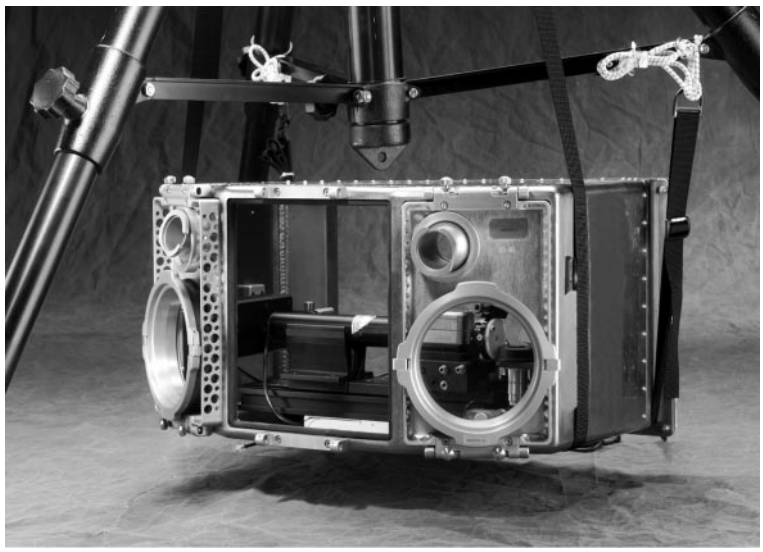

Phase-shifted, laser feedback interferometer installed in a replica of a "glovebox" used aboard the space shuttle. The light from a helium-neon laser (black cylinder) illuminates an object, which is scanned under the laser beam. The gold box between the laser and the object is a phase modulator that is used to introduce controlled phase shifts. A photodetector (black box on the far left side) is used to monitor the laser's intensity.

Scanning of an object in the interferometer. After the light leaves the phase modulator (gold box), it crosses a polarizer and is bent downward by a corner cube (glass) and focused by a microscope objective. An object is scanned across the focused laser beam to determine its topology.

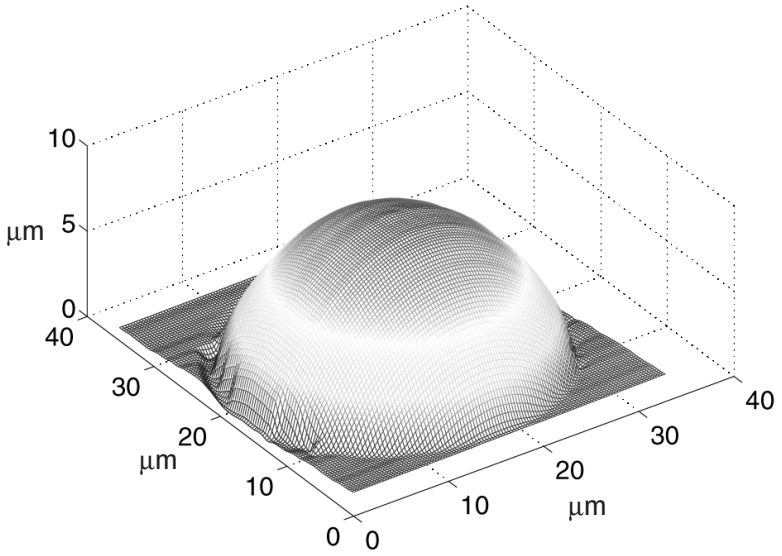

Optical path length through a silicone oil drop on a coated silicon substrate. A spherical drop has been correctly reconstructed.

coated silicone substrates. The preceding figure shows the optical path length through a silicone oil drop. This image, which was obtained by scanning the drop beneath a fixed laser beam, clearly shows the edge of the drop. We are currently pursuing the measurement of dynamic fluid-solid interfaces.

Bibliography
Ovryn, B.; and Andrews, J.H.: Phase-Shifted Laser Feedback Interferometry. Opt. Lett., vol. 23, no. 14, July 15, 1998, pp. 1078–1080.

Lewis contact:
Dr. Ben Ovryn, (216) 433–8335, Ben.Ovryn@grc.nasa.gov

Author: Dr. Ben Ovryn

Headquarters program office:
OLMSA (UG)

Programs/Projects:
Microgravity Science, ATD

Special recognition: Named Innovator of the Year 1997 by NYMA

Microgravity Experiments Being Developed for Microscopic Study of Colloidal Spheres

Microscopic spheres suspended in liquid become highly ordered under the proper conditions. Such collections of particles, called colloidal suspensions or colloids, are the subject of a series of ongoing microgravity experiments at the NASA Lewis Research Center. By studying the way these colloidal suspensions order themselves, scientists can better understand how atoms of a liquid become ordered to form a solid. In addition, highly ordered colloids have special properties that may make them useful in future high-tech applications. Work is underway at Lewis to develop an optical microscope to view these colloidal suspensions sphere by sphere in microgravity.

Previous Lewis experiments have studied the average properties and macroscopic features of colloidal suspensions using laser light scattering techniques and macrophotography. However, different techniques are needed to observe the behavior of individual spheres at specific locations within a suspension. Using a commercially available optical microscope, one can see local features and phenomena, as in the photo at the top of the next page.

The initial thrust in developing a microscope for microgravity research was to build up Lewis' expertise in applying optical microscopy to colloidal suspensions and to determine and demonstrate the core capabilities required for microgravity experiments. Many of the colloidal suspensions of interest contain 50 to 60 vol % spheres. To image beyond the surface of these high-volume-fraction colloids, one must closely match the optical index of refraction of the liquid and the spheres, rendering the spheres invisible under normal illumination. However, recently at Lewis

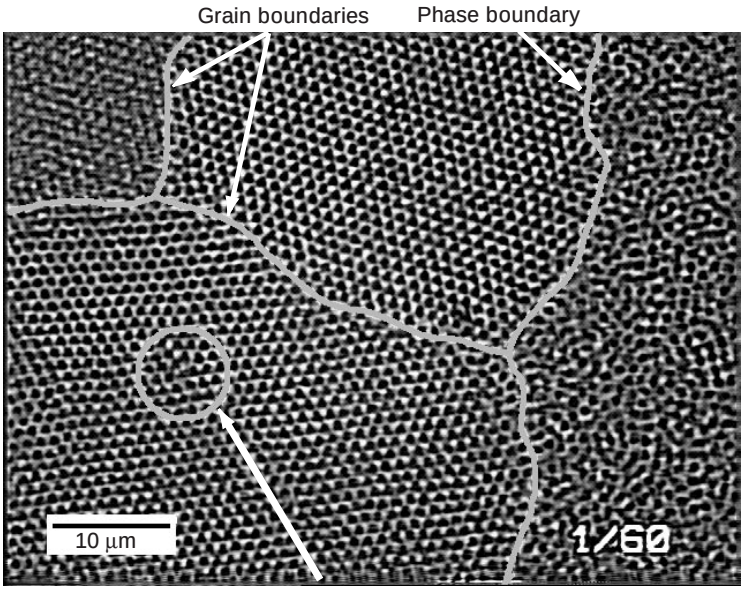

Photomicrograph illustrating various local features in a suspension of 1.0-μm-diameter spheres.

several well-established optical contrast techniques from the biological and materials science fields were combined with real-time image-processing hardware to successfully image high-volume-fraction suspensions of spheres ranging from 0.5 to 1.2 μm in diameter. Both Nomarski Differential Interference Contrast (DIC) and phase contrast techniques have produced images of colloidal crystals well beyond the walls of experiment cells. In addition, darkfield and oblique illumination techniques have been used to distinguish between colloidal crystal grains, bridging the gap between microscopic and macroscopic imaging as shown in the following figure.

NASA Lewis and Dynacs Engineering Company, Inc., engineers have begun developing concepts for the flight instrument, currently planned to be the first piece of experiment hardware in the Fluids Integrated Rack aboard the International Space Station. This microscope will support the Physics of Hard Spheres Experiment-2 (PhaSE–2; principle investigator, Paul Chaikin of Princeton University) and the Physics of Colloids in Space-2 experiments (PCS–2; principal investigator, David Weitz of the University of Pennsylvania). Current plans call for the contrast techniques described here, light-scattering optics, confocal imaging, on-orbit sample homogenization, and the capability for programmed and ground-controlled operations.

In addition to the microgravity activities just described, hardware is nearly complete for a separate series of ground-based experiments that actually depend on gravity to control the formation of colloidal crystals. These experiments, supported by the Lewis Director's Discretionary Fund (DDF), will use a fixture that allows the microscope to rotate to various angles with respect to gravity. The first use of this apparatus will be to study the sedimentation-induced growth of long, thin columns of

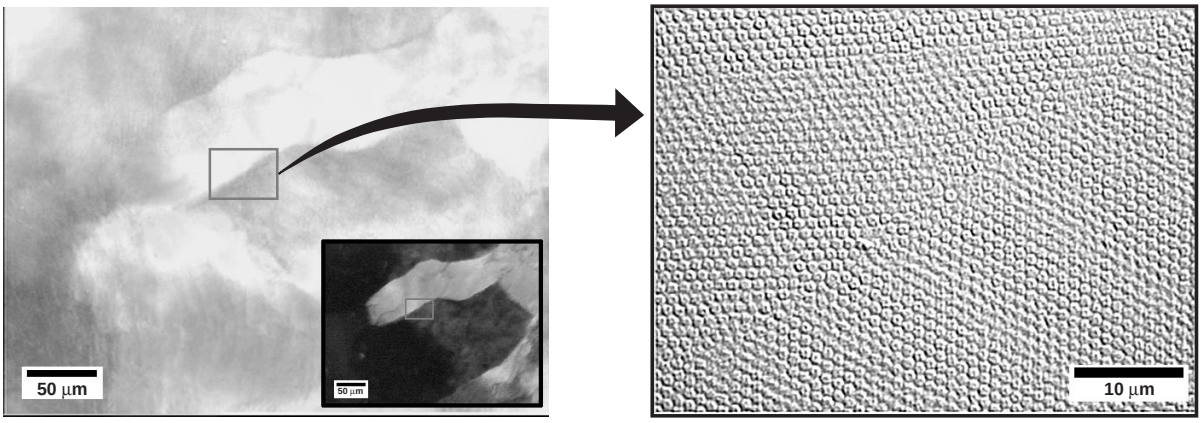

Left: Darkfield illumination. Colloidal crystal grains are delineated by color variations produced by Bragg scattering from different crystallographic planes. Inset: Oblique illumination of same region. Right: Differential Interference Contrast technique image of dark-bordered region of image on left. Note grain boundary running from lower left to upper right. The left image is shown in color in the online version of this article (http://www.grc.nasa.gov/WWW/RT1998/6000/6712rogers.htm).

colloidal crystals that bear similarities to columnar growth commonly seen in commercial metal castings. The thrust of this DDF-sponsored research is to begin applying the results of colloidal sphere experiments to a wide range of materials science topics.

Lewis contacts:
Richard B. Rogers, (216) 433–6512, Richard.B.Rogers@grc.nasa.gov; and
Michael P. Doherty, (216) 433–6641, Michael.P.Doherty@grc.nasa.gov

Author: Richard B. Rogers

Headquarters program office: OLMSA

Programs/Projects: Microgravity Science, PHASE–2, PCS–2

Onset of Convection Due to Surface Tension Variations in Multicomponent and Binary Fluid Layers

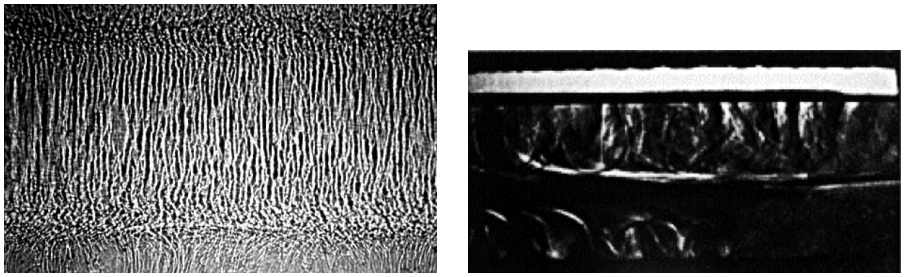

Left: Salt fingering formation. Right: Onset of double-diffusive instability (ref. 1). (Copyright Professor C.F. Chen, Univ. of Arizona; used with permission.)

Under certain conditions, such as in thin liquid films or microgravity, surface tension variations along a free surface can induce convection. Convection onset due to surface tension variation is important to many terrestrial technological processes in addition to microgravity materials processing applications. Examples include coating, drying crystallization, solidification, liquid surface contamination, and containerless processing. In double-diffusive and multicomponent systems, the spatial variations of surface tension are associated with two or more stratifying agencies, respectively. For example, both temperature and species (concentration) gradients are associated with convection in the solidification of binary alloys or salt ponds. The direction of the two (or more) gradients has a profound effect on the nature of the flow at or slightly beyond the onset of convection, as illustrated in the preceding photos. In the photo on the left, salt fingers have formed at the interface between a 10-percent sugar-water solution over a 12-percent salt-water solution. In the photo on the right, a salt-water solution, the temperature has increased from bottom to top while the salt concentration increased from top to bottom. In this case, oscillatory instability occurred via a "Hopf bifurcation," resulting in the diffusive convection pattern observed. (We are indebted to Prof. C.F. Chen for providing these photographs.) The fluid properties and operating conditions that lead to a specific convection onset behavior can be predicted from neutral stability curves and maps, like those of the remaining figures (which are shown in color in the online version of this article: http://www.grc.nasa.gov/WWW/RT1998/6000/6712skarda.htm).

Our recent work at the NASA Lewis Research Center focused on characterizing surface-tension-induced onset of convection, often referred to as Marangoni-Benard convection. Exact solutions for the stationary neutral stability of multicomponent fluid layers with interfacial deformation were derived. These solutions also permit the computation of a boundary curve that separates the long and finite wavelength instabilities, which is shown in the following graph. Computing points along this boundary using the exact solution (when possible) is more efficient than the typical numerical approaches, such as finite difference or spectral methods. Above the curve, a long wavelength instability was predicted, suggesting that convection would occur principally through one large flow cell in the layer; whereas below the curve, finite wavelength instabilities occur, which suggest multiple finite-sized circulation cells. For many common liquids with layer depths greater than 100 μm, finite wave instability is predicted under terrestrial conditions; however, with little exception, long wavelength instability is predicted in microgravity for the identical fluid systems.

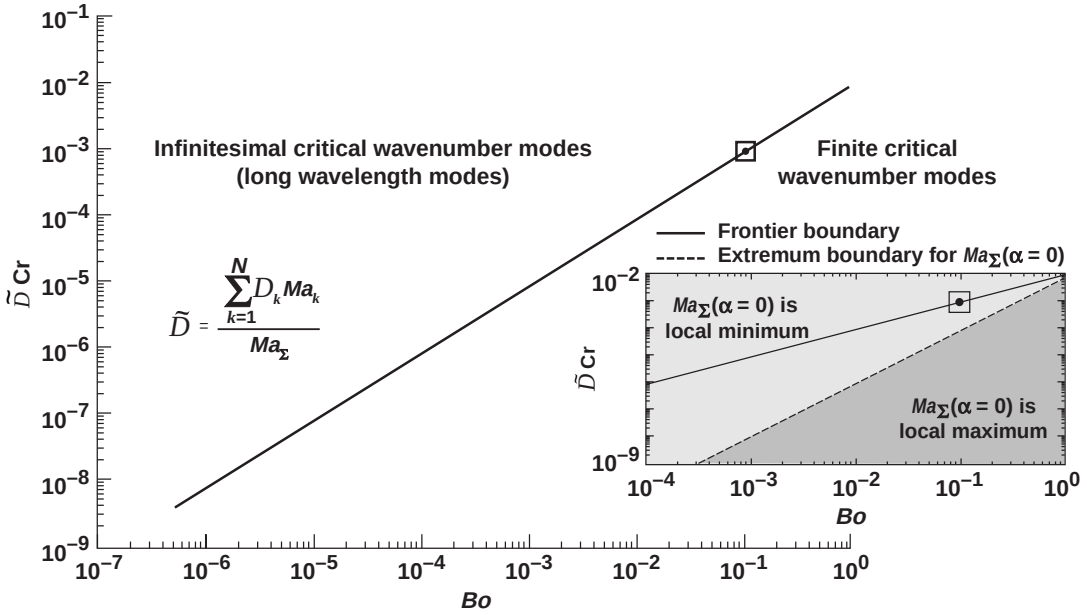

Frontier point boundaries in (Bo, $\widetilde{D}$ Cr) space. The dashed line in the insert is the extremum boundary for $Ma_\Sigma(\alpha = 0)$. Above the dashed line, $Ma_\Sigma(\alpha = 0)$ is a local minimum; below this line, it is a local maximum.

The governing equations for double-diffusive systems that include cross-diffusion, such as the Soret and Dufour effects, were rescaled for limit-zero buoyancy, and exact solutions were derived for the stationary neutral stability of these systems. An extensive investigation of stationary and oscillatory instabilities was performed. It spanned parameter values associated with binary systems, such as lead-tin alloys, to those associated with water-alcohol mixtures. Stability maps similar to the one shown in the following graph were developed to characterize the fluid behavior. Exact solutions for the location of the asymptotes, also shown in this graph, are suitable for validating the computational schemes that will ultimately be used to analyze the behavior of more complex systems.

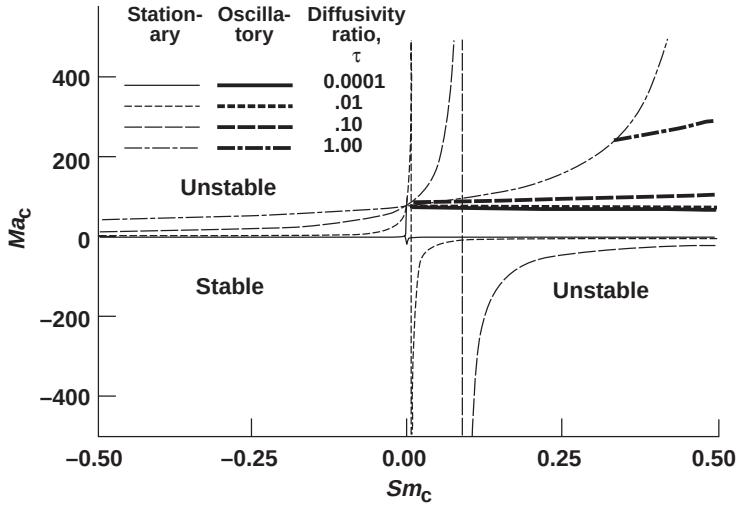

Effect of diffusivity ratio, τ, on stability maps in (Sm_c, Ma_c) space, where Sm_c and Ma_c are the critical surface tension Soret number and Marangoni number, respectively. The concentration difference is induced by an applied temperature difference. Oscillatory instability occurs above the oscillatory boundaries in the upper right quadrant.

Researchers at Lewis are also examining the response of a fluid layer to time periodic accelerations or gravity modulation. For Marangoni-Benard type convection, gravity modulation can stabilize an unstable (or destabilize a stable) unmodulated system. Results such as those in the preceding stability plots can be used to assess the sensitivity of these fluid systems to residual accelerations. The response of a double-diffusive fluid system to modulation can be more complex, exhibiting regions of quasi-periodic, subharmonic, and synchronous behavior along the neutral stability curve, as shown in the final graph. For more information and definitions of symbols used in the figures, see references 2 to 4.

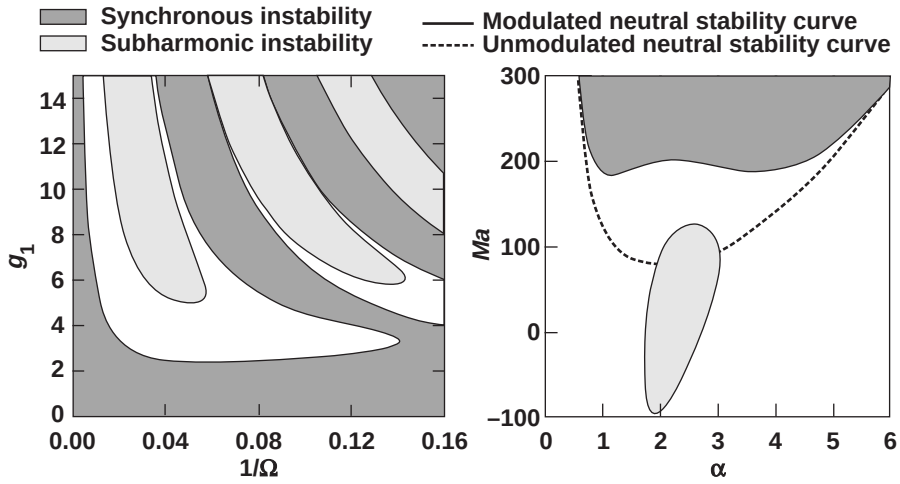

Left: Stability boundaries in (1/Ω, g_1) space; α = 2, Ra = 1000, Ma = 118.77, Pr = 1, g_o = 0. Right: Neutral stability curve; Pr = 1, g_o = 0, g_1 = 5, Ra = 1000.

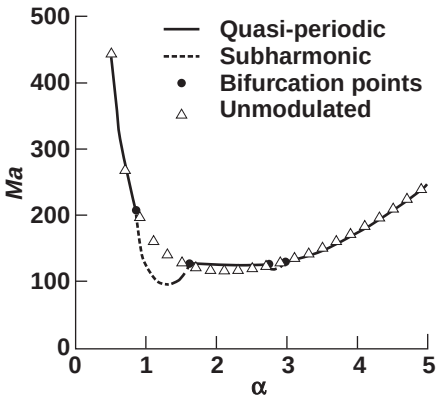

Neutral stability curves for gravity-modulated double diffusion; Ms = –700, Pr = 10, D_{22} = 0.1, Ra = 1000, g_0 = 0, g_1 = 1, Ω = 5.

References

1. Tanny, J.; Chen, C.C.; and Chen, C.F.: Effects of Interaction Between Marangoni and Double-Diffusive Instabilities. J. Fluid Mech., vol. 303, 1995, pp. 1–21.
2. Skarda, J.R.L.; Jacqmin, D.; and McCaughan, F.E.: Exact and Approximate Solutions to the Double-Diffusive Marangoni-Benard Problem With Cross-Diffusive Terms. J. Fluid Mech., vol. 366, 1998, pp. 109–133.
3. Skarda, J.R.L.; and McCaughan, F.E.: Exact Solution to Stationary Onset of Convection Due to Surface Tension Variation in a Multicomponent Fluid Layer With Interfacial Deformation. Int. J. Heat Mass Transfer, vol. 42, no. 13, 1999, pp. 2387–2398.
4. Skarda, J.R.L.: Convective Instability of a Gravity Modulated Fluid Layer With Surface Tension Variation. AIAA Paper 98–2599 (NASA TM—1998-207941), 1998.

For more information, visit us on the World Wide Web:
http://zeta.grc.nasa.gov/6712/home6712.htm
http://zeta.grc.nasa.gov/6712/people/skarda.htm

Lewis contact: Dr. J. Raymond Lee Skarda, (216) 433–8728, J.R.Skarda@grc.nasa.gov

Author: Dr. J. Raymond Lee Skarda

Headquarters program office: OLMSA

Programs/Projects:
Microgravity Fluid Physics Science

Space Acceleration Measurement System for Free Flyers

Experimenters from the fluids, combustion, materials, and life science disciplines all use the microgravity environment of space to enhance their understanding of fundamental physical phenomena caused by disturbances from events such as spacecraft maneuvers, equipment operations, atmospheric drag, and (for manned flights) crew movement. Space conditions reduce gravity but do not eliminate it. To quantify the level of these disturbances, NASA developed the Space Acceleration Measurement System (SAMS) series to collect data characterizing the acceleration environment on the space shuttles. This information is provided to investigators so that they can evaluate how the microgravity environment affects their experiments. Knowledge of the microgravity environment also helps investigators to plan future experiments.

The original SAMS system flew 20 missions on the shuttle as well as on the Russian space station Mir. Presently, Lewis is developing SAMS–II for the International Space Station; it will be a distributed system using digital output sensor heads. The latest operational version of SAMS, SAMS–FF, was originally designed for free flyer spacecraft and unmanned areas. SAMS–FF is a flexible, modular system, housed in a lightweight package, and it uses advances in technology to improve performance. The hardware package consists of a control and data acquisition module, three different types of sensors, data storage devices, and ground support equipment interfaces.

Three different types of sensors are incorporated to measure both high- and low-frequency accelerations and the roll rate velocity.

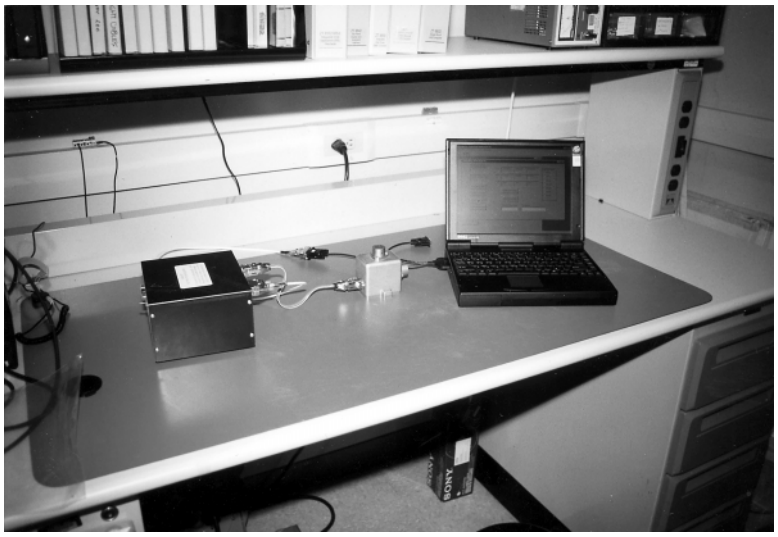

SAMS–FF–1: Implementation of TSH with laptop computer and battery.

Small, low-power triaxial sensor heads (TSH's) offer high resolution and selectable bandwidth, and a special low-frequency accelerometer is available for high-resolution, low-frequency applications. A state-of-the-art, triaxial fiber-optic gyroscope that measures extremely low roll rates is housed in a compact package.

The versatility of the SAMS–FF system is shown in the three different types of missions SAMS–FF has supported. The first mission was on a sounding rocket supporting NASA Lewis Research Center's DARTFire combustion experiment on September 10, 1997. The results indicated that a sounding rocket is a very good platform to conduct short-duration research under high-quality microgravity conditions.

A SAMS–FF TSH was used to support experiments flown on the NASA KC–135, flying parabolic arcs for low-gravity conditions. This TSH, which was utilized standalone connected to a laptop computer, served as a compact acceleration measurement system. Its small size and low power requirements allowed it to be mounted close to the area of interest.

SAMS–FF was requested by the NASA Goddard Space Flight Center to support the Hubble Space Telescope program. On STS–95, a SAMS–FF system consisting of a control and data acquisition unit and two TSH's was mounted on the Hubble Space Telescope Orbital System Test (HOST) experiment that was launched October 29, 1998. HOST was a shuttle test flight of upgraded systems for the Hubble Space Telescope, including a cryocooler for the Near Infrared Camera and Multi-Object Spectrometer (NICMOS). SAMS–FF measured the vibrations produced by the cryocooler and the ability of the vibration isolation mounts for the cooler to conduct these vibrations to the telescope. The Hubble Space Telescope has very strict requirements for a low-vibration environment. SAMS–FF was chosen to perform this task since it has small volume and weight, but high measurement resolution. The acceleration data produced by SAMS–FF were analyzed and documented by the SAMS–FF team, and the Hubble team used the report in quantifying the cryocooler vibration signature. The SAMS–FF system, which was designed and developed by Lewis and its contractors, is now manifested for support of microgravity measurement on several different platforms, including the KC–135, sounding rockets, the space shuttles, and the International Space Station (ISS).

SAMS–FF–2: TSH in hermetic enclosure.

SAMS–FF–3: Hermetically enclosed SAMS–FF system supporting HOST payload on STS–95.

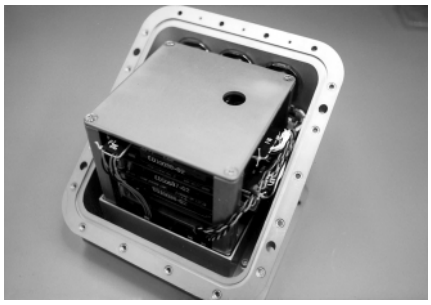

SAMS–FF–4: SAMS–FF control and data acquisition unit in hermetic enclosure.

Find out more on the World Wide Web: http://www.grc.nasa.gov/WWW/MMAP/SAMSFF

Lewis contacts:
Ronald J. Sicker, (216) 433–6498, Ronald.J.Sicker@grc.nasa.gov; and Thomas J. Kacpura, (216) 977–1057, Thomas.J.Kacpura@grc.nasa.gov

Author: Thomas J. Kacpura
Headquarters program office: OLMSA (UG)
Programs/Projects: Microgravity Science, HST, SAMS–FF

Binary Colloidal Alloy Test Conducted on Mir

Colloids are tiny (submicron) particles suspended in fluid. Paint, ink, and milk are examples of colloids found in everyday life. The Binary Colloidal Alloy Test (BCAT) is part of an extensive series of experiments planned to investigate the fundamental properties of colloids so that scientists can make colloids more useful for technological applications. Some of the colloids studied in BCAT are made of two different sized particles (binary colloidal alloys) that are very tiny, uniform plastic spheres. Under the proper conditions, these colloids can arrange themselves in a pattern to form crystals, which may have many unique properties. For example, someday these colloidal crystals may form the basis of new classes of light switches, displays, and optical devices that can fuel the evolution of the next generation of computer and communication technologies. Windows made of liquid crystals are already in the marketplace. These windows change their appearance from transparent to opaque when a weak electric current is applied. In the future, if the colloidal crystals can be made to control the passage of light through them, such products could be made much more cheaply. These experiments require the microgravity environment of space because good quality crystals are difficult to produce on Earth because of sedimentation and convection in the fluid.

The BCAT experiment hardware included two separate modules for two different experiments. The "Slow Growth" hardware consisted of a 35-mm camera with a 250-exposure photo film cartridge. The camera was aimed toward the sample module, which contained 10 separate colloid samples. A rack of small lights provided backlighting for the photographs.

The BCAT hardware was launched on the shuttle and was operated aboard the Russian space station Mir by American astronauts John Blaha and David Wolf (launched September 1996 and returned January 1997; reflown September 1997 and returned January 1998). To begin the experiment, one of these astronauts would mix the samples to disperse the colloidal particles and break up any crystals that might have already formed. Once the samples were mixed and the experiment was powered on, the hardware operated autonomously, taking photos of the colloidal samples over a 90-day period.

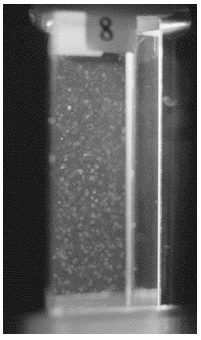

Colloidal crystal photographed by astronaut David Wolf aboard Mir, approximately 90 days after the start of the BCAT experiment.

The "Rapid Growth" hardware was set up in the Microgravity Glovebox. This experiment used a video camera with a low-magnification lens to record five separate samples. The astronauts operated the experiment by first mixing the samples and then recording each sample over a 24-hr period to monitor the colloidal behavior.

Analysis of the BCAT data is in progress and is almost complete. Results indicate that it is indeed possible to form new materials in microgravity. Some samples in the BCAT Slow Growth experiment were observed to form ordered crystalline structures in space even though they do not do so in Earth's gravity. During the BCAT Rapid Growth experiment, the colloidal structure persisted through the whole flight. The structure did not collapse as it does on Earth.

BCAT results are providing important new information about the behavior of several different colloidal systems. The investigation proved that gravity plays a central role in the formation and stability of these types of colloidal crystal structures. The investigation also helped identify the optimum conditions for the formation of colloidal crystals, which will be used for optimizing future microgravity experiments in the study of colloidal physics. Dr. David Weitz of the University of Pennsylvania and Dr. Peter Pusey of the Univer-

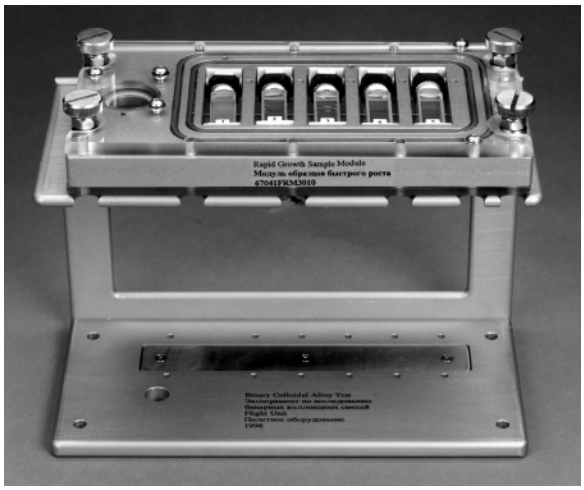

BCAT Rapid Growth hardware.

BCAT Slow Growth hardware.

sity of Edinburgh, United Kingdom, conceived the experiments. The hardware and software were designed, built, and tested by a contractor team from NYMA, Inc., and Aerospace Design & Fabrication (ADF) at the NASA Lewis Research Center in Cleveland, Ohio.

Find out more about BCAT on the World Wide Web:
http://zeta.grc.nasa.gov/expr4/bcat.htm

Find information about related research at the following web sites:
Colloidal Gelation (CGEL): http://zeta.grc.nasa.gov/expr3/cgelpage.htm
Physics of Hard Spheres Experiment (PhaSE): http://zeta.grc.nasa.gov/phase/
Physics of Colloids in Space (PCS): http://dept.physics.upenn.edu/~weitzlab/research/nasaproj.html

Lewis contacts: Rafat R. Ansari (Project Scientist), (216) 433–5008, Rafat.R.Ansari@grc.nasa.gov; and Monica I. Hoffmann (Project Manager), (216) 433–6765, Monica.I.Hoffmann@grc.nasa.gov

Authors: Monica I. Hoffmann and Rafat R. Ansari

Headquarters program office:
OLMSA (UG)

Programs/Projects:
Microgravity Science, BCAT

Coarsening in Solid-Liquid Mixtures Studied on the Space Shuttle

Ostwald ripening, or coarsening, is a process in which large particles in a two-phase mixture grow at the expense of small particles. It is a ubiquitous natural phenomena occurring in the late stages of virtually all phase separation processes. In addition, a large number of commercially important alloys undergo coarsening because they are composed of particles embedded in a matrix. Many of them, such as high-temperature superalloys used for turbine blade materials and low-temperature aluminum alloys, coarsen in the solid state. In addition, many alloys, such as the tungsten-heavy metal systems, coarsen in the solid-liquid state during liquid phase sintering. Numerous theories have been proposed that predict the rate at which the coarsening process occurs and the shape of the particle size distribution. Unfortunately, these theories have never been tested using a system that satisfies all the assumptions of the theory.

In an effort to test these theories, NASA studied the coarsening process in a solid-liquid mixture composed of solid tin particles in a liquid lead-tin matrix. On Earth, the solid tin particles float to the surface of the sample, like ice in water. In contrast, in a microgravity environment this does not occur. The microstructures in the ground- and space-processed samples (see the photos) show clearly the effects of gravity on the coarsening process. The STS–83-processed sample (right image) shows nearly spherical uniformly dispersed solid tin particles. In contrast, the identically processed, ground-based sample (left image) shows significant density-driven, nonspherical particles, and because of the higher effective solid volume fraction, a larger particle size after the same coarsening time.

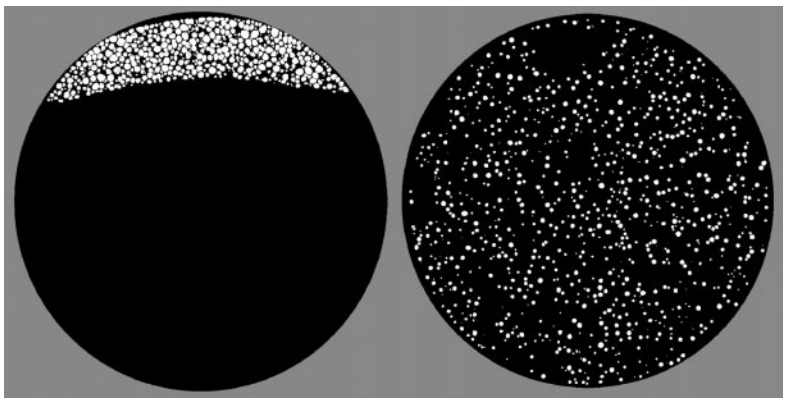

Photomicrographs of 10 vol % solid tin phase taken after samples were held 10 hr at 185 °C. Left: Ground experiment results show significant density-driven sedimentation and nonspherical particles. Because of the compacting of the particles (effective higher solid volume fraction) the coarsening rate was artificially increased and the result was a larger particle size. Right: STS–83 microgravity results show spherical, uniformly dispersed solid tin particles in a lead tin eutectic.

The "Coarsening in Solid-Liquid Mixtures" (CSLM) experiment was conducted in the Middeck Glovebox facility (MGBX) flown aboard the shuttle in the Microgravity Science Laboratory (MSL–1/1R) on STS–83/94. The primary objective of CSLM is to measure the temporal evolution of the solid particles during coarsening. The particles were coarsened four times from 0 sec to 24 hours after a 9-min heat-up to 185 °C.

Quantitative analysis of the samples with a volume fraction of 10 percent solid is yielding data that are as spectacular as the microstructures. The data are so good that the kinetics and particle size distribution can be determined with unprecedented accuracy. CSLM has provided the first careful test of theory of Ostwald ripening by conducting the study at low solid volume fractions with the solids uniformly distributed in the sample.

CSLM hardware was developed and built jointly by the NASA Lewis Research Center and NYMA, Inc. CSLM has been selected for additional flight experiments as well as continued ground studies. Several new evaluation techniques have been developed, and numerous research papers have been published from this study by the principal investigator, Prof. Peter W. Voorhees, and his team.

For more information, visit us on the World Wide Web: http://zeta.grc.nasa.gov/cslm/cslmrslt.htm

Lewis contact:
John J. Caruso, (216) 433–3324, John.J.Caruso@grc.nasa.gov

Author: John J. Caruso

Headquarters program office:
OLMSA (UG)

Programs/Projects:
HEDS, Microgravity Science, STS–83, STS–94, MSL–1, MSL–1R, CSLM

Third and Final Shuttle Mission of the Isothermal Dendritic Growth Experiment Conducted—Highest Supercooling Ever Recorded Achieved

Dendrites describe the treelike crystal morphology commonly assumed in metals and alloys that freeze from supercooled or supersaturated melts. There remains a high level of engineering interest in dendritic solidification because the size, shape, and orientation of the dendrites determine the final microstructure of a material. It is the microstructure that then determines the physical properties of cast or welded products.

Although it is well known that dendritic growth is controlled by the transport of latent heat from the moving solid-liquid interface, an accurate and predictive model has not yet been developed. The effects of gravity-induced convection on the transfer of heat from the interface have prevented adequate testing, under terrestrial conditions, of solidification models.

The Isothermal Dendritic Growth Experiment (IDGE) constituted a series of three microgravity experiments flown aboard the Space Shuttle Columbia. The apparatus was used to grow and record dendrite solidification in the absence of gravity-induced convective heat transfer, thereby producing a wealth of benchmark-quality data for testing solidification models and theories. The principal investigator is Prof. Martin E. Glicksman

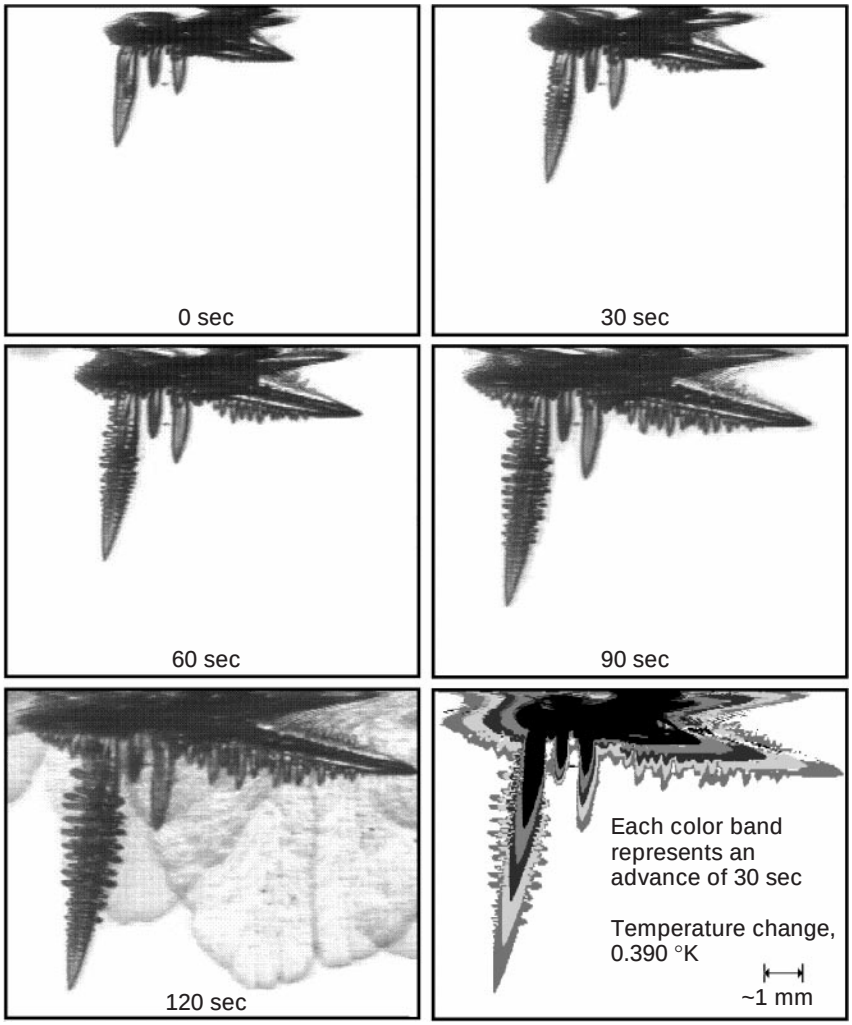

Time-elapsed photographic sequence of a PVA dendrite grown during the STS–87 mission. This figure is shown in color in the online version of this article (http://www.grc.nasa.gov/WWW/RT1998/6000/6728malarik.htm).

of Rensselaer Polytechnic Institute in Troy, New York. The project is managed by the Microgravity Sciences Division at the NASA Lewis Research Center and is supported by a contractor team of engineers and technicians employed by Aerospace Design & Fabrication (ADF), Inc., under subcontract to the NYMA, Inc.

The first two flights of IDGE (STS–62 and STS–75) aboard the Second and Third United States Microgravity Payload (USMP–2 and –3) used ultrapure succinonitrile (SCN) as the test material. SCN is an organic crystal that mimics the solidification of body-centered-cubic metals, such as ferrous metals. The third and final IDGE flight (USMP–4), which was launched on STS–87 in November 1997, employed a different test material. This flight used pivalic acid (PVA)—a face-centered-cubic organic crystal that solidifies like many nonferrous metals. PVA, like SCN, has convenient properties, such as its transparent nature and its low melting point, that make it ideal for conducting benchmark experiments. Because a different sample was used, the universality of solidification theories could be tested.

The third and final flight of IDGE was a resounding success. Dendritic growths were obtained across the full range of supercooling required. In fact, during the mission, a growth was achieved at the high end of the supercooling range, 1.25 K—something never before accomplished even under terrestrial conditions. The data and subsequent analysis from the final flight experiment are currently at a preliminary stage. Thus far, the results indicate that dendritic growth in PVA is (as in SCN) diffusion-limited, with little, if any, kinetic response. This observation conflicts with the conclusion reached by other investigators that there are large interfacial kinetic effects in PVA.

In addition to the investigation of dendritic solidification kinetics and morphology, the IDGE has been part of the development of remote, university-based teleoperations. These teleoperation tests point the way to the future of microgravity science operations on the International Space Station (ISS). NASA Headquarters and the Telescience Support Center at Lewis set a goal for developing the experience and expertise to set up remote, non-NASA locations from which to control space station experiments. Recent IDGE space shuttle flights provide proof-of-concept and tests of remote space flight teleoperations.

The IDGE flight series is now complete. The principal investigator and his team are currently completing analyses and moving toward final data archiving. The IDGE published results and archived data sets are being used actively by other scientists and engineers. In fact, they have been referenced in the classroom by a graduate-level instructor at Case Western Reserve University. In addition, the techniques and IDGE hardware systems that were

developed are being employed for future dendritic growth flight experiments.

Find out more about this research on the World Wide Web:
http://www.rpi.edu/locker/56/000756

Lewis contacts: Diane C. Malarik (Project Manager), (216) 433–3203, Diane.C.Malarik@grc.nasa.gov; Terri D. Rodgers (Deputy Project Manager), (216) 433–8740, Terri.D.Rodgers@grc.nasa.gov; and Dr. Francis D. Chiaramonte (Project Scientist), (216) 433–8040, Francis.D.Chiaramonte@grc.nasa.gov

Author: Diane C. Malarik

Headquarters program office: OLMSA

Programs/Projects: Microgravity Science

Tracker—Image-Processing and Object-Tracking System Developed

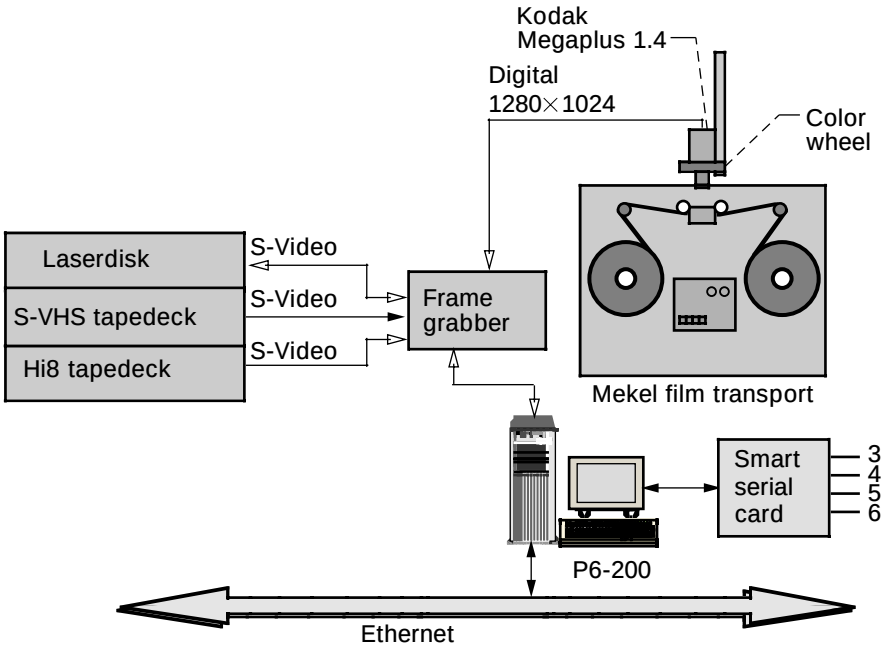

Object-tracking system hardware layout.

Tracker is an object-tracking and image-processing program designed and developed at the NASA Lewis Research Center to help with the analysis of images generated by microgravity combustion and fluid physics experiments. Experiments are often recorded on film or videotape for analysis later. Tracker automates the process of examining each frame of the recorded experiment, performing image-processing operations to bring out the desired detail, and recording the positions of the objects of interest. It can load sequences of images from disk files or acquire images (via a frame grabber) from film transports, videotape, laser disks, or a live camera. Tracker controls the image source to automatically advance to the next frame. It can employ a large array of image-processing operations to enhance the detail of the acquired images and can analyze an arbitrarily large number of objects simultaneously. Several different tracking algorithms are available, including conventional threshold and correlation-based techniques, and more esoteric procedures such as "snake" tracking and automated recognition of character data in the image. The Tracker software was written to be operated by researchers, thus every attempt was made to make the software as user friendly and self-explanatory as possible.

Tracker is used by most of the microgravity combustion and fluid physics experiments performed by Lewis, and by visiting researchers. This includes experiments performed on the space shuttles, Mir, sounding rockets, zero-g research airplanes, drop towers, and ground-based laboratories. This software automates the analysis of the flame or liquid's physical parameters such as position, velocity, acceleration, size, shape, intensity characteristics, color, and centroid, as well as a number of other measurements. It can perform these operations on multiple objects simultaneously. Another key feature of Tracker is that it performs optical character recognition (OCR). This feature is useful in extracting numerical instrumentation data that are

embedded in images. All the results are saved in files for further data reduction and graphing.

There are currently three Tracking Systems (workstations) operating near the laboratories and offices of Lewis' Microgravity Science Division researchers. These systems are used independently by students, scientists, and university-based principal investigators. The researchers bring their tapes or films to the workstation and perform the tracking analysis. The resultant data files generated by the tracking process can then be analyzed on the spot, although most of the time researchers prefer to transfer them via the network to their offices for further analysis or plotting. In addition, many researchers have installed Tracker on computers in their office for desktop analysis of digital image sequences, which can be digitized by the Tracking System or some other means. Tracker has not only provided a capability to efficiently and automatically analyze large volumes of data, saving many hours of tedious work, but has also provided new capabilities to extract valuable information and phenomena that was heretofore undetected and unexploited.

Find out about Tracker on the World Wide Web:
http://zeta.grc.nasa.gov/Tracker/Tracker.html

Lewis contacts: Robert B. Klimek, (216) 433–2837, Robert.B.Klimek@grc.nasa.gov; and Dr. Theodore (Ted) W. Wright, (216) 433–5341, Theodore.W.Wright@grc.nasa.gov

Authors: Robert B. Klimek and Dr. Theodore W. Wright

Headquarters program office: OLMSA (UG)

Programs/Projects:
Microgravity Science, Investigations of the behavior of flames and fluids: ***On the shuttles and Mir—***SSCE, CFM, WIF, ICE, FSDC, FFFT, RITSI, DCE, CHT, LSP, ELF, TGDF, ALB, OFFS, Behavior of Rapidly Sheared Bubbly Suspensions, TIGER–3D, SIBAL ***On sounding rockets—***SAL, DARTFire ***In aircraft and ground-based facilities—***Measurement of Flame Temperatures in Reduced-Gravity and other combustion experiments, Bubble Formation and Detachment in Cross Liquid Flow Under Reduced and Normal Gravity and other fluid behavior experiments, General Motors R&D Center, Engine Research Department

Special recognition:
NASA Tech Brief; runnerup for NASA Software of the Year award

Engineering and Technical Services

Computer Services

NASA Lewis Launch Collision Probability Model Developed and Analyzed

There are nearly 10 000 tracked objects orbiting the Earth. These objects encompass manned objects, active and decommissioned satellites, spent rocket bodies, and debris. They range from a few centimeters across to the size of the MIR space station. Anytime a new satellite is launched, the launch vehicle with its payload attached passes through an area of space in which these objects orbit. Although the population density of these objects is low, there always is a small but finite probability of collision between the launch vehicle and one or more of these space objects. Even though the probability of collision is very low, for some payloads even this small risk is unacceptable.

To mitigate the small risk of collision associated with launching at an arbitrary time within the daily launch window, NASA performs a prelaunch mission assurance Collision Avoidance Analysis (or COLA). For the COLA of the Cassini spacecraft, the NASA Lewis Research Center conducted an in-house development and analysis of a model for launch collision probability. The model allows a minimum clearance criteria to be used with the COLA analysis to ensure an acceptably low probability of collision. If, for any given liftoff time, the nominal launch vehicle trajectory would pass a space object with less than the minimum required clearance (see the following figure), launch would not be attempted at that time.

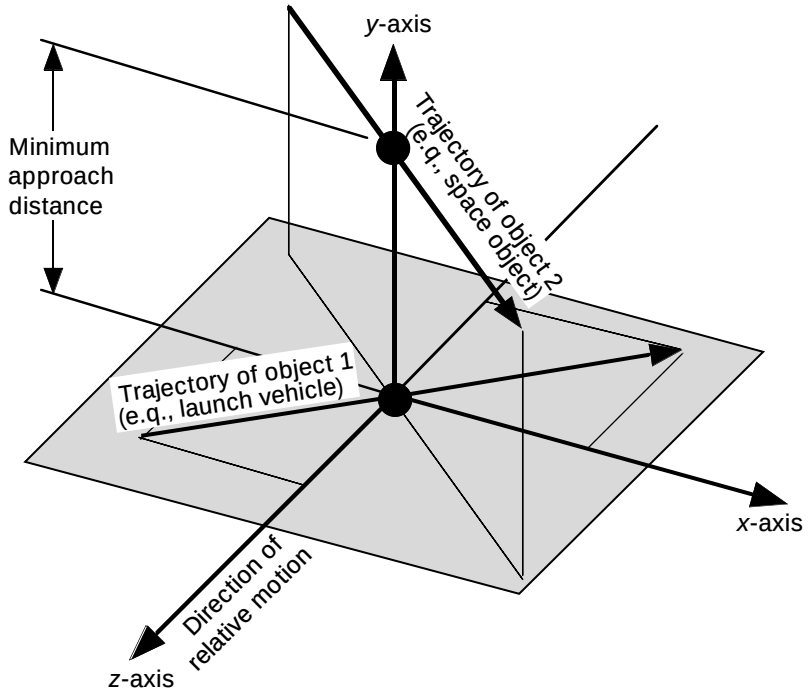

Launch vehicle and orbiting object nominal trajectories and miss distance.

The model assumes that the nominal positions of the orbiting objects and of the launch vehicle can be predicted as a function of time, and therefore, that any tracked object that comes within close proximity of the launch vehicle can be identified. For any such pair, these nominal positions can be used to calculate a nominal miss distance. The actual miss distances may differ substantially from the nominal miss distance, due, in part, to the statistical uncertainty of the knowledge of the objects' positions. The model further assumes that these position uncertainties can be described with position covariance matrices. With these, and some additional simplifying assumptions, a closed-form solution for the probability of collision is obtained. This solution provides clear insights into how each of the independent parameters affects the probability of collision. It shows that for a given maximum probability of collision and prior knowledge of the objects' position uncertainties and sizes, only knowledge of the nominal closest approach distance is required to make the launch/no launch decision.

The model was completed and used for the mission assurance COLA analysis for the Cassini spacecraft, which was launched on a Titan IV/Centaur rocket on October 15, 1997. Although the model was specifically developed for the Cassini mission, it is clearly applicable for other launches as well.

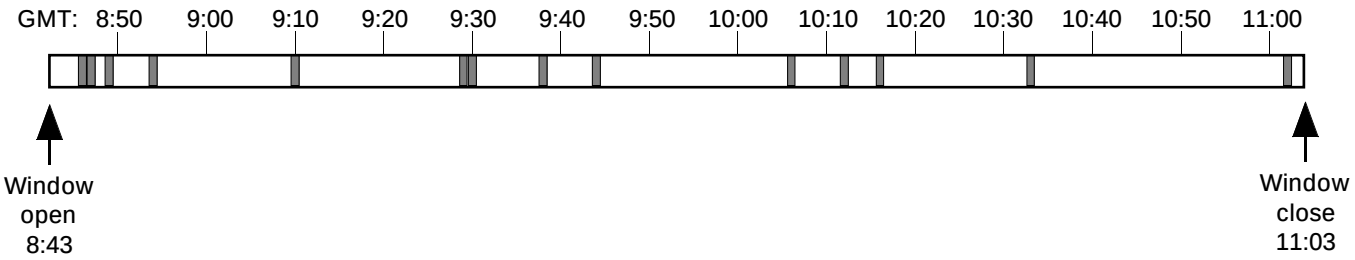

October 15 Cassini launch window (launch was not allowed in darkened areas because of the risk of collision). GMT, Greenwich Mean Time.

This figure illustrates the effect of COLA closures on the launch window. The bar represents the entire 140-min launch window on October 15, 1997; the blackened areas represent the loss of launch opportunities due to the potential for a collision with an orbiting object.

Find out more on the World Wide Web:

Launch vehicle history: http://www.grc.nasa.gov/WWW/PAO/html/lvpo.htm
Cassini: http://www.jpl.nasa.gov/cassini

Bibliography

Bollenbacher, G.; and Guptill, J.D.: Launch Collision Probability. NASA TP—1999-208852, 1999.

Lewis contacts:
Gary Bollenbacher, (216) 433–2276, Gary.Bollenbacher@grc.nasa.gov; and James D. Guptill, (216) 433–5213, James.D.Guptill@grc.nasa.gov

Authors:
Gary Bollenbacher and James D. Guptill

Headquarters program office: OSF

Programs/Projects: Cassini

Manufacturing Engineering

Customized Hermetic Feedthrough Developed to Isolate Fluids

A common problem occurs when refrigerant fluids wick inside the insulation of thermocouple wires through a compressor's casing feedthrough and then leak into the adjacent disconnect box outside the casing. Leaking fluids create an unfavorable situation inside the disconnect box and may contaminate the fluids. To address this problem, NASA Lewis Research Center's Manufacturing Engineering Division developed a customized hermetic feedthrough for a bank of Worthington compressors.

In these compressors, bearing temperatures are measured by internal thermocouples embedded in bearings located inside the compressor casings. The thermocouple wires need to be routed outside the casing and read at

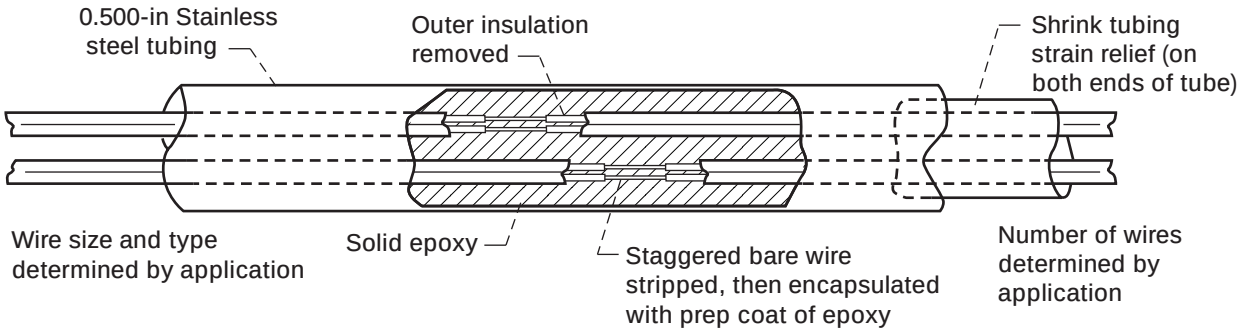

Cutaway diagram of a customized hermetic feedthrough.

another location. These wires are short and are terminated to a disconnect strip inside the casing. The bearings operate at about 170 °F, but because the casing is filled with R12 refrigerant oil, the casing has a maximum temperature of about 100 °F.

The operating conditions of these compressors permit the use of an epoxy that is compatible with the R12 fluid. The desired finished product is a stainless steel tube that has been filled solid with epoxy after thermocouple wires bonded and sealed by epoxy have been inserted through its length. Shrink tubing extends from both ends of the tube. The process that was developed to isolate the thermocouple wires from the R12 fluid follows.

For this application, use an 8-in.-long piece of 0.500-in. 304 stainless steel tube with six pairs of 24-gauge stranded, PTFE-insulated (polytetrafluoroethylene) type "T" thermocouple wires for each feedthrough. Use shrink tubing to strain relief the insulated wires at their exit from the stainless steel tube.

Cut the wire to length and identify the location of the stainless steel tube sleeve with masking tape. Then, remove the outer insulation from a 2-in. section of wire that will be inside the tube, and carefully strip to bare wire a 1-in. section in the middle of the section with the outer insulation removed. For an effective seal, the epoxy must penetrate between the strands when stranded conductors are used. Make the seal with epoxy bond on the bare wire. The bare wire must be encapsulated with a thin layer of the epoxy that leaves only a very low profile. These encapsulated wires must cure before the assembly can be continued. Then, inspect the cured wires for complete encapsulation before going to the next step.

Insert the wires in the stainless steel tube and orient them so that the epoxied stripped sections are staggered within the tube (see the illustration); then, apply shrink tubing to one end of the cleaned wires, positioning it inside the edge of the tube. The small gaps between the wires on the other end will be used to inject the epoxy into the tube. Let the epoxy cure inside the tube, free of any voids. Then, continue to fill the tube until the entire 8-in. length is nearly filled, allowing room for the other strain-relieving shrink tubing.

Since this first design, the process has been adjusted to fit many needs and situations. Customized feedthroughs have been assembled from various wire types, wire gauges, and/or stainless steel tube passages. The fittings selected to mount these feedthroughs allow their use in other areas, such as pressure or vacuum systems.

Lewis contact:
Roger D. Meredith, (216) 433–2103, Roger.D.Meredith@grc.nasa.gov

Author: Roger D. Meredith

Headquarters program office: OAT

Programs/Projects:
Turbomachinery and combustion research, wind tunnel research

Engineering Design and Analysis

Pyroshock Environments Characterized for Spacecraft Missions

Pyrotechnic shock, or pyroshock, is the transient response of a structure to loading induced by the ignition of pyrotechnic (explosive or propellant activated) devices. These devices are typically used to separate structural systems (e.g., separate a spacecraft from a launch vehicle) and deploy appendages (e.g., solar panels). Pyroshocks are characterized by high peak acceleration, high-frequency content, and short duration. Because of their high acceleration and high-frequency, pyroshocks can cause spaceflight hardware to fail. Verifying by test that spaceflight hardware can withstand the anticipated shock environment is considered essential to mission success.

The Earth Observing System (EOS) AM–1 spacecraft for NASA's Mission to Planet Earth is scheduled to be launched on an Atlas IIAS vehicle in 1999, and the NASA Lewis Research Center is the launch vehicle integrator for this NASA Goddard Space Flight Center spacecraft. The EOS spacecraft was subjected to numerous ground

EOS spacecraft following shock separation testing at Lockheed Martin Missiles & Space, Valley Forge, Pennsylvania.

shock tests to verify that its scientific instruments and avionics components will withstand the shock-induced vibration produced when the spacecraft separates from the launch vehicle. Shock test data from these tests represent the third largest available pyroshock data base in the United States. Future spacecraft missions will directly benefit from the knowledge gained from these tests.

The payload separation system used for EOS is a new system that operates by firing six separation nuts. This system was tested to verify its functional operation and to characterize the resulting shock levels. The launch vehicle contractor (Lockheed Martin Astronautics) and spacecraft contractor (Lockheed Martin Missiles & Space) completed 16 separation test firings. This resulted in an unusually large amount of pyroshock data. Typically, only one or two pyroshock test firings are performed for a spacecraft mission.

Because of the size of this separation system shock data base, engineers were able to perform unique statistical analyses to characterize the distribution of the test data. For example, it was proven that the shock data follow a lognormal distribution, a concept often assumed but rarely proven. The test-to-test repeatability of the shock source level was analyzed, and the effects of various test configurations and separation nut production lots were examined and quantified.

Engineers investigated the change in shock level as the shock traveled from the spacecraft separation interface to the avionics components of the upper stage and analyzed the effects of the structural fidelity (simulator versus real) of the components and their weight on vibrational response. In addition, the shock attenuation with distance and across joints was quantified and compared with concepts originally generated in 1970, and the effects of separation nut preload and firing sequences effects were examined.

Because of this EOS shock testing and the analyses performed at NASA Lewis, a significant amount of new information on pyroshock and its characteristics is now available to the aerospace industry. We hope that this information will help future spacecraft test planners to perform better and cheaper spacecraft separation shock tests and to better understand their test data.

Find out more about EOS on the World Wide Web:
http://eos-am.gsfc.nasa.gov/spacecraft.html
http://eospso.gsfc.nasa.gov
http://www.earth.nasa.gov/

Bibliography

Hughes, W.O.; and McNelis, A.M.: Statistical Analysis of a Large Sample Size Pyroshock Test Data Set. NASA TM—1998-206621, 1998.

Hughes, W.O.; and McNelis, A.M.: Characterization of the Pyroshock Environment for the EOS Mission, Proceedings of the 44th IES Annual Technical Meeting of the Institute of Environmental Sciences and Technology, Mount Prospect, IL, 1998, pp. 93–104.

Lewis contacts: William O. Hughes, (216) 433–2597, William.O.Hughes@grc.nasa.gov; and Anne M. McNelis, (216) 433–8880, Anne.M.McNelis@grc.nasa.gov

Authors: William O. Hughes and Anne M. McNelis

Headquarters program office: OES

Programs/Projects: MTPE, EOS

Traversing Microphone Track Installed in NASA Lewis' Aero-Acoustic Propulsion Laboratory Dome

The Aero-Acoustic Propulsion Laboratory is an acoustically treated, 65-ft-tall dome located at the NASA Lewis Research Center. Inside this laboratory is the Nozzle Acoustic Test Rig (NATR), which is used in support of Advanced Subsonics Technology (AST) and High Speed Research (HSR) to test engine exhaust nozzles for thrust and acoustic performance under simulated takeoff conditions. Acoustic measurements had been gathered by a far-field array of microphones located along the dome wall and 10-ft above the floor. Recently, it became desirable to collect acoustic data for engine certifications (as specified by the Federal Aviation Administration (FAA)) that would simulate the noise of an aircraft taking off as heard from an offset ground location. Since nozzles for the High-Speed Civil Transport have straight sides that cause their noise signature to vary radially, an additional plane of acoustic measurement was required. Desired was an arched array of 24 microphones, equally spaced from the nozzle and each other, in a 25° off-vertical plane.

The various research requirements made this a challenging task. The microphones needed to be aimed at the nozzle accurately and held firmly in place during testing, but it was also essential that they be easily and routinely lowered to the floor for calibration and servicing. Once serviced, the microphones would have to be returned to their previous location near the ceiling. In addition, there could be no structure between the microphones and the nozzle, and any structure near the microphones would have to be designed to minimize noise reflections. After many concepts were considered, a single arched truss structure was selected that would be permanently affixed to the dome ceiling and to one end of the dome floor.

This structure, which was mostly installed in November 1997, forms a track on which each microphone rides on its own "carriage." The 150-ft-long, roller-coaster-like track consists of three 1-in.-diameter tubular rails, a 4-in.-diameter structural tube, diagonal stiffeners, and web plates that hold the components together. Twenty-four carriages constructed of light aluminum tubing traverse in series along the track. Each carriage engages all three rails and is shaped like a tripod, with wheels at each leg to provide complete support to each microphone. This configuration also allows each carriage to nest into the next when the microphones are brought to the ground for calibration and servicing. As a tow cable attached to the lead carriage is pulled up by a winch on the ground, the other carriages follow in series and are properly spaced along the cable. The tow cable is guided along the truss by rollers on each web. Most of the wheels and rollers are roller-skate wheels—a likely choice because of their rugged urethane construction (like that of the roller-coaster wheels used at the Cedar Point amusement park in Sandusky, Ohio), integral dual ball bearings, and availability.

Each microphone extends from its carriage on a "stinger" tube. These stingers can be offset from the carriage enough to place the microphones in different planes, up to 5° to either side of the 25° track plane, extending the research capability of the system. This new traversing microphone system will greatly increase the amount of valuable research data that can be collected during future nozzle tests in this already highly productive research facility.

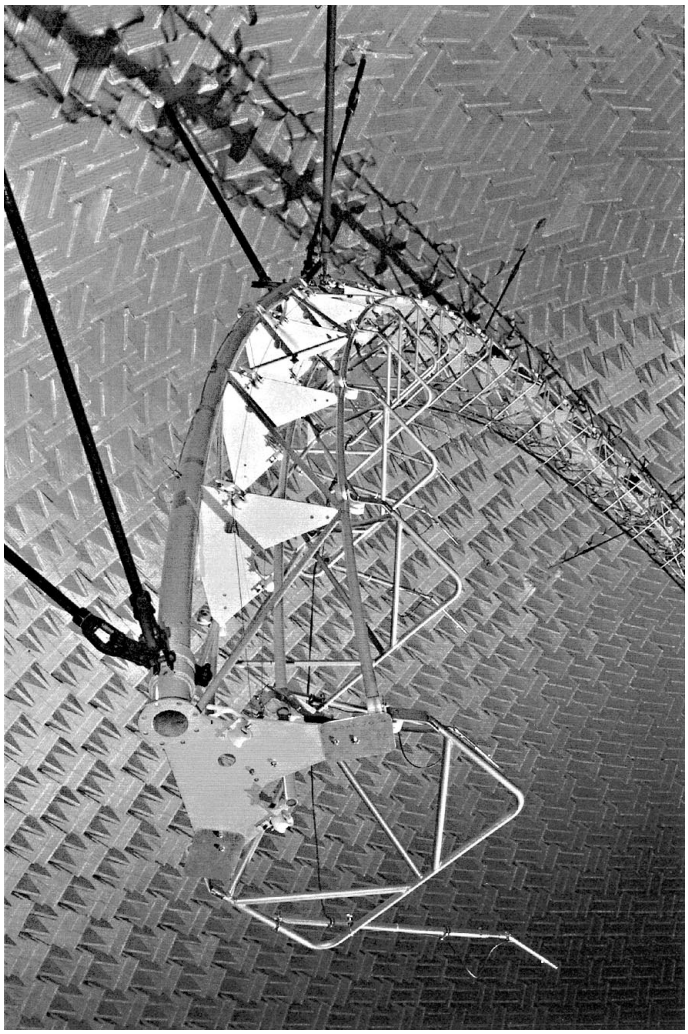

Traversing microphone track assembly in Lewis' Aero-Acoustic Propulsion Laboratory.

Find out more about the AAPL facility on the World Wide Web:

http://www.grc.nasa.gov/WWW/Aapl/traverse.htm
http://www.grc.nasa.gov/WWW/AFED/facilities/aapl.html
http://www.grc.nasa.gov/WWW/Aapl/traverse.htm

Lewis contacts:
Steven W. Bauman, (216) 433–3826, Steven.W.Bauman@grc.nasa.gov, and Gail P. Perusek, (216) 433–8729, Gail.P.Perusek@grc.nasa.gov

Authors:
Steven W. Bauman and Gail P. Perusek

Headquarters program office: OAT

Programs/Projects: Propulsion Systems R&T, HSR, HSCT, AST

Virtual Interactive Classroom: A New Technology Developed for Distance Learning

The Virtual Interactive Classroom (VIC) allows Internet users, specifically students, to remotely control and access data from scientific equipment. This is a significant advantage to school systems that cannot afford experimental equipment, have Internet access, and are seeking to improve science and math scores with current resources. The VIC concept was initially identified as an application of Embedded Web Technology in June of 1997. VIC uses the 1998 NASA Software of the Year Award winner, *Tempest*, an embedded web server developed at the NASA Lewis Research Center (ref. 1). VIC and *Tempest* were developed by the same civil servant team at Lewis.

A VIC Development Lab was established at Lewis to demonstrate that scientific equipment can be controlled by remote users over the Internet. Current projects include a wind tunnel, a room camera, a science table, and a microscope:

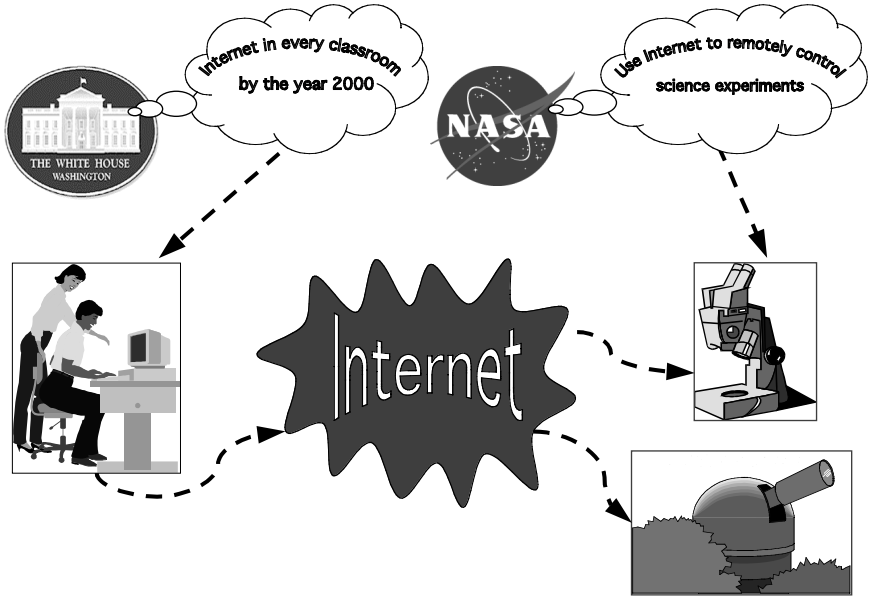

Virtual Interactive Classroom concept. Lewis' Virtual Interactive Classroom leverages the vision of "Internet in every classroom," allowing students to remotely control scientific experiments.

• The wind tunnel project accesses the 6- by 6-in. laminar flow test section of a research-grade wind tunnel. Users can read pressure transducers located in the upper and lower surfaces of a wing as well as an airflow transducer in the test section. Remote users can turn the airflow on and off, set wind velocity, adjust the wing angle of attack, and read the pressure values.

• The room camera project uses a charge-coupled discharge (CCD) device mounted to a pan/tilt mechanism. Users can control the pan, tilt, zoom, and focus. The image received by the user is refreshed at regular intervals.

• The science table project includes a horizontal surface with a two-axis servomechanism that positions a color camera. The table has interchangeable surfaces. Several surfaces are available with fossils, Native American artifacts, geology samples, and antique tools. The user, from any remote location, can select a specific position for the camera and retrieve either high-speed or high-quality images in real time.

• The microscope comprises a two-axis servomechanism that positions a microscope camera and lens, and a microscope slide holder that can contain up to 360 slides. Remote users can position the microscope over any of the slides in the holder and download high-quality color images.

Metrics are being collected, as well as feedback from users, to determine the desirability, popularity, and educational benefits of each project. Modifications will be made in response to user feedback. After the projects have been developed and tested, they will be duplicated at remote VIC Operations Labs. These labs may be owned and/or operated by institutions of learning. Students will be able to operate these remote labs to learn about the Internet or study the subjects made available by VIC projects. These opportunities are directly related to careers in science and engineering.

Find out more about Lewis' Virtual Interactive Classroom on the World Wide Web:
Learning Technologies Project:
http://www.grc.nasa.gov/WWW/K-12/
Embedded Web Technology:
http://vic.grc.nasa.gov/

Reference

1. Daniele, C.J.: Embedded Web Technology: Internet Technology Applied to Real-Time System Control. Research & Technology 1997, NASA TM—98-206312, 1998, pp. 165–166. (Available online: http://www.grc.nasa.gov/WWW/RT1997/7000/7750daniele.htm)

Lewis contacts:
David W. York, (216) 433–3162, David.W.York@grc.nasa.gov;
Maria Babula, (216) 433–5221, Maria.Babula@grc.nasa.gov;
Lisa M. Lambert, (216) 433–3994, Lisa.M.Lambert@grc.nasa.gov; and
Joseph G. Ponyik, (216) 433–8592, Joseph.G.Ponyik@grc.nasa.gov

Authors:
David W. York and Maria Babula

Headquarters program office:
OLMSA, External Programs

Programs/Projects:
SEMAA, LTP, FCF, EWT

Special Recognition: *Tempest* received the 1998 NASA Software of the Year Award.

Commercial Technology

Silicon Carbide Being Developed for High-Definition Television Transmitter Modules

Through a Space Act Agreement, the NASA Lewis Research Center has helped develop the base silicon carbide (SiC) epitaxial growth technology for Westinghouse's efforts to bring silicon carbide products to the marketplace. SiC is a high-temperature, high-voltage semiconductor that can deliver greater than three times the power of conventional silicon devices. The technology was initially disclosed in the 1994 R&T report (refs. 1 to 3). NASA Lewis' High Temperature Integrated Electronics and Sensors (HTIES) team is developing SiC as a material for advanced semiconductor electronic device applications because SiC-based electronics and sensors can operate in hostile environments where conventional silicon-based electronics cannot function.

SiC transmitters hold great promise for television stations because they can convert broadcasts from analog to digital signals. A modular solid-state design provides broadcasters with an option to gradually add modules, increasing the power of their transmitters as they expand their high-definition television (HDTV) coverage. Using these high-power transistors will significantly reduce the space needed for high-power transmitters at television stations and will offer a solid-state solution, reducing long-term maintenance costs. Thus, transmitter manufacturers will be able to abandon their reliance on tube-based technology for high-power transmitters and will be able to build smaller, high-power, solid-state transmitters.

Find out more about this research on the World Wide Web:
http://www.grc.nasa.gov/WWW/SiC/SiC.html

References

1. Neudeck, P.G.; and Powell, J.A.: Performance-Limiting Micropipe Defects Identified in SiC Wafers. Research & Technology 1994, NASA TM–106764, 1995, p. 8. (Available online: http://www.grc.nasa.gov/WWW/RT1994/Aeronautics/02Instrumentation.html)
2. Neudeck, P.G.; and Larkin, D.J.: Silicon Carbide Junction Field-Effect Transistors Developed. Research & Technology 1994, NASA TM–106764, 1995, pp. 10–11. (Available online: http://www.grc.nasa.gov/WWW/RT1994/Aeronautics/02Instrumentation.html)
3. Larkin, D.J., et al.: Site-Competition Epitaxy Controls Doping of Silicon Carbide. Research & Technology 1994, NASA TM–106764, 1995, pp. 11–12. (Available online: http://www.grc.nasa.gov/WWW/RT1994/Aeronautics/02Instrumentation.html)

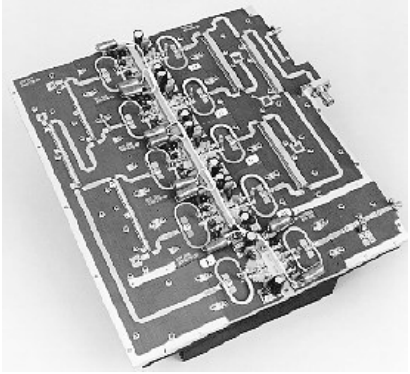

SiC transmitter module.

Lewis contacts:
Donald E. Costello, (216) 433–6635, fax (216) 433–2555, Donald.E.Costello@grc.nasa.gov; and Dr. Philip G. Neudeck, (216) 433–8902, Philip.G.Neudeck@grc.nasa.gov

Author: Donald E. Costello

Headquarters program office: OAT

Programs/Projects: HTIES, HDTV

NASA Has Joined America True's Design Mission for 2000

The agreement between Lewis and America True calls for detailed analysis of different sail and mast designs.

Engineers at the NASA Lewis Research Center will support the America True design team led by America's Cup innovator Phil Kaiko. The America's Cup is an international sailing competition, and its trophy is the oldest in professional sports. America True is the San Francisco Yacht Club's challenger for the America's Cup race in the year 2000. The joint effort between NASA and America True is encouraged by Mission HOME, the official public awareness campaign of the U.S. space community.

NASA Lewis and America True have entered into a Space Act Agreement to focus on the interaction between the airfoil and the large deformation of the pretensioned sails and rigs along with the dynamic motions related to the boat motions. This work will require a coupled fluid and structural simulation. Included in the simulation will be both a steady-state capability, to capture the quasi-state interactions between the air loads and sail geometry and the lift and drag on the boat, and a transient capability, to capture the sail/mast pumping effects resulting from hull motions.

This agreement is segmented into two phases of a fluid structure interaction (FSI) simulation. FSI simulations will enable validation and improvements of the boat design, with higher fidelity, more reliable predictions of what will happen during testing, and will reduce the number of design iterations. Phase I is the generation of an FSI simulation template. This template will provide America True with a baseline simulation that can be used in generating subsequent models. Phase II consists of production FSI simulations. In this phase, the templates will be used to simulate potential and final boat designs.

Find out more on the World Wide Web: http://www.americatrue.org

Lewis contacts:
Laurel J. Stauber, (216) 433–2820, Laurel.J.Stauber@grc.nasa.gov;
Matthew E. Melis, (216) 433–3322, Matthew.E.Melis@grc.nasa.gov

Author: Gynelle C. Steele

Headquarters program office: OAT

Programs/Projects:
Smart composites, hypersonics

National Combustion Code, a Multidisciplinary Combustor Design System, Will Be Transferred to the Commercial Sector

The NASA Lewis Research Center and Flow Parametrics will enter into an agreement to commercialize the National Combustion Code (NCC). This multidisciplinary combustor design system utilizes computer-aided design (CAD) tools for geometry creation, advanced mesh generators for creating solid model representations, a common framework for fluid flow and structural analyses, modern postprocessing tools, and parallel processing. This integrated system can facilitate and enhance various phases of the design and analysis process.

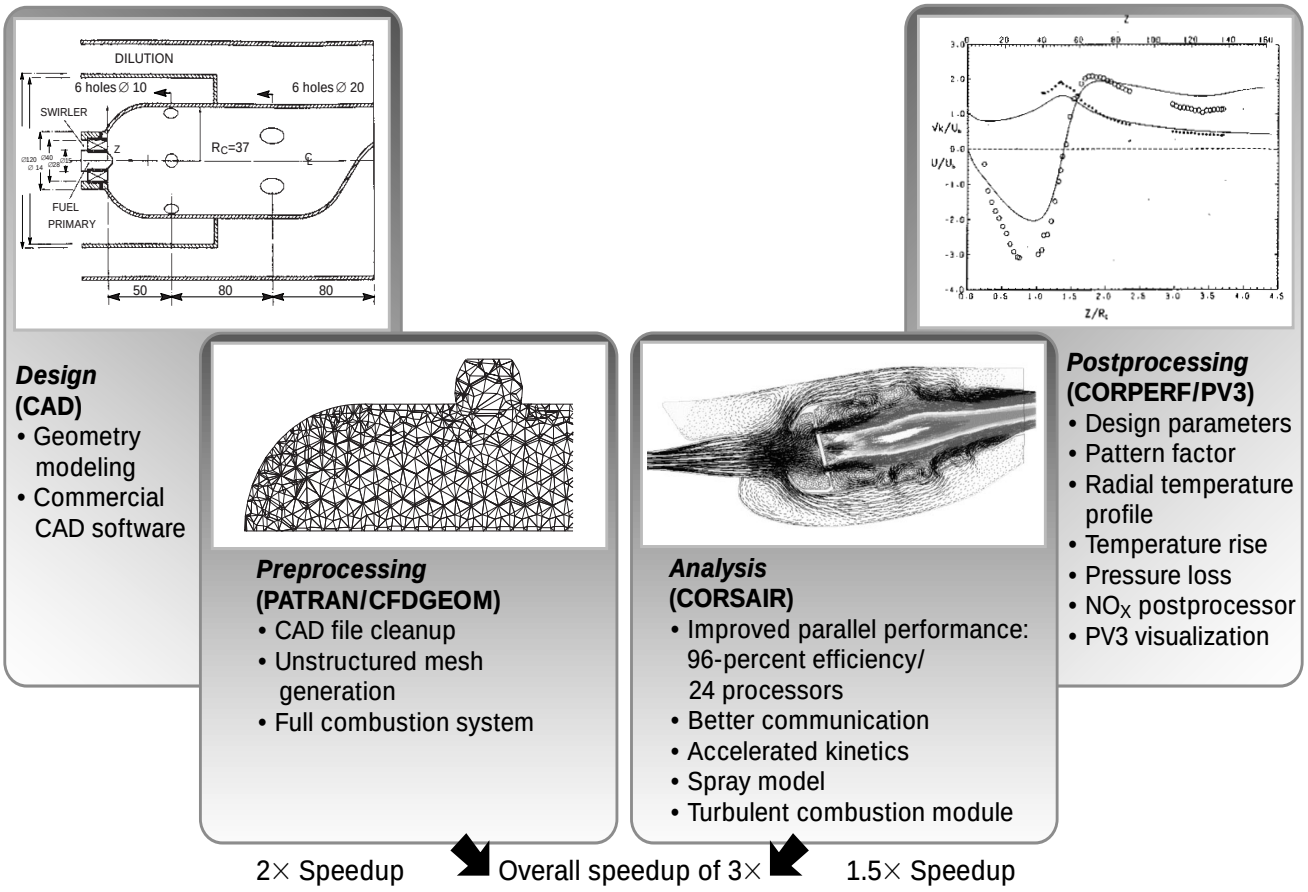

Typical results for the National Combustion Code (NCC), a combustor design and analysis system.

The National Combustion Code was developed under a NASA/Department of Defense/Department of Energy/U.S. industry partnership. Recent efforts have been focused on developing a computational combustion dynamics capability that will meet combustor designer requirements for model accuracy and analysis turnaround time, incorporating both short and long-term technology goals. As a first step, a baseline solver for turbulent combustion flows, CORSAIR–CCD, was developed under a joint modeling and code development effort between the aeronautics industry and NASA Lewis. CORSAIR–CCD is a Navier-Stokes flow solver based on an explicit four-stage Runge-Kutta scheme that uses unstructured meshes and runs on networked workstations. The solver can be linked to any computer-aided design system via the Patran file system. Turbulence closure is obtained via the standard k-ε model with a high Reynolds number wall function. The following combustion models have been implemented into the code: finite-rate chemical kinetics emulations for Jet–A and methane fuels, turbulence-chemistry interactions via an assumed probability density function for temperature fluctuations, and thermal emissions of nitrogen oxides. CORSAIR–CCD can switch between a parallel virtual machine interface and a message-passing interface by using compiler flags. Its parallel performance on several platforms has been analyzed; and on the basis of the results, several improvements have been made. Applications of the CORSAIR–CCD code to date include simulating swirling flow and simulating ignition-delay experiments; computing a generic swirling flow for a can-combustor and a multishear flow for a low-NO_x fuel nozzle; calculating a multiwalled production fuel nozzle and an IMFH/Cyclone "1-cup sector" (which contains one cyclone and an integrated set of mixing and flame holder tubes); and providing computational support for tests of the NASA LDI–MVS sector rig combustor (which uses lean direct injection and a multiple venture swirler).

Lewis contacts:
Gynelle C. Steele, (216) 433–8258, Gynelle.C.Steele@grc.nasa.gov; and Dr. Nan-Suey Liu, (216) 433–8722, Nan-Suey.Liu@grc.nasa.gov

Author: Gynelle C. Steele

Headquarters program office: OAT

Programs/Projects: Propulsion Systems R&T, HPCCP, SGE, P&PM

Definitions of NASA Headquarters Program Offices

OA Office of the Administrator
- **DDF** Director's Discretionary Fund

OAT Office of Aeronautics and Space Transportation Technology

OES Office of Earth Sciences

OLMSA Office of Life & Microgravity Sciences & Applications
- **LS** Life Sciences
- **UG** Microgravity Research

OSF Office of Space Flight

OSS Office of Space Science
- **ATMS** Advanced Technology & Mission Studies

Definitions of Programs and Projects

ACESE	Attitude Control and Energy Storage Experiment
ACTS	Advanced Communications Technology Satellite
AITP	Aerospace Industry Technology Program
ALB	Angular Liquid Bridge Experiment
AOS	Aviation Operation Systems
ASCR	Advanced Subsonic Combustor Rig
AST	Advanced Subsonic Technology
ASTP	Advanced Space Transportation Program
ATD	Advanced Technology Development
ATM	Asynchronous Transfer Mode
AXAF	Advanced X–Ray Astrophysics Facility
BCAT	Binary Colloidal Alloy Test
CARES	Ceramics Analysis and Reliability Evaluations of Structures
CETDP	Cross Enterprise Technology Development Program
CFM	Candle Flames in Microgravity Experiment
CHT	Capillary-Driven Heat Transfer Investigation
CSLM	Coarsening in Solid-Liquid Mixtures
CSOC	Consolidated Space Operations Contract
D^3	Direct Data Distribution
DARTFire	Diffusive and Radiative Transport in Fires
DCE	Droplet Combustion Experiment
EAPU	Electric Auxiliary Power Unit
ELF	Enclosed Laminar Flames
EMA	Electromechanical Actuator
EOS	Earth Observing System
EPM	Enabling Propulsion Materials
EWT	Embedded Web Technology
FCF	Fluids & Combustion Facility for the International Space Station
FFFT	Forced Flow Flame Spreading
FSDC	Fiber Supported Droplet Combustion
GAS	Get Away Special experiment
GEO	Geosynchronous Earth orbit
HDTV	High-definition television
HEDS	Human Exploration and Development of Space
HEUS	High Energy Upper Stage
HISTEC	High Stability Engine Control
HITEMP	Advanced High Temperature Engine Materials Technology Program
HOST	Hubble Space Telescope Orbital System Test
HPCCP	High Performance Computing and Communications Program
HREC	High Reliability Engine Control
HSCT	High-Speed Civil Transport
HSR	High-Speed Research
HST	Hubble Space Telescope
HTIES	High Temperature Integrated Electronics and Sensors Program

ICE	Interface Configuration Experiment
IMAPS	International Microelectronics and Packaging Society
In-STEP	In-Space Technology Experiment Program
ISS	International Space Station
LCBT	Low Cost Booster Technology Program
LEO	Low Earth orbit
LSP	Laminar Soot Processes Experiment
LTP	Learning Technologies Project
MGBX	Microgravity (or Middeck) Glovebox
Mir	Russian space station
MSL	Microgravity Science Laboratory
MSL–1R	Microgravity Science Laboratory–First Reflight
MTPE	Mission to Planet Earth
NCMR	National Center for Microgravity Research
NCP	National Cycle Program
NII/GII	National and Global Information Infrastructure
NPSS	Numerical Propulsion System Simulation
NSTAR	NASA Solar Electric Propulsion Technology Application Readiness
OFFS	Opposed Forced Flame Spread Experiment
PHSV	Propulsion for Highly Survivable Vehicles
POSA	Passive Optical Sample Assembly
P&PM	Physics and Process Modeling
RITSI	Radiative Ignition and Transition to Spread Investigation
RLV	Reusable Launch Vehicles
SAL	Spread Across Liquids
SAMS	Space Acceleration Measurement System
SBIR	Small Business Innovation Research
SDFD	Solar Dynamic Flight Demonstration project
SD GTD	Solardynamic Ground Test Demonstration
SEMAA	Science/Engineering/Mathematics & Aerospace Academy
SGE	Smart Green Engine
SIBAL	Solid Inflammability Boundary at Low Speed
SOMO	Space Operations Management Office
SSCE	Solid Surface Combustion Experiment
SSP	Space Solar Power
STS	Space Transportation System
TGDF	Turbulent Gas-Jet Diffusion Flames
TIGER–3D	Transition From Ignition to Flame Growth Under External Radiation in 3D
TTCP	The Technical Cooperative Program
TURBO–AE	Three-dimensional viscous propulsion aeroelastic computer code
USML	United States Microgravity Laboratory
USMP	United States Microgravity Payload
WIF	Wire Insulation Flammability experiment
X2000	Deep space development program
X–33	Replacement for space shuttles

Index of Authors and Contacts

Both authors and contacts are listed in this index. Articles start on the page numbers following the names. When two articles start on the same page, the first article is indicated by an “a” after the number and the second article by a “b.”

REPORT DOCUMENTATION PAGE

Form Approved
OMB No. 0704-0188

1. AGENCY USE ONLY (*Leave blank*)	2. REPORT DATE	3. REPORT TYPE AND DATES COVERED
	April 1999	Technical Memorandum

4. TITLE AND SUBTITLE

Research & Technology 1998

5. FUNDING NUMBERS

None

6. AUTHOR(S)

7. PERFORMING ORGANIZATION NAME(S) AND ADDRESS(ES)

National Aeronautics and Space Administration
Glenn Research Center
Cleveland, Ohio 44135–3191

8. PERFORMING ORGANIZATION REPORT NUMBER

E–11414

9. SPONSORING/MONITORING AGENCY NAME(S) AND ADDRESS(ES)

National Aeronautics and Space Administration
Washington, DC 20546–0001

10. SPONSORING/MONITORING AGENCY REPORT NUMBER

NASA TM—1999-208815

11. SUPPLEMENTARY NOTES

Responsible person, Walter S. Kim, organization code 9400, (216) 433–3742.

12a. DISTRIBUTION/AVAILABILITY STATEMENT

Unclassified - Unlimited
Subject Categories: 01 and 31 Distribution: Nonstandard

This publication is available from the NASA Center for AeroSpace Information, (301) 621–0390.

12b. DISTRIBUTION CODE

13. ABSTRACT ***(Maximum 200 words)***

This report selectively summarizes the NASA Lewis Research Center's research and technology accomplishments for the fiscal year 1998. It comprises 134 short articles submitted by the staff scientists and engineers. The report is organized into five major sections: Aeronautics, Research and Technology, Space, Engineering and Technical Services, and Commercial Technology. A table of contents and an author index have been developed to assist readers in finding articles of special interest. This report is not intended to be a comprehensive summary of all the research and technology work done over the past fiscal year. Most of the work is reported in Lewis-published technical reports, journal articles, and presentations prepared by Lewis staff and contractors. In addition, university grants have enabled faculty members and graduate students to engage in sponsored research that is reported at technical meetings or in journal articles. For each article in this report, a Lewis contact person has been identified, and where possible, reference documents are listed so that additional information can be easily obtained. The diversity of topics attests to the breadth of research and technology being pursued and to the skill mix of the staff that makes it possible. At the time of publication, NASA Lewis was undergoing a name change to the NASA John H. Glenn Research Center at Lewis Field. For more information about research at NASA Glenn, visit us on the World Wide Web (http://www.grc.nasa.gov). This document is available on the World Wide Web (http://www.grc.nasa.gov/WWW/RT/). For publicly available reports, visit the Glenn Technical Report Server (GLTRS) on the World Wide Web (http://gltrs.grc.nasa.gov/GLTRS/).

14. SUBJECT TERMS	15. NUMBER OF PAGES
Aeronautics; Aerospace engineering; Space flight; Space power; Materials; Structures; Electronics; Space experiments; Technology transfer	208
	16. PRICE CODE: A10

17. SECURITY CLASSIFICATION OF REPORT	18. SECURITY CLASSIFICATION OF THIS PAGE	19. SECURITY CLASSIFICATION OF ABSTRACT	20. LIMITATION OF ABSTRACT
Unclassified	Unclassified	Unclassified	